

**FINITE ELEMENT MODELING OF RING SPLITTING TEST TO
PREDICT RESIDUAL STRESSES IN SPIRAL WELDED PIPE**

BY

AHMED SALEH AL-OMARI

A Thesis Presented to the
DEANSHIP OF GRADUATE STUDIES

KING FAHD UNIVERSITY OF PETROLEUM & MINERALS

DHAHRAN, SAUDI ARABIA

In Partial Fulfillment of the
Requirements for the Degree of

MASTER OF SCIENCE

In

MECHANICAL ENGINEERING

MAY 2010

KING FAHD UNIVERSITY OF PETROLEUM & MINERALS
DHAHRAN 31261, SAUDI ARABIA

DEANSHIP OF GRADUATE STUDIES

This thesis, written by Ahmed Saleh Al-Omari under the direction of his thesis advisor and approved by his thesis committee, has been presented to and accepted by the Dean of Graduate Studies, in partial fulfillment of the requirements for the degree of MASTER OF SCIENCE IN MECHANICAL ENGINEERING.

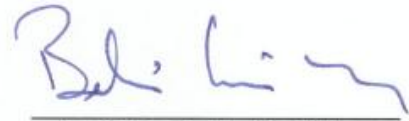
Thesis Committee



Prof. Dr. AbulFazal M. Arif
(Thesis Advisor)



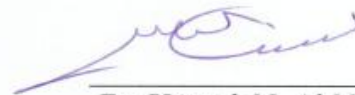
Dr. Amro M. Al-Qutub
Department Chairman



Prof. Dr. Bekir S. Yilbas
(Member)



Dr. Salam A. Zummo
Dean of Graduate Studies



Dr. Yagoub N. Al-Nassar
(Member)

16/10/10

Date

I dedicate this work to my wife,
children, brothers, sisters and to
the memory of my parents

ACKNOWLEDGMENT

First of all, I thank Allah for giving me the strength and ability to complete this work. Then, there are many people who have helped me along the road that has led to the completion of this master program. I thank my twin brother, Abdullah, for the constant encouragement to pursue my dreams. My success would not have been possible without the support of my wife. I am very grateful for her enduring love throughout the whole process and for her patience and encouragement. Thanks to my beloved kids, Nawaf and Reem, for their smiling faces. Special thanks to my brothers and sisters, for their patience and support.

I thank Prof. Dr. Abul-Fazal Arif and Dr. Yagoub Al-Nassar for their encouragement and assistance during my study. Their guidance throughout my thesis work has been very valuable and is greatly appreciated. My sincere appreciation to Prof. Dr. Bekir Sami Yilbas for his assistance during the laser welding part of this thesis. I am grateful to Prof. Dr. Anwar Khalil Sheikh for his assistance in the statistical analysis and regression models.

I want to thank all the staff of National Pipe Company (NPC) for their help and support. Thanks also are due to all of my colleagues from Saudi Aramco for providing guidance and technical information.

TABLE OF CONTENTS

ACKNOWLEDGMENT	iv
TABLE OF CONTENTS	v
LIST OF TABLES	viii
LIST OF FIGURES	x
THESIS ABSTRACT	xv
CHAPTER 1	1
INTRODUCTION	1
1.1 BACKGROUND	1
1.2 OVERVIEW OF LINE PIPE PRODUCTION	2
1.3 MANUFACTURING OF SPIRAL WELDED PIPE.....	5
1.3.1 SPIRAL PIPE PRODUCTION IN INTEGRATED FORMING AND WELDING.....	13
1.3.2 SPIRAL PIPE PRODUCTION WITH SEPARATE FORMING AND WELDING	19
1.4 INTRODUCTION TO WELDING	21
1.5 OVERVIEW OF RESIDUAL STRESSES.....	31
1.6 SPIRAL WELDED PIPE RESIDUAL STRESSES.....	39
1.7 RESIDUAL STRESSES MEASUREMENT TECHNIQUES.....	48
1.8 PIPE STRESS RELIEVING	54
1.9 INDUSTRY EXPERIENCE WITH SPIRAL WELDED PIPE	56
1.10 PROBLEM STATEMENT	58
1.11 OBJECTIVES OF THE THESIS	58
CHAPTER 2	60
LITERATURES REVIEW	60
2.1 PRODUCTION OF PIPES	60
2.2 WELD MODELING	61
2.3 HEAT SOURCE MODELING.....	63
2.4 WELDING RESIDUAL STRESSES	64
2.5 EXPERIMENTAL MEASUREMENTS OF RESIDUAL STRESSES	65
2.6 FEM RESIDUAL STRESSES MEASUREMENTS.....	66
2.7 PROBABILISTIC ANALYSIS AND REGRESSION MODEL	68

2.8	LASER WELDING	70
CHAPTER 3		73
PROBABILISTIC ANALYSIS AND REGRESSION MODEL		73
3.1	INTRODUCTION	73
3.2	EXPERIMENTAL PROCEDURE.....	76
3.3	DATA COLLECTION AND ANALYSIS.....	79
3.4	PROCESS CAPABILITY ANALYSIS (USING DATA SET A).....	81
3.5	PROBABILISTIC ANALYSIS (USING DATA SET B).....	86
3.6	REGRESSION MODELING (USING DATA SET B).....	95
CHAPTER 4		103
DRILLING HOLE TECHNIQUE MEASUREMENTS		103
4.1	DRILLING HOLE EXPERIMENTAL PROCEDURE	103
4.2	EXPERIMENTAL RESULTS.....	106
CHAPTER 5		115
FINITE ELEMENT ANALYSIS: 3D MODELING		115
5.1	OVERVIEW OF MODELING AND FINITE ELEMENT SIMULATION	115
5.2	IDEALIZATION OF THE FINITE ELEMENT MODEL.....	121
5.3	FEM ANALYSIS TYPE	123
5.4	ELEMENT TYPES (THERMAL & STRUCTURAL).....	125
5.5	MATERIAL PROPERTIES (THERMAL & MECHANICAL).....	127
5.6	GEOMETRICAL MODELING	131
5.7	FINITE ELEMENT MESH	137
CHAPTER 6		141
THERMAL ANALYSIS USING FINITE ELEMENT METHOD		141
6.1	OVERVIEW OF HEAT TRANSFER ANALYSIS	141
6.2	HEAT SOURCE MODELING FOR SPIRAL WELDED PIPE	144
6.3	TRANSIENT NON-LINEAR THERMAL ANALYSIS PROCEDURE.....	155
6.4	SOLUTION CONTROL	158
6.5	THERMAL BOUNDARY CONDITIONS	163
6.6	VALIDATION OF THE FEM THERMAL MODEL.....	164
6.7	FEM THERMAL RESULTS AND DISCUSSIONS	173
6.8	EFFECT OF WELDING SPEED ON THE TEMPERATURE FIELD PREDICTION.....	179

CHAPTER 7	183
STRUCTURAL ANALYSIS USING FINITE ELEMENT METHOD	183
7.1 STRUCTURAL ANALYSIS (SEQUENTIALLY COUPLED THERMAL-STRESS ANALYSIS) ...	183
7.2 MECHANICAL BOUNDARY CONDITIONS	189
7.3 TRANSIENT NON-LINEAR STRUCTURE ANALYSIS PROCEDURE	191
7.4 VALIDATION OF FE STRUCTURAL MODEL	191
7.5 FEM STRUCTURAL ANALYSIS RESULTS AND DISCUSSIONS	195
7.6 EFFECT OF WELDING SPEED ON THE RESIDUAL STRESS MEASUREMENTS	209
CHAPTER 8	213
LASER WELDING	213
8.1 INTRODUCTION	213
8.2 MATHEMATICAL MODEL OF LASER WELDING	214
8.2.1 THERMAL ANALYSIS.....	214
8.2.2 HEAT SOURCE MODEL	217
8.2.3 STRESS ANALYSIS	219
8.3 FINITE ELEMENT MODEL	220
8.4 RESULTS AND DISCUSSIONS	227
8.5 EFFECT OF WELDING SPEED	239
CHAPTER 9	244
CONCLUSIONS	244
CHAPTER 10	249
FUTURE WORK	249
REFERENCES	250
VITA	258

LIST OF TABLES

Chapter 1

Table 1.1: Spiral welded pipe sizes [NPC]	10
Table 1.2: Examples of root face details	30
Table 1.3: Graphical explanation of residual stress behavior	46

Chapter 3

Table 3.1: Process capability analysis	85
Table 3.2: Capability indices	86
Table 3.3: Process capability summery	86
Table 3.4: Statistics summary for 19 groups of data	87
Table 3.5: Summary of the multiple regression model.....	98
Table 3.6: Analysis of variance (ANOVA)	99

Chapter 4

Table 4.1: Selected pipes for hole drilling method (Compressive)	107
Table 4.2: Selected pipes for hole drilling method (Tensile)	107
Table 4.3: Microscopic residual stress parallel to weld bead in spiral pipes with tensile RSTP values	108
Table 4.4: Microscopic residual stress parallel to weld bead in spiral pipes with compressive RSTP values.....	110
Table 4.5: Microscopic residual stress perpendicular to weld bead in spiral pipes with tensile RSTP values.....	111
Table 4.6: Microscopic residual stress perpendicular to weld bead in spiral pipes with compressive RSTP values.....	112

Chapter 5

Table 5.1: Temperature-dependent thermal conductivity of mild steel [Mahapatra et al. 2006]	129
Table 5.2: Temperature-dependent enthalpy properties used for mild steel	130
Table 5.3: Temperature-dependent mechanical properties of mild steel [Mahapatra et al. 2006]	130
Table 5.4: Meshing details.....	139

Chapter 6

Table 6.1: Numerical values of heat source parameters used.....	149
Table 6.2: Welding process parameters	149
Table 6.3: Weld measurements for experimental samples	172
Table 6.4: Solution plan for welding speed=0.0192 m/s with 300 load steps.....	174
Table 6.5: Cases for welding speed effect study	179

Chapter 7

Table 7.1: SMYS and acceptable residual stress values for X65 pipe	192
Table 7.2: Cases foe welding speed effect study	210

Chapter 8

Table 8.1: Pipe and welding parameters.....	222
Table 8.2: Temperature-dependent thermal conductivity of steel [Mahapatra et al. 2006]	222
Table 8.3: Temperature-dependent enthalpy properties used for steel.....	223
Table 8.4: Temperature-dependent mechanical properties of steel [Mahapatra et al. 2006]	223
Table 8.5: Heat source parameters.....	227
Table 8.6: Details of locations.....	228

LIST OF FIGURES

Chapter 1:

Figure 1.1: Seamless Pipes	3
Figure 1.2: Welded Pipe	4
Figure 1.3: Geometric dependence of pipe diameter (D) on forming angle (α) and strip width (B), [Franz and Baldur 2004].....	6
Figure 1.4: Geometrical detail to specify a spiral welded pipe	7
Figure 1.5: Strip width relation with the pipe diameter, [Bresing and Sommer]	8
Figure 1.6: Pipe diameter relation with the helix angle.....	9
Figure 1.7: Spiral welded pipe production steps, [Ozmak Boru Co.].....	11
Figure 1.8: Carbon steel coil used for spiral welded pipe production	12
Figure 1.9: Helix forming of spiral welded pipe [Hall Longmore]	14
Figure 1.10: Three-roll bending system with outside roller cage [Franz and Baldur 2004] .	15
Figure 1.11: Internal and external welding of spiral welded pipe [Hall Longmore]	16
Figure 1.12: Internal welding of the SWP where laser-controlled seam tracking system used [NPC].....	17
Figure 1.13: External welding of spiral welded pipe [NPC]	17
Figure 1.14: Monitoring of spiral welded pipe process at the pipe mill [NPC]	18
Figure 1.15: Shielded Metal Arc Welding (SMAW) Process [Lee 2006].....	23
Figure 1.16: Gas Tungsten Arc Welding (GTAW) [Lee 2006].....	24
Figure 1.17: Gas Metal Arc Welding (GMAW) [Lee 2006]	24
Figure 1.18: Submerged Arc Welding (SAW) [Lee 2006].....	25
Figure 1.19: Elements of a SAW circuit diagram [Lee 2006].....	26
Figure 1.20: Double-V-Groove welded joint details	28
Figure 1.21: Example of welding data sheet for spiral welded pipe [NPC]	29
Figure 1.22: Generation of residual stresses by heating and cooling of the material [Horn 2002]	32
Figure 1.23: Schematic representation of changes in temperature ΔT and stresses during welding [Weisman 1976].....	34
Figure 1.24: Representation of parallel (longitudinal) and perpendicular (Transverse) measured residual stress	38
Figure 1.25: Representation of different stresses on a pipe.....	38
Figure 1.26: Spiral and longitudinal welded pipes stresses	41
Figure 1.27: Stress dependence of the weld angle [Franz and Sommer 2004].....	42
Figure 1.28: Influence of the colder side in the sheet deformation [Hidveghy et al. 2003] ..	43
Figure 1.29: Residual stresses distribution across the thickness in rolling direction L and transverse direction T [Hidveghy et al. 2003]	44
Figure 1.30: Requirements for line pipe and control points in manufacturing.....	47
Figure 1.31: Depth ranges of measurement techniques compared with typically observed .	49
Figure 1.32: RS-200 mill guide used for drilling hole technique	51
Figure 1.33: Setup of the blind drilling hole device [ASTM-E837 2008].....	52
Figure 1.34: X-ray diffraction residual stress measurement [Proto Manufacturing].....	53

Chapter 3:

Figure 3.1: Spiral welded pipe.....	74
Figure 3.2: (a) Preparation for splitting ring test, (b) Ring cut from spiral welded pipe.....	77
Figure 3.3: Ring splitting method.....	77
Figure 3.4a: Histogram of ΔC values for ring splitting tests conducted on data set A.....	81
Figure 3.5: Normal probability plot for data set A	82
Figure 3.6: Process capability for the change in circumference ΔC in data set A.....	85
Figure 3.7: Pie-chart for data set B.....	88
Figure 3.8: Change of circumferences (\pm) verses different wall thicknesses for grade X65 pipes.....	89
Figure 3.9a: Change in circumferences for pipe groups 1 to 6.....	90
Figure 3.10: Normal probability plots for all groups of data set B (Separate).....	93
Figure 3.11: Normal probability plot in percent for all groups of data set B (Combined)....	94
Figure 3.12: Median plots with 95% confidence intervals for data set B.....	95
Figure 3.13: Predicted versus observed ΔC values.....	101

Chapter 4:

Figure 4.1: Hole-drilling rosettes.....	104
Figure 4.2: Setting positions of drilling hole rosettes.....	105
Figure 4.3: Microscopic residual stress parallel to weld bead in spiral pipes with tensile RSTP values.....	109
Figure 4.4: Microscopic residual stress parallel to weld bead in spiral pipes with compressive RSTP values.....	110
Figure 4.5: Microscopic residual stress perpendicular to weld bead in spiral pipes with tensile RSTP values	112
Figure 4.6: Microscopic residual stress perpendicular to weld bead in spiral pipes with compressive RSTP values.....	113

Chapter 5:

Figure 5.1: Coupling between different fields	118
Figure 5.2: Simulation scheme in welding analysis	120
Figure 5.3: Algorithm of thermo-structural analysis	121
Figure 5.4: Scheme of 3D heat flow [Sorenson 1999]	122
Figure 5.5: Scheme of 2D heat flow [Sorenson 1999]	122
Figure 5.6: SOLID70, 3D thermal solid element [ANSYS 2007].....	126
Figure 5.7: SOLID45, 3D structural solid element [ANSYS 2007].....	127
Figure 5.8: Pipe geometric that will be modeled.....	132
Figure 5.9: 3D model of 56-inch spiral welded pipe for one complete pitch.....	133
Figure 5.10: Geometry of 56-inch weld joint	134
Figure 5.11: Spiral welding of the weld joint	134
Figure 5.12: Basic concept for weld spiral path	135
Figure 5.13: Spiral weld line (path) for one complete pitch.....	136
Figure 5.14: Spiral weld path code	136
Figure 5.15: Final model of the ring.....	137

Figure 5.16: (a) Free meshing (b) Mapped meshing [ANSYS 2007].....	138
Figure 5.17: Finite element mesh of the ring model.....	140
Chapter 6:	
Figure 6.1: Schematic of the welding thermal model.....	143
Figure 6.2: The three stages in the welding time problem	144
Figure 6.3: Double ellipsoidal heat input distribution (W/m^3) [Sorenson 1999]	145
Figure 6.4: ANSYS code to get the elements centroidal positions.....	151
Figure 6.5: Array parameters for the elements centroidal positions in X-direction (Radial)	152
Figure 6.6: Array parameters for the elements centroidal positions in Y-direction (Angles)	152
Figure 6.7: Array parameters for the elements centroidal positions in Z-direction (Axial)	153
Figure 6.8: Modification of the arc's direction.....	154
Figure 6.9: Mapping of three different gauss points from global to local coordinates	155
Figure 6.10: Heat distribution (heat spot top view).....	157
Figure 6.11: Unfolding spiral welded pipe showing the spiral line as straight line	160
Figure 6.12: 150-mm ring spiral path (XY length).....	161
Figure 6.13: Stepped versus ramped loads [ANSYS 2007]	163
Figure 6.14: Metallographic specimen extraction location	165
Figure 6.15: Cross Section showing the macrograph of the spiral weld joint.....	166
Figure 6.16: Cross section showing the spiral weld configuration.....	167
Figure 6.17: Temperature gradients across the weld joint for mild steel	168
Figure 6.18: Weld bead shape as per the welding data sheet	169
Figure 6.19: Temperature contours throughout the spiral weld joint at the end of bottom and top welding	169
Figure 6.20: Representation of the nodes within the weld area at the ring end side	170
Figure 6.21: Temperature profile at selected nodes along the pipe ID at the end of the bottom welding (Load Step#100)	170
Figure 6.22: Temperature profile at selected nodes along the pipe OD at the end of the bottom welding (Load Step#100)	171
Figure 6.23: Temperature profile at selected nodes along the pipe ID at the end of the top welding (Load Step#250)	171
Figure 6.24: Temperature profile at selected nodes along the pipe OD at the end of the top welding (Load Step#250)	172
Figure 6.25: Temperature distributions at different stages	175
Figure 6.26: Temperature distributions after final cooling stage	176
Figure 6.27: Temperature profiles for selected nodes on pipe ID	177
Figure 6.28: Temperature profiles for selected nodes on pipe OD.....	178
Figure 6.29: Temperature distributions after final cooling stage for different welding speeds	180
Figure 6.30: Temperature variations at a single node (#6409) located at the OD for different speeds.....	181
Figure 6.31: Temperature contours through the wall thickness at the end of bottom welding (Load Step#100) for the three welding speed cases	182

Chapter 7:

Figure 7.1: Idealized flow curves from uniaxial tension test [Hsu 1986] 185

Figure 7.2: A schematic representation of the isotropic hardening model [Horn 2002] 187

Figure 7.3: A schematic representation of the kinematic hardening model [Horn 2002] ... 188

Figure 7.4: Mechanical boundary conditions 189

Figure 7.5: Mechanical boundary conditions applied on the ring 190

Figure 7.6: Close-up to the lines that were restrained in both the radial and tangential directions..... 190

Figure 7.7: Surface contours of the von Mises stress after final cooling 192

Figure 7.8: Residual stress measured by drilling hole technique for 56-inch spiral welded pipe 193

Figure 7.9: Residual stress measured by cutting method for 56-inch spiral welded pipe ... 194

Figure 7.10: Stress distribution throughout the OD of spiral welded ring 198

Figure 7.11: Stress distribution throughout the ID of spiral welded ring 199

Figure 7.12: Temperature fields and von Mises stress distributions during bottom welding 201

Figure 7.13: Temperature fields and von Mises stress distributions during at the end of the cooling 202

Figure 7.14: Temperature fields and von Mises stress distributions during top welding.... 203

Figure 7.15: Temperature distributions after cooling 204

Figure 7.16: Equivalent (von Mises) plastic strain after the welding..... 205

Figure 7.17: Selected nodes across the spiral weld on the OD surface 206

Figure 7.18: von Mises stress distributions across the weld on the OD 207

Figure 7.19: X-Component stress distributions across the weld on the OD..... 207

Figure 7.20: Y-Component stress distributions across the weld on the OD..... 208

Figure 7.21: Z-Component stress distributions across the weld on the OD 208

Figure 7.22: von Mises stresses for different welding speeds 210

Chapter 8:

Figure 8.1: View of laser welding process 215

Figure 8.2: The spatial heat distribution in the volumetric heat input model 218

Figure 8.3: Basic concept for weld spiral path in cylindrical coordinate system 221

Figure 8.4: (a) 3D model of 75 mm spiral welded tube for one complete pitch, 222

Figure 8.5: Finite element mesh 225

Figure 8.6: Showing the movement of the heat source along the unfolded spiral weld path 226

Figure 8.7: Schematic showing welding direction and distance measured across weld at four locations. 227

Figure 8.8: Temperature distribution on the outer surface at different times. 230

Figure 8.9: Temperature distribution along the spiral weld path on the outer and inner surfaces. 231

Figure 8.10: Temperature Distribution across the weld at location 4..... 233

Figure 8.11: Temporal variation of temperature at three different locations. 234

Figure 8.12: von Mises stress distribution along the spiral weld path on the outer and inner surfaces. 236

Figure 8.13: von Mises stress distribution on outer surface at different times.....	237
Figure 8.14: Temporal variation of von Mises stress at three different locations.	238
Figure 8.15: Residual stress across the weld path at three different locations.	239
Figure 8.16: Effect of welding speed on the temporal variation of von Mises stress at Location# 2.	241
Figure 8.17: Residual stress distribution across the weld at three different locations after cooling at three welding speeds.	243

THESIS ABSTRACT

Name : Ahmed Saleh Awadh Al-Omari
TITLE : Finite Element Modeling of Ring Splitting Test to Predict Residual Stresses in Spiral Welded Pipe
FIELD : Mechanical Engineering
DATE : May 2010

Spiral welded pipe offers cost benefits over other types of pipes. It is used for low pressure applications, water supply, and structural components successfully. However, acceptance of this product for wet sour hydrocarbon is controversial among oil and gas producers. It is well known that residual stresses are formed during the manufacturing of spiral welded pipes which will affect the integrity of the produced pipe. The main objective of this thesis work is to develop an appropriate finite element model of ring splitting technique that can be used to predict the residual stresses due to welding in spiral welded pipe. In addition, validation experiments were conducted whereby Finite Element Analysis “FEA” simulation outputs were compared to the experimentally measured data. Moreover, the effect of welding speed on the level of the residual stresses was studied. Furthermore, finite element method (FEM) is used to predict the temperature and stress fields in a laser spirally welded tube with 1.6 mm wall thickness and 75 mm diameter. Finally, statistical analysis and linear-regression modeling were used to study the effect of several structural, material and welding parameters on ring splitting test opening for spiral welded pipes.

Master of Science

King Fahad University of Petroleum & Minerals

Dhahran, Saudi Arabia

خلاصة الرسالة

اسم الطالب الكامل : أحمد بن صالح بن عوض الحاسن العُمري
عنوان الدراسة : محاكاة طريقة قطع الحلقة للتنبؤ بالإجهادات المتبقية في الأنابيب
الملحومة لوليباً باستخدام طرائق العناصر المنتهية.
التخصص الرئيسي : الهندسة الميكانيكية
التاريخ : مايو 2010

الأنابيب الملحومة لوليباً (بشكل حلزوني) تعتبر ذات قيمة مادية أقل مقارنة بالأنواع الأخرى من الأنابيب. حالياً هذا النوع من الأنابيب يستخدم لتطبيقات الضغط المنخفض ، وإمدادات المياه ، وكذلك في الأعمال الإنشائية بشكل فعال. ومع ذلك ، قبول هذا المنتج في نقل المنتجات الهيدروكربونية مازال محط للجدل بين منتجي النفط والغاز. ومن المعروف جيداً أن الإجهادات المتبقية والتي تشكلت خلال مراحل التصنيع للأنابيب الملحومة لوليباً تؤثر على جودة و سلامة الأنابيب المنتجة.

إن الهدف الرئيسي من هذه الرسالة هو تطوير نموذج مناسب باستخدام طرائق العناصر المنتهية لطريقة قطع الحلقة (جزء من الأنبوب) والتي يمكن استخدامها للتنبؤ عن الإجهادات المتبقية بسبب لحام الأنابيب لوليباً. بالإضافة إلى ذلك ، تم مقارنة عدد من نتائج التجارب العملية للمصادقة على نتائج المحاكاة المستخلصة من طرائق العناصر المنتهية. كما تمت دراسة تأثير سرعة اللحام على مستوى الإجهادات المتبقية في الأنابيب الملحومة لوليباً. وأخيراً، اللحام بواسطة الليزر على هذا النوع من الأنابيب تمت محاكاته بواسطة طرائق العناصر المنتهية والنتائج المستخلصة تمت مقارنتها بنتائج التجارب العملية.

دراسة الماجستير في العلوم
جامعة الملك فهد للبترول والمعادن
الظهران - المملكة العربية السعودية

CHAPTER 1

INTRODUCTION

1.1 BACKGROUND

Industrial pipes have a fundamental role in different sectors of the chemical, petrochemical, nuclear and oil industries. The use of line pipes has a long history in different industrial applications. Line pipes play an important role in many applications primarily for conveying of fluids and are made of diverse materials and dimensions according to the purpose for which they are intended. The manufacturing methods of line pipes can be divided as seamless and welded. Depending on the application requirements, line pipes are manufactured in different sizes and shapes. The pipe industries face many challenges to produce high quality piping in a cost effective and productive way in today's marketplace.

Spiral welded pipe is one type of the line pipes and it is used throughout the world for large-diameter, oil and gas transmission pipelines with some restriction to critical services (wet sour hydrocarbon). As the industry needs for production increase, the operating demands on spiral welded pipe also increase. These demands include larger diameters, higher operating pressures, increased mechanical strength and low level of residual stresses.

The relative structural weakness of spiral welded pipe, due to larger welded area and high residual stresses, limited the growth of its use in the oil and gas industry. The main characteristic failure mechanism in spiral welded pipes is a propagation of any cracks along the length of the pipe in a spiral pattern where the residual stresses will facilitate the failure. So, high residual stress is the main disadvantage of spiral welded pipes compared with longitudinal welded pipes. Currently, the popularization of spiral welded pipes is limited although it is cheaper to produce than any types of pipe.

Although the process for forming spiral welded pipe is widely used, little work has been conducted to establish unique residual stress characteristics of pipe formed from this process. In order to eliminate doubts in respect of quality of spiral welded pipes, the need for studying the residual stresses in this type of line pipes is required to use it in higher pressure and in critical operating conditions with confidence.

1.2 OVERVIEW OF LINE PIPE PRODUCTION

The steel pipes are very wide used in all kinds of application. Pipes are usually distinguished by their way of production. They can be produced either seamless or with seam (welded) by longitudinal welding or spiral welding from rolled strip or thick plate. The following two sections briefly point out main features of different pipe processes.

1.2.1 SEAMLESS PIPE

Seamless pipes (Figure 1.1) are being the preference for small diameters pipes of 305 mm (12 inches) or less. The production process for seamless pipe begins by heating a metal billet at high temperature which is usually done in a rotary hearth furnace. The red-hot billet is rotated and drawn by rolls over a piercing rod or mandrel. The action of the rolls causes the metal to flow over and about the mandrel to create a hollow pipe shell. The shell is then moved forward over a support bar and is hot-rolled or cold-rolled in several reducing/sizing stands to obtain the desired wall thickness and diameter. For high quality requirements, heat treatment is carried out after final rolling. Hot extrusion process is also used for producing seamless pipes of approximately up to 230 mm (9 inches) outside diameter. Another method of manufacturing seamless pipes is casting. Seamless pipe has outstanding homogeneity in the circumferential direction and is thus highly resistant to internal pressure and torsion.

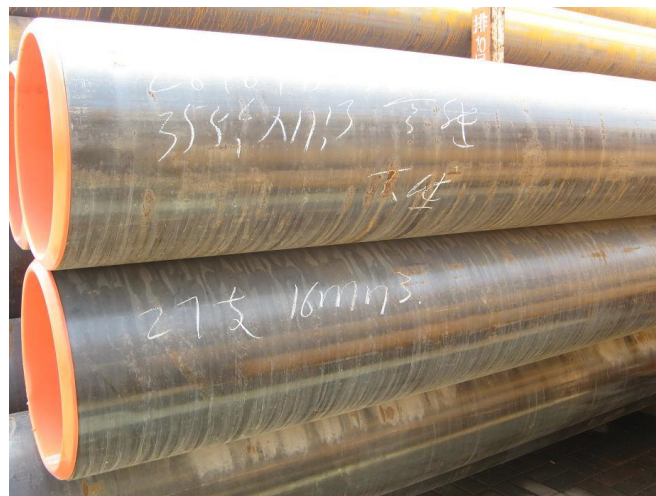


Figure 1.1: Seamless Pipes

1.2.2 WELDED PIPE

Welded pipe is made by bending metal strips (skelp) or plate into the form of a pipe by roll forming and welding the seam by various welding processes. Currently around two thirds of the steel pipe productions in the world are accounted for by welding processes. There are two types of welded pipes as shown in

Figure 1.2, longitudinal (straight seam) welded pipes and spiral welded pipes.



a) Longitudinal Welded Pipe



b) Spiral Welded Pipe

Figure 1.2: Welded Pipe

Longitudinal welded (Straight Seam) pipe is commonly used for oil and gas pipelines. Each pipe starts as a steel plate which is formed into the pipe by pressing, for example in a UOE mill, or rolling, for example in a roll bending mill. At the end of the

formation stage, the pipe is tack welded to maintain its form before being welded inside (ID) and outside (OD) by the submerged arc welding process. Longitudinal welded pipes are made from a steel plate with only one weld seam joining the two edges of the rolled plate.

Spiral welded pipes are manufactured by helical rolling of steel coils. In contrast to longitudinally welded pipe production where each pipe diameter requires a certain plate width, spiral pipe production is characterized by the fact that various pipe diameters can be manufactured from a single strip or plate width.

1.3 MANUFACTURING OF SPIRAL WELDED PIPE

Spiral welded pipe, as the name implies, is a steel pipe that has a seam running its entire length in a spiral form. ASME B31.3 “Process Piping” defines the spiral welded pipe as a pipe having a helical seam with a butt, lap, or lock-seam joint which is welded using an electrical resistance, electric fusion or double-submerged arc welding process.

A major advantage of spiral pipe production is its high flexibility. Various spiral welded pipe diameters can be produced from the same strip width (with a ratio of pipe diameter to width of between 1:2 and 1:2.2) by changing the forming angle α which is also called helix angle. Large diameter pipe ranging from approximately 500–2500 mm (20-98 inches) is the current state-of-art in spiral welded pipe production. Normal

operation of spiral pipe mills includes control of the mill forming angle. This has an effect on pipe diameter while also being critical to pipe formation and good weld quality. The forming angle is defined as the angle between the incoming strip and the leaving pipes (Figure 1.3).

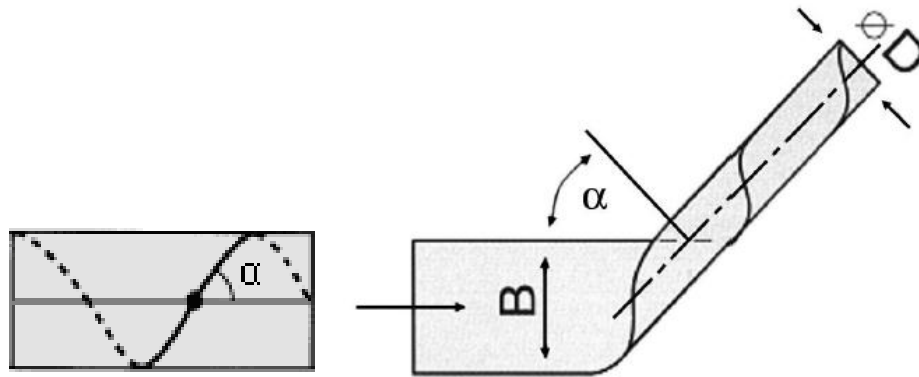


Figure 1.3: Geometric dependence of pipe diameter (D) on forming angle (α) and strip width (B), [Franz and Baldur 2004]

The forming angle (α) is a function of such parameters as the width of the strip (B) and the diameter pipe (D) to which the strip is rolled and it can be calculated using one of the following formulas:

$$\alpha = \sin^{-1}\left(\frac{B}{\pi D}\right) \quad (1.1)$$

$$\alpha = \tan^{-1}\left(\frac{P}{\pi D}\right) \quad (1.2)$$

where:

α = forming "helix" angle

$D = \text{Pipe Diameter}$

$B = \text{Coil width} - \text{trim loss} = \text{Coil width} - 15 \text{ mm}$

$P = \text{Pitch}$

Spiral Pitch (P) is defined as the distance between successive turnings as shown in Figure 1.4.

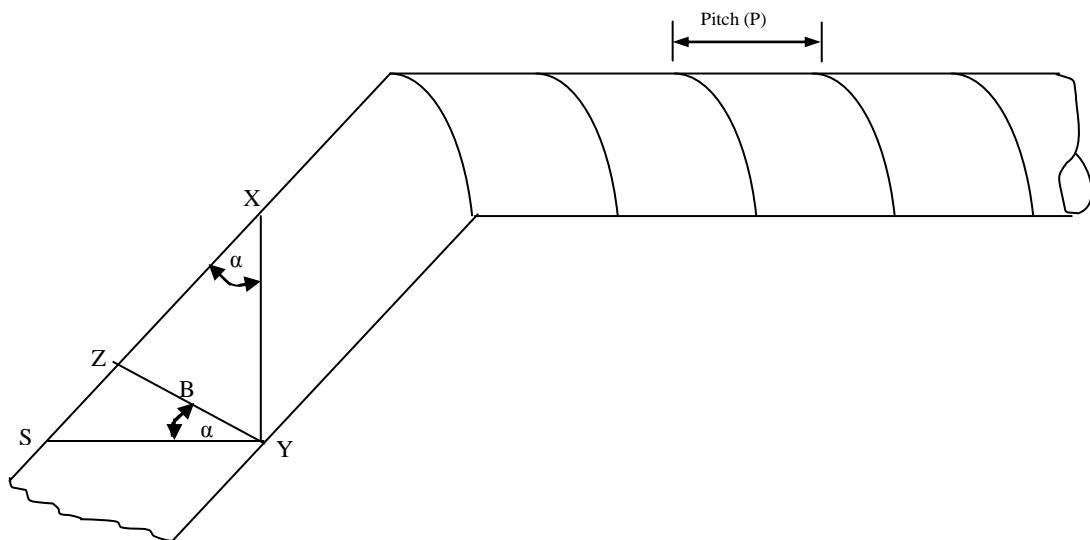


Figure 1.4: Geometrical detail to specify a spiral welded pipe

To determine the pitch distance (P), the following formulas are used:

$$P = YS = \tan \alpha \times (\pi D) \quad (1.3)$$

or

$$P = \frac{B}{\cos \alpha} \quad (1.4)$$

Figure 1.5 shows the ratio of pipe diameter to starting material width in a comparison between longitudinally welded and spiral pipe production, and also the mathematical dependences which apply in spiral pipe production between feed angle, strip/skelp width and pipe diameter. Forming angle and the pipe diameter where the pipe diameter increases as the forming angle decrease.

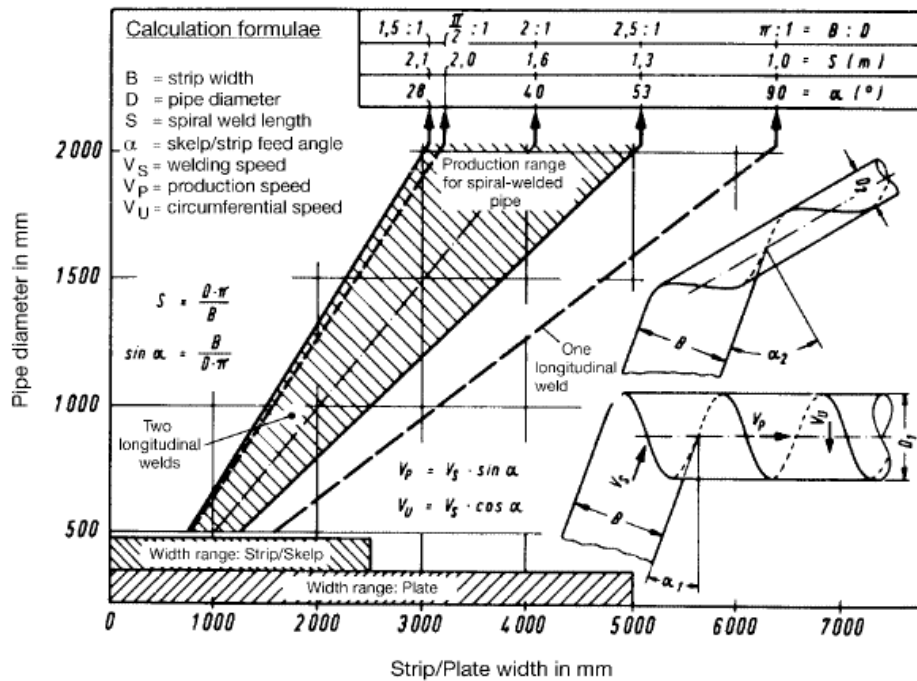


Figure 1.5: Strip width relation with the pipe diameter, [Brensing and Sommer]

Figure 1.6 shows an example of two different forming angles. The change in angle will have an effect on the pipe diameter for the same strip width as explained before.

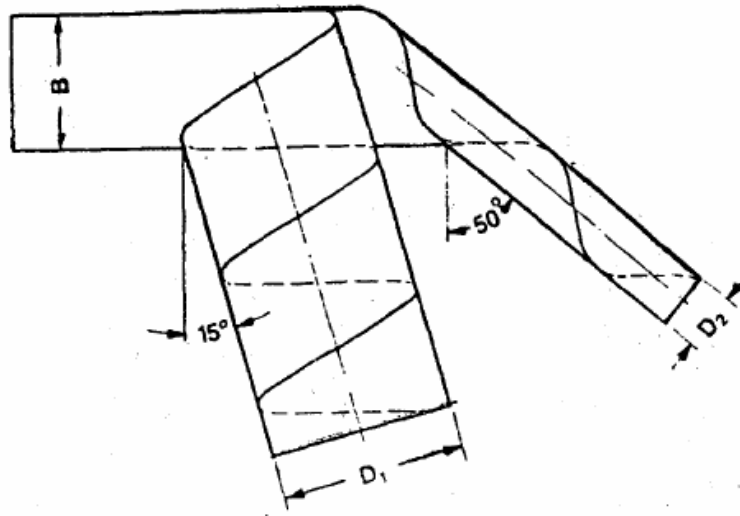


Figure 1.6: Pipe diameter relation with the helix angle

Basically, 10 to 45 degrees are the range of forming angles used by the spiral welded pipe manufacturers. This is also in compliance to paragraph 5.3.1 of API Spec 5L which specifies the width of plate or skelp used to manufacture helical seam pipe (shall be less than 0.8 or more than 3.0 times the outside diameter of the pipe). Table 1.1 shows different pitch spiral distances for different pipe sizes used in spiral pipe production mills.

Table 1.1: Spiral welded pipe sizes [NPC]

Size & Grade				Coil Width	Coil Width - Trim Loss	Forming Angle (Degrees)	Welding Speed (M/Min)	Pitch (mm)	
OD	WT		GR						
56	1422 "	0.649	16.48 "	65	1630	1615	21	2.15	1719
36	914 "	0.250	6.35 "	60	1630	1615	34	2.10	1946
40	1016 "	0.444	11.28 "	60	1630	1615	31	2.25	1860
40	1016 "	0.640	16.26 "	60	1650	1635	31	1.80	1886
24	610 "	0.250	6.35 "	60	1320	1305	43	2.10	1775
24	610 "	0.305	7.75 "	60	1320	1305	43	2.25	1774
42	1067 "	0.438	11.13 "	70	1630	1615	29	2.25	1832
42	1067 "	0.625	15.88 "	70	1630	1615	29	1.90	1827
56	1422 "	0.467	11.86 "	65	1630	1615	21	2.20	1723
60	1524 "	0.500	12.70 "	65	1630	1615	20	1.90	1706
60	1524 "	0.679	17.25 "	70	1520	1505	18	1.55	1574
60	1524 "	0.661	16.79 "	70	1520	1505	18	1.55	1574
30	762 "	0.375	9.53 "	65	1320	1305	33	2.15	1546
30	762 "	0.542	13.77 "	65	1520	1505	39	1.65	1919
30	762 "	0.437	11.10 "	65	1600	1585	42	2.00	2102
56	1422 "	0.534	13.56 "	70	1630	1615	21	2.05	1722
56	1422 "	0.640	16.26 "	70	1600	1585	21	1.80	1683
56	1422 "	0.640	16.26 "	70	1600	1585	21	1.80	1683
60	1524 "	0.551	14.00 "	70	1640	1625	20	1.80	1717
30	762 "	0.502	12.75 "	65	1520	1505	39	1.75	1920

The starting material employed for pipe wall thicknesses up to approx. 20 mm takes the form of wide hot-rolled strip. Plates in individual lengths up to 30 meter are usually required for pipe wall thicknesses in excess of 20 mm. There are two type of steel materials used to fabricate the spirally welded pipe for oil and gas industries ,based on the operating service, which are sour and non-sour. Oil and Gas Companies usually purchased 20” to 60” OD pipe size with API Grade B, X52 or X60 steel grade. The trend for the last five years is to use bigger pipe sizes with higher steel grade. The maximum supplied pipe size was of 66” OD and maximum steel grade of API X70.

Generally, spiral welded pipes are produced from forming and welding plate or strip material. The steel is leveled and passed through a forming station that spirals the steel to the required outside diameter. The spiral seam is then welded both internally and externally as part of the one forming operation. The pipe shell thus formed is cut to the required length as it travels out of the forming and welding machine. Figure 1.7 summarizes the production and quality control steps during the manufacture of spiral welded pipe.

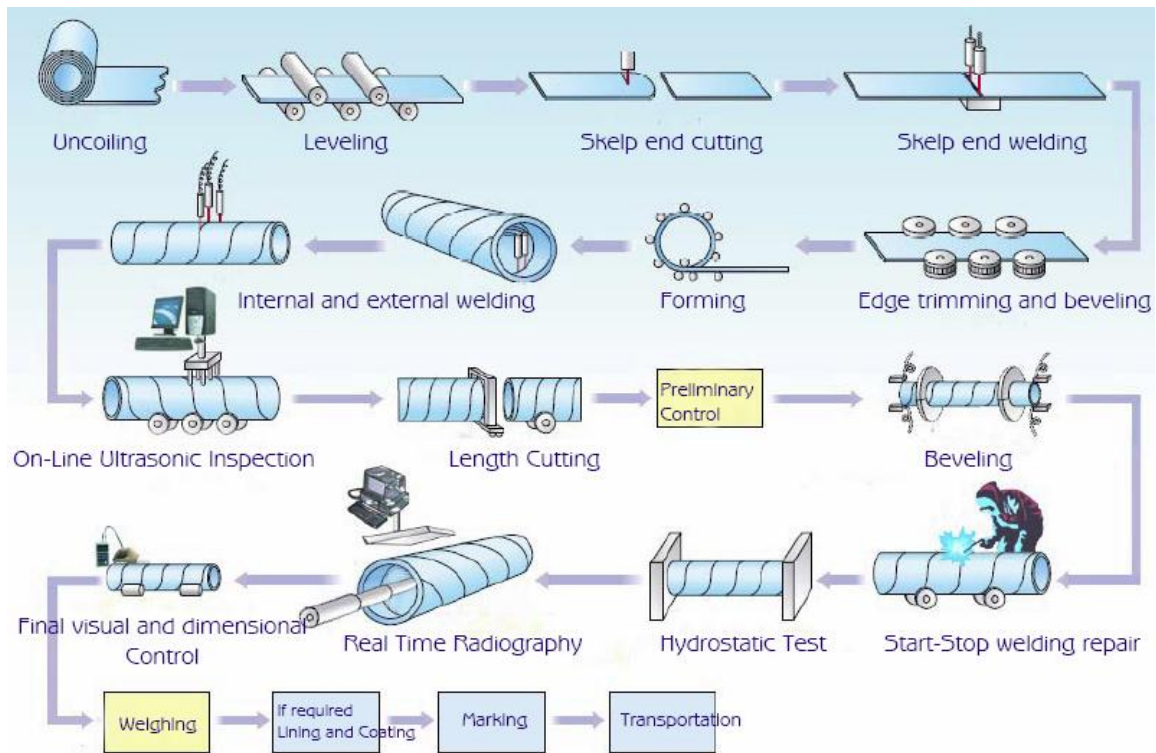


Figure 1.7: Spiral welded pipe production steps, [Ozmaç Boru Co.]

Spiral pipe welding mills consist of:

- De-coiling device (Figure 1.8)
- Strip connecting welder

- Straightening rollers
- Edge preparation tools (shearing and trimming)
- Forming devices, three roller bending and cage forming system
- Internal and external welders
- Ultrasonic testing apparatus
- Cutting devices
- Hydrostatic Pressure Testing



Figure 1.8: Carbon steel coil used for spiral welded pipe production

Specifically, spiral pipe production methods fall into two main categories:

- Facilities with integrated forming and Submerged Arc welding (SAW) lines.
- Facilities with separate forming and SAW welding lines.

1.3.1 SPIRAL PIPE PRODUCTION IN INTEGRATED FORMING AND WELDING

The integrated forming and SAW welding line can be regarded as the more conventional spiral pipe manufacturing facility. In this configuration, the production process comprises:

- Strip preparation stage.
- Pipe forming operation with simultaneous inside and outside pass submerged-arc welding.

In an integrated facility, the strip preparation stage is immediately followed by the forming process with simultaneous inside and outside submerged-arc welding. A pinch-roll unit feeds the skelp at a predetermined entry angle into the forming section of the machine. (Figure 1.9). The forming unit consists of a three-roll bending system with an outside roller cage. The purpose of the forming section is to bend the exactly prepared skelp of width (B) at a certain feed angle (α) into a tubular cylinder of diameter (D) in line with the mathematical relationships illustrated in Figure 1.5.



Figure 1.9: Helix forming of spiral welded pipe [Hall Longmore]

Various forming techniques may be applied to produce the spiral pipes. Aside from the direct forming shoe process – which has its limitations – there are two main methods which are generally employed:

- 3-roll bending with an inside diameter roller cage.
- 3-roll bending with an outside diameter roller cage (Figure 1.10).

In a 3-roll bending system, numerous individual shaping and guiding rollers are employed rather than a single forming roll. The roller cage serves to fix the pipe axis and maximize the roundness of the pipe in order to ensure offset-free convergence of the strip edges at the welding point. This facilitates attainment of accurate pipe dimensions, so that the pipe exiting from the machine is already manufactured to within the standardized

diameter, roundness and straightness tolerances. Expansion/sizing of the pipes after welding is therefore not necessary.

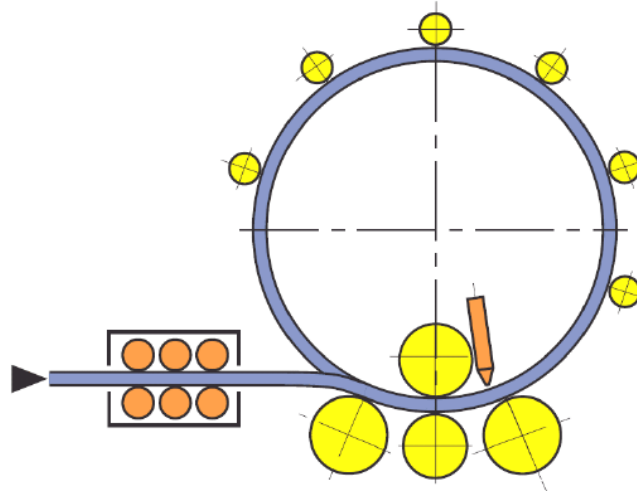


Figure 1.10: Three-roll bending system with outside roller cage [Franz and Baldur 2004]

The formed spiral welded pipes are subsequently fed to one of the three computer-controlled internal/external submerged arc welding stations for final welding (Figure 1.11). The welding of the spiral welded pipes is based on the Double-Sided Submerged Arc Welding (DSAW) process. Arc welding works by using electric current to produce an electric arc in a gas environment. The arc's heat brings the metal to fusion point. The submerged arc welding is carried out first internally (at approximately the 6 o'clock position), and then, 1 pitch turn further, outside-welded in the 12 o'clock position using the multi-wire technique. Welding head alignment to the weld centre, and gap control, are performed automatically. The two- or three-wire method is employed for the inside and outside pass welding operations.

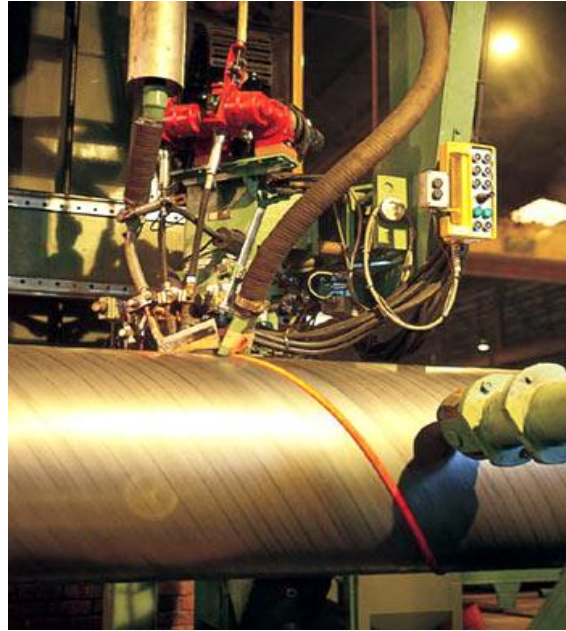


Figure 1.11: Internal and external welding of spiral welded pipe [Hall Longmore]

A laser-controlled seam tracking system shown in Figure 1.12 guarantees exact positioning of the weld seam and optimized overlapping. Figure 1.13 shows part from the external welding done for spiral welded pipe.



Figure 1.12: Internal welding of the SWP where laser-controlled seam tracking system used [NPC]



Figure 1.13: External welding of spiral welded pipe [NPC]

The manufactured pipe string is subsequently cut to length by a flying parting-off device. The individual pipes are then taken to the finishing department where the production process is completed by machining of the pipe ends and the performance of

any necessary rework. Prior to pipe edge machining, the pipes undergo a hydrostatic test. The entire weld region is then ultrasonically inspected, with the weld zones at the pipe ends also being x-rayed. In addition, each pipe end is also ultrasonically inspected over its full circumference for laps/laminations. If required, the weld zone and also the parent metal may be ultrasonically inspected following the hydrostatic test.

As part of the quality assurance regime, both in-process nondestructive inspections and offline mechanical tests are performed as production proceeds. After the pipes have successfully passed through all the test and inspection stages, including the dimensions check, they are presented for final inspection and acceptance. The process of the spiral pipe production in any mills is monitored continuously. All input data are recorded such as the pre-heat/post-heat temperatures, welding temperature, welding arc voltage and current for all internal and external electrodes. Figure 1.14 shows mill monitoring screen at one of the pipe production station.



Figure 1.14: Monitoring of spiral welded pipe process at the pipe mill [NPC]

The productivity of the integrated forming and welding process is determined by the speed of the submerged-arc welding operation. The pipe forming process is capable of substantially higher production speeds.

In order better to utilize the efficiency of the spiral pipe forming section, newer plants are being designed on the basis of separate forming and SAW welding lines. In this case, the spiral pipe forming machine features a tack-welding facility which is capable of production speeds commensurate with those of the forming section. The submerged-arc welding of the seams is then performed offline in a number of separate welding stands. Details of this process are explained in the next section.

1.3.2 SPIRAL PIPE PRODUCTION WITH SEPARATE FORMING AND WELDING

The main feature of this new technology is that there are two separate manufacturing processes:

- Stage 1 – Pipe forming with integral tack welding
- Stage 2 – Inside and outside submerged-arc welding on separate welding stands.

Aside from the higher cost-efficiency of this process (achieved owing to the faster forming and tacking operation) there are also technical benefits derived from separating the pipe forming stage from the main welding stage, as both operations can be

individually optimized. In the spiral pipe forming section, the merging strip edges (one on the already formed pipe section and the other on the incoming skelp) are continuously joined by inside tack welding.

The tack-welding process is performed by the Metal Active Gas welding (MAG) method at a speed of 12 m/min in the region of the 6 o'clock position. The shield gas employed is carbon dioxide. The weld edges below the welding position run with virtually no gap over a rigidly fixed guide roller. A flying parting-off device cuts the tack-welded pipe string into the required individual lengths. This pipe cutting process constitutes the last operation performed in the spiral forming machine. Because of the high tack-welding speeds achieved, it has become necessary to replace the conventional oxyacetylene torch cutter by high-speed plasma torches operating with water injection. The cut-to-length pipes are then fed to the downstream combined two-pass SAW stands for final welding.

A special roller table rotates the pipe in precise accordance with its spiral joint, so enabling the SAW welding heads to perform first the inside and then the outside passes. Precise weld centerline alignment control of the inside and outside welding heads is required in this operation in order to minimize weld offset. Aside from a few modifications, the subsequent production stages such as pipe end machining, hydrostatic testing and also the nondestructive examinations and mechanical tests, are in principle the same as those applied in the conventional spiral pipe manufacturing with integrated

process that was explained in section 1.3.1. Here again, a high standard of quality is achieved by in-process quality control activities which are performed after every stage of production. The results of these tests and inspections are immediately fed back to the individual production stage concerned in order to ensure continuous product quality optimization.

1.4 INTRODUCTION TO WELDING

Generally, welding can be defined as any process in which two or more pieces of metal are joined together by the application of heat, pressure, or a combination of both. Most of the processes may be grouped into two main groups: pressure welding, in which the weld is achieved by pressure; and heat welding, in which the weld is achieved by heat. Heat welding is the most common welding used today.

Based on the heat source of sufficient intensity required to maintain a molten liquid metal pool, Heat welding can be divided into three different categories: gas welding, arc welding and high-energy beam welding.

Arc welding, which is heat-type welding, is one of the most important manufacturing operations for the joining of structural elements for a wide range of applications, including guide way for trains, ships, bridges, building structures, automobiles, and nuclear reactors, to name a few. It requires a continuous supply of either direct (DC) or alternating electric current (AC), which creates an electric arc to

generate enough heat to melt the metal and form a weld. In arc welding, energy is transferred from the welding electrode to the base metal by an electric arc. When the welding started, both the base metal and the filler metal are melted to create the weld. This melting is possible because a sufficient amount of power (energy transferred per unit time) and energy density is supplied to the electrode. The arc welding process is a remarkably complex operation involving extremely high temperatures, which produce severe distortions and high levels of residual stresses. These extreme phenomena tend to reduce the strength of a structure, which becomes vulnerable to fracture, buckling, corrosion and other type of failures. The most widely used arc welding processes are Shielded Metal Arc (SMAW), Gas Tungsten Arc (GTAW), Gas Metal Arc (GMAW), and Submerged Arc Welding (SAW).

In shielded metal-arc welding (Figure 1.15), a metallic electrode, which conducts electricity, is coated with flux and connected to a source of electric current. The metal to be welded is connected to the other end of the same source of current. By touching the tip of the electrode to the metal and then drawing it away, an electric arc is formed. The intense heat of the arc melts both parts to be welded and the point of the metal electrode, which supplies filler metal for the weld.

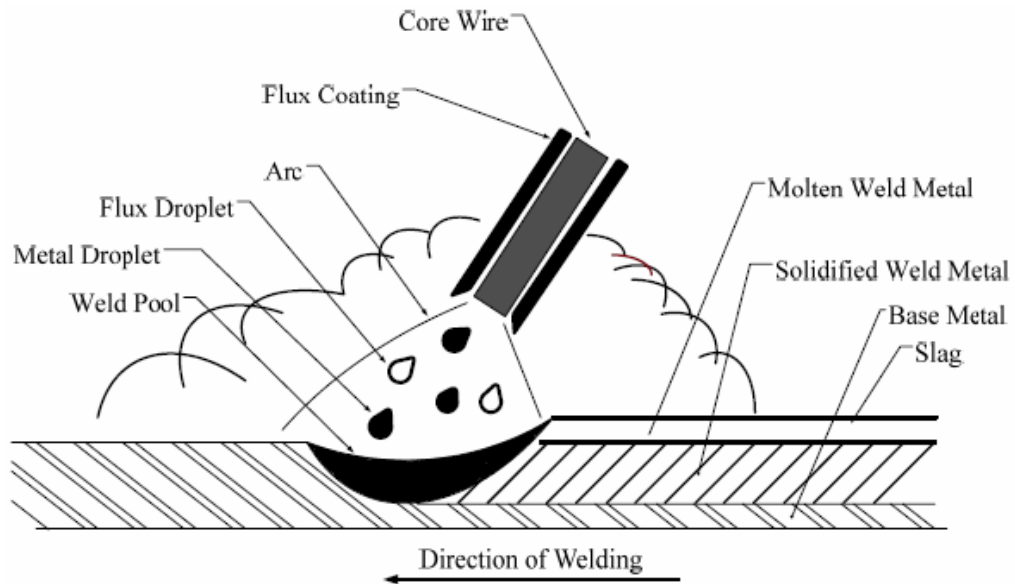


Figure 1.15: Shielded Metal Arc Welding (SMAW) Process [Lee 2006]

In gas tungsten arc welding (Figure 1.16), a tungsten electrode is used in place of the metal electrode used in shielded metal arc welding. A chemically inert gas, such as argon, helium, or hydrogen, is used to shield the metal from oxidation. The heat from the arc formed between the electrode and metal melts the edges of the metal. Metal for the weld may be added by placing a bare wire in the arc or the point of the weld. The GTAW process could be used with almost all metals and produces a high-quality weld. However, the rate of welding is considerably slower than in other processes.

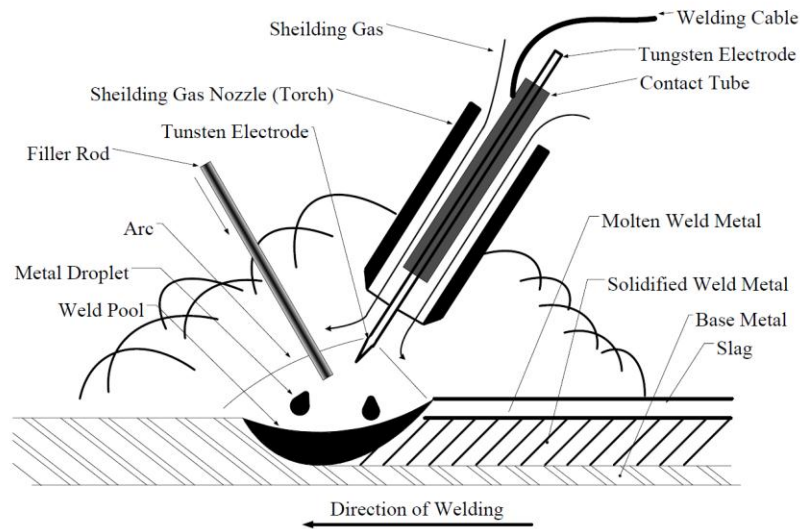


Figure 1.16: Gas Tungsten Arc Welding (GTAW) [Lee 2006]

In gas metal arc welding (Figure 1.17), a bare electrode is shielded from the air by surrounding it with argon or carbon dioxide gas or by coating the electrode with flux. The electrode is fed into the electric arc, and melts off in droplets to enter the liquid metal that forms the weld.

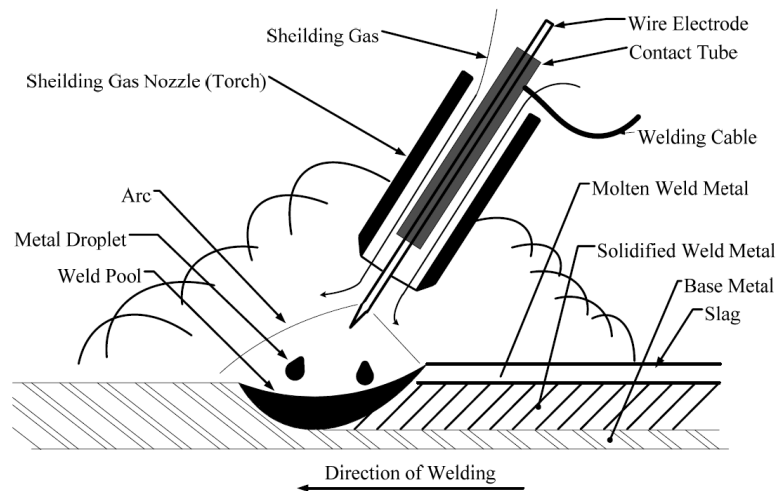


Figure 1.17: Gas Metal Arc Welding (GMAW) [Lee 2006]

Submerged arc welding (SAW) is similar to gas metal arc welding, but in this process no gas is used to shield the weld. Instead, the arc and tip of the wire are submerged beneath a layer of granular, fusible material formulated to produce a proper weld. This process is very efficient but is only used with steel. Submerged arc welding is one of the most common arc welding processes and is widely used for the production of line pipe as well as the fabrication of pressure vessels and steel structures. All welding for spiral welded pipe forming is carried out using the automatic submerged arc process. Submerged arc welding is a mechanized process in which a continuous solid wire is fed through a welding head immediately above the work piece, Figure 1.18.

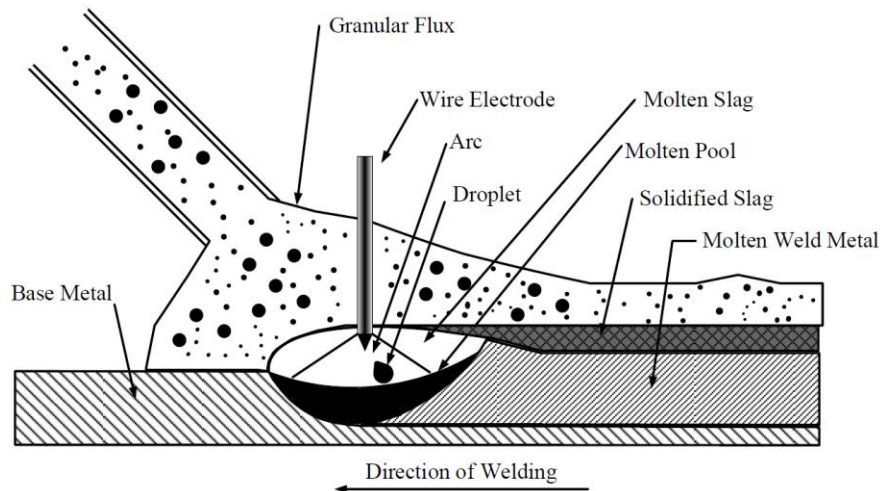


Figure 1.18: Submerged Arc Welding (SAW) [Lee 2006]

Figure 1.19 shows the elements required to perform Submerged Arc Welding (SAW)

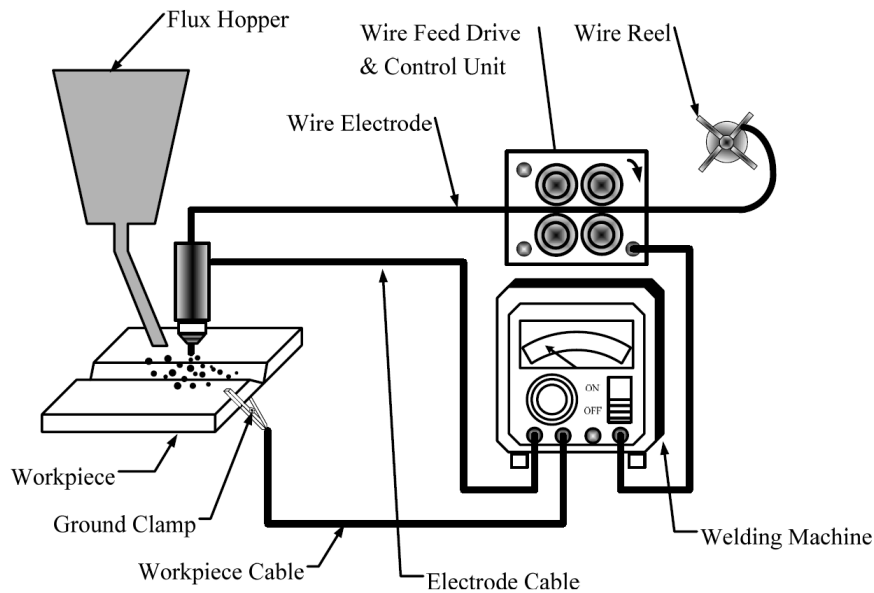


Figure 1.19: Elements of a SAW circuit diagram [Lee 2006]

The wire picks up current from the welding head and an arc is formed between the tip of the wire and the work piece thus generating the energy which both makes the weld pool and melts the end of the wire which is transferred across the arc. The arc and weld pool are protected from atmospheric contamination by a blanket of granular flux which fuses to form a liquid protective layer. De-oxidation and alloying additions to the weld pool can be made through control of the composition of the filler wire and from reactions with the flux. The submerged-arc welding of pipes in the usually applied two-pass method (i.e. first run followed by sealing or backing run) is normally performed with the inside pass first and the outside pass second. This ensures that the two passes sufficiently overlap. The efficiency of this welding process is characterized by the rate of filler metal deposited per unit time (rate of deposition) and the resultant – invariably high – welding speed which is possible.

The rate of deposition can be raised by increasing the welding current. However, owing to the limited current carrying capacity of the welding flux, performance can only be increased in single-wire welding up to a maximum input of around 1200 amps. Any increase in the rate of deposition beyond this limit requires the employment of several wire electrodes. This then allows a higher overall current to be applied for the welding work without the danger of the current carrying capacity of the flux being exceeded at any of the individual wire electrodes. In practical operations, increased performance is obtained by employing a multi-wire welding configuration with 2, 3 or 4 electrodes. The higher rate of deposition available with multi-wire welding converts readily into a higher welding speed under practical production conditions. In practice, the welding speeds attained range between 1 and 2.5 m/min, increasing in some cases to 3 m/min, depending on the welding process, wall thicknesses and type of flux used. The welding data sheets for several spiral welded pipe diameters (20" – 60" OD) have been collected. These sheets demonstrate the welding related information needed in the production of the spiral welded pipes.

Figure 1.20 shows the geometrical detail of the double-V-groove weld where:

α : Groove Angle

R: Root Opening

f: Root Face

T: Joint Thickness

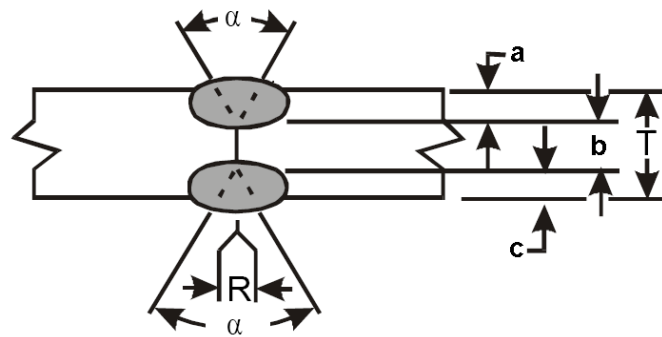


Figure 1.20: Double-V-Groove welded joint details

The following list indicates some of the variables that are included in the welding data sheets:

- Joint type and dimensions
- Pipe size and grade
- Filler material specification
- Flux classification
- Welding speed
- Current range
- Voltage range
- Electrode type and diameter

Figure 1.21 shows example of a welding data sheet where the above information are found.

WELDING DATA (SPIRAL, T-CROSS & W/R)

W.O. No. : _____ Ref. No.: _____ Rev. _____
 Specification : _____ Grade : _____ Date : _____
 Ref. WPS No.: SAW _____ SMAW : _____

Mill No. _____		Size: _____ in. O.D. x _____ mm W.T.	
Beam No. _____		Coil Width : _____ mm	

ITEM	SPIRAL		T-CROSS	
	INSIDE	OUTSIDE	INSIDE	OUTSIDE
Position	P mm	mm	X	mm
Tip Height	1P mm	mm	mm	mm
	2P mm	mm	mm	mm
Angle of Wire	1P deg.	deg.	deg.	deg.
	2P deg.	deg.	deg.	deg.
Distance	c mm	mm	mm	mm
	-	X	X	X

INSIDE

OUTSIDE

ITEM	SPIRAL WELDING		T-CROSS	
	INSIDE	OUTSIDE	INSIDE	OUTSIDE
	1P	2P	1P	2P
WIRE TYPE (Brand)				
WIRE DIAMETER (mm)				
FLUX				
AMPERE (A)				
VOLTAGE (V)				
WELDING SPEED (m/min)				
HEAT INPUT (KJ/cm)				
PRE-HEATING TEMP.(°C)				

ROOT FACE

a = mm

b = mm

c = mm

MACRO

a

b

c

d

e

dtl.	SPIRAL	T-CROSS
a	mm	mm
b	mm	mm
c	mm	mm
d	mm	mm
e	mm	mm

ITEM	SPIRAL WELDING			T-CROSS	
	INSIDE	OUTSIDE	INSIDE	OUTSIDE	
	1P	2P	1P	2P	
ELECTRODE BRAND					
ELECTRODE DIA. (mm)					
CURRENT (A)					
VOLTAGE (V)					
WELDING SPEED (mm/min)					
PRE-HEATING TEMP.(°C)					

W/R

ELECTRODE BRAND	
ELECTRODE DIA. (mm)	
CURRENT (A)	
VOLTAGE (V)	
WELDING SPEED (mm/min)	
PRE-HEATING TEMP.(°C)	

Remarks:

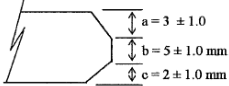
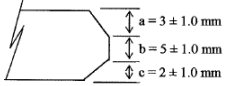
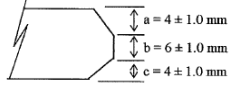
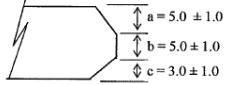
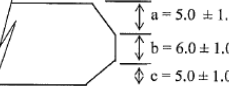
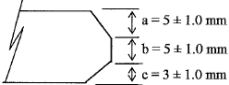
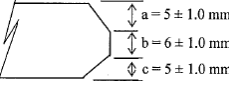
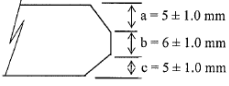
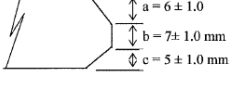
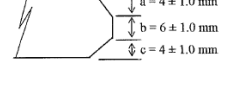
Spindle shim = mm

Cutter shim = mm

Figure 1.21: Example of welding data sheet for spiral welded pipe [NPC]

Table 1.2 shows examples of root face details for different pipe outside diameters, wall thicknesses and grades.

Table 1.2: Examples of root face details

No.	OD (Inch)	Thickness (mm)	Grade	Root Face Detail
1	20	9.53	B	
2	24	9.53	X65	
3	28	14.22	X65	
4	32	12.70	X60	
5	36	15.88	B	
6	40	12.70	X60	
7	46	15.88	X60	
8	48	15.88	X60	
9	56	16.26	X70	
10	60	13.99	X70	

The pipe fabrication process including mechanical forming and welding are the most common sources for residual stresses. Residual stresses in welds are due mainly to thermal contractions and phase transformations induced by the welding process. In submerged arc welding, the magnitude of residual stress acting in the seam weld is a function of the wall thickness, sequence and number of passes, heating and cooling rates and other variables. The following section will describe briefly the effect of the residual stresses in the pipe integrity.

1.5 OVERVIEW OF RESIDUAL STRESSES

Residual stress is defined as “the stress resident inside a component or structure after all applied forces have been removed”. SI unit for stress is the Mega Pascal (MPa). US Customary unit for stress is kilo pound-force per square inch (ksi).

$$6.895 \text{ MPa} = 1 \text{ ksi}$$

Residual stresses are generated, upon equilibrium of material, after plastic deformation that is caused by applied mechanical loads, thermal loads or phase changes. Mechanical and thermal processes applied to a component during service may also alter its residual stress state. Like other processes involving heating and cooling such as for instance preheating and flame bending, welding produces thermal strains and stresses. Residual stresses are generated by the welding process, due to the local heating and

cooling of the material. This causes the material to expand and shrink locally, while the rest of the material is restraining this expansion and shrinkage. In the simple example in Figure 1.22 the generation of residual stresses is shown, where the weld is replaced by a bar and the surrounding material by a spring.

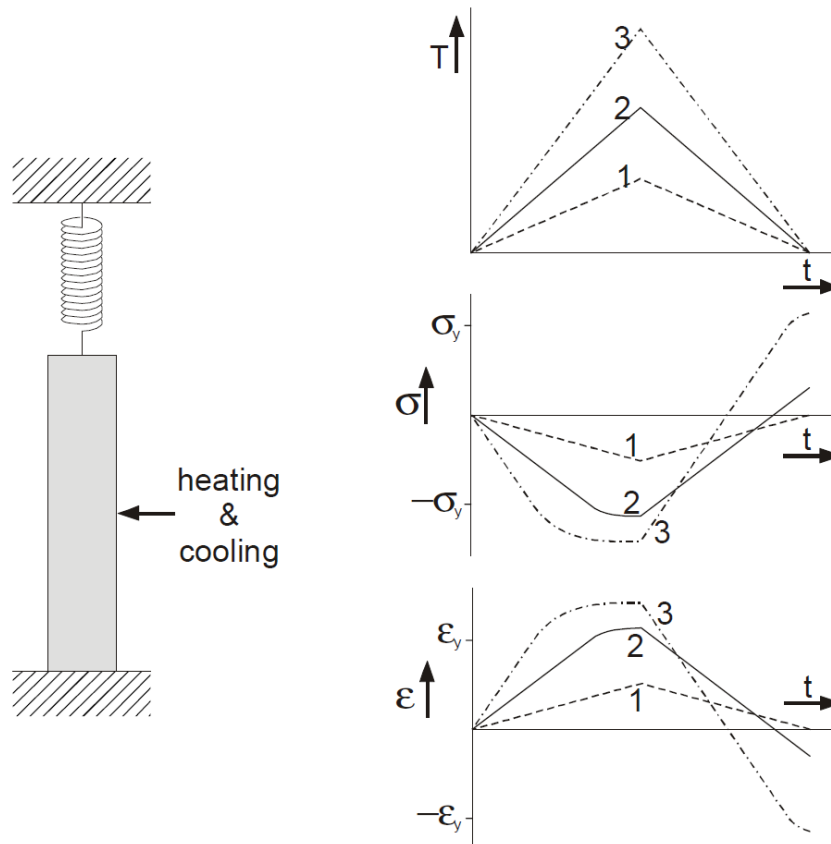


Figure 1.22: Generation of residual stresses by heating and cooling of the material [Horn 2002]

Three situations are shown with their corresponding temperature (T), stress (σ) and strain (ϵ) histories. The strains shown for the strain histories are the combination of the thermal strain due to the expansion and the mechanical strain due to the generated stresses. For curve 1 of Figure 1.22, the material is heated to a temperature where the

stresses generated by the thermal expansion of the material do not reach the yield stress (σ_y). Upon subsequent cooling to the starting temperature, the stresses return to zero and the bar will have the same length as before without the presence of residual stresses. The maximum temperature reached for curve 2 is higher than for curve 1. This causes higher stresses due to the thermal expansion than for curve 1. In fact, the stresses generated for curve 2 are higher than the yield strength of the material, which results in plastic deformation of the material in the heating stage. The result is that the bar will be shorter than if the material had remained elastic. Upon subsequent cooling of the material to the starting temperature, the shrinkage will be so large that the final length of the bar will be smaller than its original length; this will then cause residual tensile stresses in the bar. For curve 3, the maximum temperature is even higher than for curve 2. Similar to curve 2, curve 3 will show plastic deformation in the heating stage. However, with the higher maximum temperature, more shrinkage will occur in the cooling stage for curve 3. In fact, so much shrinkage occurs that the generated residual tensile stress exceeds the yield strength and further plastic deformation occurs.

To illustrate physically how residual stresses are formed during welding, a simple case of a bead fillet on a plate will be described. Figure 1.23 shows schematically the changes in temperature and stresses during the welding process.

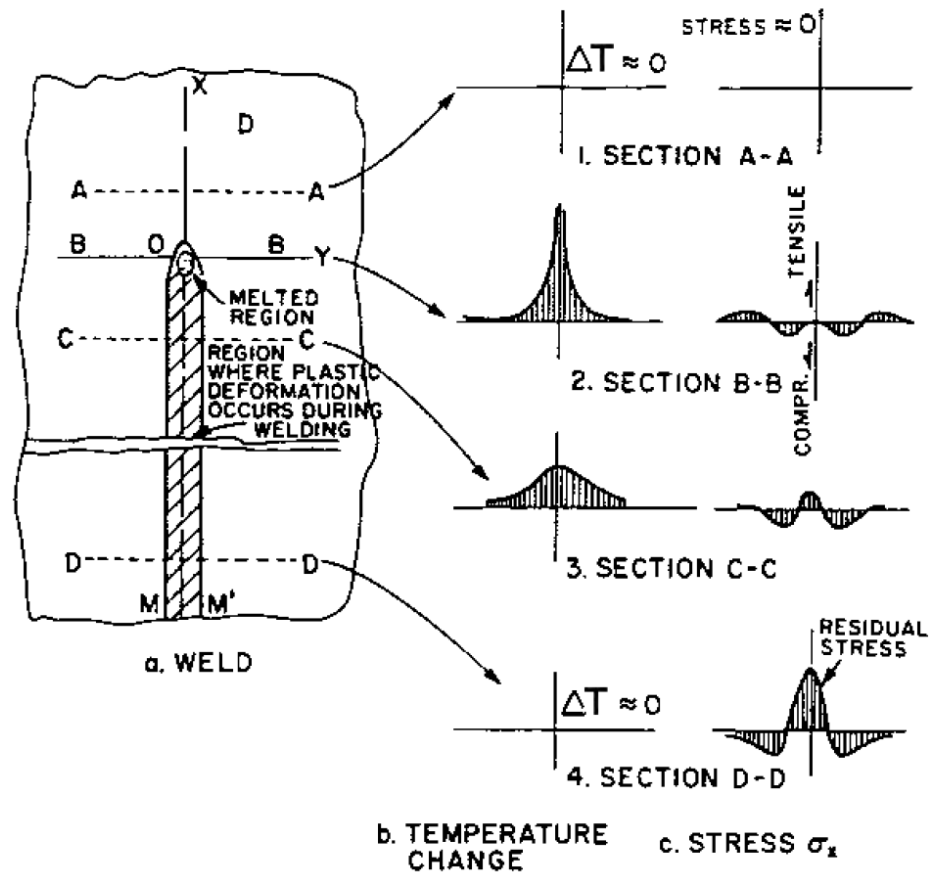


Figure 1.23: Schematic representation of changes in temperature ΔT and stresses during welding [Weisman 1976]

The welding arc, which is moving at a speed v , is located at the origin O as shown in Figure 1.23(a). Figure 1.23(b) shows the temperature distributions at several cross-sections.

- Along section A-A, which is ahead of the welding arc, the temperature change due to the welding ΔT is almost zero.

- Along section B-B, which crosses the welding arc, the temperature change is extremely rapid and the distribution is very uneven.
- Along section C-C, which is some distance behind the welding arc, the temperature change becomes more even, and finally,
- At section D-D, which is very far from the welding arc, the temperature change due to welding has vanished.

Figure 1.23(c) shows the distribution of longitudinal stresses, σ_x , along these sections. Normal stresses in the y-direction, σ_y , and shearing stresses, τ_{xy} , also exist, but are usually much smaller than σ_x .

- In front of the welding, section A-A, the thermal stresses due to welding are almost zero.
- Because molten metal does not support a load, stresses underneath the welding arc, section B-B, are close to zero. Stresses in regions at a short distance from the arc are compressive, because the expansion of these areas is restrained by surrounding metal where the temperature is lower. The temperature in these areas is high and the yield strength of material is hence low, and the stresses are as high as the yield strength of the material at the corresponding temperature. The magnitude of compressive stresses passes through a maximum with increasing distance from the weld or with decreasing temperature. However, stresses in areas

away from the weld are tensile to balance with the compressive stresses in areas near the weld.

- In section C-C, when the weld metal and base metal regions near the weld have cooled, the result is in tensile stresses in regions near the weld and compressive stresses at greater distances.
- Section D-D represents a finally cooled-down region, where high-tensile stresses are present in regions near the weld.
- The hatched area, M-M', in Figure 1.23(a) shows the region where plastic deformation occurs during the welding.
- The egg-shaped region near the origin O indicates the region where the metal is melted. The metal outside the hatched area remains elastic during the entire welding cycle.

Since the temperatures are highest in the region near the welding torch, this region expands more than regions further away. During the heating, the stresses in the region near the weld are compressive plastically because the thermal expansion in this region is restrained by surrounding metal with lower temperature and higher yield stress. When the welding has been completed and the work-piece starts to cool, it deforms in the opposite direction. If the material was completely elastic during the entire period of the heating and cooling cycle, the work-piece would return to its initial shape with no residual distortion.

The generated residual stresses are usually very high, sometimes approaching the material yield strength, but their effects are not evident until the structure is fully loaded or exposed to service environment. Tensile surface residual stresses are detrimental as they increase the susceptibility of the component to fatigue damage, stress corrosion and even fracture. Stresses in a welded plate can be divided in two directions; transverse and longitudinal to the weld. Longitudinal residual stresses can arise from different causes, the most common of which is the longitudinal contraction of the weld as it cools down. Transverse residual stresses are generated by the transverse contraction of the weld during the cooling phase. It can also be generated indirectly due to the longitudinal contraction. Longitudinal stress is normally referred to the stress that is parallel to the weld bead while the transverse stress is referred to the stress that is perpendicular to the weld bead (Figure 1.24).

For pipes (Figure 1.25), the stress in axial direction (longitudinal/parallel to weld line) at a point in the pipe wall can be expressed as σ_a while the stress in circumferential direction (perpendicular/transverse to the weld line) at a point in the pipe wall is known as the hoop stress (σ_c). The stress in tangential direction at a point in the pipe wall can be denoted by σ_r .

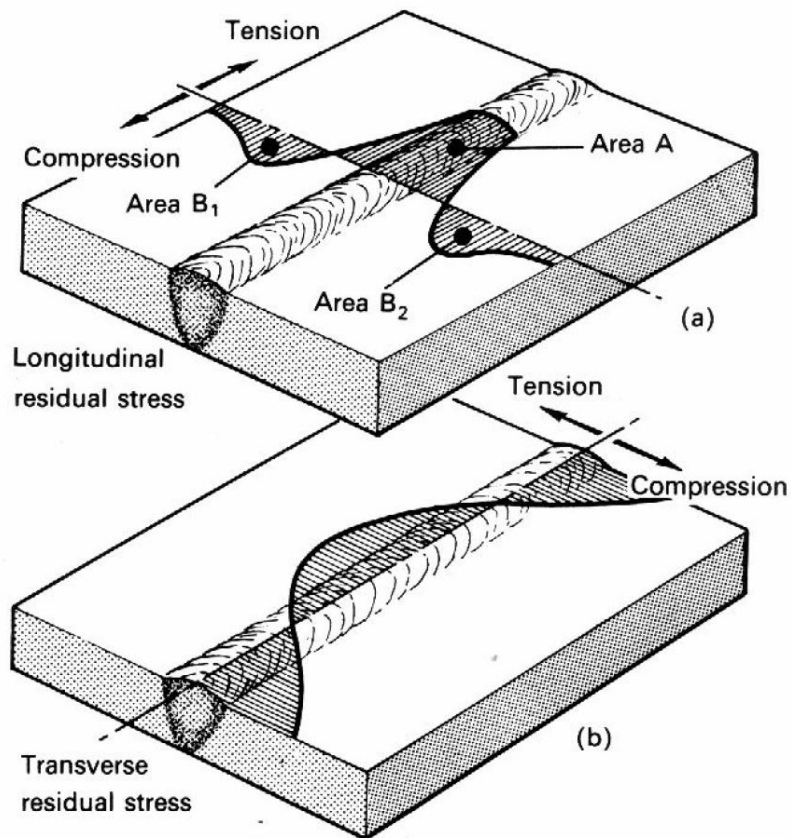


Figure 1.24: Representation of parallel (longitudinal) and perpendicular (Transverse) measured residual stress

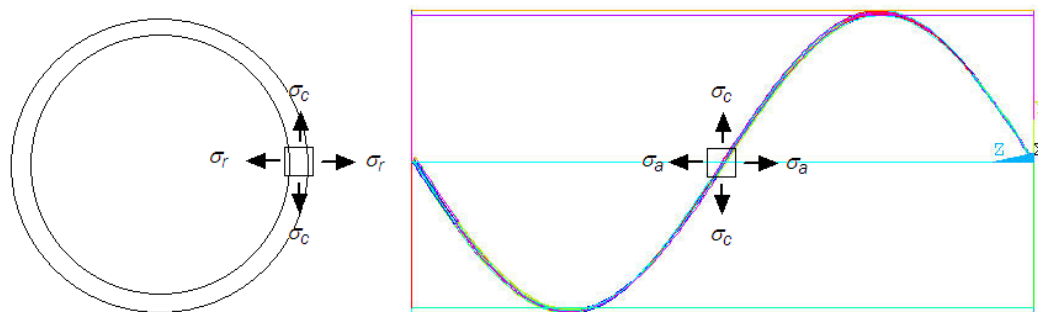


Figure 1.25: Representation of different stresses on a pipe

Residual stresses and welding distortion are two faces of the same problem, namely the thermally induced plasticity. Prediction and control of residual stresses and distortions are crucial in manufacture of welded structures. The residual stresses also affect the fatigue, buckling and yielding strength. The shape of the welding residual stress field depends on several factors like the structural restraint, the wall thickness over diameter ratio for pipes, the heat input, the number of weld passes and weld pass sequence. Hence, the through-the-thickness variation of the residual stress components may be very complex. It becomes fundamentally important to understand the behavior of welding residual stresses to assure the integrity of industrial pipes. Consequently, the residual stress for spiral welded pipe will be discussed in the next section with more details.

1.6 SPIRAL WELDED PIPE RESIDUAL STRESSES

Pipelines are normally designed for service pressures which develop a hoop stress of 72% of the yield strength of the base materials. The safety factor, i.e. the difference between the developed hoop stress and yield strength, is dependent upon the location of the pipeline. The actual stress seen by the pipe can be higher than the applied hoop stress as generally no account is made of the residual stresses or constructional stresses, these stresses can be additive and result in stresses of the order of yield point.

Fabrication-induced residual stresses have received increasing attention in gas, oil and petrochemical industry. The driving force for this interest can be attributed to the fact that application of modern structural integrity assessment procedures for defective welded components, such as API RP-579, requires more accurate information on the weld residual stress state to give a more realistic assessment. Residual stress distribution and distortion in a welded pipe are strongly affected by many parameters and by their interaction. In particular, there are structural, material and welding factors. The structural parameters include geometry of the pipe, wall thickness and welding joint type.

During the production of oil and gas line pipe, the plate should go through bending, forming, welding, etc. These mechanisms interact to produce a complex three-dimensional residual stress field. For spiral welded pipe, there are more factors influencing the forming process (forming angle, power of sending, the intervals among three roller, relative altitudes of three rollers, distribution of inside or outside rollers, etc.). In addition the spiral welded pipes have no cold expansion process after welding just like longitudinal welding pipe, this also makes it have complicated, various, distributed irregularly residual stress, relatively high peak value, and vary greatly among pipe mills.

Having higher internal residual stress is one of the main reasons that restrain spiral welded pipe's application. The residual tensile stress would become the driving force of crack propagation with operation pressure together. On the other hand, the unbalanced

residual stress makes some location of weld pipe have relatively high residual stress. This probably may lead to stress corrosion cracking or corrosion fatigue fracture to pipeline in the case of having corrosive medium. This is also one of reasons why people think the spiral welded pipe have a lower reliability than seam pipe. In the meanwhile, people propose more and stricter requirements to the residual stress of spiral welded pipe in order to assure the safety and reliability of pipeline.

Figure 1.26 shows the stresses in spiral and longitudinal welded pipes. There is a relation between the weld seam angles, relative to the pipe axis, and the residual stresses in spiral welded pipes. In longitudinal welded pipe, the seam is subjected to the maximum applied hoop stress; in spiral welded pipe, the stress is some fraction therefore, depending on angle of the weld with the longitudinal axis.

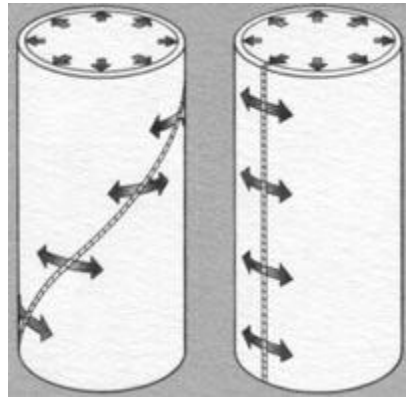


Figure 1.26: Spiral and longitudinal welded pipes stresses

As the circumferential stress σ_u is the maximum stress that occurs in a pipeline, the longitudinal weld that is located perpendicular to direction of stress is subjected to the maximum load. The more the seam angle deviates from the direction of the pipe axis, the

more the 'normal stress' σ_N acting perpendicular to the weld seam decreases when neglecting the longitudinal stress. This relationship is given by the following equation:

$$\sigma_N = \sigma_U \cos^2 n \quad (1.5)$$

Considering the longitudinal stresses that actually occur in practice, the ratio of normal stress and circumferential stress, σ_N / σ_U , as a function of the weld angle is shown in Figure 1.27 for three cases of loading, $\sigma_L / \sigma_U = 0, 0.3$ and 0.5 .

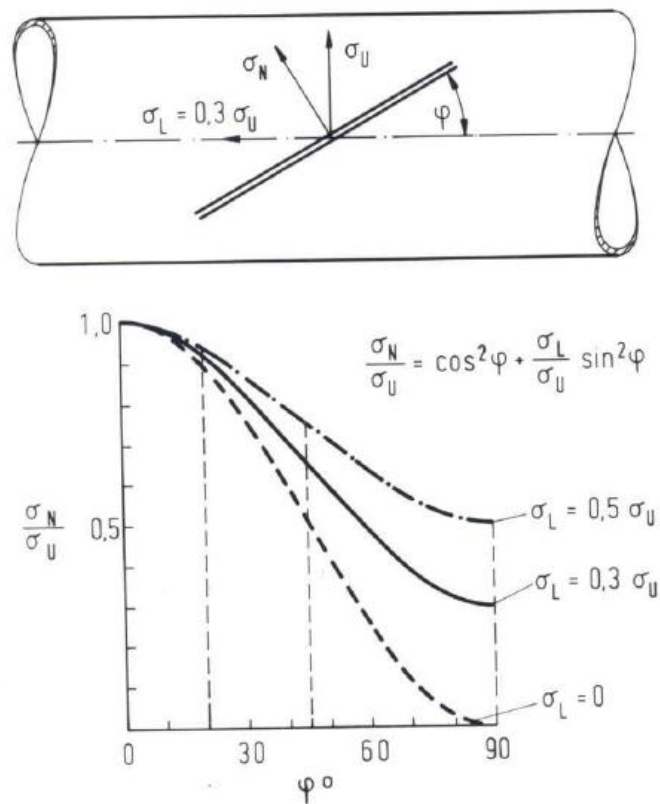


Figure 1.27: Stress dependence of the weld angle [Franz and Sommer 2004]

It was shown that all three typical cases of loading, longitudinal weld seams are subjected to the highest loads, and circumferential seams to the lowest loads. The spiral weld is situated in between, and the load it has to withstand is between 50 and 75 % of the load that is acting upon a longitudinal weld.

The residual stress fields in spiral welded pipe may also cause due to the production technology, for instance hot or cold rolling, the coiling, the coil cooling and the cold deformation during uncoiling or flattening. The thermal residual stress fields are due to uneven strip cooling during the rolling when the sides of the sheet are colder than the middle as shown in Figure 1.28.

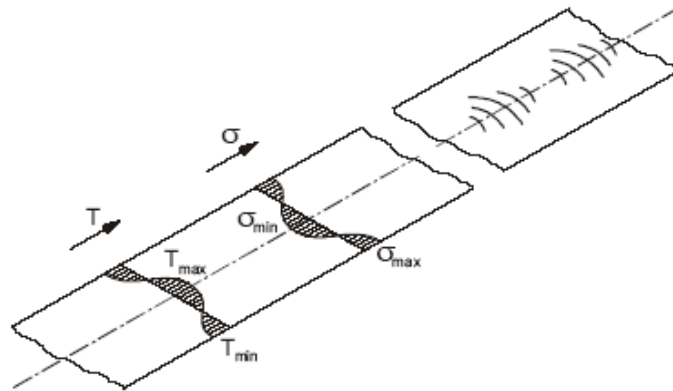


Figure 1.28: Influence of the colder side in the sheet deformation [Hidveghy et al. 2003]

Uncoiling produces residual stress: tension in the upper surface and compression in the lower surface as shown in Figure 1.29.

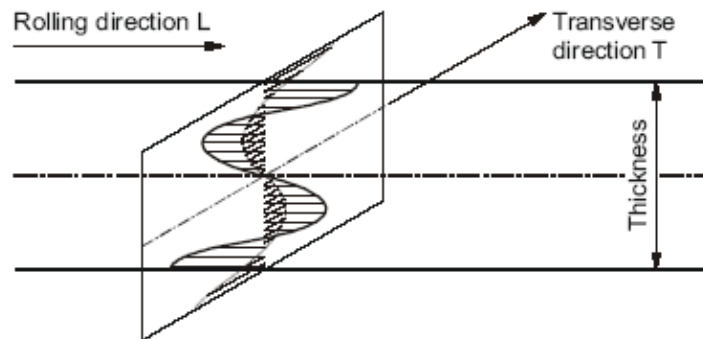


Figure 1.29: Residual stresses distribution across the thickness in rolling direction L and transverse direction T [Hidveghy et al. 2003]

Residual stresses can be characterized by the scale at which they exist within a material. So, there are two types of residual stresses are found in the spiral welded pipe. These stresses are macroscopic stresses and microscopic stresses. Macroscopic stresses, or macro-stresses, which extend over large distances relative to the grain size of the material, are the stresses of general interest in design and failure analysis. Macro-stresses are tensor quantities, and are determined for a given location and direction by measuring the strain in that direction at a single point. Macro-stresses produce uniform distortion of many crystals simultaneously, shifting the angular position of the diffraction peak selected for residual stress measurement.

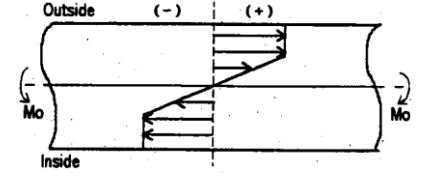
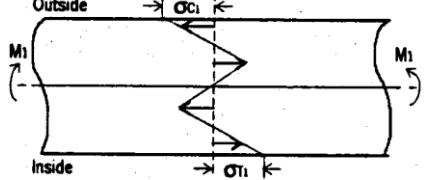
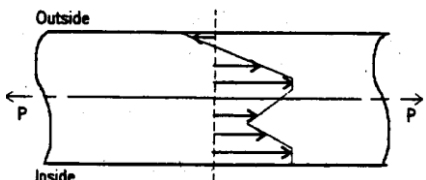
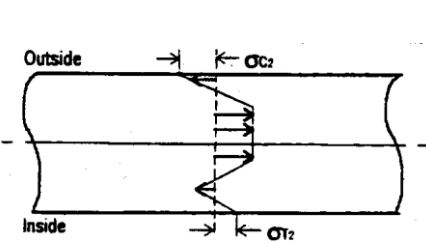
Microscopic stresses, or micro-stresses, are treated as scalar properties of the material, related to the degree of cold working or hardness, and result from imperfections in the crystal lattice. Micro-stresses arise from variations in strain between the "crystallites" bounded by dislocation tangles within the grains, acting over distances less

than the dimensions of the crystals. Micro-stresses vary from point to point within the crystals, producing a range of lattice spacing and broadening of the diffraction peak. Interaction of the macroscopic and microscopic stresses orients the plastic strains such that deformation occurs beyond the volume change resulting in transformation plasticity. The total stress experienced by the material at a given location within a component is equal to the residual stress plus the applied stress.

$$\text{TOTAL STRESS} = \text{RESIDUAL STRESS} + \text{APPLIED STRESS} \quad (1.6)$$

Table 1.3 shows the graphical explanation of the residual stress behavior for the spiral welded pipes. Figure 1.30 summarizes the controlling points for manufacturing of sour service line pipe materials. As can be seen, the residual stress on spiral welded pipes can be controlled during the pipe making by heat treatment, cold expansion and hydrotesting.

Table 1.3: Graphical explanation of residual stress behavior

Process	Residual Stress Distribution	Explanation
During Pipe Forming		Residual Stress is generated with 3-roll bender during pipe forming
After Welding Guided by inner Supports		In pipe mill, inner support is adapted in which the formed pipe is guided from inside applying the force to open the pipe. At this point welding is done.
During Hydrotest		The pipe wall is yielded lower than 100% SMYS due to existence of residual stress as a result slight expansion is brought even at 90% SMYS.
After Hydrotest		<p>Due to plastic deformation, The residual stress tends to be released consequently similar opening of ΔC is observed:</p> <p>$\sigma_{T2} < \sigma_{T1}$</p> <p>$\sigma_{C2} < \sigma_{C1}$</p>

Note: M_o , $M1$ =Bending Moments, P =Tension due to Hydrotest, σ_T =Tension Residual Stress, σ_C =Compression Residual Stress

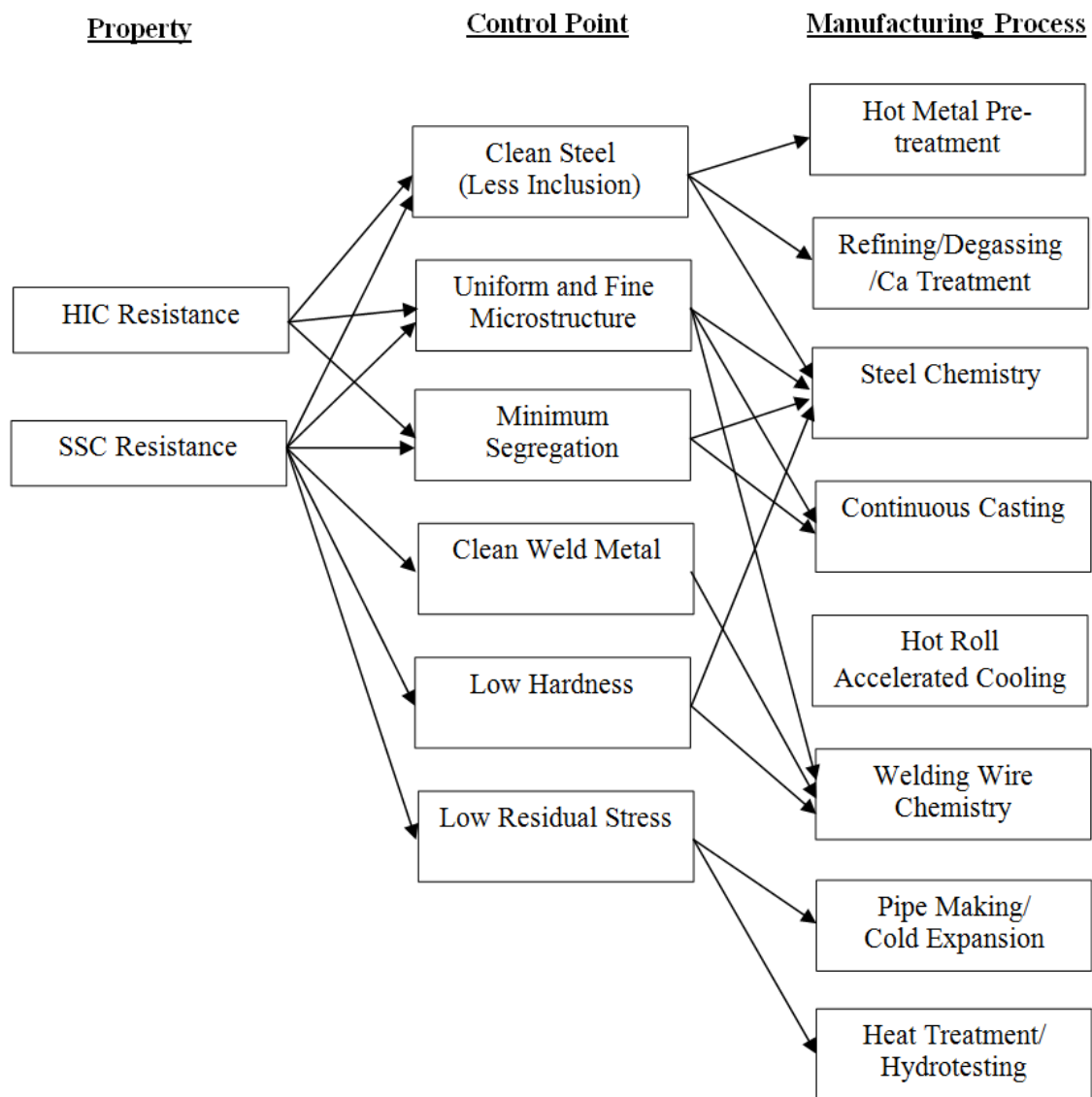


Figure 1.30: Requirements for line pipe and control points in manufacturing

1.7 RESIDUAL STRESSES MEASUREMENT TECHNIQUES

Quantifying the residual stresses present in a component, which may either accelerate or arrest fatigue or stress corrosion cracking, is frequently crucial to understanding the cause of failure. Because stress is not a measurable quantity, another quantity must be measured from which the stress can be calculated. The most commonly used quantity is strain. There are many methods to measure the residual stress in welded components. These test methods are as X-ray diffraction, drilling hole test, mechanical cutting stress releasing test, ring splitting test, and other destructive and non-destructive methods. X-ray method and drilling hole method give accurate measurement of the surface residual stress; on the other hand, they are unable to describe the distribution of the residual stress through the depth so it can not reflect the true residual stress condition of the pipe.

The identification of the residual stresses can be also carried out experimentally by means of destructive techniques known as Ring Splitting Test. The mechanical cutting stress releasing test data are stable, this test method has good stability, and it is a suitable method to analyze and study residual stress of welded pipe. But this measurement is complex and not feasible during actual production of spiral welded pipe. Usually, ring splitting test is adopted as the method of measuring residual stress by many pipe mills and the circumferential opening is regarded as the reference of residual stress.

Figure 1.31 shows the approximate depth ranges over which the various methods are able to resolve residual stress variations. The depth range shown for x-rays is for non-destructive measurements. Profiles up to 1 mm depth are commonly made with x-rays by electrochemically etching away material. The figure illustrates the need to consider two important factors when choosing a residual stress measurement method for a particular application: (1) the depth of residual stresses that was generated in manufacturing the part of interest, and (2) the depth to which residual stresses will contribute to the potential failure mechanism.

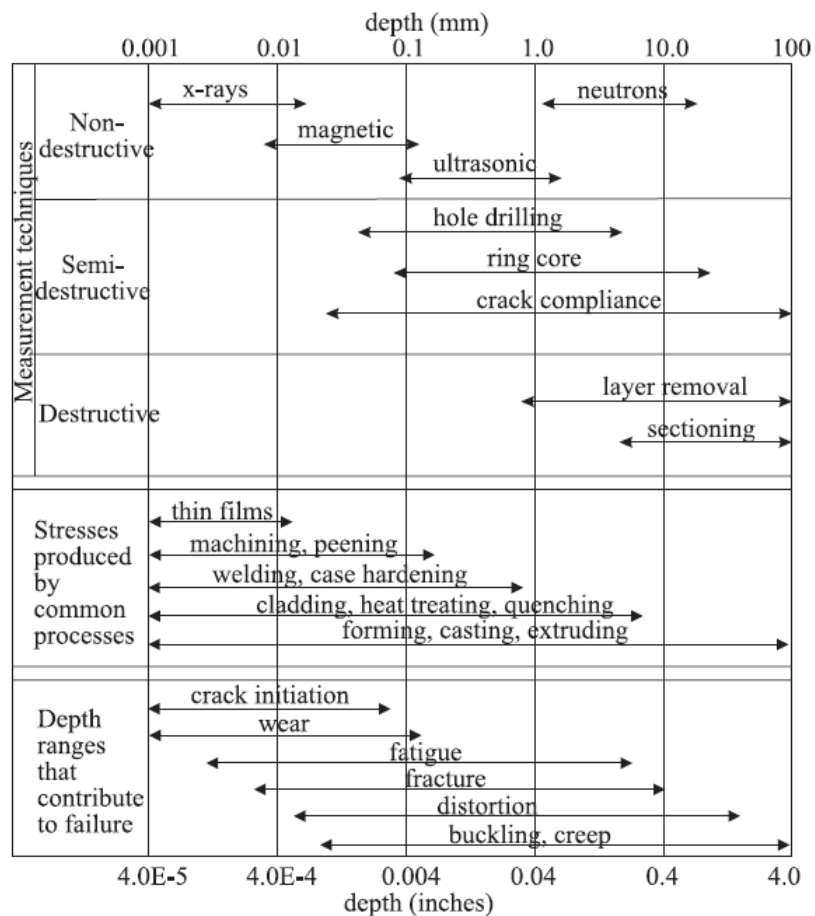


Figure 1.31: Depth ranges of measurement techniques compared with typically observed profiles and failure mechanisms [Prime 1999]

Numerical method is also an important method to determine the residual stresses. There are a large number of literatures on the application of FEM to determine residual stresses existing in piping components.

1.7.1 DRILLING HOLE METHOD

Drilling hole is the most widely used technique for residual stress measurement. The hole-drilling (Figure 1.32) is one of the stress-relaxing methods that analyze the stress-relaxation produced in a metal part when material is removed. By measuring the deformation caused by the relaxation, the values of the residual stress present in the part before the metal was removed can be determined by analyzing the successive state of equilibrium.



Figure 1.32: RS-200 mill guide used for drilling hole technique

The principle involves introduction of a small hole (of about 1.8 mm diameter and up to about 2.0 mm deep) at the location where residual stress is to be measured. Due to drilling of the hole the locked up residual stresses are relieved and the corresponding strains on the surface are measured using suitable strain gauges bonded around the hole on the surface. From the strains measured around the hole, the residual stresses are calculated using appropriate calibration constants derived for the particular type of strain gauge rosette used as well as the most suitable analysis procedure for the type of stresses expected. The procedure for residual stress measurement using hole drilling is described

in ASTM standards with designation E837 for uniform residual stress fields. Center hole drilling is limited to stresses less than nominally 60% of the yield strength.

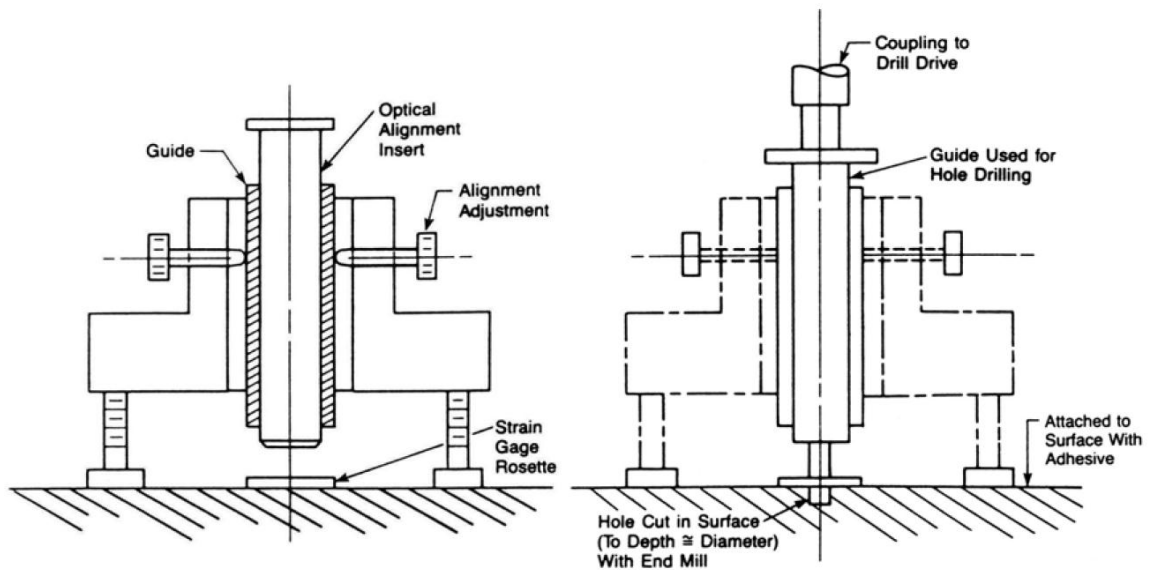


Figure 1.33: Setup of the blind drilling hole device [ASTM-E837 2008]

In most practical cases, the residual stresses are not uniform with depth. The incremental hole drilling method is an improvement on the basic hole drilling method, which involves carrying out the drilling in a series of small steps, which improves the versatility of the method and enables stress profiles and gradients to be measured. A high-speed pneumatic drill is used to drill the hole without introducing any further machining stresses and thereby modifying the existing stress system. The strain data at pre-determined depths are precisely acquired.

1.7.2 X-RAY DIFFRACTION METHOD

X-ray diffraction (XRD) can be used to measure residual stress using the distance between crystallographic planes, i.e., d-spacing, as a strain gauge (Figure 1.34). A change in stress results in a modification of the inter-planar spacings which alters the angular position of the diffraction peaks. When the material is in tension, the d-spacing increases and, when under compression the d-spacing decreases. Stresses can be determined from the measured d-spacings.

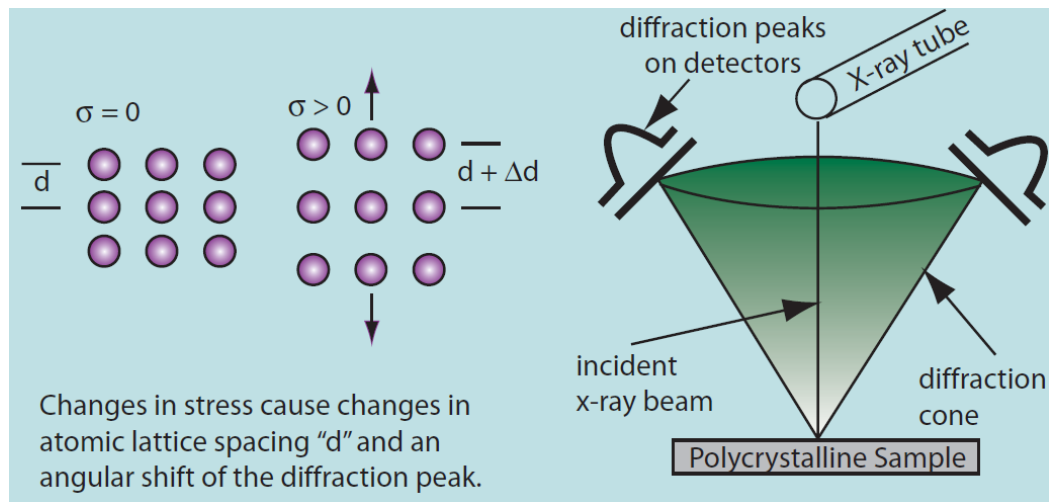


Figure 1.34: X-ray diffraction residual stress measurement [Proto Manufacturing]

This technique is non-destructive because no material destruction is needed to release the energy (stress / volume) stored in the material. XRD residual stress measurement is applicable to fine grained crystalline materials that produce a diffraction peak of suitable intensity, and free of interference in the high back-reflection region for any orientation of the sample surface.

1.7.3 RING SPLITTING TEST

One of the industry practices to measure the residual stress in spiral welded pipes is the use of Ring Splitting method. The principal of this mode of determination of residual stresses lies in their releasing inside the worked ring and in the measurement of induced strains. Details of this method are explained in chapter 3.

1.8 PIPE STRESS RELIEVING

1.8.1 COLD EXPANSION

For many years, cold expansion of pipe for work hardening, sizing and rounding has been utilized for long sections of large diameter pipe of the type formed with a longitudinally welded seam. Cold expansion often significantly reduces residual tension stresses. In the production of pipe, it is the weld seam which usually requires more attention by way of manufacturing steps and equipment to insure the production of reliable and quality products. When work hardening by cold expansion is utilized, provision must be made to insure that the integrity of the weld seam is not destroyed or compromised in any way.

It is difficult to mechanically expand pipe of the type having a spiral weld seam since there are no expander has a helical groove which corresponds to the helical weld

seam of the pipe. So, spiral welded pipes cold expanded are rarely available. Most of the spiral welded pipe manufacturers do not consider the cold expansion in the case of the helical pipe to stress-relieve the pipe after edge forming and welding process. Non cold expanded spiral welded pipe exhibits highly stressed regions close to the seam weld caused during the edge forming and welding processes. It is for this reason that residual stresses in spiral pipes continue to be a subject of considerable interest.

1.8.2 HEAT TREATMENT

Post-weld heat treatment is widely acceptable mean of stress control in structural steel components. Post-weld heat treatment is the uniform heating of a structure or portion of a structure to a sufficient temperature below the critical range to relieve the major portion of the residual stresses, followed by uniform cooling. Minimum residual stresses, which are beneficial for a better stress corrosion and fatigue resistance, were obtained through heat treatment.

Although residual stresses can be relieved by means of a proper heat-treatment, this is generally not practical for spiral welded pipes. However, post-weld heat treatment suffers from several disadvantages: the cost of treatment in terms of equipment and energy is high; the growth of oxide scale on the surface implies the need for a subsequent finishing process to remove the scale; in many metals, annealing relieves residual stresses at the cost of mechanical properties.

1.9 INDUSTRY EXPERIENCE WITH SPIRAL WELDED PIPE

Spiral-welded pipe is used extensively throughout the world for large-diameter, gas transmission pipelines. As the industry needs for gas production increase, the operating demands on spiral-welded pipe also increase. These demands include larger diameters, higher operating pressures and increased mechanical strength. Although the process for forming spiral welded pipe has been used for nearly 100 years, little work has been done to predict the residual stresses in spiral welded pipes accurately. A disadvantage of the spiral weld pipe is its longer weld line in comparison with the longitudinal welded pipe. It is known that cracks and defects are more likely to exist in the welding area. Therefore, the possibility of finding cracks in the spiral weld pipes is more than the longitudinal weld pipes. The cracks in the spiral weld pipes are generally subjected to mixed mode loading.

After welding, the spiral welded joint contains residual stresses which, together with service loading (especially alternating loading) in the conditions of corrosive media greatly increase the extent of local corrosion of the zones of the welded joint. So, the high residual stresses exist in spiral welded pipe can contribute to the Stress Corrosion Cracking (SCC) process by creating dis-homogeneity in the mechanical properties of the material. Residual stresses can act as sites for crack initiation, either under the effect of a superimposed stress or in combination with environmental factors. The initiation and growth of SCC requires an environment conducive to crack formation (environmental

factor); a tensile stress (stress factor such as applied or inherent residual stresses); and a material susceptible to SCC in a particular cracking environment (pipe factor). If one of the above components is missing or varies over time, the opportunity for initiation and propagation can be minimized or maximized. Moreover, Stress Oriented Hydrogen induced Cracking “SOHIC” is also one of the industry failures found in spiral welded pipe in situations where the hydrogen activity is very high and where some sort of localized straining occurs due to local softening and or high residual stresses from plate forming or welding processes.

1.10 PROBLEM STATEMENT

Within the welding procedures of Spiral Welded Pipe manufacturing, there are many factors such as welding process parameters, pre-heat and post-heat patterns, level of constraint and joint details that contribute to the pipe residual stresses. Knowing which parameters have an effect on the quality of the Spiral Welded Pipe and which parameters give the most significant effect on the weld quality are the main issues in welding industry. The benefit of wider adoption of spiral welded pipe for oil and gas services will result in reduced capital expenditure for pipeline development and replacement. The results of this work may serve as the basis for the future research to optimize the spiral welded pipe manufacturing processes and minimize the residual stresses at the products. The motivation for this industrial M.S. project is the need for a better understanding of a very important problem in spiral welded pipe industry which is the induced welding residual stresses.

1.11 OBJECTIVES OF THE THESIS

The main objective of this thesis work is to develop an appropriate finite element model of ring splitting technique that can be used to predict the residual stresses due to welding in spiral welded pipe. In addition, validation experiments were conducted whereby Finite Element Analysis “FEA” simulation outputs were compared to the experimentally measured data. Moreover, the effect of welding speed on the level of the residual stresses was studied. Furthermore, finite element method (FEM) is used to predict the temperature and stress fields in a laser spirally welded tube with 1.6 mm wall

thickness and 75 mm diameter. Finally, statistical analysis and linear-regression modeling were used to study the effect of several structural, material and welding parameters on ring splitting test opening for spiral welded pipes.

CHAPTER 2

LITERATURES REVIEW

2.1 PRODUCTION OF PIPES

Avagianos and Papamantellos [2002] introduced the principals of the spiral manufacturing technology from coil by the two-step-method and they outlined the innovations of Corinth Pipework's production facility in detail, including the sophisticated NDT techniques and the Quality Management System. Permyakov et al. [2006] showed that controlled rolling of plates and coils or heat treatment of the product need to be applied in order to obtain a higher strength in line pipes of diameter up to 1420 mm. They showed also that the metallurgical design based on purification, low carbon content, micro-alloying and controlled rolling has increased yield stress. They also studied the effect of quench and tempering in maximizing the homogeneity of the structure for both the base metal and the weld joint and minimizing residual stresses, which is beneficial for a better stress corrosion and fatigue resistance. Franz and Baldur [2004] described in details the modern technology of HTS (Helical Seam Two Step) manufacturing process they explained the qualitative and economical advantages over the conventional process.

2.2 WELD MODELING

The research activity in welding simulation started decades ago. Understanding of the theory of heat flow is essential in order to study the welding process analytically, numerically or experimentally. Considerable interest in the thermal aspects of welding was expressed by many researchers such as Goldak et al. [1984, 1986] and Nguyen et al. [1999]. The most critical input data required for welding thermal analysis are the parameters necessary to describe the heat input to the weldment from the arc. Goldak et al. [1984, 1986] derived a mathematical model for welding heat sources based on a Gaussian distribution of power density. They proposed a doubled ellipsoidal distribution in order to capture the size and shape of the heat source of shallow and deeper penetrations. Goldak et al. [1984] presented an overview of the aims and methods of computational weld mechanics. They described the numerical methods, algorithms, software and computer hardware needed for computing the temperature, displacement, strain and stress fields associated with the welding process. They discussed in some detail the modeling heat sources, non-linear thermal properties, the heats of fusion and transformation, and work piece geometry and boundary conditions. Sunar et al. [2006] computed the temperature and stress fields during the heating process of a cantilever assembly. A control volume approach is introduced for the numerical solution of heat transfer equations while the finite element method is adopted for stress field predictions. It was found that the temperature distribution in the transverse direction does not vary considerably, but varies significantly in the longitudinal direction. They found that

maximum magnitude of the von Mises stress is less than the yield strength of the substrate material. Zhang et al. [2004] investigate the heat transfer and free surface flow during gas metal arc fillet welding of mild steel. Dimensional analysis was used to understand the importance of heat transfer by conduction and convection and the role of various driving forces on convection in the liquid weld pool. The effect of welding parameters on important weld bead characteristics was quantitatively studied using the numerical model. They found that the results indicate a significant promise for understanding and control of gas metal arc fillet welding processes based on fundamental principles of transport phenomena.

Poorhaydari et al. [2005] presented an innovative method for estimating the actual cooling rate in a welded section. The model can be used to predict the peak temperature profile across the HAZ. Kubel and Edward [1986] provides an overview on the modeling of arc and other welding systems with scientific principles from many disciplines including physics, chemistry, mechanics, electronics, and materials. Taylor et al. [1999] presented a computational modeling of welding phenomena within a versatile numerical framework. Wu and Sun [2002] developed a numerical model to compute the temperature field and history in double-sided arc weldment. They use this model to compute the temperature distributions and profiles at different cross-sections and along different lines of interest and then they compared their results with the results in regular plasma arc welding. They found that DSAW process has advantages in obtaining deep narrow penetration with low the thermal distortion and residual stress.

2.3 HEAT SOURCE MODELING

Over the past few years, finite element methods have been used extensively in an attempt to predict distortion and residual stresses due to welding operations. Generally, the finite element method has already been proven to be a successful tool to simulate the complex welding process. Dittmer et al. [2006] employed a genetic algorithm to iteratively re-mesh 3-D surfaces and tend toward an optimal mesh based on the quality metric. The optimization approach was implemented on two components. Results indicate that this approach is effective in generating high-quality meshes without altering the mesher itself, developing new meshing algorithms or post-processing meshes to improve element quality. Fassani and Trevisan [2003] did a comparison between thermal cycles obtained from analytical models regarding point (concentrated) and Gaussian (distributed) heat sources. They found that the comparison shows that the thermal cycles obtained from the distributed heat source model are more reliable than those obtained from the concentrated heat source model. Yeung and Thornton [1999] developed a parametric model to predict the transient thermal behavior of a typical spot welding electrode cap. The analysis indicated that convective and radiant heat losses were not important. A simple linear relationship between the maximum temperature and the input power was found.

Gery et al. [2005] presented a moving heat source model based on Goldak's double-ellipsoid heat flux distribution. They predicted the transient temperature distributions and temperature variations of the welded plates during welding. They also

investigated the effects of the heat source distribution, energy input and welding speed on temperature changes. Okada et al. [1988] proposed the details of the frame heat source model formed by line heat segments which correspond to heat transfers due to the plasma stream and molten metal flow using a personal computer system designed. They also developed a system to predict hardness and micro-structural constituents in the heat affected zone and to determine optimum welding conditions. Nguyen et al. [1999] derived the analytical solution for a double-ellipsoidal power density moving heat source in a semi-infinite body with conduction-only consideration. Malik et al. [2007] described a combination of numerical simulation and experimental validation to study the temperature distribution and prediction of fusion zone (FZ) and heat affected zone (HAZ) in gas tungsten arc welding of low carbon steel. Tsai and Eagar [1984] presented weld width, penetration, and cross-sectional area as a function of heat input and arc heat distribution parameter in dimensionless forms. The theory was based on a closed form solution to a travelling gaussian heat source. The results indicate both welding process parameters (current, arc length, travel speed) and material parameters have significant effects on weld pool shape.

2.4 WELDING RESIDUAL STRESSES

Most of the welding research in the past was conducted to investigate the distribution of residual stress and distortion of welded metal. Not only the welding residual stress and distortion have been studied by welding researchers, but the effects of

welding parameter, welding sequence, welding joint geometry, and root opening has also been investigated by several researchers in the past. Withers and Bhadeshia [2001] summarized the effect of residual stresses on fatigue lifetimes and structural integrity, followed by the definition and measurement of residual stresses. Different types of stress are characterized according to the characteristic length scale over which they self-equilibrate. They also assessed the capability of a range of techniques. Moreover, they examined the different nature and origins of residual stress for various classes of material.

2.5 EXPERIMENTAL MEASUREMENTS OF RESIDUAL STRESSES

Tanala et al. [1995] conducted ultrasonic velocity measurements to determine residual stresses induced by welding processes. The results of surface residual stress distribution are compared with those obtained with an X-ray diffraction technique.

Macura and Fiala [2002] measured of the residual stresses after spiral welding, pressure testing and annealing. The measurements were performed by means of the hole-drilling strain gage method. Paul [1996] presented a theoretical development of x-ray diffraction residual stress measurement is emphasizing practical engineering applications of the plane-stress model, which requires no external standard. He briefly described the determination of the full stress tensor. He also compared alternate mechanical, magnetic, and ultrasonic methods of residual stress measurements. He also described sources of error arising in practical applications. Barsoum [2007] carried out a three-dimensional

welding simulation in the FE software ANSYS in order to predict transient temperatures and the residual stresses in a three-pass welded tubular joint structure Silva and Farias [2008] presented experimental results on the profile of residual stresses in manually welded butt joints. They carried out the residual stress measurements on the external surface with a mini-diffractometer X-ray. The results show that significant variations can occur in the welding residual stress behavior even under similar welding conditions.

2.6 FEM RESIDUAL STRESSES MEASUREMENTS

Dong et al. [2006] used an advanced computational simulation procedure to simulate the detailed forming and welding interactions and their combined effects on thermal and residual stress development for spiral welded pipe. Their results show steep through-wall gradients in the hoop and axial components, with levels for some components well above the yield stress. Cold expansion is shown to be beneficial in terms of relief of the hoop component, but potentially detrimental for the longitudinal weld component. The utility of split-ring testing is evaluated analytically, and compared to typical results for expanded line pipe. Qureshi et al. [2009] conducted parametric studies where they employed three-dimensional FE models to study the effects of a critical geometric, that is, tack weld on the corresponding residual stress fields in circumferentially welded thin-walled cylinders. Dhingra and Murphy [2005] presented a sequentially coupled thermal stress analysis approach for modeling temperature and distortion profiles resulting from welding thin-walled structures. The heat source is

modeled as a three dimensional (3-D) double ellipsoid, and 3-D finite element (FE) models are employed for predicting ensuing distortions. Jiang et al. [2005] developed a full three-dimensional (3D) thermo-mechanical finite element (FE) model to simulate the step-by-step multipass welding process. Stamenković and Vasović [2009] studied the manual metal arc welding of carbon steel plates. They performed finite element analysis of residual stresses in butt welding of two similar plates with the ANSYS software. The welding simulation was considered as a sequential coupled thermo-mechanical analysis and the element birth and death technique was employed for the simulation of filler metal deposition. The residual stress distribution and magnitude in the axial direction was obtained. A good agreement between the computation and experimental results was obtained.

Abid and Siddique [2005] presented a 3-D finite element simulation of a pipe-flange joint to describe the numerical procedure for modeling of tack welds in circumferential joints. Sequentially coupled nonlinear transient thermo-mechanical analysis is performed to simulate Metal Inert Gas (MIG) welding. Lu and Hassan [2001] presented a finite element scheme for simulation of welding residual stresses. They performed detailed thermal and residual stress analyses for butt-welded and socket-welded pipes using ANSYS and ABAQUS. The calculated distribution of axial stress and hoop stress at welded joint are validated against experimental results. They studied the relaxation of residual stress under high amplitude cyclic loading. Cho et al. [2004] determined the residual stress distribution after welding and after a post weld heat

treatment by a finite element transient heat flow analysis in conjunction with a coupled thermal–mechanical analysis. They found that the maximum residual stress of 316 MPa was found in the 56mm plate, but was reduced to 39 MPa after the post weld heat treatment. A. Yaghi et al. [2006] discussed the residual stresses in welded components they presented a brief review of weld simulation is. They explained the general methodology of the FE analysis methods used for welded sections of steel pipes. They plotted the residual axial and hoop stresses for the considered range of pipe diameters for the two simulated pipe wall thicknesses and they discussed the differences.

2.7 PROBABILISTIC ANALYSIS AND REGRESSION MODEL

Walton [2002] provides a low-cost, easy method of determining if residual stresses are the cause of component distortion during manufacture. He developed a mathematical derivation for simple cases based on the saw-cut methods which include the calculation of circumferential residual stresses for thick tube. Conway and Nickola [1965] did a theoretical analysis of the stresses induced in thin elastic strips which are bent into arcs with substantially constant radii of curvatures. Qingren et al. [2002] analyzed the problems related to the measurement and control of residual stress in the production of spiral welded pipes pipe. Yang et al. [1993] have used linear-regression equations for computing the weld features (melting rates, total fusion area, penetration, deposit area, bead height and bead width) from SAW process variables (electrode extensions range, welding voltage, welding current, welding speed and electrode

diameter) using both positive and negative electrode polarity. They managed to develop regression equations for each weld feature in both polarity conditions. Their results indicated that the linear-regression equations were equally useful for computing the various features of the SAW process. The effect of process parameters (welding current, travel speed, gap width, bead height and arc deflection current) on the bead shape in a narrow gap-GTAW process with magnetic arc oscillation was studied by Starling et al. [1995]. Statistical experimental design and linear-regression modeling were used in this investigation to develop the model. Kim et al. [2003] have studied the interrelationship between robotic CO₂ arc welding parameters and bead penetration by developing mathematical models using factorial techniques to predict the desired bead penetration. Partial-penetration and single-pass welds were fabricated in 12 mm SS400 plates based on controlling four different process parameters (arc voltage, welding current, welding speed and welding angle). They found that all the investigated parameters affect the bead penetration. They suggested extending the empirical formulae to plates of varying thickness and many other parameters which were not included in their research. Kim et al. [2003] have employed factorial design to correlate the robotic GMAW process parameters (welding voltage, welding speed and arc current) to three responses (bead width, bead height and penetration) for optimization purposes. Their results showed that all process parameters influenced the responses and the models developed are able to predict the responses with 0–25% accuracy.

2.8 LASER WELDING

Considerable research studies were carried out to examine the laser welding process. Mackwood and Crafer [2005] carried out an extensive review on laser welding and related processes. They presented the applications laser welding process under different welding categories such as laser spot welding, laser butt welding, etc. Laser welding characteristics of cold rolled carbon steel were examined by Shin et al. [2007]. They showed that the optimal welding conditions resulting in no defect sites in the vicinity of the welded area was possible for a certain combination of laser output power, welding speed, and focus setting of focusing lens. Nd:YAG laser repair welding of tool steels and microstructural changes in the weld site was examined by Vedani [2004]. He indicated that heat affected zone was narrow and carbides dissolve during the heating phase of the welding process. Laser welding of steel and residual stress distribution were examined by Olabi et al. [2007]. They examined the effect of laser parameters on the residual stress developed through statistical analysis. Application of high-energy sources as plasma or laser for welding improves joint geometry, but requires post-welding treatment or preheating for high strength steels (Permyakov et al. [2006]).

Laser welding of low carbon steel sheets was carried out by Yilbas et al. [2010]. Temperature and stress fields developed during the welding were computed using the finite element method. The residual stress developed in the weld region was measured using the XRD technique while metallurgical and morphological changes in the weld

zone were examined using the optical microscopy, SEM and EDS. They found that the temperature decay in the molten zone was lower than in the solid due to absorption and dissipation of the laser energy in the molten zone generated in the surface region. Laser welding and temperature fields simulations were carried out by Zeng-rong et al. [2007]. They indicated that the finite element method provided results in agreement with the experimental findings. Sundar et al. [2007] carried out Finite Element Analysis on a single pass butt-welding model to illustrate the temperature distribution, distortion and residual stress field developed in the weldment. They found that the geometric distortion and residual stress induced during welding can be minimized by selecting appropriate process parameters. De et al. [2003] considered 2-D axisymmetric finite element analysis of heat flow during laser spot welding. They predicted the transient temperature isotherms and the weld pool dimensions. Lundback and Runnemalm [2005] described a 3-D finite element model for the prediction of the distortion and residual stresses induced during electron beam welding. They used combined conical and double ellipsoid heat source to model the deep penetration characteristic of the electron beam. Balasubramanian et al. [2008] employed a three dimensional conical Gaussian heat source in the analysis. Frewin and Scott [1999] presented a three-dimensional finite element model of the heat flow during the pulsed laser beam welding. The results suggested that temperature profiles and weld dimensions were strong functions of the absorptivity and energy distribution of the laser beam. For this reason, it is essential to incorporate an accurate description of the heat source. Arif [2010] presented a moving volumetric heat source model and he used it to simulate the laser cutting process in order

to predict the residual stress generated in the cutting region. Safdar et al. [2007] investigated the effects for various laser beam geometries on the laser tube bending. Wu et al. [2006] established a model for the keyhole plasma arc welding (PAW) incorporating the heat source in the simulation.

CHAPTER 3

PROBABILISTIC ANALYSIS AND REGRESSION MODEL

3.1 INTRODUCTION

Spiral welded pipe (SWP), as the name implies, is a steel pipe that has a seam running its entire length in a spiral form as shown in Figure 3.1. It is used extensively throughout the world for large-diameter, gas transmission pipelines. As the industry needs for gas production has increased, there is more demands for SWP having larger diameters, higher operating pressures and increased mechanical strength. SWP is produced from forming and welding plate or strip material. The steel is leveled and passed through a forming station that spirals the steel to the required outside diameter. The spiral seam is then welded both internally and externally as part of the one forming operation. The pipe shell thus formed is cut to the required length as it travels out of the forming and welding machine.

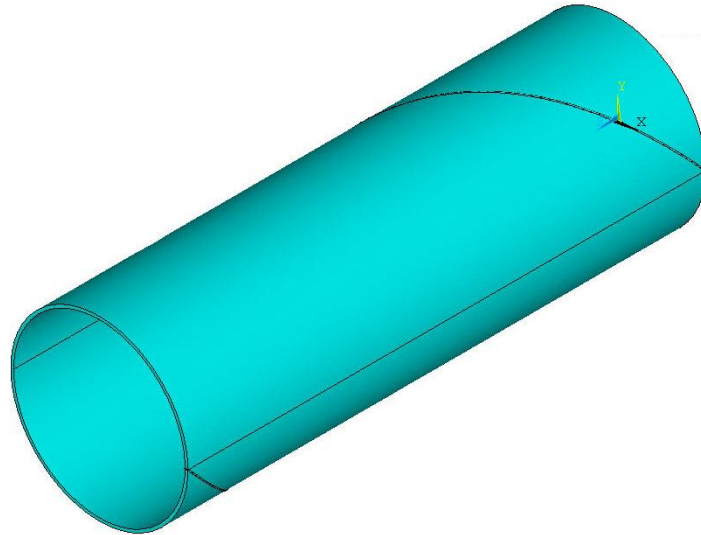


Figure 3.1: Spiral welded pipe.

Quality of spiral welded pipe is directly influenced by forming and welding input parameters. During the production of SWP, the plate or strip material goes through bending, forming, and welding. These mechanisms interact to produce a complex three-dimensional residual stress field. Having higher internal residual stress is one of the main reasons that restrain SWP's application. The residual tensile stress would become the driving force of crack propagation with operation pressure together. On the other hand, even relatively small unbalanced state of residual stress at some locations could lead to stress corrosion cracking or corrosion fatigue fracture to pipeline in the presence of a corrosive medium. Therefore, a common problem faced by the spiral welded pipes manufacturers is the control of process input parameters to obtain a good pipe quality with minimal detrimental residual stresses.

Residual stresses in spiral welded pipes may be measured by non-destructive techniques and locally destructive techniques. The non-destructive techniques include X-ray and neutron diffraction methods, magnetic methods, and ultrasonic techniques and the locally destructive techniques include hole drilling methods or ring splitting technique. The selection of the optimum measurement technique should consider volumetric resolution, material, geometry and access. To get the desired spiral welding residual stresses, it is essential to know interrelationships between process parameters and the change in circumference during the ring splitting test. The process of developing this relationship is not an easy task because there are some unknown, nonlinear process parameters. The relationship between process variables and ring splitting opening are complex because of the number of variables and their interrelationships involved. Knowing which parameters have an effect on the quality of the spiral welded pipe and which parameters give the most significant effect on the weld quality are the main issues in piping industry.

However, no serious attempt has so far been made to predict residual stresses in spiral welded pipes due to the combination of input and output welding and processing variables. The difficulty of getting sufficient real data of residual stress tests done in the industries has limited the full utilization of the regression models to predict spiral welded pipes residual stresses. Fortunately, a substantial amount of real life data was acquired which is generated over several years in a most appropriate environment of utilization of such pipes. Based upon this valuable data the objective of this chapter is to develop a

regression model explaining relationship between spiral pipe process/welding variables in order to predict the residual stresses by ring splitting test. Several factors were included in this study. These factors are pipe diameter, wall thickness, pipe grade, coil width, forming angle, welding speed, and pitch distance.

3.2 EXPERIMENTAL PROCEDURE

Residual stress measurement can be carried out experimentally by means of destructive techniques known as Ring Splitting Test. Figure 3.2 shows a ring-like sample with a length of approximately 150 mm is taken from a long pipe and split open in the longitudinal direction for all measurements. The residual stresses are distributed across the wall thickness of pipe. In ring splitting method, a cut, by flame or sawing, is made along a straight line parallel to the longitudinal axis of the pipe and in the opposite direction of the spiral weld (180 degrees from the spiral weld) in order to release the residual moment as shown in Figure 3.3. Prior to cutting the ring, fiducial marks shall be placed on either side of the proposed cut location. The direction and magnitude of the residual stress can be estimated from the magnitude of a ring opening or a ring closing resulting from a longitudinal cut made in the pipe. If the residual moment is an expanding one, the cut in the sample opens up. If the residual moment is a contracting one, on the other hand, the cut closes. The amount by which the cut opens ($+\Delta C$) and the amount by which the cut closes ($-\Delta C$) are collectively known as the magnitude of a ring opening.



Figure 3.2: (a) Preparation for splitting ring test, (b) Ring cut from spiral welded pipe.

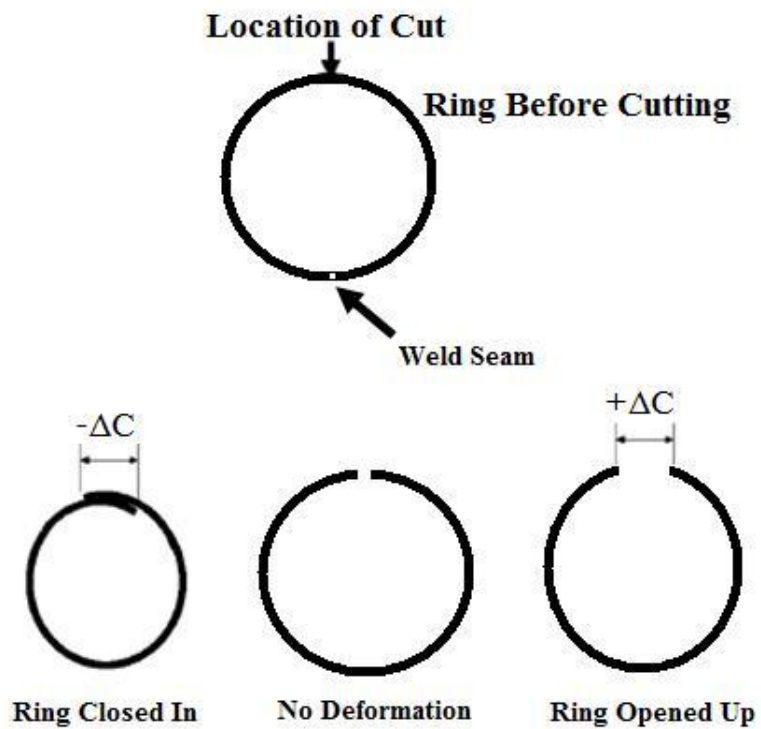


Figure 3.3: Ring splitting method

Many researchers have worked on developing relationships between the

circumferential opening, in cut-ring test, and the residual stress of spiral welded pipe so that residual stress can be estimated from the circumferential opening conveniently. For example, one company uses the following formula [Saudi Aramco Materials System Specification, 01-SAMMS-035]:

$$\sigma_r = Et \left(\frac{1}{D_o} - \frac{1}{\frac{\Delta C}{\pi} + D_o} \right) = \frac{Et \Delta C}{2R \Delta C + 4\pi R^2} \quad (3.1)$$

Where:

σ_r = residual stress in MPa (psi)

ΔC = \pm change in circumference, mm (in)

t = nominal thickness, mm (in)

E = Young's Modulus of Elasticity 200,000 MPa (29×10^6 psi)

R = nominal pipe radius mm (in)

The above equation is based on a linear distribution of stress through the thickness of the material. Although this is an approximation, the values obtained for residual stresses are believed to be reasonably accurate. This technique can only assess hoop stresses and it is not possible to determine longitudinal residual stresses.

Acceptance Criterion: In industry, the computed stresses in spiral welded pipe are limited to $\pm 10\%$ of the pipe Specified Minimum Yield Stress (SMYS) due to a fairly

broad consensus that these stresses increased the possibility of sulfide stress cracking (when operating in sour environment) and that large computed stresses would contribute to a longer rupture, regardless of cause [Saudi Aramco Materials System Specification, 01-SAMMS-035].

3.3 DATA COLLECTION AND ANALYSIS

Continuously pursuing high quality and low cost in every kind of industrial processes has made statistical and probabilistic analysis common and fundamental practices in several business environments. One main problem with these techniques can be the data availability, which means costs and time required for experimental investigations. The recorded data by the spiral welded pipes manufacturers (before, during and after pipe production) offer enormous potential as sources of new knowledge. Making use of these large volumes of collected data is important for the discovery of hidden knowledge by transforming them into useful predictive models. The extracted knowledge can be used to model, classify, and make predictions for numerous applications. Data can be analyzed to identify hidden relationships or patterns in the parameters that control manufacturing processes or to determine and improve the quality of products.

All the data for this work were collected in collaboration with National Pipe Company, Saudi Arabia [NPC], a leading local manufacturer of large diameter helical as well as longitudinal steel welded pipes. The plant has annual production capacity of 180,000 metric tons of spiral Submerged Arc Welded (SAW) pipe. The establishment can thus be treated as a representative SAW pipe manufacturing facility, and the work presented in this chapter can be used as a benchmarking tool for evaluating pipe defect due to high residual stress and plant performance of a plant operating at high quality standard. Following two sets of data were collected and analyzed in this work:

Data Set A: 2090 ring splitting tests data for 56 inch (1422mm) outer diameter spiral welded pipe having 0.875 inch (22.2mm) wall thickness were collected. The pipes were manufactured from X65 grade steel. The industrial acceptance criteria of $-0.1\sigma_Y \leq \sigma_{Res} \leq 0.1\sigma_Y$ yields $-64\text{mm} \leq \Delta C_{max} \leq 64\text{mm}$. Based on this criterion, only 9% of the rings (205 tests) failed during test for this data set.

Data Set B: 262 ring splitting tests data for 24-60 inch outer diameter spiral welded pipes having wall thickness in the range of 0.25-0.66 inch were collected. The pipes were manufactured from three different grades of steel.

3.4 PROCESS CAPABILITY ANALYSIS (USING DATA SET A)

The distributions of the opening and closing value (ΔC) for 2090 test data shows that 72% of these tests predict a closing mode with negative ΔC value (Figure 3.4). This implies that most of the stresses on the samples are compressive. An examination of the graph (Figure 3.4a) shows that it is apparently normal distributed (approximately reflected by a bell shaped curve) as the raw (empirical) distribution matches closely to the normal curve. The normal probability plot for the data set is given in Figure 3.5.

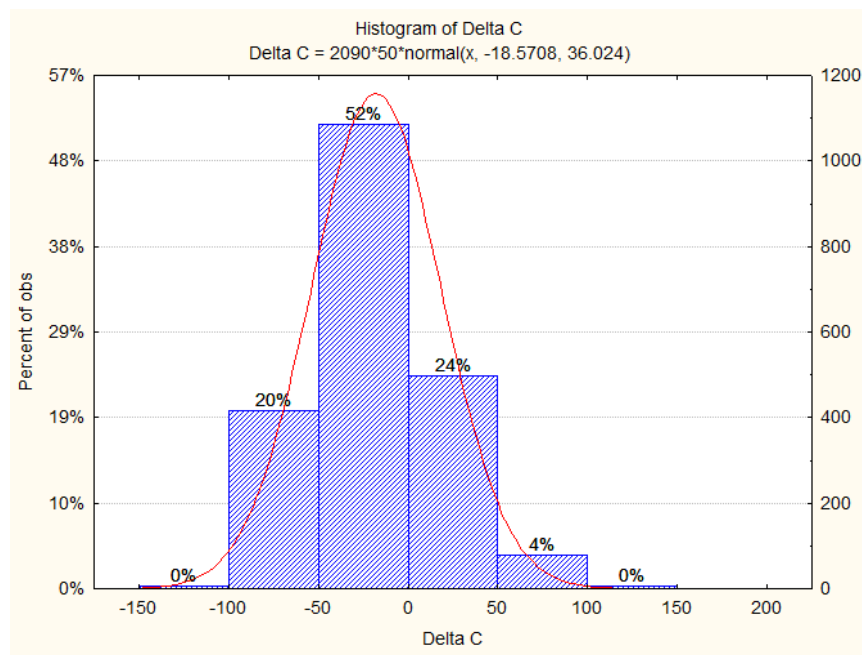


Figure 3.4a: Histogram of ΔC values for ring splitting tests conducted on data set A

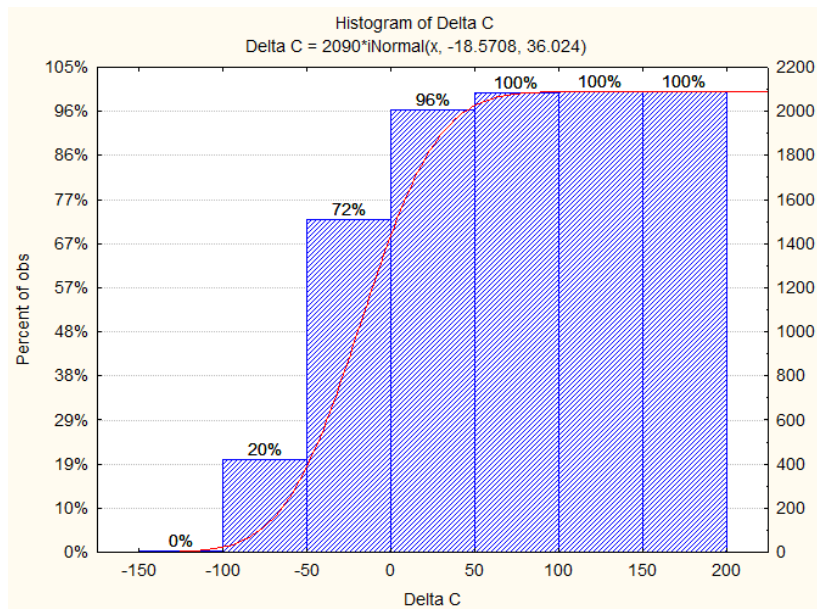


Figure 3.4b: Cumulative ΔC values for ring splitting tests conducted on data set A

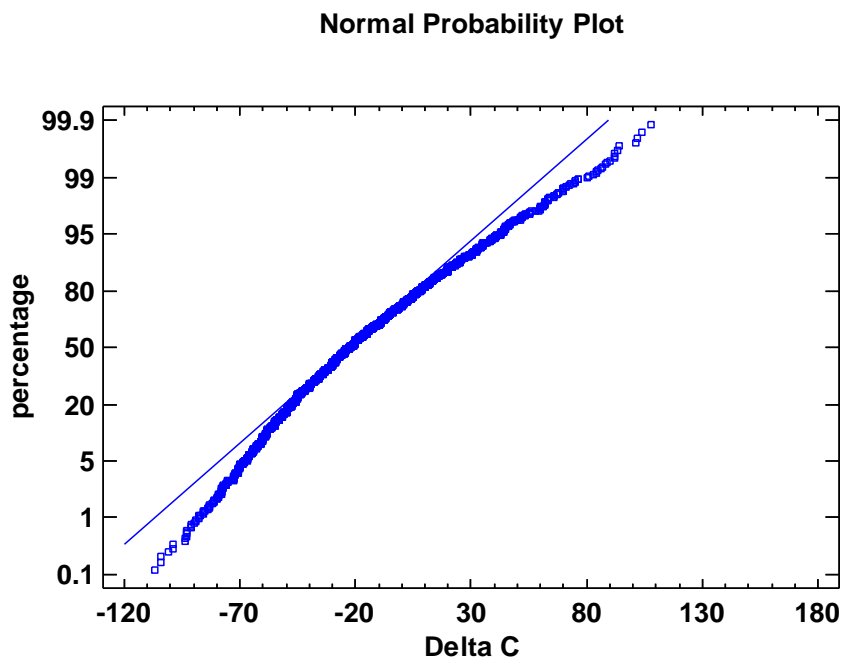


Figure 3.5: Normal probability plot for data set A

The Process Capability Analysis is designed to compare a set of data against a set of specifications. The goal of the analysis is to estimate the proportions of the population from which that data come will fall outside the specification limits. Process capability in the context of spiral pipes means ability of the pipe manufacturing process to meet the technological or other requirements, i.e. to fulfill acceptable residual stress demands put on it. The residual stress demand is measured by (USL and LSL) which are the upper and lower specification limits of the quality characteristic ΔC respectively and for this case $USL-LSL = \Delta C_{max} = (\pm 64mm)$, and the manufacturing process variability is represented by σ =standard deviation of measurements of ΔC by split ring test. Thus, the Process Capability Ratio (PCR) or (C_p) was studied for the collected data using the following formula:

$$PCR = \frac{USL - LCL}{6\sigma} \quad (3.2)$$

A normal distribution was fit to the set of collected data for the variable ΔC as shown in Figure 3.6. 11.4589% of the fitted distribution lies outside the specification limits as shown in Table 3.1. Several capability indices have been computed to summarize the comparison of the fitted distribution to the specifications (Table 3.2 and 3.3). If the process is centered, measurement process is always capable when capability index value (C_p , C_{pk} , respectively C_{pm}) exceeds 1. Since certain variability is always present and process is never fully in statistically controlled state. Therefore indexes value 1.33 is recommended for established processes such as SAW. Practical recommendation considers minimal admissible value 1.33. Table 3.2 indicate that C_p is much away from

1.33 and thus indicate a need to reduce the scatter in the SAW process to realize the goal of $C_p=1.33$. Another common index is P_p , which in the case of the normal distribution equals the distance between the specifications limits divided by 6 times the standard deviation. In this case, P_p equals 0.592198, which is usually considered to be not good. P_{pk} is a one-sided capability index, which in the case of the normal distribution divides the distance from the mean to the nearer specification limit by 3 times the standard deviation. In this case, P_{pk} equals 0.420361. The rather large difference between P_p and P_{pk} is a sign that the distribution is not centered well between the specification limits. K equals the mean minus the nominal, divided by one-half the distance between the specs. Since K equals -0.290169, the mean is located 29.0169% of the way from the center of the specs toward the lower specification limit. Since capability indices are statistics, they will vary from one sample of data to another. The 95.0% confidence intervals show how much these statistics might vary from the true values given the fact that only 2090 observations were taken.

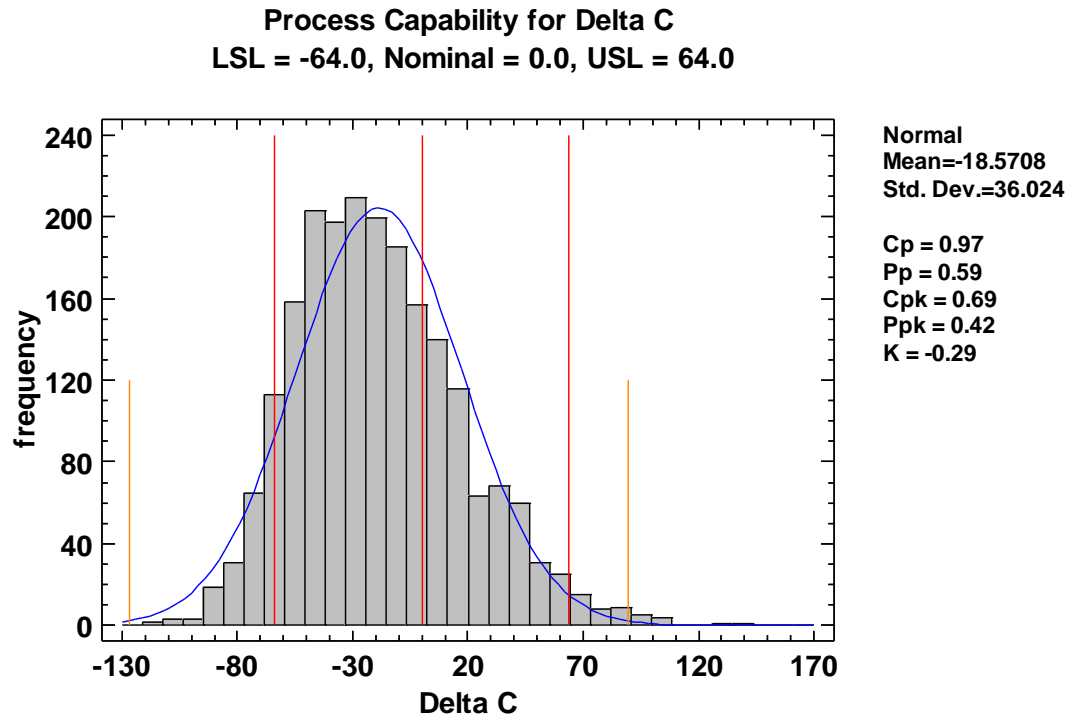


Figure 3.6: Process capability for the change in circumference ΔC in data set A.

Table 3.1: Process capability analysis

<i>Specifications</i>	<i>Observed</i>		<i>Estimated</i>	<i>Defects</i>
	<i>Beyond Spec.</i>	<i>Z-Score</i>	<i>Beyond Spec.</i>	<i>Per Million</i>
USL = 64.0	2.057416%	2.29	1.094965%	10949.65
Nominal = 0.0		0.52		
LSL = -64.0	7.799043%	-1.26	10.363926%	103639.26
Total	9.856459%		11.458891%	114588.91

Table 3.2: Capability indices

<i>Index</i>	<i>Lower Limit</i>	<i>Upper Limit</i>
Cp	0.944308	1.00336
Pp	0.574239	0.61015
Cpk	0.665894	0.716632
Ppk	0.401211	0.43951

Table 3.3: Process capability summary

	<i>Short-Term</i>	<i>Long-Term</i>
	<i>Capability</i>	<i>Performance</i>
Sigma	21.9064	36.024
Cp/Pp	0.973841	0.592198
Cpk/Ppk	0.691263	0.420361
K	---	-0.290169
DPM	19131.2	114589.

3.5 PROBABILISTIC ANALYSIS (USING DATA SET B)

19 groups of data with different pipe diameters, wall thicknesses and grades have been analyzed. Table 3.4 shows the summary of the analyzed data. The residual stress on the parent metal were measured and calculated by the ring splitting method. The total observations of 2090 represent 19 groups of data. Number of observations in each group divide by total data points provides the proportion of each group data set in the total

observations which could be treated as parent population of 2090 values. These values are plotted in the pie chart of Figure 3.7.

Table 3.4: Statistics summary for 19 groups of data

Group#	Diameter mm (in)	Wall Thickness mm (in)	Grade	Count	Average	Standard Deviation	Coeff. of Variation	Minimum	Maximum	Range
Group 1	914.4 (36)	6.35 (0.250)	X60	15	0.0108	0.0169798	157.221%	-20	42	62
Group 2	1016 (40)	11.3 (0.444)	X60	20	0.00425	0.0138027	324.768%	-10	43	53
Group 3	1016 (40)	16.256 (0.640)	X60	7	-0.0188571	0.0116108	-61.5722%	-36	-20	34
Group 4	610 (24)	6.35 (0.250)	X60	24	0.00345833	0.00606472	175.365%	-12	13	25
Group 5	610 (24)	7.747 (0.305)	X60	20	-0.00185	0.00434408	-234.815%	-8	5	13
Group 6	1067 (42)	11.125 (0.438)	X70	14	-0.0178571	0.0167785	-93.9593%	-50	8	58
Group 7	1067 (42)	15.875 (0.625)	X70	20	0.01235	0.0116541	94.3653%	10	30	40
Group 8	1422 (56)	11.86 (0.467)	X65	9	0.00455556	0.030175	662.377%	-40	50	90
Group 9	1524 (60)	12.7 (0.500)	X65	14	-0.0222857	0.0318468	-142.902%	-63	45	108
Group 10	1524 (60)	17.25 (0.679)	X70	20	-0.01075	0.0302096	-281.019%	-62	44	106
Group 11	1524 (60)	16.79 (0.661)	X70	8	0.00475	0.0372702	784.637%	-55	45	10
Group 12	762 (30)	9.525 (0.375)	X65	8	0.01925	0.00645313	33.5227%	10	30	20
Group 13	762 (30)	13.76 (0.542)	X65	13	-0.00576923	0.00434269	-75.2733%	-14	3	17
Group 14	762 (30)	11.1 (0.437)	X65	10	0.0085	0.0101571	119.495%	-4	28	32
Group 15	1422 (56)	13.563 (0.534)	X70	9	0.0242222	0.0190708	78.7326%	-5	45	50
Group 16	1422 (56)	16.256 (0.640)	X70	20	0.0112	0.0224349	200.312%	-35	47	82
Group 17	1422 (56)	16.256 (0.640)	X70	5	0.0334	0.034897	104.482%	-20	75	95
Group 18	1524 (60)	14.0 (0.551)	X70	12	-0.00775	0.0315224	-406.74%	-45	50	95
Group 19	762 (30)	12.751 (0.502)	X65	14	0.00314286	0.011967	380.768%	-15	26	41
Total				262	0.00165649	0.0227221	1371.7%	-63	75	138

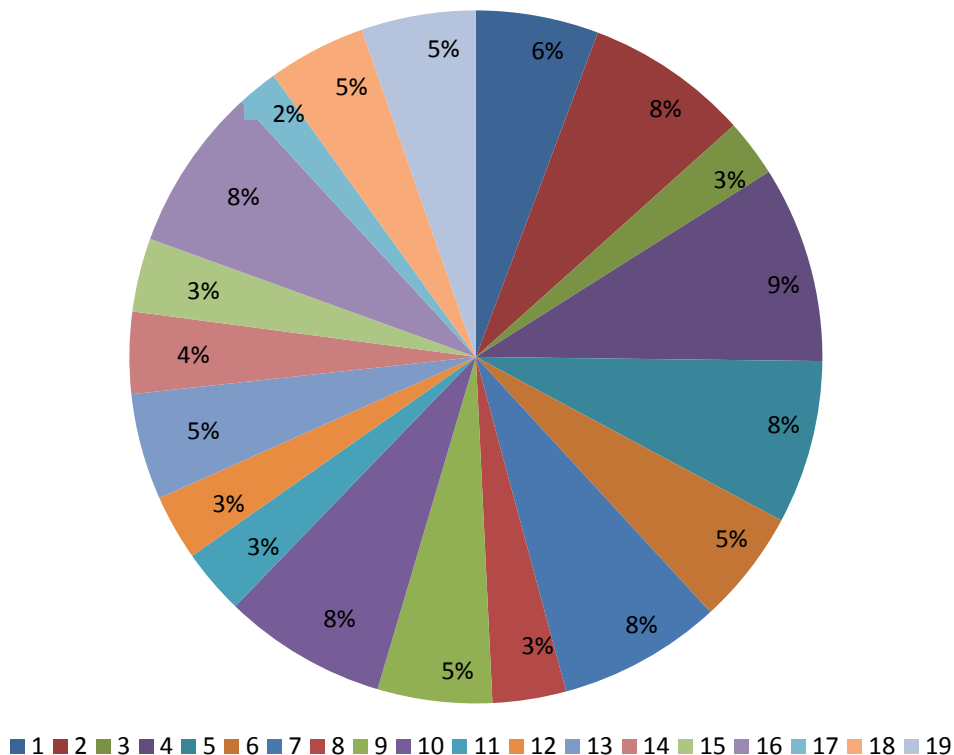


Figure 3.7: Pie-chart for data set B.

Figure 3.8 illustrate ΔC versus pipe thickness t for different pipe diameters for X65 Steel pipes. The changes in circumference versus residual stresses of individual test of pipe element sample sets of pipes ranging from 40 inches to 60 inches and two materials X60 and X65 steels are given. The empirical cumulative distribution function (CDF) of function change in circumferences ΔC , $F(\Delta C) = P(\Delta C \leq \Delta C) = \text{number of observations in a cell for the cell under consideration} / \text{total number of observations in the group}$, illustrated by the cell interval bars for all of the 19 groups are shown in Figure 3.9. Each of the empirical CDF is superimposed by a continuous curve representing a normal distribution $F(\Delta C) = \Phi[(\Delta C - \mu) / \sigma]$ where μ and σ are the mean and standard

deviation respectively of all ΔC values in each group. The normalized versions of these fitted continuous plots and linearly transformed data is plotted in Figure 3.10 shows that that the normal probability distribution characterizes the data in each of the 19 group with an acceptable goodness of fit (measured by the regression coefficient). The fitted line annotated by all is the normal fitted distribution to the pooled data of 19 groups (2090) data point .This normal distribution is also plotted in form of cumulative distribution function in Figure 3.11. This represents a global model of typical ranges and thickness of pipes of common pipe materials in oil and gas industry.

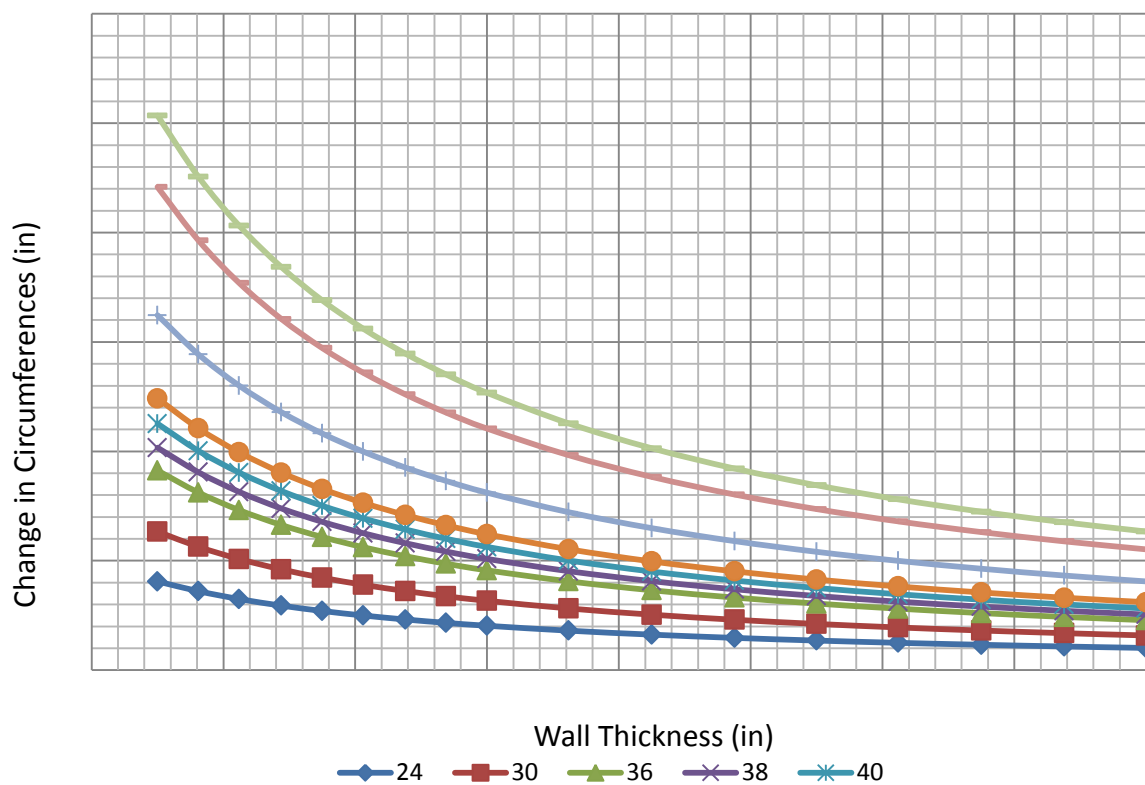


Figure 3.8: Change of circumferences (\pm) verses different wall thicknesses for grade X65 pipes

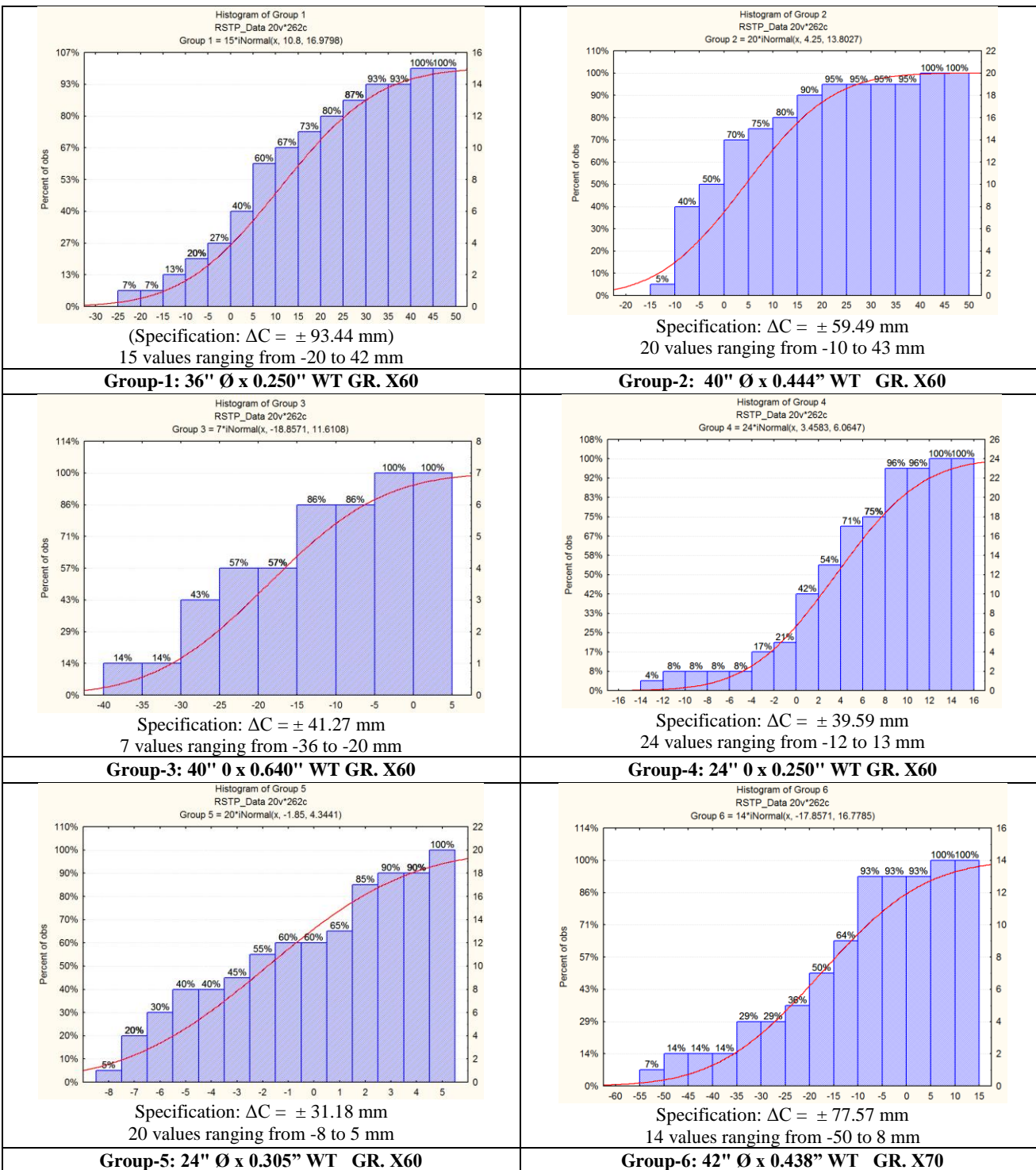


Figure 3.9a: Change in circumferences for pipe groups 1 to 6

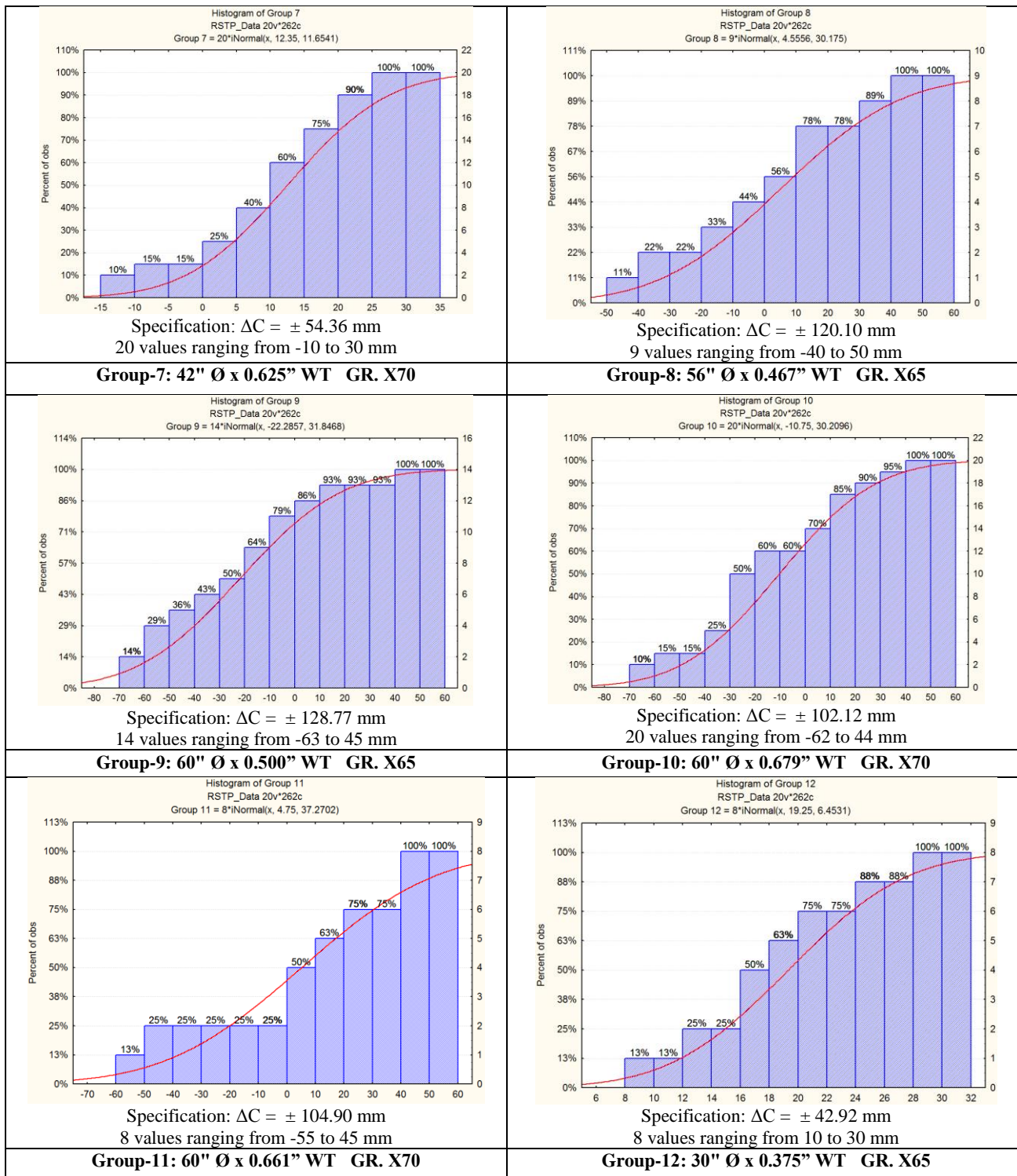


Figure 3.9b: Change in circumferences for pipe groups 7 to 12

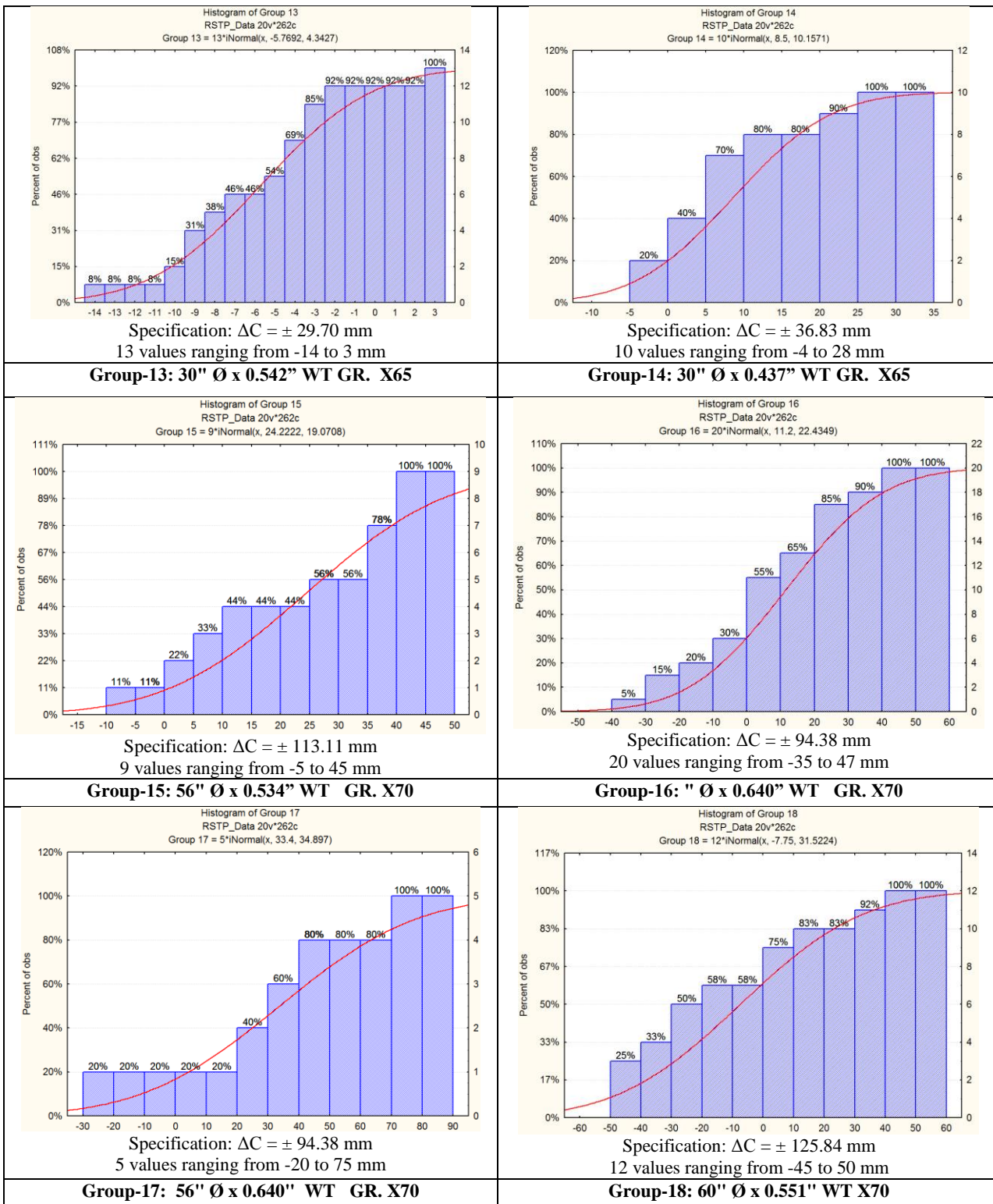


Figure 3.9c: Change in circumferences for pipe groups 13 to 18

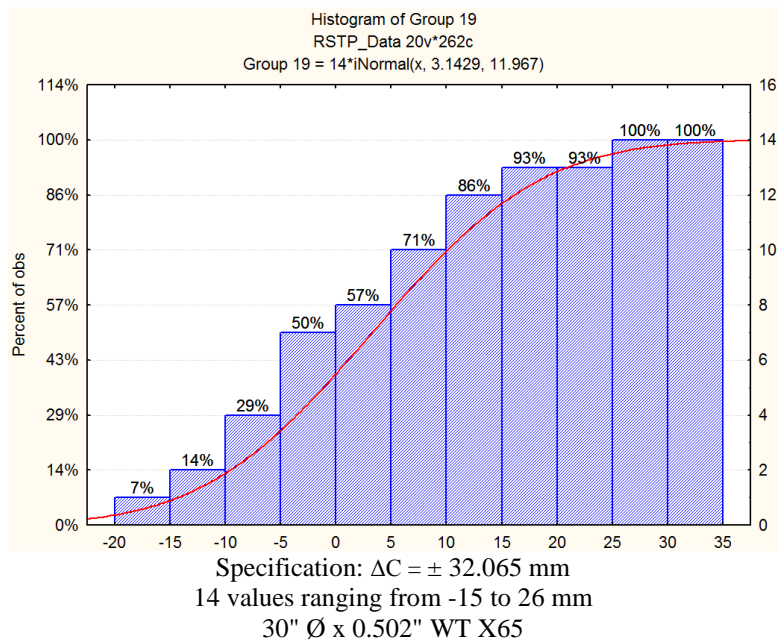


Figure 3.9d: Change in circumferences for pipe group-19

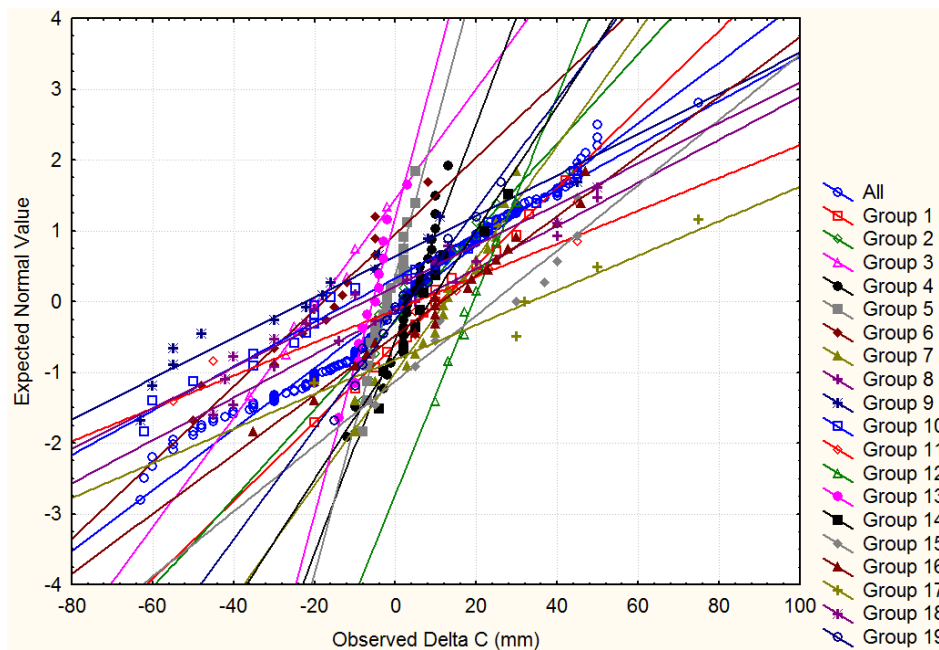
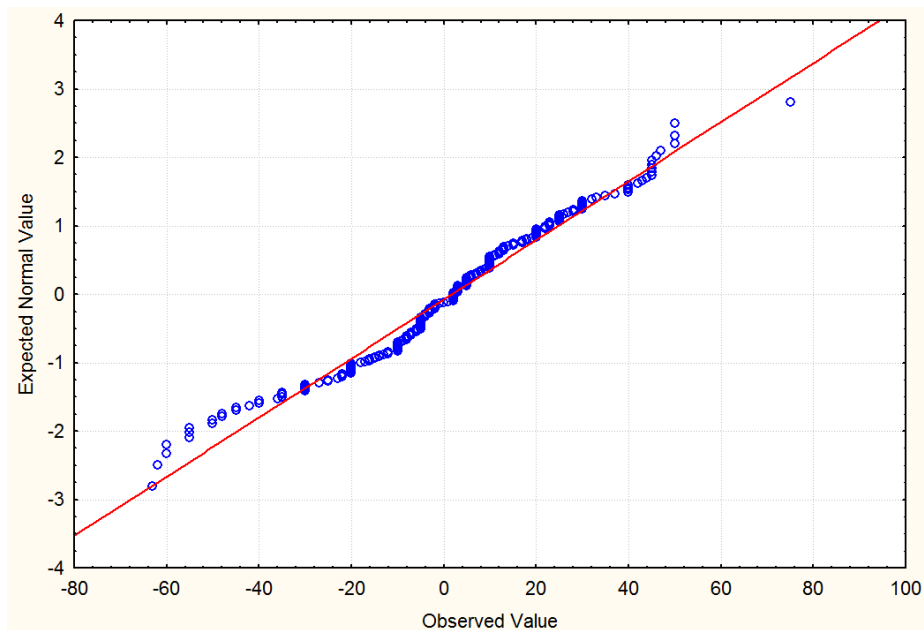


Figure 3.10: Normal probability plots for all groups of data set B (Separate).



Normal Probability Plot

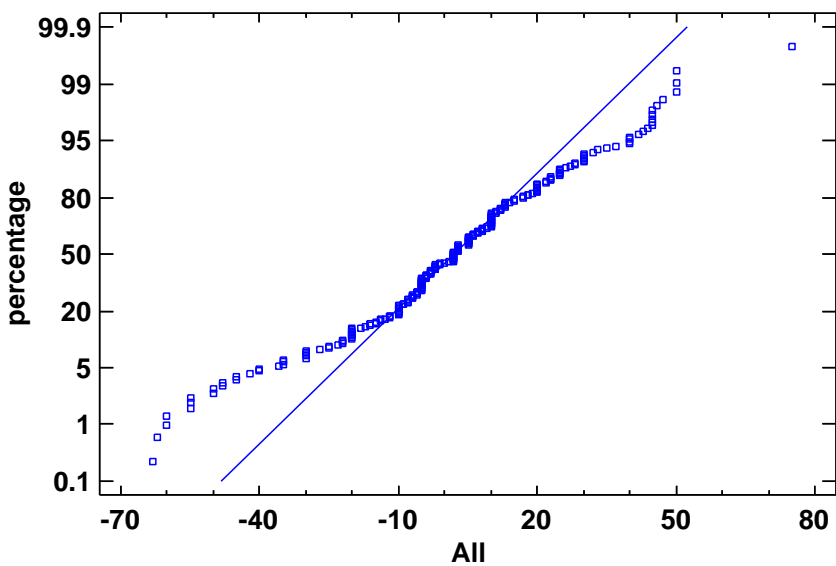


Figure 3.11: Normal probability plot in percent for all groups of data set B (Combined)

The mean (same as median in case of normal distribution) in fitting above normal models are estimated as a point estimates ,these point estimates do have uncertainty and depends upon sample size in each group and level of confidence in which the range of

such estimates. Figure 3.12 is the plots of such interval estimates of medians (same as mean for normal distribution) with 95% confidence intervals for all the 19 groups of data.

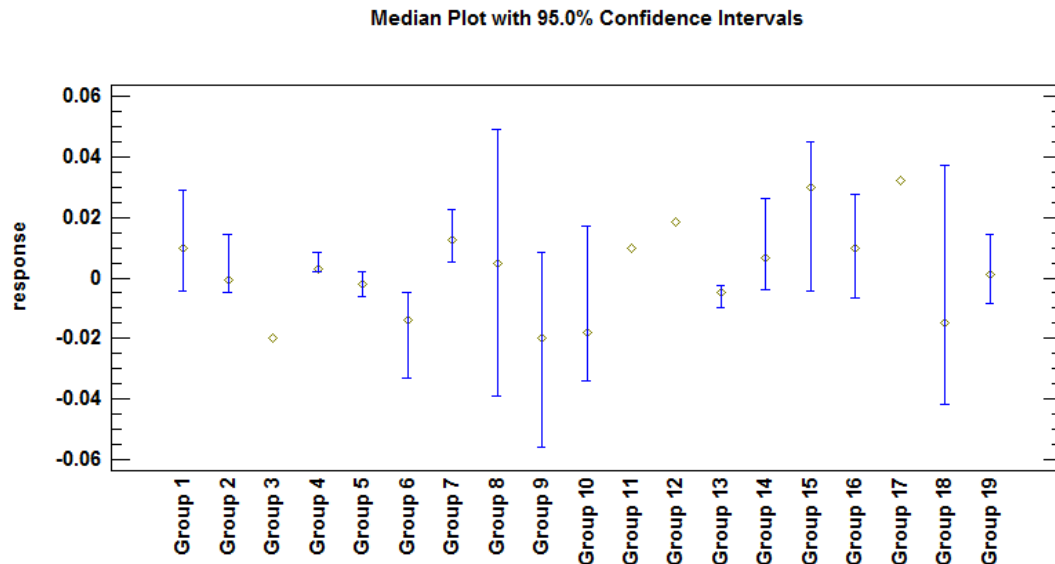


Figure 3.12: Median plots with 95% confidence intervals for data set B

3.6 REGRESSION MODELING (USING DATA SET B)

One basic goal of modeling is to extract the useful part of the information contained in the experimental data and summarize it in mathematical expressions of easier interpretation and handling. Variable selection and multiple regressions were both performed using a commercial statistical software package. Multiple regressions are used when there are one or more predictor variables and one continuous dependent variable. It allows for the testing of a theoretical model about how a set of predictors account for a particular outcome variable of interest. It can be used to assess the relative importance of

predictor variables. It develops a weighted linear composite that maximizes the variance accounted for in the dependent variable. Simple regression is when there is only one predictor variable. In this instance, regression is quite similar to correlation.

The dependent variable should be continuous or at least ordinal. Predictor variables can be continuous or binary. Nominal predictors need to be dummy coded before they can be used as predictors. There are several methods for selecting the best model, such as backward regression, forward regression and mixed regression. To investigate the influences of different factors on the measured ΔC which has a direct effect on the calculated residual stresses in detail, the multiple regression analysis was conducted on the collected data of 19 groups of different pipe specifications. The change in circumferences ΔC was considered as dependent variable while the independent variables that were considered are as follow:

1. D: Pipe Diameter (m)
2. T: Wall Thickness (m)
3. S_y : Pipe Grade (SMYS in MPa)
4. W: Coil Width (m)
5. α : Forming Angle (degree)
6. V: Welding Speed (m/s)
7. P: Spiral Pitch Distance (m)

The multiple regression equation obtained finally is as follow after taking the log of the absolute values of the ΔC with the assumption that it was adequate at the 95% confidence level:

$$|\Delta C| = \exp[\beta_0 + \beta_1 D + \beta_2 T + \beta_3 S_y + \beta_4 W + \beta_5 \alpha + \beta_6 V + \beta_7 P] \quad (3.3)$$

Table 3.5 shows the model summary which summarizes how well the overall multiple linear regression model predicts the dependent variable. The table also describes the relationship between $\ln(|\Delta C|)$ and seven independent variables mentioned before. It is worth mentioning that R-squared describes the percentage of variance in the dependent variable explained by the regression equation. It ranges from 0 to 1. It is used to evaluate the effectiveness of the regression to predict. R-squared somewhat overestimates the population variance explained in the dependent variable by the regression model. The degree of this overestimation is greater when there are more predictors and when the sample size is smaller. Adjusted R-squared attempts to obtain an unbiased estimate of variance explained in the population. The larger R-squared, the bigger the sample size and the smaller the number of predictors, the more powerful this test will be. In this case the regression model based on the seven predictors account for 36.47% of variable in the data. The analysis summary is as follow:

- R-squared = 36.4766 %
- R-squared (adjusted for d.f.) = 34.719 %
- Standard Error of Est. = 0.801987

- Mean absolute error = 0.661699
- Durbin-Watson statistic = 1.86738 (P=0.1424)
- Lag 1 residual autocorrelation = 0.0642195

Table 3.5: Summary of the multiple regression model

<i>Parameter</i>	<i>Estimate</i>	<i>Standard Error</i>	<i>T Statistic</i>	<i>P-Value</i>
β_0	-27.5576	24.8522	-1.10886	0.2685
β_1	-0.745752	6.76477	-0.110241	0.9123
β_2	-0.774656	0.391253	-1.97993	0.0488
β_3	2.60424	1.33116	1.95636	0.0515
β_4	9.36933	5.92781	1.58057	0.1152
β_5	0.093708	6.68668	0.0140141	0.9888
β_6	-1.24101	0.789606	-1.57169	0.1173
β_7	-8.52493	3.93075	-2.16878	0.0310

A value of 0.36 for R-squared indicates moderate reliability, whereas values above 0.8 are considered highly reliable [Franzblau 1958]. Table 3.6 is the ANOVA analysis output for the ring opening. As seen in this table, it can be assumed that the following interaction model for the weld bead height was adequate at the 95% and 99% confidence level. The analysis of variance (ANOVA) has efficiently been used for identifying the significance of main and interaction effects of process parameters. Since the P-value in the ANOVA table is less than 0.05, there is a statistically significant

relationship between the variables at the 95.0% confidence level. The R-Squared statistic indicates that the model as fitted explains 36.4766% of the variability in $\ln(|\Delta C|)$. The adjusted R-squared statistic, which is more suitable for comparing models with different numbers of independent variables, is 34.719%. The standard error of the estimate shows the standard deviation of the residuals to be 0.801987. This value can be used to construct prediction limits for new observations. The mean absolute error (MAE) of 0.661699 is the average value of the residuals. The Durbin-Watson (DW) statistic tests the residuals to determine if there is any significant correlation based on the order in which they occur in your data file. Since the P-value is greater than 0.05, there is no indication of serial autocorrelation in the residuals at the 95.0% confidence level.

Table 3.6: Analysis of variance (ANOVA)

<i>Source</i>	<i>Sum of Squares</i>	<i>D_f</i>	<i>Mean Square</i>	<i>F-Ratio</i>	<i>P-Value</i>
Model	93.4406	7	13.3487	20.75	0.0000
Residual	162.725	253	0.643183		
Total (Corr.)	256.166	260			

Figure 3.13 shows the observed values against the predicted change in circumferences (ΔC) values obtained from the developed model. In determining whether the model can be simplified, notice that the highest P-value on the independent variables is 0.9888, belonging to the forming angle (α). Since the P-value is greater or equal to 0.05, that term is not statistically significant at the 95.0% or higher confidence level.

Welding processes often encounter disturbances that effectively change the process outputs, resulting in a weld of undesirable characteristics. Such disturbances may include thermal distortion, pipe forming and automated systems errors. The residual stress distribution in welded joints depends on a number of process and design parameters such as the heat input, speed of the welding arc, preheat, thickness of the pipe, weld joint geometry, and other factors. Welding engineers have long used trial and error to obtain a suitable combination of these parameters in order to control the residual stresses. Variables studied so far in this research include pipe diameter, wall thickness, pipe grade, coil width, forming angle, welding speed and spiral pitch distance. There are other factors that need to be included which were not available. These variables may include pre-heat and post-heat temperatures, cooling rate, welding arc voltage and current, electrode wire feed rate, number of internal and external welding electrodes with their positioning and orientations, forming roller setup and weld joint configuration.

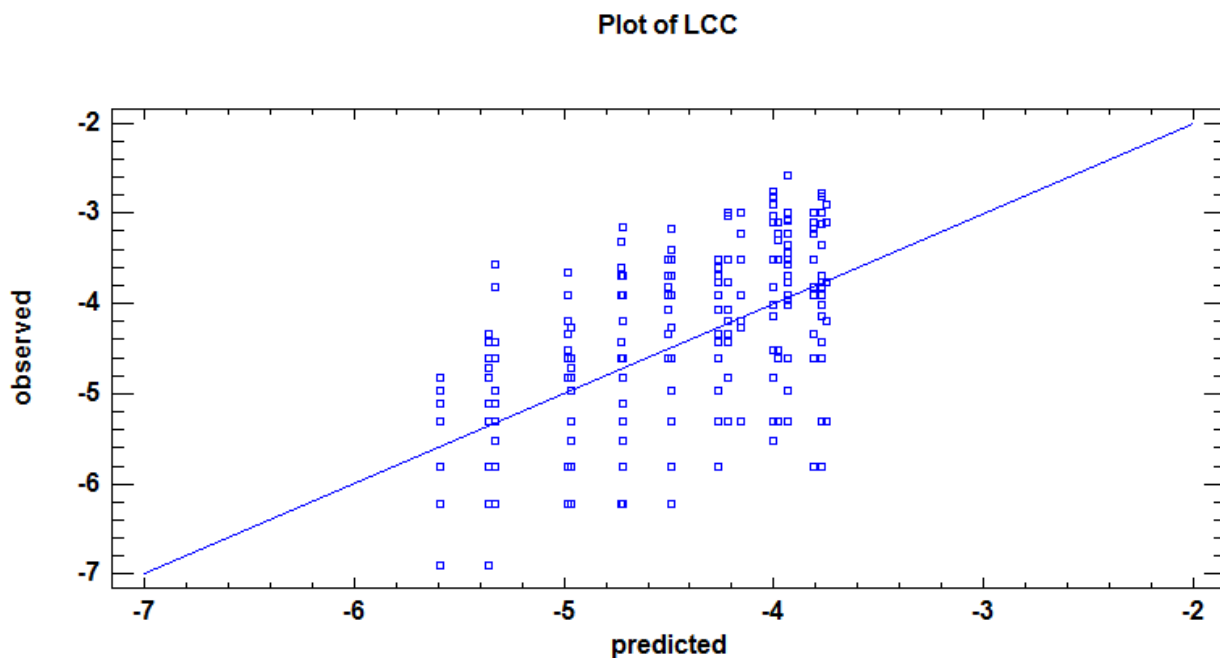


Figure 3.13: Predicted versus observed ΔC values

Another primary measure of the welding process quality is the microstructure, which determines the weld material properties as a result of heat input during the welding process as well as a possibility of inclusions introduced as a part of flux layer deposited and maintained over the arc during the SAW process. This manifestation of the quality is not directly measurable in real time, i.e., it is unobservable. So, more efforts and researches are needed to move beyond mere analysis of residual stresses and distortions to aggressively controlling other materials and metallurgical process variables. These variables that may be considered are pipe and electrode material properties, hardness, strength, microstructure, welding discontinuities (cracks, inclusions, porosity, etc.). Metallurgy of the weld has a great effect on the cracks propagation in addition to the pipe residual stresses. Failure mechanisms in spiral welded pipes by cracking may be

separated into two stages: initiation and propagation. Each is influenced by microstructure features (grain structure, intermetallics, matrix precipitation) and/or by “mechanical” features (presence of residual stresses or pores). Because weld quality is not directly measurable, identifying variables with a high correlation with residual stress test results will be desirable.

CHAPTER 4

DRILLING HOLE TECHNIQUE MEASUREMENTS

4.1 DRILLING HOLE EXPERIMENTAL PROCEDURE

In collaboration with National Pipe Company (NPC), a leading local manufacturer of large diameter helical as well as longitudinal steel welded pipes, the results of the Microscopic Residual Stress (MIRS) tests that were conducted by NPC have been used to validate the Finite Element Model. Microscopic Residual Stress (MIRS) tests were conducting by hole-drilling and cutting method. The test pipes have been selected from both acceptable and unacceptable pipes evaluated by Macroscopic Residual Stress (MARS) test (Ring Splitting Test) that was explained in the previous chapter. The pipe samples for testing were selected from sections of pipes with the following size:

- Outside Diameter: 56" (1422mm)
- Wall thickness: 0.875" (22.2 mm)
- Length: 1.5 meter (1500 mm)

In this test, strain released by drilling a hole in a specimen is recorded by strain gages distributed around the drilled hole on the surface of the pipe. The recorded strains

are converted to stress using equations provided by ASTM E837. The hole-drilling rosettes consist of three single or pairs of strain gauge grids. An example of hole-drilling rosette recommended in ASTM E837 is shown in Figure 4.1.

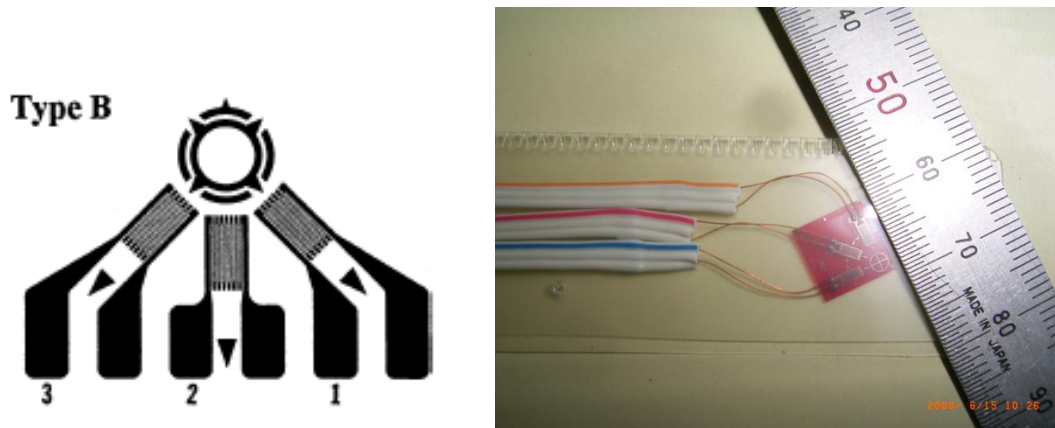


Figure 4.1: Hole-drilling rosettes

The Microscopic Residual Stress (MIRS) Test Procedure is as follow:

1. Install a special three strain gauge rosette at the point where stresses are to be measured (Figure 4.1).
2. Wire the strain gauges to a static strain indicator.
3. Attach and accurately position a drilling device over the target of the rosette.
4. Balance the gauge circuits.
5. Drill hole in increments, being careful not to generate heat that would induce residual stresses.
6. Record strains after the strain indicator has stabilized.
7. Calculate stresses using strain data averaging.

The MIRSs were measured on seven points at welded portion on the inside surfaces of pipes as shown in Figure 4.2 and they are as follow:

- Bead center (1 location marked as 2 in Figure 4.2)
- $\pm 15\text{mm}$ from the bead center (2 locations marked as 5 & 6 in Figure 4.2)
- $\pm 20\text{mm}$ from the bead center (2 locations marked as 1 & 3 in Figure 4.2)
- $\pm 30\text{mm}$ from the bead center (2 locations marked as 4 & 7 in Figure 4.2)

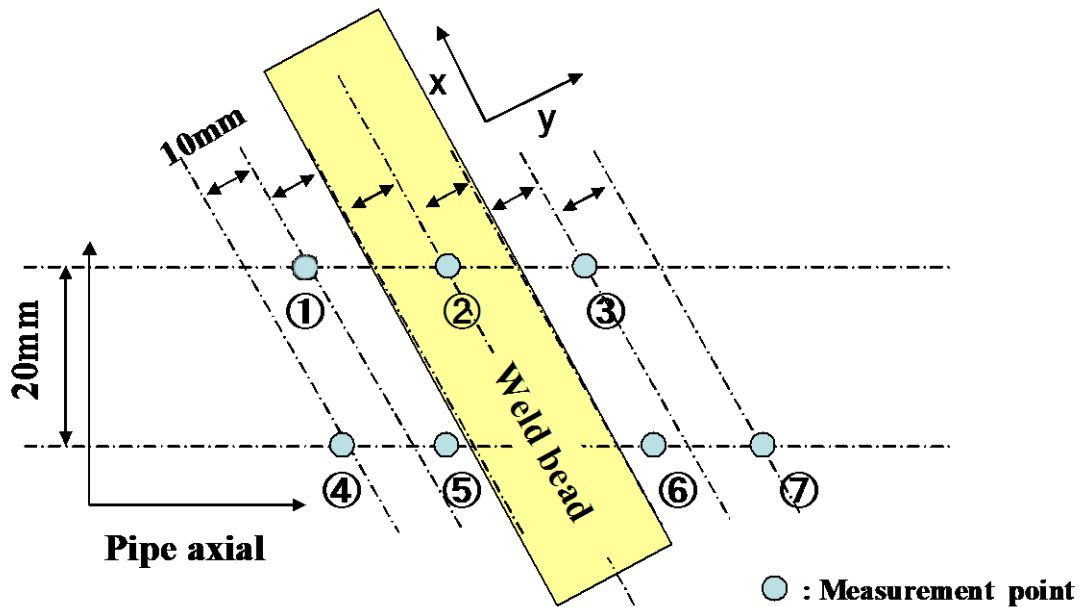


Figure 4.2: Setting positions of drilling hole rosettes

Each hole drill provides the principal stresses and the angle to the principal stresses in the plane of the specimen surface at the hole drilling location. The stresses calculated per the ASTM E 837 equations represent the average stress over about half the whole depth and across the hole diameter.

4.2 EXPERIMENTAL RESULTS

Much of the residual stress field comes from coiling and uncoiling the steel strip that is used to produce the spiral welded pipes by forming the uncoiled strip with angle before welding. The coiling and forming process compresses the inner face of the coiled strip (this becomes the inner wall of the pipe) and stretches the outer face of the pipe. When the strip is formed into the pipe shape the outer surface has tensile stresses and the inner wall has compressive stresses imposed. This generates the more linear stress distributions. The axial stress component was the greatest in magnitude. The stress profile from forming operations may be the most important factor in the stresses in addition to the residual stresses as a result of the welding process.

Residual stresses measured by drilling hole technique for the 56-inch spirally weld pipe (Grade X65) are shown in Table 4.1, Table 4.2 and Figure 4.3 and Figure 4.4. The reported stresses are as high as the specified minimum yield strength of the X65 pipe materials which is 448 MPa (65,000 psi). The residual stress in the pipes are influenced by coil forming and by the following production steps such as the internal & external welding, cold expansion (if any) and hydrotesting. Table 4.1 shows the selected pipe for drilling hole method were these pipe joints showed compressive macro residual stresses during the ring splitting test (samples with spring-in mode during ring splitting test).

Table 4.1: Selected pipes for hole drilling method (Compressive)

	<i>Acceptable pipe</i>		<i>Unacceptable pipe</i>			
Compressive MARS	CA1	CF1	CF2	CF3	CF4	CF5
RST Gap (mm)	-64	-101	-100	-99	-93	-91
MARS (MPa)	-44.7	-70.6	-69.9	-69.2	-65.0	-63.6

Table 4.2 shows the selected pipe for hole drilling method were these pipe joints showed tensile macro residual stresses during the ring splitting test (samples with spring-out mode during ring splitting test).

Table 4.2: Selected pipes for hole drilling method (Tensile)

	<i>Acceptable pipe</i>		<i>Unacceptable pipe</i>			
Tensile MARS	TA1	TF1	TF2	TF3	TF4	TF5
RST Gap (mm)	63	141	115	104	102	101
MARS (MPa)	44.0	98.6	80.4	72.7	71.3	70.6

Table 4.3 and Figure 4.3 illustrate the microscopic residual stress data obtained in the parallel (axial) direction to the weld from spiral welded pipe with tensile ring splitting test (RST) values. A measurement of 60% of the SMYS was produced along the weld bead center. These high values of residual stresses emphasize the degree of scatter of residual stress values which was probably due to the lack of cold expansion or heat treatment. The parallel residual stresses were around 56% to 95% of SMYS measured 30 mm from the spiral weld line.

It should be noted that there is a significant difference in the stress values between the right and left side of the spiral center bead in most of the measurements for both parallel and perpendicular stress measurements. For example, the peak axial stresses occur at approximately 30 mm of the distance away from one side of the weld center line for most of the failed pipes while these stresses were low at 30 mm from the weld center line from the other side.

Table 4.3: Microscopic residual stress parallel to weld bead in spiral pipes with tensile RSTP values

Rosette ID	Distance from bead center (mm)	TA1	TF1	TF2	TF3	TF4	TF5
④	-30	319	286	141	171	153	151
①	20	287	360	333	418	361	257
⑤	15	304	356	350	427	349	310
②	0	289	274	287	267	341	253
⑥	-15	311	356	320	374	309	281
③	-20	313	384	381	393	330	266
⑦	30	261	415	387	440	396	330
RST Gap (mm)		63	141	115	104	102	101
MARS (MPa)		44	99	80	73	71	71

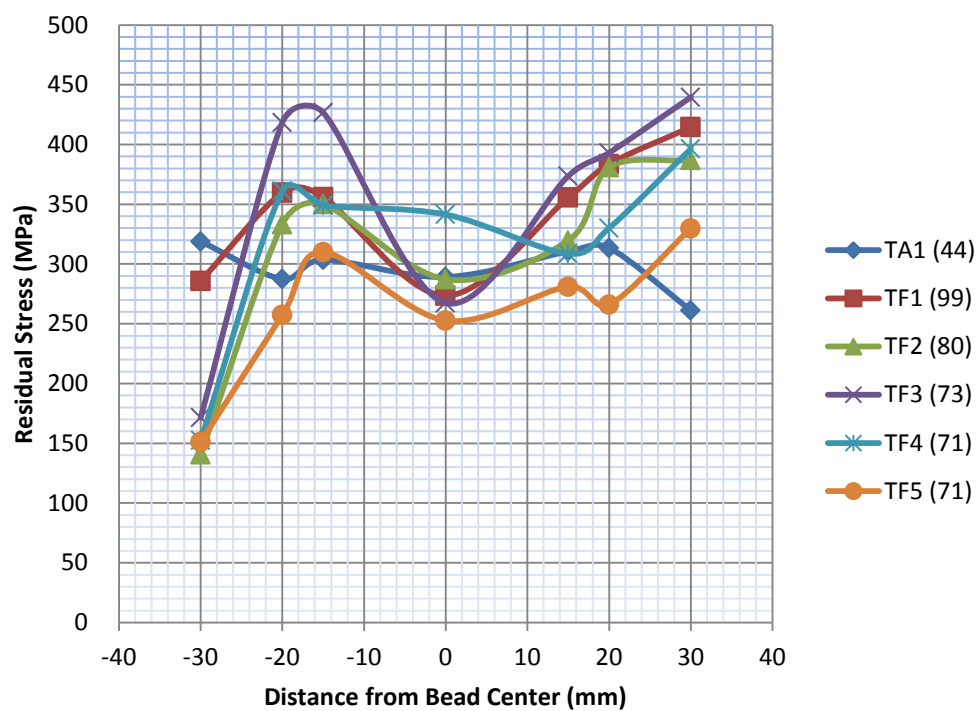


Figure 4.3: Microscopic residual stress parallel to weld bead in spiral pipes with tensile RSTP values

For the microscopic residual stress data obtained in the parallel direction to the weld from spiral welded pipe with compressive ring splitting test (RST) values, Table 4.4 and Figure 4.4 show the distribution of these stresses.

Table 4.4: Microscopic residual stress parallel to weld bead in spiral pipes with compressive RSTP values

Rosette ID	Distance from bead center (mm)	CA1	CF1	CF2	CF3	CF4	CF5
④	30	169	211	202	165	-21	158
①	20	239	339	275	294	226	178
⑤	15	245	353	259	273	236	215
②	0	246	209	313	259	203	285
⑥	-15	182	325	253	234	268	235
③	-20	211	322	259	222	257	236
⑦	-30	254	404	270	264	222	238
RST Gap (mm)		-64	-101	-100	-99	-93	-91
MARS (MPa)		-45	-71	-70	-69	-65	-64

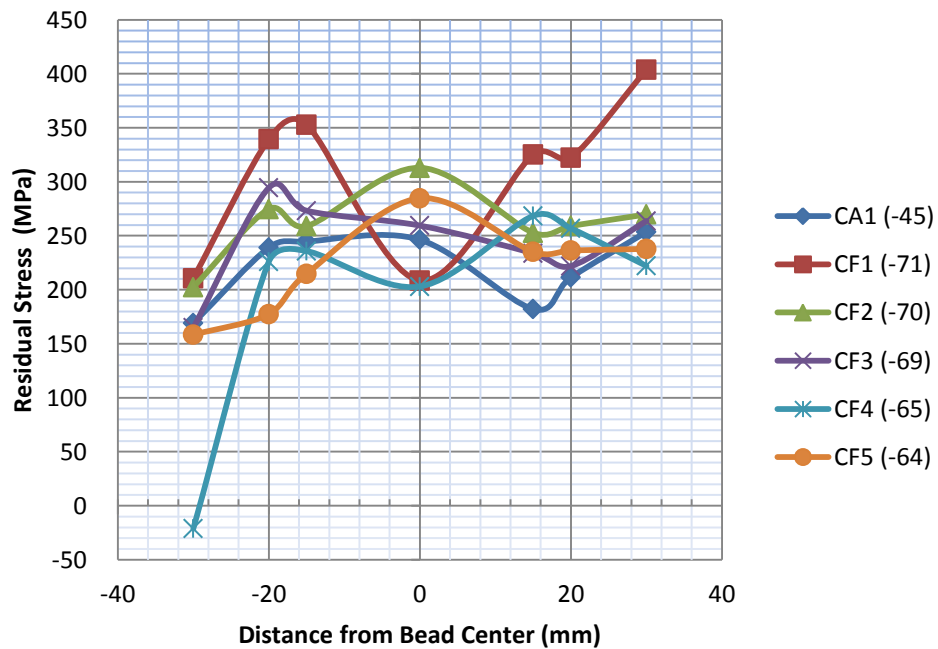


Figure 4.4: Microscopic residual stress parallel to weld bead in spiral pipes with compressive RSTP values

The perpendicular (hoop) microscopic residual stresses, for spiral pipes with tensile ring splitting test values, were low along the center of the weld bead and they were high at 15 and 20 mm far from the weld center line approaching the SMYS value of 448 MPa and exceeding it for one pipe joint as shown in Table 4.5 and Figure 4.5. The low hoop stresses in the weld (compared to those seen in the parent material) are a result of the weld contraction being restrained by the adjacent parent material, which is also heated by the weld. The weld metal yields under tensile stress. When the adjacent parent metal cools and contracts, low tensile hoop stresses are the result.

Table 4.5: Microscopic residual stress perpendicular to weld bead in spiral pipes with tensile RSTP values

Rosette ID	Distance from bead center (mm)	TA1	TF1	TF2	TF3	TF4	TF5
④	30	318	433	350	405	321	278
①	20	386	409	428	528	410	353
⑤	15	387	318	425	483	392	376
②	0	140	92	91	67	133	145
⑥	-15	411	433	352	403	272	354
③	-20	441	438	420	424	283	310
⑦	-30	418	384	393	347	368	311
RST Gap (mm)		63	141	115	104	102	101
MARS (MPa)		44	99	80	73	71	71

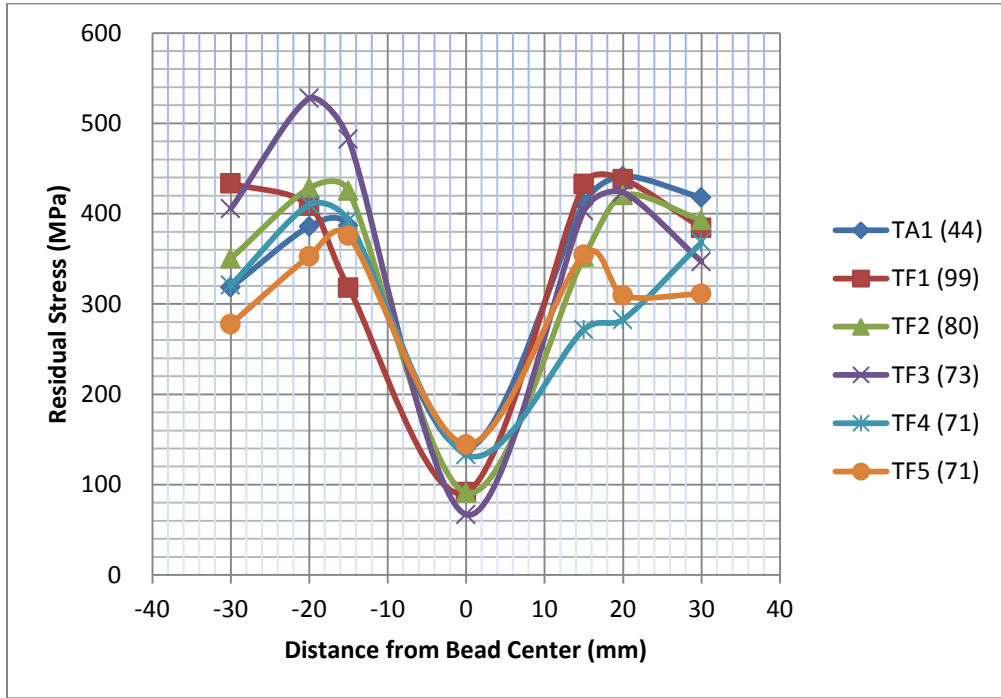


Figure 4.5: Microscopic residual stress perpendicular to weld bead in spiral pipes with tensile RSTP values

Table 4.6: Microscopic residual stress perpendicular to weld bead in spiral pipes with compressive RSTP values

Rosette ID	Distance from bead center (mm)	CA1	CF1	CF2	CF3	CF4	CF5
④	30	258	366	318	359	132	263
①	20	365	454	401	474	237	306
⑤	15	271	405	313	432	179	305
②	0	105	73	81	211	-13	122
⑥	-15	248	363	308	292	230	329
③	-20	236	329	262	280	200	329
⑦	-30	263	408	259	287	123	264
RST Gap (mm)		-64	-101	-100	-99	-93	-91
MARS (MPa)		-45	-71	-70	-69	-65	-64

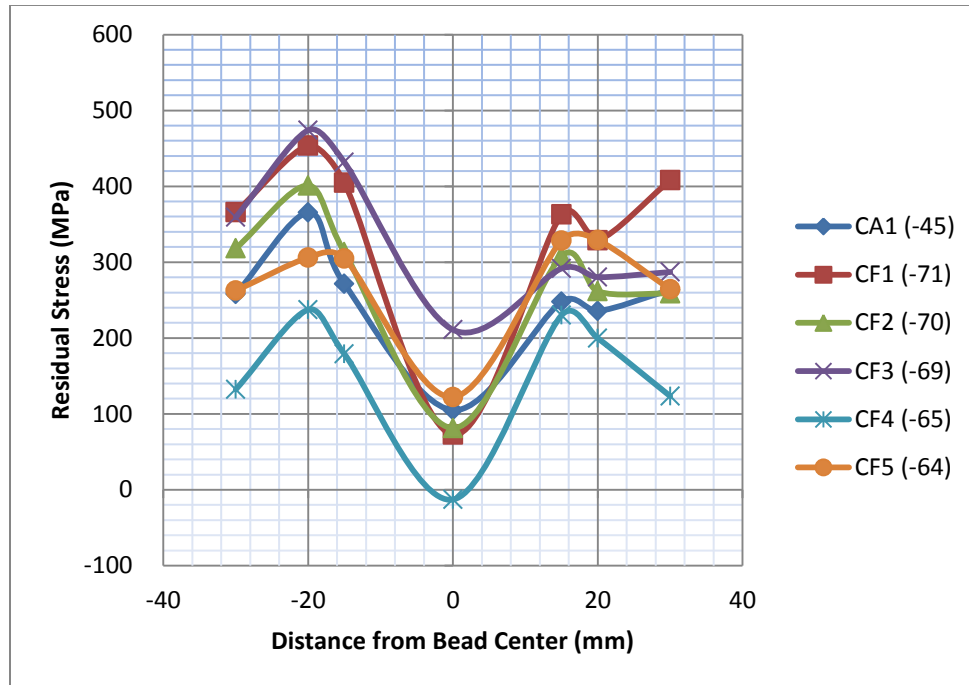


Figure 4.6: Microscopic residual stress perpendicular to weld bead in spiral pipes with compressive RSTP values

It was concluded that from the drilling hole test analysis of the previous shown results that:

- In the weld bead, large MIRS parallel to weld bead was formed and the MIRS perpendicular to weld bead was small.
- In HAZ, MIRS both parallel and perpendicular to weld bead was more than 200 MPa.
- The maximum MIRS measured in this study was around 500 MPa.
- The MIRS values in acceptable pipes were much the same as unacceptable pipes.

- The effect of MARS on MIRS is a little because the MIRS values were significantly higher than MARS values.

Results from the ring splitting test and drilling hole techniques are not expected to be identical as the ring splitting method averages the bending contribution from all residual stresses at each depth and position over the entire ring. The stresses predicted by ring splitting method are a linearized measure, while the drilling hole stresses are direct measurements at discrete locations. The measured maximum stress values by drilling hole technique are higher than those calculated from the ring splitting method. It is important to re-emphasize that this stress pattern is specific to this particular pipe (56-inch outside diameter with 22.22 mm wall thickness) and should not be misconstrued to represent a generalized result for spiral weld pipe.

CHAPTER 5

FINITE ELEMENT ANALYSIS: 3D MODELING

5.1 OVERVIEW OF MODELING AND FINITE ELEMENT SIMULATION

Weld modeling is aimed at relating processing conditions to the structure and properties of weldments, thereby defining optimum welding conditions. Such models ultimately will provide welding engineers with the means to obtain highest quality welds through process control. The accuracy of model prediction of micro-structural and property changes in welds depends on the accuracy of defined boundary conditions of heat transfer and stress analyses. The rapid growth in weld-modeling research is a result of more readily available computer facilities, software packages, and computational fluid mechanics. In addition, this growth is stimulated by an industrial need for consistently higher quality welds produced by automated operations. Advanced structural integrity assessment of structures containing welds implies the use of numerical methods for welding residual stress assessment and subsequent life assessment analysis. This may be required by the need to reduce the conservatism of residual stress evaluation when using simplified assumptions or bounding profiles or by the lack of provisions of assessment procedures for certain geometries or considered materials.

There is a growing trend towards the use of advanced finite element (FE) systems for modeling the generation of residual stresses and material phenomena during welding. This fact yields also an improvement of structural integrity assessment procedures. The use of finite element analysis (FEA) in pipe manufacturing industry to optimize the tool design, manufacturing processes parameters and finally the performance of the pipe product is advancing at higher pace. The current applications of the FEA in piercing, drawing, extrusion, bending, roll forming, welding are very common. There is no doubt that industry cannot survive without the computer-based simulation and optimization of some of the key manufacturing processes with which it is working. As commercial finite element codes have become increasingly available, the use of some of the general-purpose codes for residual stress analysis has become highly desirable. This is mainly because residual stress analysis procedures based on commercial codes can be readily transferred to industrial applications. Therefore, finite element modeling is an excellent numerical technique that can predict the values of the residual stresses that a pipe contained. Modeling of welding process is a highly multi-physics problem. The phenomenon of arc welding is described by the flow of electrons between anode and cathode by applying the electromagnetic field. The arc initiates because of the flow of electrons between cathode and anode. The shielding gas plays a key role in ionization.

The heat input supplied by the welding arc produces complex thermal cycles in the weldment and these, in turn, cause changes in the microstructure of the heat-affected

zone. The high heat concentration is necessary because metallic materials diffuse the heat and cause transient, inhomogeneous thermal stress and metal movement. The transient temperature field causes thermal expansion, stress and strain that usually plastically deforms in the weld neighborhood and results in residual stress and strain that remains when the weldment cools and the structure is distorted from its original shape. Numerical simulation of residual stresses due to welding need to accurately take account of the interactions between heat transfer, metallurgical transformations and mechanical fields. The phenomena involved in the heat input such as arc, material/laser interactions as well as fluid dynamics in the weld pool are not accurately described. From the thermo-mechanical point of view, the heat input can be seen as a volumetric or surface energy distribution, and the fluid flow effect, which leads to homogenize the temperature in the molten area, can be simply taken into account by increasing the thermal conductivity over the fusion temperature.

The main phenomena identified in a welding process can be summarized as follows:

a) Heat input;

- Amount of added welding material per unit time;
- Heat generated by the welding process;
- Speed of the welding machine; and
- Number of welding passes.

b) Heat flow;

- Latent heat;

- Heat lost by convection and radiation;
 - Heat conducted in the welded structure.
- c) Solidification;
- Temperature change in the weld during phase change.
- d) Microstructure changing; and
- Volumetric change of the material during cooling
- e) Plastic deformation and stress/strain accumulation.

In order to carry out the welding simulation, the multi-physics problem is reduced to coupled thermo-mechanical models. Welding analysis has to consider three main coupled fields, which interact more or less with each other's as shown in Figure 5.1.

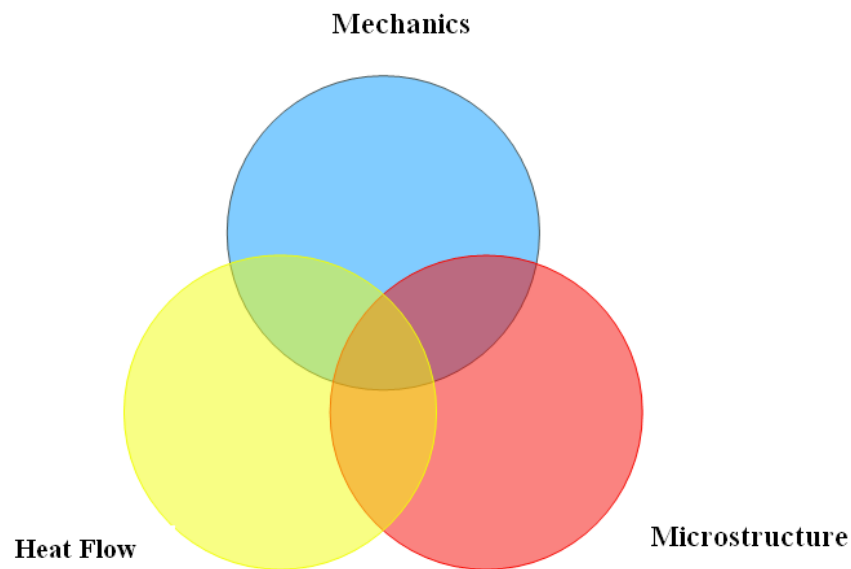


Figure 5.1: Coupling between different fields

There are currently no models that integrate all these phenomena together with the deformation behavior of the welded component. In this thesis, the mechanical effect of welding induced residual stress was calculated utilizing the thermal and mechanical coupling only. The field of microstructure can be accounted for by more or less sophisticated techniques for material modeling. Nowadays, the finite element method (FEM) is the most used tool for solving this kind of problems to predict temperature fields, residual stresses and deformation due to welding in 2- & 3-dimension. Because there is a weak coupling from mechanics to heat flow (heat generation by deformation can be neglected), the most used approach is a sequentially coupled thermal and mechanical analysis, unless the structure deformation during welding significantly changes thermal boundary conditions. This approach gives also the possibility for the use of general purpose finite element computer codes. Accurate and reliable residual stress predictions are essential for structural integrity and fatigue assessment of components containing residual stresses. However, finite element simulation of residual stresses due to welding involves in general many phenomena e.g. non-linear temperature dependent material behavior, 3D nature of the weld pool and the welding processes and microstructural phase transformation. Despite the simplification by excluding various effects, welding simulations are still CPU time-demanding and complex. Hence, simplified welding simulation procedures are required in order to reduce the complexity and thus maintain the accuracy of the residual stress predictions. Figure 5.2 shows the simulation scheme and coupling fields in welding analysis used in this thesis.

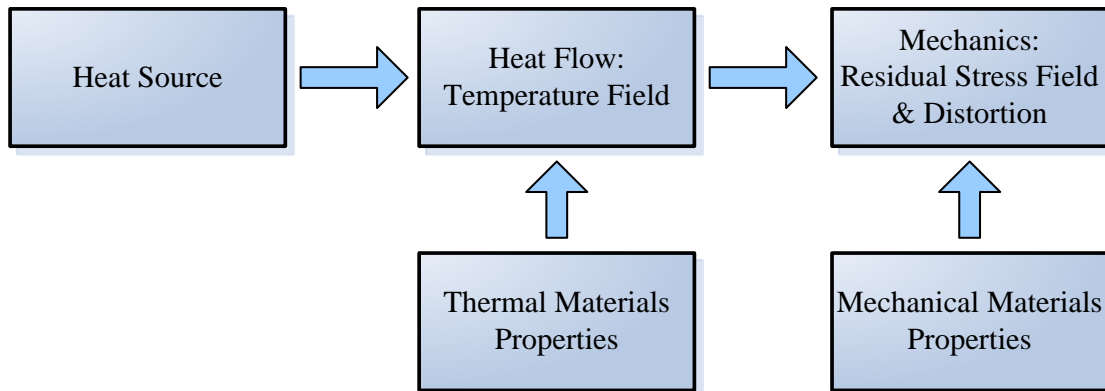


Figure 5.2: Simulation scheme in welding analysis

The basis of the finite element technique (to tackle the thermal elastic–plastic problem) is to change the nonlinearity relation of the stress and strain into a linear one during the loading process. The external force does not have any effect on welding. But loading is due to the change in temperature. The procedure to tackle this problem is to calculate the increment of the load with change in temperature then add up these to the structural elements. The flow diagram of the program is shown in Figure 5.3. First, a transient heat transfer analysis is performed, determining the temperature history in all nodes. Then, a static mechanical analysis is performed, having as loading the temperature field previously determined. Each step of the mechanical analysis corresponds to a time step in the thermal analysis.

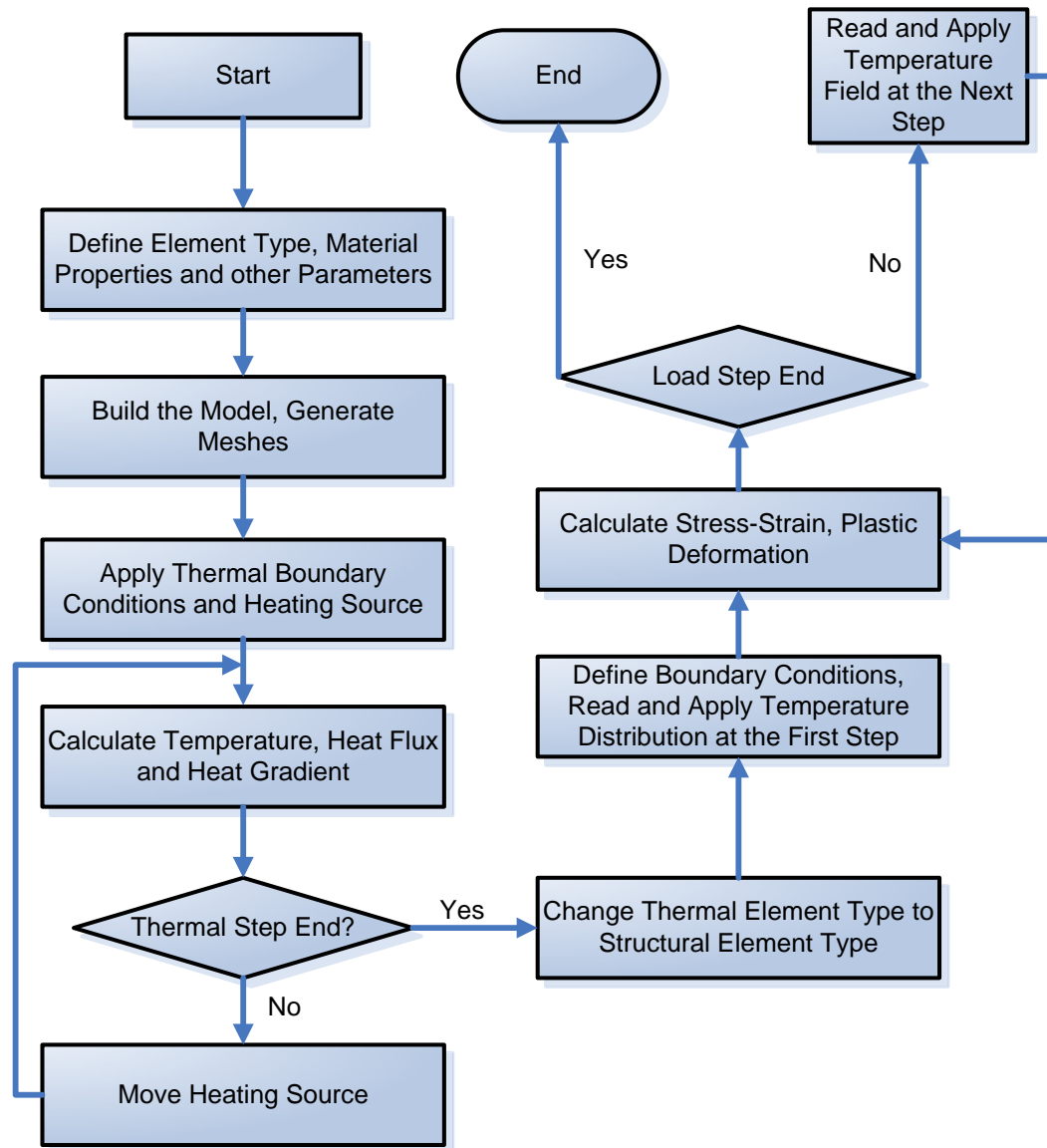


Figure 5.3: Algorithm of thermo-structural analysis

5.2 IDEALIZATION OF THE FINITE ELEMENT MODEL

Prediction of weld residual stresses foremost relies on accurate prediction of the weld thermal cycle. Two types of heat flow occur: Two-dimensional (thin wall thickness) and three dimensional (Thick wall thickness) are considered. The heat flow is sketched in

Figure 5.4 and Figure 5.5.

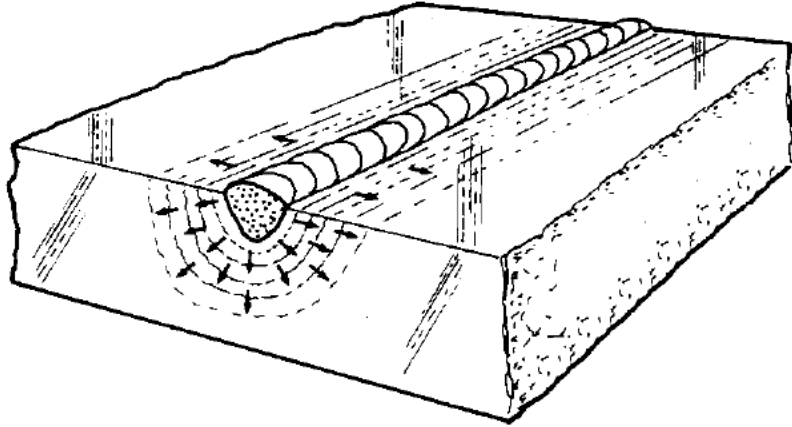


Figure 5.4: Scheme of 3D heat flow [Sorenson 1999]

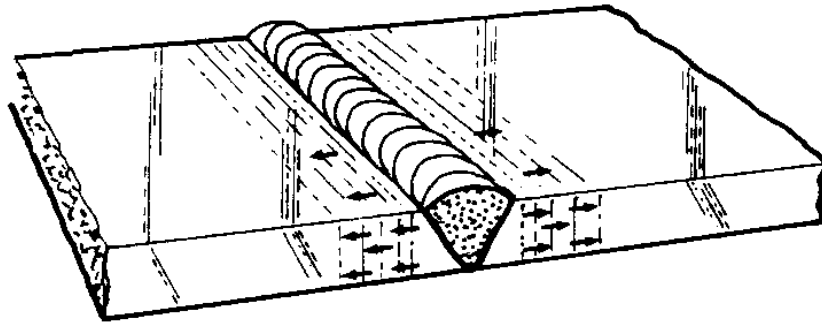


Figure 5.5: Scheme of 2D heat flow [Sorenson 1999]

In general, it can be stated that regions with high temperatures i.e. adjacent to the heat source should be calculated by a 3D solution, and the far field could be approximated by 2D heat flow solutions. Some 2-D predictions of residual stresses for materials exhibiting phase transformations show extremely large differences with experimental measurements. This discrepancy is attributed to the use of the plane strain condition in which plane sections remain planar.

However, full three-dimensional (3D) models contain more information than the two-dimensional (2D) ones, because structures normally experience responses in all three dimensions. Of course such three dimensional (3D) models can only represent a small portion of a structure due to the required CPU time.

In this thesis work, a nonlinear, transient, 3-D analysis of the spiral welding process was adopted since it is essential for practical problems and can provide accurate residual stress results that cannot be obtained from 2-D simulations. Moreover, temperature-dependent thermal properties were assumed, therefore non-linear equations were solved, with all complexity related to their solutions. This assumption was made observing that the temperature changes (gradients) encountered in the heat-affected-zone is so large that the change of thermal properties could not be neglected. To evaluate residual stress distributions, the thermal analysis was performed first in order to find nodal temperatures as a function of time. Once defined temperature history for each node, temperature nodal temperature loads were applied to the structural model.

5.3 FEM ANALYSIS TYPE

Most of the welding processes are based on a local heating of manufacturing parts up to melting temperature and then cooling them down. The temperature distribution is highly non-uniform both in spatial co-ordinates and in time. This non-uniform heating is a reason causing residual stresses and/or deformations in a welded structure. It can be

seen that the stress/displacement solution is significantly dependent on a temperature field. From this concept, ANSYS also has a special module, which is so called a coupled-field analysis, used to solve a combination of analyses from different engineering disciplines (physical fields) that interact to solve a global engineering problem. When the input of one field analysis depends on the results from another analysis, the analyses are coupled. Load transfer coupled analysis (One-way coupling analysis): if the stress/displacement is dependent on a temperature field but there is no inverse dependency, a sequentially coupled thermal-stress analysis can be conducted. In the other words, the temperature field introduces thermal strains in the structural field, but the structural strains generally do not affect the temperature distribution. Thus, there is no need to iterate between the two field solutions. Thermal-stress analysis is performed by first solving the pure heat transfer problem (thermal analysis), and then nodal temperatures from the thermal analysis are applied as "body force" loads by using in the LDREAD command in ANSYS specification in subsequent stress analysis. This kind of analysis was involved in the models used in this thesis work. A fully coupled analysis (Two-way coupling analysis) is used when the thermal and structural analyses affect each other strongly. It may not be advantageous, in thermal-stress problem, to use this approach because it is complicated procedure and time consuming procedure.

5.4 ELEMENT TYPES (THERMAL & STRUCTURAL)

After defining the analysis type, next step is selecting compatible element types across physic environments used to calculate the thermal-stress problem in welding process. In this study, the elements called SOLID70 and SOLID45 were selected for load transfer coupled analysis in the thermal and structural analyses, respectively. The reason for this selection is due to the fact that such elements maintain a consistent base geometry which is the most important factor to reach a precise result.

SOLID70 has a 3-D thermal conduction capability. The element has eight nodes with a single degree of freedom, temperature, at each node. The element is applicable to a 3-D, steady-state or transient thermal analysis. The element also can compensate for mass transport heat flow from a constant velocity field. If the model containing the conducting solid element is also to be analyzed structurally, the element should be replaced by an equivalent structural element such as SOLID45. An option exists that allows the element to model nonlinear steady-state fluid flow through a porous medium. With this option, the thermal parameters are interpreted as analogous fluid flow parameters. For example, the temperature degree of freedom becomes equivalent to a pressure degree of freedom. The geometry, node locations, and the coordinate system for this element are shown in Figure 5.6.

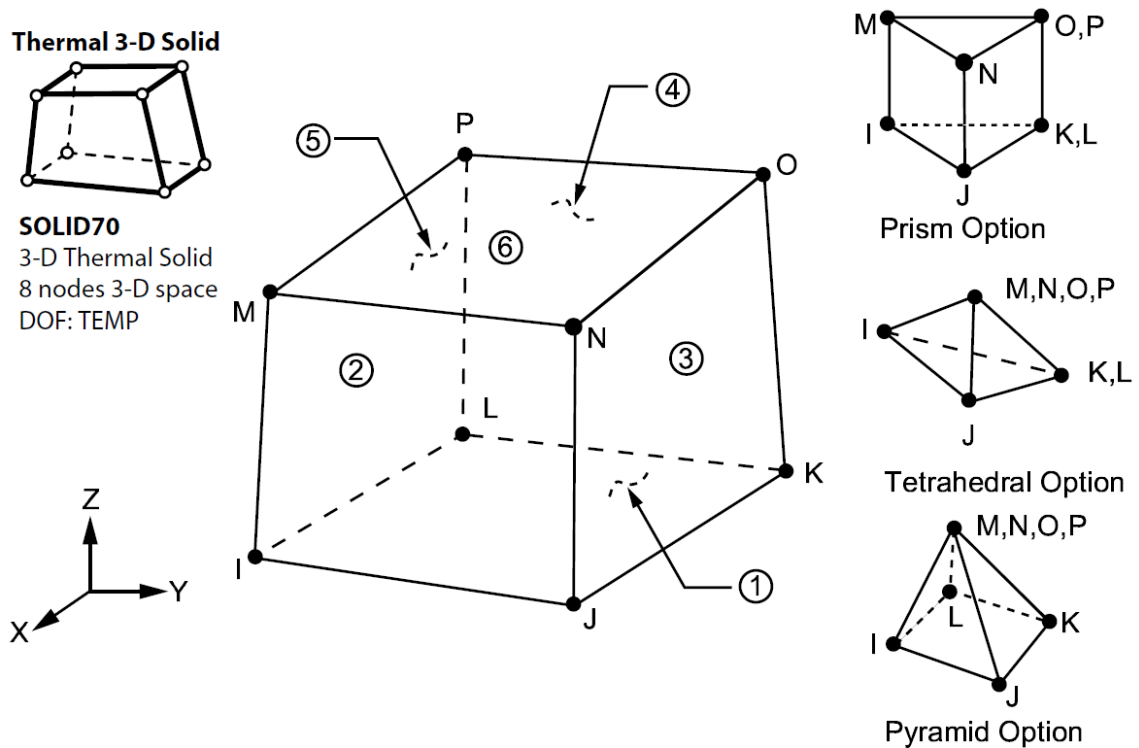


Figure 5.6: SOLID70, 3D thermal solid element [ANSYS 2007]

SOLID70 element is defined by eight nodes and the orthotropic material properties. Orthotropic material directions correspond to the element coordinate directions. Specific heat and density are ignored for steady-state solutions. Convection or heat flux (but not both) and radiation may be input as surface loads at the element faces as shown by the circled numbers in the Figure 5.6. Heat generation rates may be input as element body loads at the nodes. Convection heat flux is positive out of the element; applied heat flux is positive into the element.

For the structural analysis, SOLID45 element was used which has a large deformation capabilities and extra displacement shapes. SOLID45 is used for the 3-D

modeling of solid structures. The element is defined by eight nodes having three degrees of freedom at each node: translations in the nodal x, y, and z directions. The element has plasticity, creep, swelling, stress stiffening, large deflection, and large strain capabilities. The geometry, node locations, and the coordinate system for this element are shown in Figure 5.7. The element is defined by eight nodes and the orthotropic material properties. Orthotropic material directions correspond to the element coordinate directions.

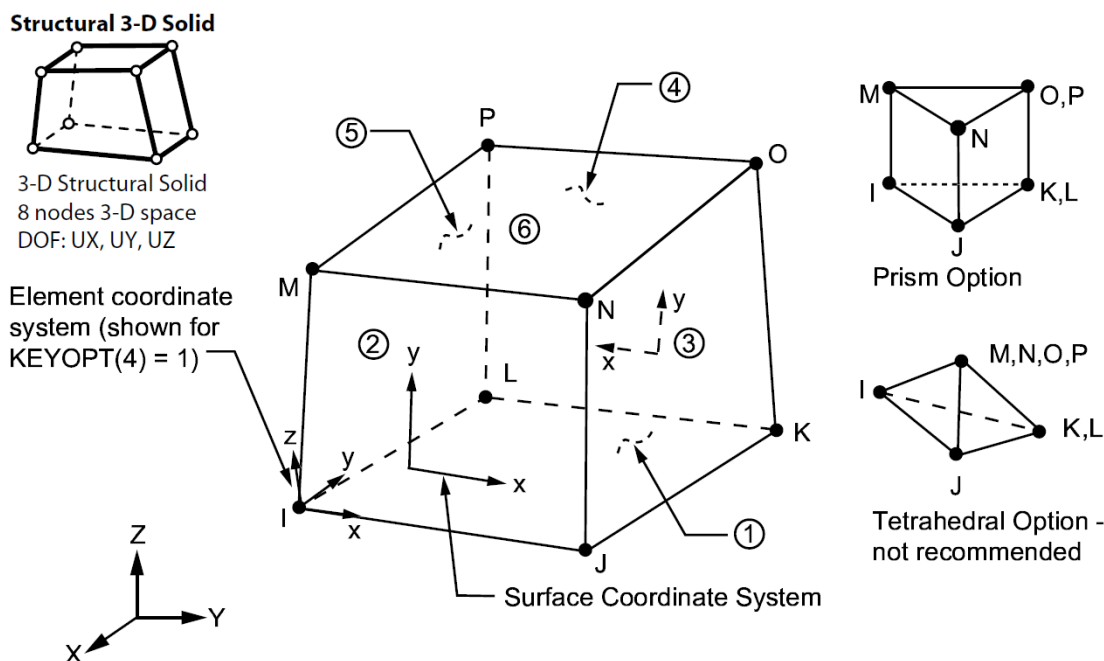


Figure 5.7: SOLID45, 3D structural solid element [ANSYS 2007]

5.5 MATERIAL PROPERTIES (THERMAL & MECHANICAL)

Most element types require material properties. Depending on the application, material properties can be linear or nonlinear. As with element types and real constants, each set of material properties has a material reference number. The table of material

reference numbers versus material property sets is called the material table. Within one analysis, you may have multiple material property sets (to correspond with multiple materials used in the model). ANSYS identifies each set with a unique reference number. Linear material properties can be constant or temperature-dependent, and isotropic or orthotropic. Nonlinear material properties are usually tabular data, such as plasticity data (stress-strain curves for different hardening laws), magnetic field data (B-H curves), creep data, swelling data, hyperelastic material data, etc. The thermal material characteristic values are in reality temperature-dependent and not constant, the extent of the change varying according to the kind of material. When the values of thermal properties are treated as variables that change with the temperature, the analysis becomes non-linear and the mathematical analysis becomes extremely complex. The phase change during heating and cooling of typical low-alloy steels also has an influence on accurate modeling of the temperature field and the residual stress formation. It is evident that the material model needs to represent the real material behavior with sufficient accuracy.

Material properties are divided in two groups; the temperature-dependent thermo-physical properties (thermal conductivity, enthalpy and density) used for the thermal analysis and the temperature-dependent mechanical properties (thermal expansion, Young's modulus, Poisson's ratio and yield stress) used for the coupled thermo-mechanical analysis. The metal adjacent to a weld is exposed to rapid thermal cycles and often undergoes changes in microstructure when it is subjected to elevated temperatures. These phase changes in turn influence the thermal properties, making them time- as well

as temperature-dependent. The microstructure and hardness of the heat-affected zone depend upon the cooling rate, and this rate is influenced by various factors including pipe wall thickness, welding conditions, preheat, the length of the weld, joint geometry, etc. The heat distribution during welding is governed by material constants such as the density, the enthalpy, the thermal conductivity and the surface transmission coefficient. In this thesis work, temperature-dependent thermo-physical properties were assumed to be the same for both parent and weld materials. Density, young's modulus, thermal conductivity, enthalpy, poisson's ratio, coefficient of thermal expansion and reference temperatures (ANSYS support up to 6 temperatures, using TB command to define non-linear properties) for different temperatures have been gathered from literature for carbon steel pipes. These thermo-physical parameters change with the change in temperature.

Mild steel is the most common structural material for welded pipes. The Melting temperature (solidus to liquidus) is in the range of 1435 to 1500 degree C (1735 to 1800 K). The temperature-dependent thermal properties of mild steel used for the heat transfer and temperature distribution calculations are shown in Table 5.1 and Table 5.2.

Table 5.1: Temperature-dependent thermal conductivity of mild steel [Mahapatra et al. 2006]

<i>Temperature (K)</i>	273	373	573	723	823	873	993	1073	1783	1853
<i>Thermal Conductivities (W/m.K)</i>	51.9	51.1	46.1	41.05	37.5	35.6	30.64	26	29.7	31

Table 5.2: Temperature-dependent enthalpy properties used for mild steel

<i>Temperature (K)</i>	<i>300</i>	<i>1,640</i>	<i>1,809</i>	<i>3000</i>
<i>Enthalpy (J/m³)</i>	<i>0</i>	<i>5.02E+09</i>	<i>7.12E+09</i>	<i>1.12E+10</i>

During the welding process, mechanical properties change as a function of the temperature. The main mechanical properties are Young's modulus, yield strength and Poisson's ratio. These properties can change drastically at temperatures as low as 500°C-600°C (773 to 873 K). Mechanical properties of the mild steel used for the simulation are given as follows:

- The density of carbon steel pipe used in the program is 7800 Kg/m³.
- Mechanical properties are shown in Table 5.3. Young's modulus and yield stress are given small, finite values at high temperatures to avoid difficulties with numerical convergence.

Table 5.3: Temperature-dependent mechanical properties of mild steel [Mahapatra et al. 2006]

Temperature (K)	Yield Stress, σ_y (MPa)	Young's Modulus, E (GPa)	Poisson's Ratios	Thermal Expansion Coefficient, α (1/°C)
273	290.0	200.0	0.2786	1.0E-05
373	260.0	200.0	0.3095	1.1E-05
573	200.0	200.0	0.3310	1.2E-05
723	150.0	150.0	0.3380	1.3E-05
823	120.0	110.0	0.3575	1.4E-05
873	110.0	88.0	0.3738	1.4E-05
993	9.8	20.0	0.3738	1.4E-05
1073	9.8	20.0	0.4238	1.4E-05
1473	2.0	20.0	0.4538	1.5E-05
1783	2.0	2.0	0.4738	1.5E-05
1853	1.0	0.2	0.4990	1.5E-05

In order to define the non-linearity of the material with increase in temperature in ANSYS, TB command is used with BISO. BISO is the bilinear isotropic hardening using von Mises. The material behavior is described by a bilinear stress-strain curve starting at the origin with positive stress and strain values. This behavior is defined by the elastic modulus E , Poisson's ratio ν , the yield strength σ_Y , and the tangent modulus G . The initial slope of the curve is taken as the elastic modulus of the material. At the specified yield stress, the curve continues along the second slope defined by the tangent modulus. It is possible to define up to six (for six temperature values) stress-strain curves, which is not sufficient to describe all the changes of the temperature-dependent material properties in detail. Consequently, some tradeoff is necessary to define the best approximation avoiding possible ill-behavior of the solution process and thus facilitating convergence.

5.6 GEOMETRICAL MODELING

The general purpose FE package ANSYS is used for both the thermal and stress analyses performed sequentially with an appropriate combination of elements as described before. The main features of the 3D model are the moving heat input, the heat loss, the temperature-dependent material properties, and the application of ANSYS parametric design language (APDL) to model the moving heat source and adaptive boundary conditions. In the current 3D thermo-mechanical FE model, all non-linearities associated with welding, such as the moving heat source, temperature- dependent

material properties, and others, were taken into account in order to simulate the real-life spiral welding process for pipes. The FEA work scope includes:

1. Geometrical modeling of 56-inch spiral welded pipe.
2. Materials modeling.
3. Weld modeling, assuming that the modeled geometry (pipe) is already spirally formed (Figure 5.8).
4. Heat source modeling.
5. Analysis of the weld residual stresses.
6. Studying the effects of varying the welding speed on the temperature distributions and residual stress level.

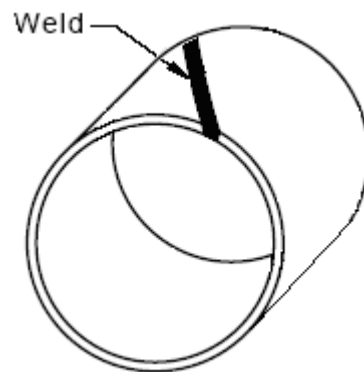


Figure 5.8: Pipe geometric that will be modeled

Building a finite element model requires more time than any other part of the analysis. First, a job name and analysis title is specified. Then, PREP7 preprocessor is used to define the element types, element real constants, material properties, and the

model geometry. The ANSYS program does not assume a system of units for analysis. Except in magnetic field analyses, any system of units can be used so long as units are consistent for all input data. Using the /UNITS command, a marker can be set in the ANSYS database indicating the system of units being used. This command does not convert data from one system of units to another; it simply serves as a record for subsequent reviews of the analysis. In this thesis work, the SI “International System” (m, kg, s, K,..) was considered.

The simulations were carried out for a pipe with a dimension of 56-inch in diameter. The simulated pipe piece was fabricated from carbon steel materials. It was formed by spiral wrapping nominally 0.875-inch (22.22 mm) thick coil (1400 mm in width) to form a 14 helix angle which was then butt-welded. The finite element model for the spiral welded pipe is shown in Figure 5.9. The length of the simulated pipe is 5.9-inch (150 mm) and the nominal diameter is 56-inch (1422 mm).

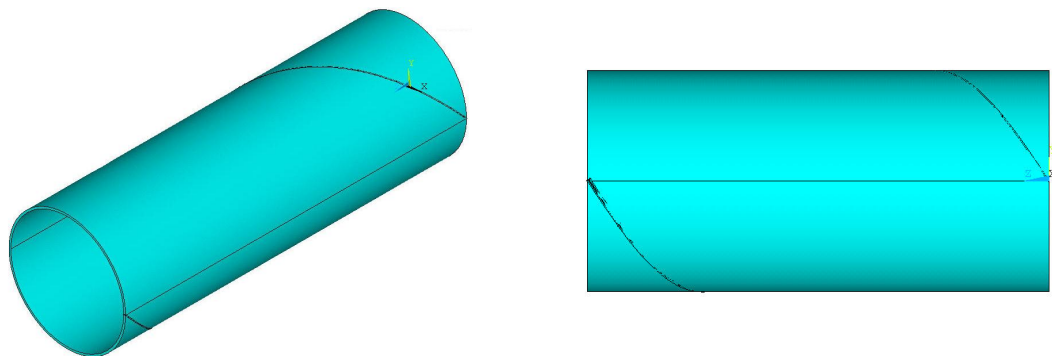


Figure 5.9: 3D model of 56-inch spiral welded pipe for one complete pitch

Control of weld-bead shape is essential as the mechanical properties of welds are affected by the weld-bead shape. Therefore, it is clear that precise selection of the process parameters is necessary. The weld joint dimensions were taken from the welding data sheet of the 56-inch spiral welded pipe. The geometry of the weld considered in this study is shown in Figure 5.10.

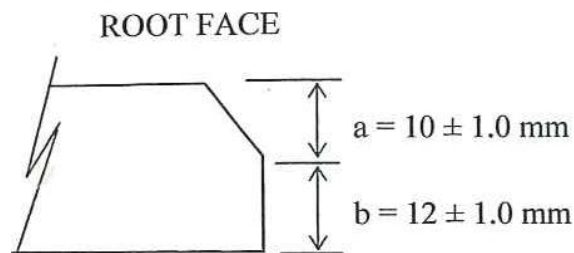


Figure 5.10: Geometry of 56-inch weld joint

Figure 5.11 shows the spiral welding of this type of weld joint type.

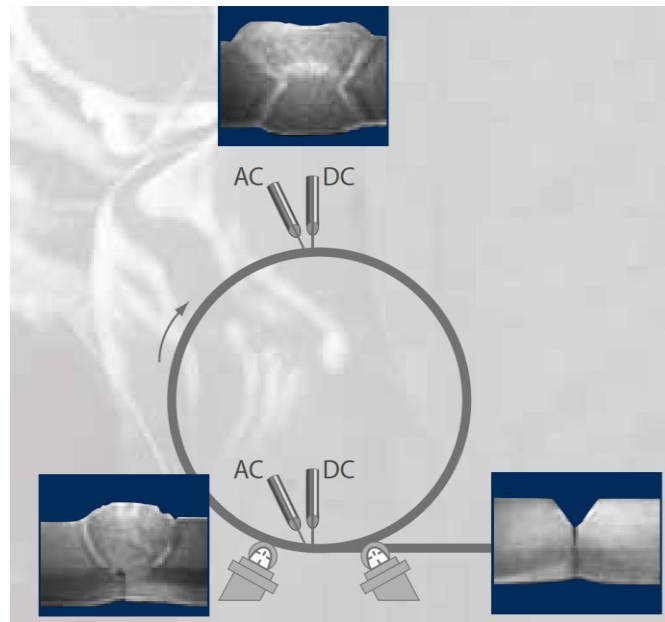


Figure 5.11: Spiral welding of the weld joint

The cylindrical coordinate system was adopted to build the geometrical Model. The distance from the axis is called the radial distance or radius (X-coordinate), while the angular coordinate is referred to as the angular position (Y-coordinate). The third coordinate is called the axial (horizontal) direction (Z-coordinate). A spiral weld path can be described by the global cylindrical coordinate system whose origin coincides with the curve passing through the pipe's cross section center. This spiral line is characterized by the pitch length, pipe diameter (D) and forming angle (α). Figure 5.12 represents, schematically, a weld joint model dragged over a spiral weld line with a pitch (P) $= \pi D \times \tan \alpha$ and pipe diameter (D).

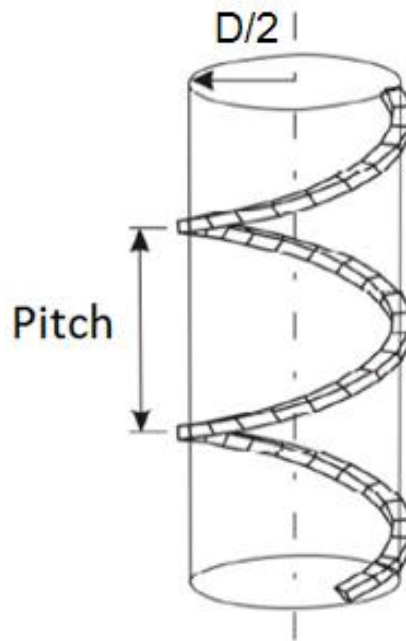


Figure 5.12: Basic concept for weld spiral path

The spiral weld path is defined by n discrete points equally positioned along the spiral path (Figure 5.13). The x , y , z points are created to cover only the 150 mm pipe section which represent the ring. To generate the weld path, the weld joint model

developed before is revolved (dragged) along a spiral weld path. The code, that was developed to create these points for spiral welds path and then creating the line, is shown in Figure 5.14.

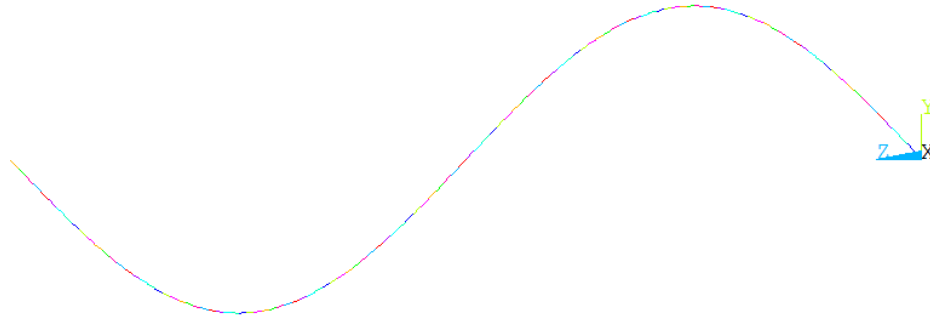


Figure 5.13: Spiral weld line (path) for one complete pitch

```

!***** Creating spiral Line *****
CSYS,1
beta= 200e-3/Pitch
DZ=Pitch/Ndiv
DY=Tangle/Ndiv

*DO, I, 1, (beta*Ndiv)+1
      X1=RO
      Y1=(I-1)*DY
      Z1=(I-1)*DZ
      K,I+200,X1,Y1,Z1
*ENDDO

*DO, I, 1, beta*Ndiv
      L,I+200,I+201
*ENDDO

FLST,2,41,4,ORDE,2
FITEM,2,1
FITEM,2,-41
LCOMB,P51X, ,0

```

Figure 5.14: Spiral weld path code

After creating the weld joints areas and the spiral line, dragging has been performed in order to create the weld volume. The final model for the 56-inch spiral welded ring is shown in Figure 5.15.

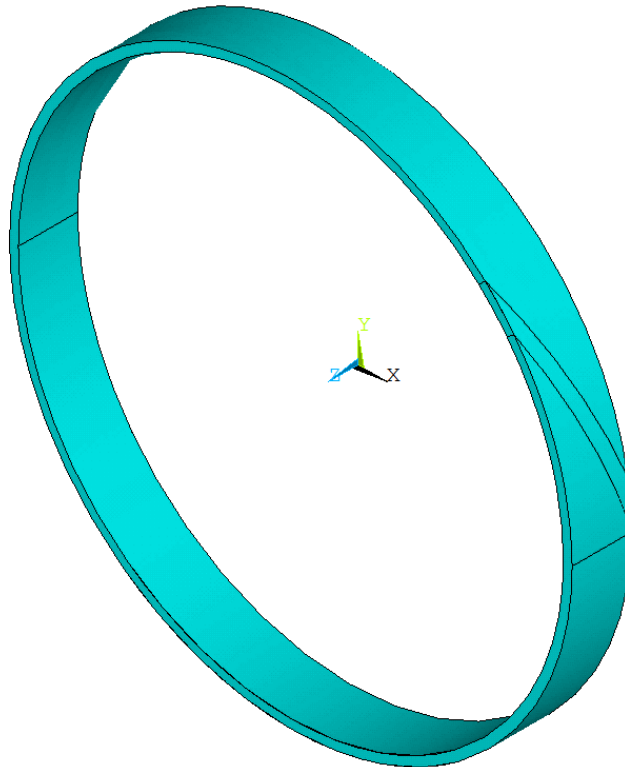


Figure 5.15: Final model of the ring

5.7 FINITE ELEMENT MESH

Once the material properties are defined and the model was created, the next step is to generate the elements by meshing the model. There are two methods to create the finite element model: solid modeling and direct generation. With solid modeling, once the geometric shape of the model is described, then the ANSYS program automatically

meshes the geometry with nodes and elements. Size and shape of the elements that the program creates can be controlled by the user. "Manually" defined several convenient operations, such as copying patterns of existing nodes and elements, symmetry reflection, etc. are available in ANSYS. Before meshing the model, and even before building the model, it is important to think about whether a free mesh or a mapped mesh is appropriate for the analysis (Figure 5.16).

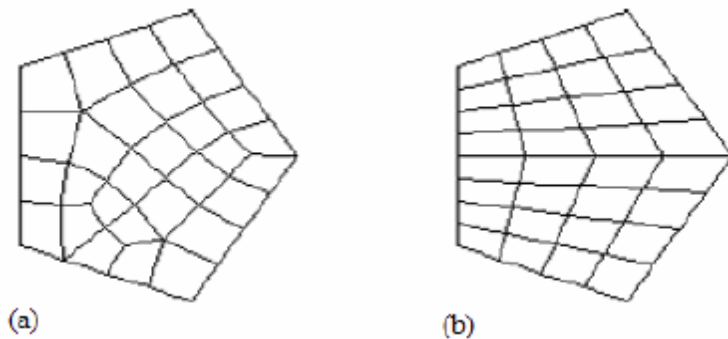


Figure 5.16: (a) Free meshing (b) Mapped meshing [ANSYS 2007]

A free mesh has no restrictions in terms of element shapes, and has no specified pattern applied to it. Compared to a free mesh, a mapped mesh is restricted in terms of the element shape it contains and the pattern of the mesh. A mapped area mesh contains either only quadrilateral or only triangular elements, while a mapped volume mesh contains only hexahedron elements. In addition, a mapped mesh typically has a regular pattern, with obvious rows of elements. To use mapped meshing, the geometry has to be built as a series of fairly regular volumes and/or areas that can accept a mapped mesh.

Since the shape of weld path (spiral) along the pipe does not have regular pattern, a free mesh was adopted in this thesis work for 56-inch spiral welded pipe. The meshes used for both simulations (thermal and structural) are the same, and they are shown in Figure 5.17. Element size increases progressively with distance from the weld centerline. Table 5.4 shows the number of nodes and elements for the modeled volumes.

Table 5.4: Meshing details

<i>Volume#</i>	<i>No. of Nodes</i>	<i>No. of Elements</i>
1	24527	185124
2	4838	56495

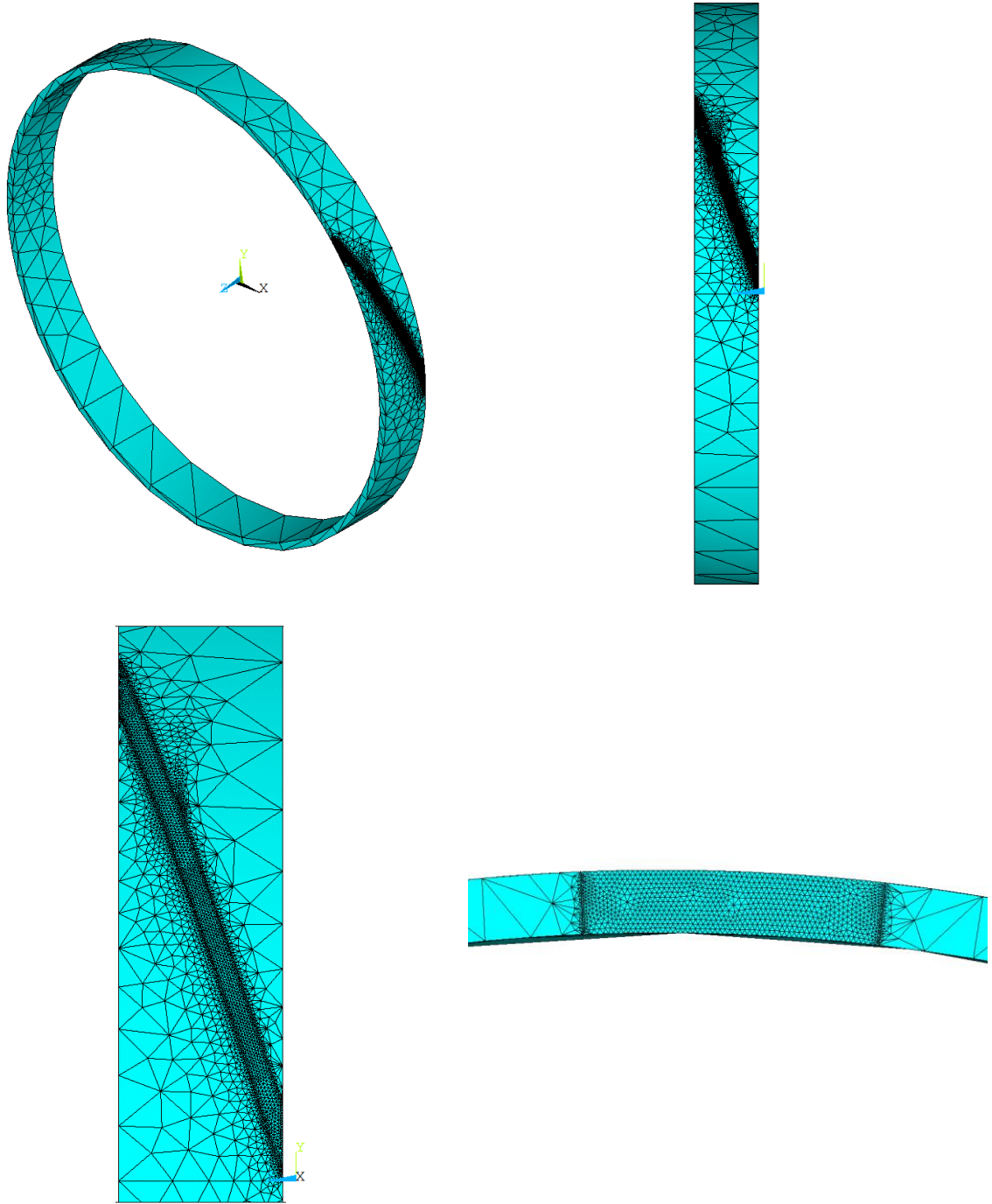


Figure 5.17: Finite element mesh of the ring model

CHAPTER 6

THERMAL ANALYSIS USING FINITE ELEMENT METHOD

6.1 OVERVIEW OF HEAT TRANSFER ANALYSIS

To determine the thermal field during the welding process, two different analyses are required, namely heat conduction and thermal analyses. The most significant factors affecting both analyses are the heat input rate, the moving speed of the heat source and the thickness of the base material. One of the fundamental problems in the analysis of heat flow during welding is how to take into account physical material changes due to temperature changes during the welding process. The fundamental behavior of heat conduction is that a flux, Q (W/m^2), of energy flows from a hot region to cooler regions, linearly dependent on the temperature gradient, ∇T . The non-linear isotropic Fourier heat flux constitutive equation 6.1 is employed:

$$Q = -k\nabla T \quad (6.1)$$

where

k is the thermal conductivity of the material and

$$\nabla = \left(\frac{\partial}{\partial x}, \frac{\partial}{\partial y}, \frac{\partial}{\partial z} \right) \quad (6.2)$$

It should be noted that the minus sign (-) is necessary in order to make Q positive, because heat is always transferred in the direction of decreasing temperature. The energy required to change the temperature of the materials is defined by specific heat c or enthalpy H. The conservation of energy is expressed in a differential form having the terms for specific heat, thermal flux and a distributed volume heat-source term Q (W/m³) and it is given as:

$$\rho c T = Q''' + \nabla(k \nabla T) \quad (6.3)$$

or

$$\rho \frac{\partial c T}{\partial t} = Q + \frac{\partial(k_x \frac{\partial T}{\partial x})}{\partial x} + \frac{\partial(k_y \frac{\partial T}{\partial y})}{\partial y} + \frac{\partial(k_z \frac{\partial T}{\partial z})}{\partial z} \quad (6.4)$$

Where c is the specific heat, k thermal conductivity, T temperature, Q is the external heat input per unit volume and t is time. If the material properties are considered temperature independent the equation (specific heat and thermal conductivity do not change with temperature) is reduced to a linear differential equation (6.5).

$$\rho c \frac{\partial T}{\partial t} = Q + k \left(\frac{\partial(\frac{\partial T}{\partial x})}{\partial x} + \frac{\partial(\frac{\partial T}{\partial y})}{\partial y} + \frac{\partial(\frac{\partial T}{\partial z})}{\partial z} \right) \quad (6.5)$$

There are losses from the pipe surfaces in the form of convection and radiation. Therefore, to evaluate the amount of heat, Q [J], absorbed by the pipe as a portion of the total heat generated the following formula (equation 6.6) was used.

$$Q = \eta V I \quad (6.6)$$

Where η is arc efficiency, V is the voltage and I the current.

Convection losses (heat flow q [J/s]) are evaluated using the equation 6.7:

$$q = h(T - T_{\infty}) \quad (6.7)$$

Where h is the film convection coefficient, T is the pipe temperature and T_{∞} is the ambient temperature. Heat losses due to radiation in welding are taken into account by the heat efficiency η which depends on the welding process.

Figure 6.1 shows a schematic model of the temperature distribution when a surface weld bead is being deposited at a speed v . The colored bands represent isothermal areas.

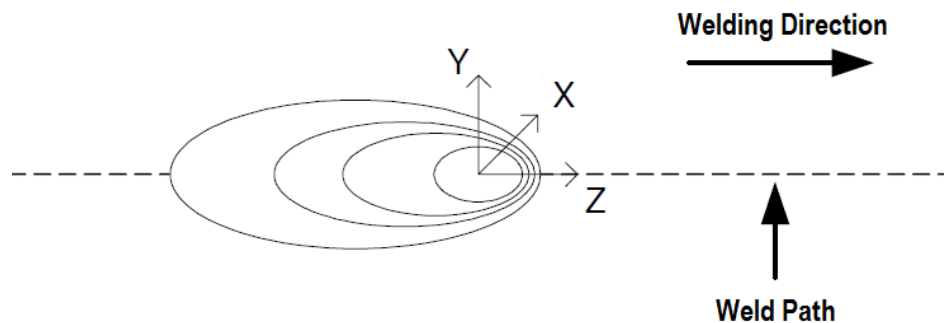


Figure 6.1: Schematic of the welding thermal model

The heating in the welding process involves three stages, sketched in Figure 6.2:

1. A transient stage at which the temperature around the heat source is still rising, often called the initiation stage.
2. The quasi-stationary stage at which the temperature distribution is stationary in a co-ordinate system moving with the heat source.

3. A second transient stage at which the temperature decrease after the welding arc is extinguished.

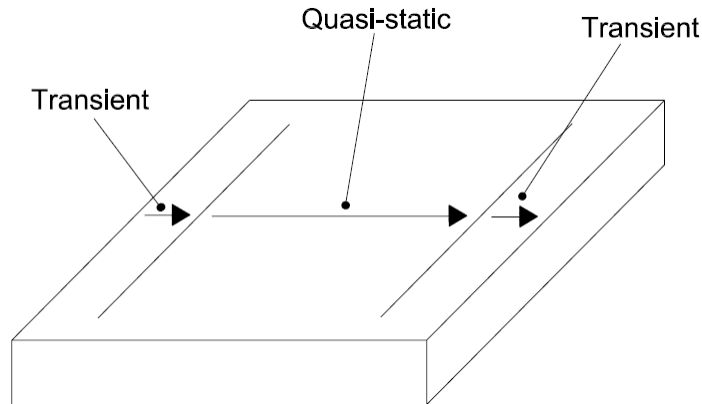


Figure 6.2: The three stages in the welding time problem

The majority of the thermal expansion and shrinkage in the base material and in the HAZ occurs at the quasi-stationary stage.

6.2 HEAT SOURCE MODELING FOR SPIRAL WELDED PIPE

Heat generation in welding is based on the concept of instantaneous heat sources. From the literature review, it is noticed that a lot of researches are in progress to define reliable heat source for the welding processes. Knowledge of the heat transfer from the welding source to the base material is essential for determination of the molten pool or bead shape and the subsequent solidification pattern. The heat source model developed by Goldak is used in this thesis research, which distributes the heat throughout the

volume of the molten zone. The heat source is modeled as a distributed heat flux depending on the arc spread observed during experiments by varying the electrode diameter, current, voltage, and rate of travel of the electrode. The Goldak heat source model is defined spatially by a double ellipsoid as is shown in Figure 6.3. The front half of the source is the quadrant of one ellipsoidal source, and the rear half is the quadrant of a second ellipsoidal source. Precise heat source modeling is the key to get the accurate results. The power density distribution is assumed to be Gaussian along the weld path.

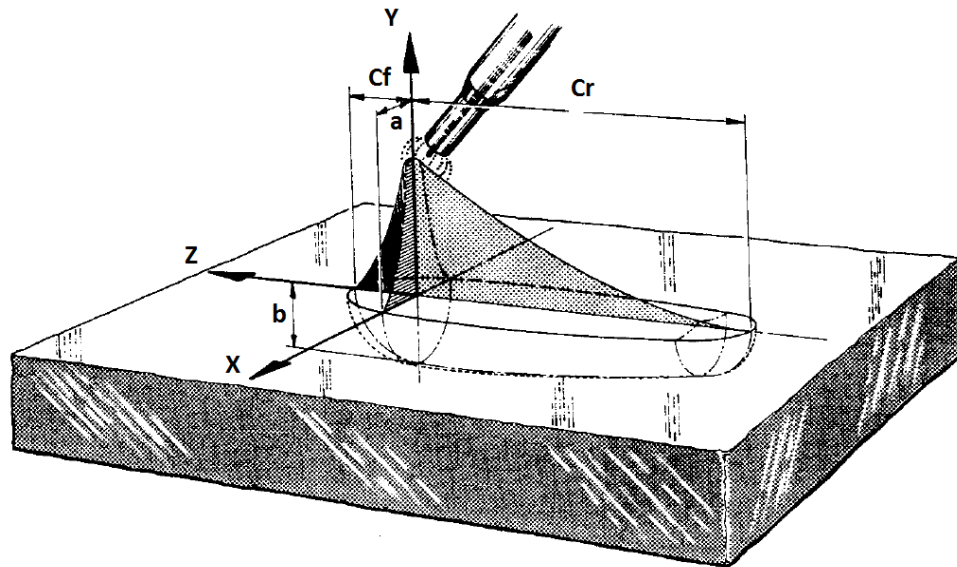


Figure 6.3: Double ellipsoidal heat input distribution (W/m^3) [Sorenson 1999]

The double ellipsoid geometry is used so that the size and shape of the heat source can be easily changed to model both the shallow penetration arc welding processes and the deeper penetration laser and electron beam processes. The size and the shape of the "double ellipsoid" are determined by its semi-axes. It is centered at the origin of the heat source. The double ellipse consists of two separate ellipses, one in the front quadrant and

the other in the rear quadrant. The hatched surface describes the one dimensional flux along the z-axis. Four characteristic lengths must be determined which physically correspond to the radial dimensions of the molten zone. The geometrical constants must be chosen so that the heat distribution describes the two most important zones correctly, namely the FZ (Fusion Zone) and the HAZ (Heat Affected Zone). If the cross-section of the molten zone is known from experiment, this information can be used to set the heat source dimensions. Though a first starting guess can be, if there are experimental values available, to set the variable “a” to the same value as the FZ. To set the other variables experience and “trial and error” is the only solution yet. For this reason, the welding data for 56-inch pipe was used. If precise data does not exist, Goldak et al. suggest that it is reasonable to take the distance in front of the source equal to one half the weld width ($c_f=2a$) and the distance behind the source equal to two times the weld width ($c_r=4a$). The variables a, b, c_f and c_r are geometrical constants as shown in Figure 6.3.

The heat input is defined separately over two regions; one region is the front of the arc center represented by the equation 6.8 and the other is behind the arc center represented by equation 6.9.

For $Z \geq 0$: Front Region

$$q_f(x, y, z) = \frac{6\sqrt{3}f_f Q}{abc_f \pi \sqrt{\pi}} e^{(-3\frac{x^2}{a^2})} e^{(-3\frac{y^2}{b^2})} e^{(-3\frac{z^2}{c_f^2})} \quad (6.8)$$

For $Z < 0$: Rear Region

$$q_r(x, y, z) = \frac{6\sqrt{3}f_r Q}{abc_r \pi \sqrt{\pi}} e^{(-3\frac{x^2}{a^2})} e^{(-3\frac{y^2}{b^2})} e^{(-3\frac{z^2}{c_r^2})} \quad (6.9)$$

The variable, Q is the energy input rate (W) and η is dependent on the current (I) the voltage (V) and the efficiency as follows:

$$Q = \eta VI \quad (6.10)$$

In this model, the fractions f_f ($Z > 0$) and f_r ($Z < 0$) of the heat deposited in the front and rear quadrants are needed, where

$$f_f + f_r = 2 \quad (6.11)$$

This is done because the temperature gradient in front of the heat source is steeper than in the tailing edge.

The maximum value of the power density ($\frac{6\sqrt{3}f_r Q}{abc_r \pi \sqrt{\pi}}$) is at the center of the ellipsoid when x, y and z equals zero.

Based on the FE mesh generated by the ANSYS, definitions of the welding process parameters and characteristics of the heat source transient heat fluxes representing the moving distributed heat source can be calculated on specific positions in welding areas. The heat source is assumed to move through volume and calculated heat is applied to elements as volumetric heat generation so that the elements lying on the surface can be used for modeling of surface heat convection. The mathematical expression for the double ellipsoidal power density distribution is coded directly in the APDL file to be used in the FEM program. The welding speed, the fraction values f_f , f_r , the semi-axis of Goldak heat source parameters used in the calculation are shown in Table 6.1 and they are based on the actual weld bead profile. The first thing to note is the correlation of the heat source parameters to the molten zone size is not one to one, and therefore some values (such as b) are oversized in order to get the required shape of the welding and heat affected zone. So, it was necessary to increase the ellipsoid dimensions of the heat source. This is due primarily to the interaction between the heat source power which is Gaussian along the longitudinal weld arc axis and the volume specified by the double ellipsoid dimensions as shown in Figure 6.3.

Table 6.1: Numerical values of heat source parameters used

<i>Symbol</i>	<i>Description</i>	<i>Value</i>	<i>Unit</i>
C_f	Front heat spot distance	16e-3	m
C_r	Rear heat spot distance	24e-3	m
a	Welding heat spot half width	11e-3	m
b	Welding heat spot depth	12e-3	m
f_f	Goldak front factor	0.4	--
f_r	Goldak rear factor	1.6	--
v	Welding speed	0.01917	m/sec
		1.15	m/min

Welding parameters for the 56-inch spiral welded pipe are shown in Table 6.2 for both internal and external electrodes.

Table 6.2: Welding process parameters

		Internal Welding		External Welding	
		1 st Electrode	2 nd Electrode	1 st Electrode	2 nd Electrode
Current, I	(amps)	1075 ±160	700 ±100	1050 ±150	750 ±110
Voltage, V	(volts)	27 ±2	31 ±2	29 ±2	30 ±2
Power (Watt)		50725		52950	
Welding Speed, v	(m/min)	1.15 ±0.10			

The amounts of heat generated by the internal and external electrodes are calculated per the following formulas:

$$Q_{\text{internal}} = \eta \times (V_{\text{electrode\#1}} I_{\text{electrode\#1}} + V_{\text{electrode\#2}} I_{\text{electrode\#2}}) \quad (6.12)$$

$$Q_{\text{external}} = \eta \times (V_{\text{electrode\#1}} I_{\text{electrode\#1}} + V_{\text{electrode\#2}} I_{\text{electrode\#2}}) \quad (6.13)$$

Heat input was also calculated which is a relative measure of the energy transferred per unit length of weld. It is an important characteristic because, like preheat temperature, it influences the cooling rate, which may affect the mechanical properties and metallurgical structure of the weld and the HAZ. Heat input is typically calculated as the ratio of the power (i.e., voltage x current) to the velocity of the heat source (i.e., the arc) as follows (equation 6.14):

$$\text{Heat Input} = \frac{60 \times V \times I}{1000 \times v} \quad (6.14)$$

where,

H = heat input (kJ/in or kJ/mm)

V = arc voltage (volts)

I = current (amps)

S = welding travel speed (in/min or mm/min)

This equation is useful for comparing different welding procedures for a given welding process. Heat input to the nodes under the arc is calculated by the Gaussian distribution shown in equation 6.8 and 6.9. To pick up the arc heat input completely,

there must be a certain minimum number of elements/nodes under the arc heat input during welding.

To be able to map the heat source model along the predetermined weld path, the FE-program or actually the user subroutine must know the weld arc's position, direction and the local coordinate system. A number of calculations and preparations must be performed before this information can be obtained. The origin of the coordinate system is located at the center of the moving arc and the movement of the heat source is achieved through developed user subroutine (Figure 6.4). Another user subroutine is used to calculate the centroidal distances of elements from the instantaneous position of the moving arc center. The spatial distribution of heat is calculated from equations 6.8 & 6.9 and it is applied on elements as volumetric heat generation.

```

!*****Element Counts &Centroidal Position *****
/POST1
ALLSEL,ALL
CSYS,1

*GET,NE,ELEM,0,COUNT, , ,

*DIM,ECX,ARRAY,NE,1,1, , ,
*DIM,ECY,ARRAY,NE,1,1, , ,
*DIM,ECZ,ARRAY,NE,1,1, , ,

*VGET,ECX,ELEM,1,CENT,X, ,
*VGET,ECY,ELEM,1,CENT,Y, ,
*VGET,ECZ,ELEM,1,CENT,Z, ,

ALLSEL,ALL

```

Figure 6.4: ANSYS code to get the elements centroidal positions

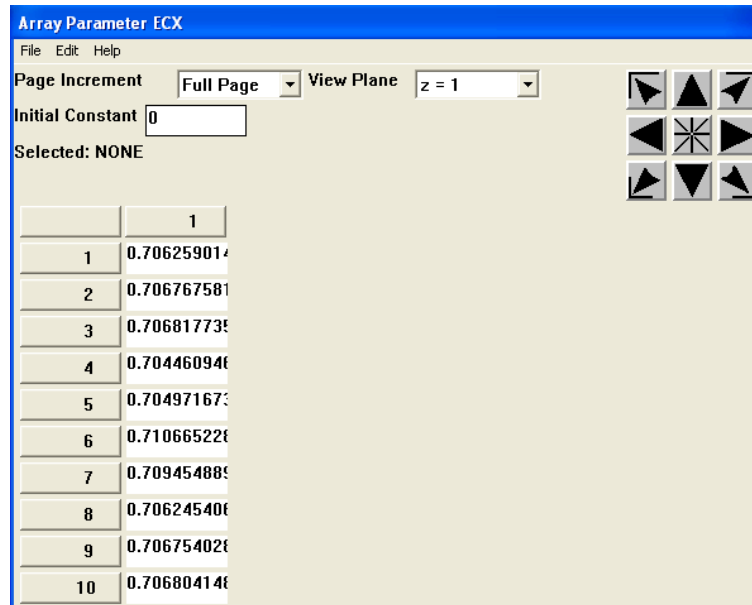


Figure 6.5: Array parameters for the elements centroidal positions in X-direction (Radial)

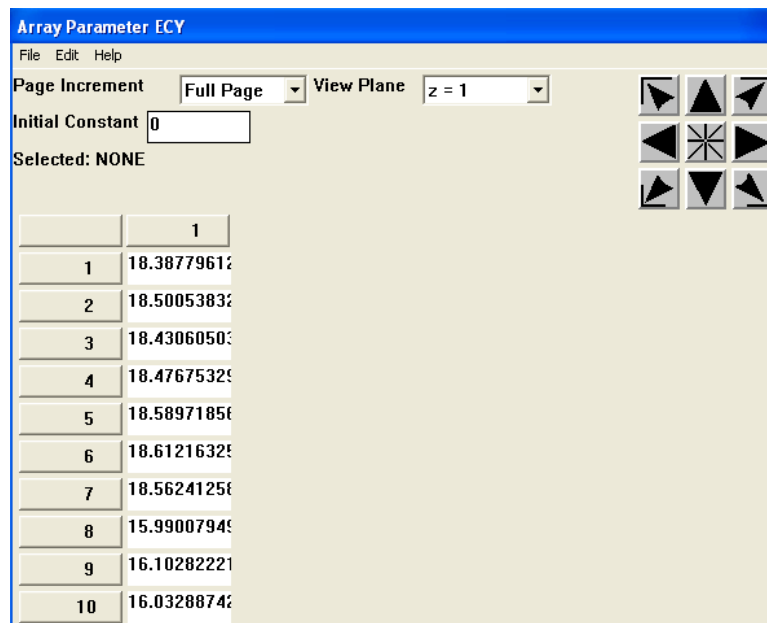


Figure 6.6: Array parameters for the elements centroidal positions in Y-direction (Angles)

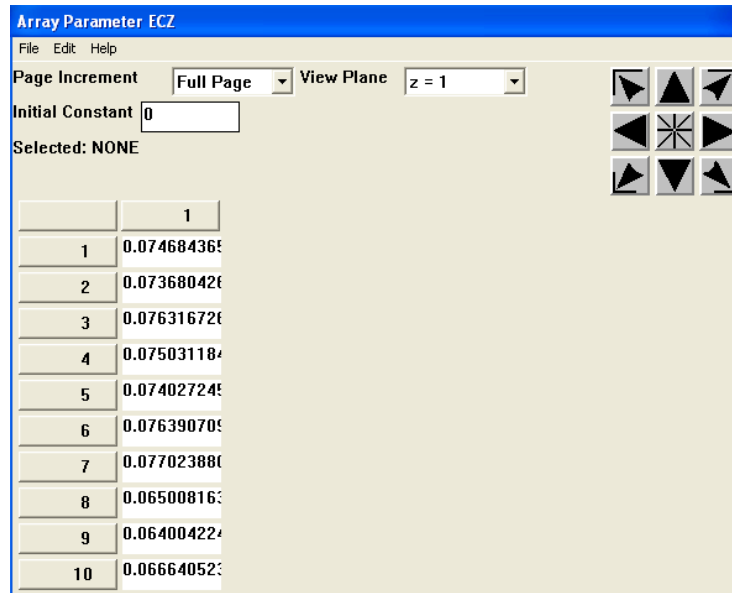


Figure 6.7: Array parameters for the elements centroidal positions in Z-direction (Axial)

Now, we will describe how the heat source was moved and a short introduction of the mapping between the local and the global coordinate system will be presented. The direction of the arc along the spiral weld path can be easily modified with the parameter α as shown in Figure 6.8. Mapping between the local and the global coordinate system for any points has been done through a user subroutine. The moving coordinate system can be defined with weld speed, time and fixed global coordinate system (X, Y, Z). The local coordinates system (x, y, z) is defined by translation and rotation transformation at location “A” which is the center of the heat source at each load step.

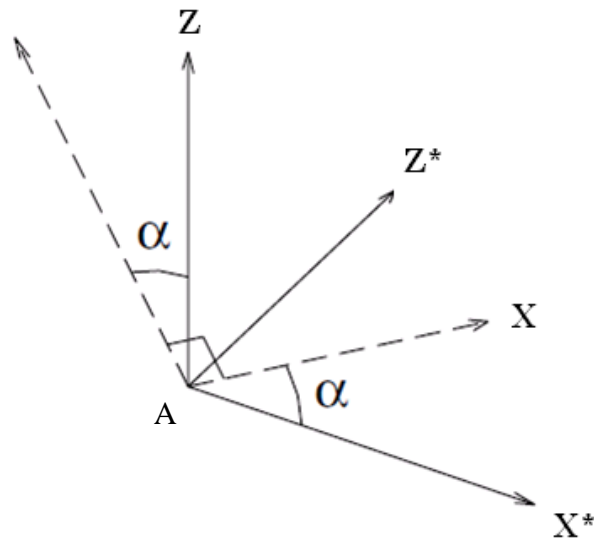


Figure 6.8: Modification of the arc's direction

$$\begin{Bmatrix} x \\ y \\ z \end{Bmatrix} = \begin{bmatrix} \cos 45 & \sin 45 & 0 \\ -\sin 45 & \cos 45 & 0 \\ 0 & 0 & 1 \end{bmatrix} \begin{Bmatrix} X - X_0 \\ Y - Y_0 \\ Z - Z_0 \end{Bmatrix} \quad (6.15)$$

Where X_0 , Y_0 , Z_0 are coordinate values of point A in the global coordinate system. The moving coordinate is fixed at the arc position. Point "C" located in the weldment can be described by two different coordinate systems. During the movement of the heat source (thermal load step), each centroidal position (gauss point: x , y , z) will be checked if it should be given any energy. In order to determine whether a gauss point is affected by the heat input, a mapping between the local and the global coordinate system has been done. In Figure 6.9, it is shown how the three gauss points, p1, p2 and p3 are mapped by adding the transformation matrix corresponding to the point. Here in this example it is only point p3 that will receive energy from the heat flux formula. The other

points, p1 and p2, are placed outside the goldak heat source model at a specific thermal load step and will therefore receive no energy.

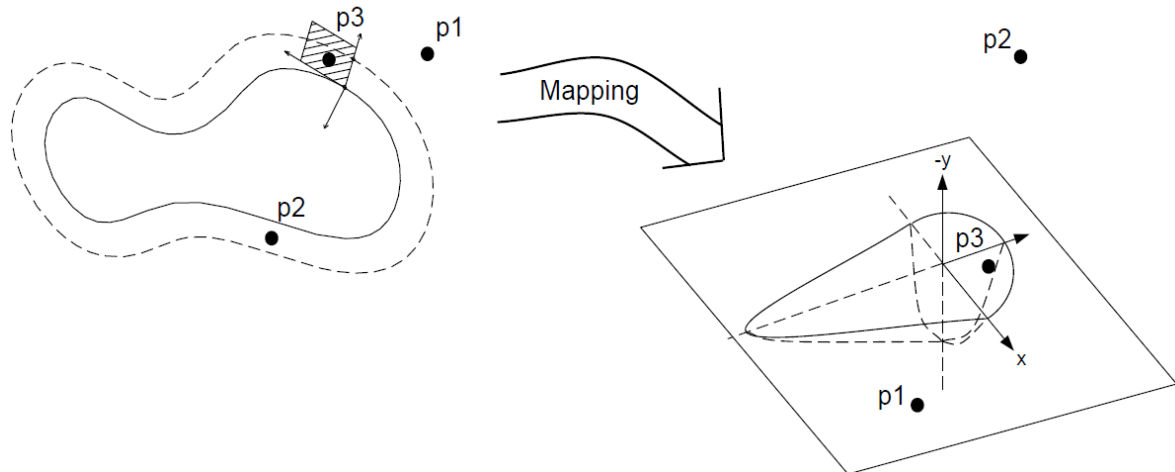


Figure 6.9: Mapping of three different gauss points from global to local coordinates

6.3 TRANSIENT NON-LINEAR THERMAL ANALYSIS PROCEDURE

The finite element analysis of the thermal elastic–plastic stress was conducted using ANSYS software. As a first step, the component was divided into several finite elements. The thermo-physical parameters were entered and the distribution of thermal field of welding was found out. The determination of stress field followed. Automatic time stepping was used for the solution of this non-linear transient heat transfer problem. A user sub-routine is used to achieve the heat source movement. The coordinate system is at the center of the heat source. To apply heat on the weld pool, a heat table is defined. A “3 plane” heat table is created with the name of “HEATGEN”. The number of rows and columns must equal to the number of elements in that particular directions. A user sub-

routine is used to calculate the coordinates of all elements in the modeled pipe geometry. In the user sub-routine to calculate the heat source, first the numerical values are defined. Equations 6.8 and 6.9 are used to find out heat. A loop is used to read the values in z-direction. “IF ELSE” command is used to apply equation 6.8 for the front side of the arc and equation 6.9 for the rare side of the arc. The following procedure was adopted for the transient non-linear thermal analysis:

1. Create a solid model.
2. Define element type which is SOLID70 in this study.
3. Define the material properties.
4. Free-mesh the model.
5. Define the convection by using room temperature of 300 K (27 °C).
6. Define the heat table and generate the heat source table.
7. Go to SOLUTION and activate
 - Transient analysis using “ANTYPE,4”
 - Full Newton Raphson method using “NROPT, Full,, ON”. During analysis (both thermal and structural), a “Full Newton–Raphson” iterative solution technique with a direct sparse matrix solver is used for obtaining the solution. During the thermal cycle, temperature, and consequently temperature-dependent material properties, changes very rapidly; thus, a Full Newton–Raphson scheme, which uses a modified material properties table and reformulated stiffness matrix after equilibrium iterations, believed to give

more accurate results than other options such as Modified or Initial Newton–Raphson schemes.

- Automatic time stepping using “AUTOTS, ON”
 - Ramped changed loads using “KBC,0”
 - 150 iterations using “NEQIT, 150”
 - Write only NSOL, RSOL, NLOAD, STRS, FGRAD, and FFLUX records to the results file and database using “OUTRES, BASIC, LAST”
8. User sub-routine for moving the heat source.
 9. Loop for element selection to distribute the heat source:

Loop is used to distribute the temperatures available in “HEATGEN” table. Refer to Figure 6.10. Temperature is maximum at point 1 (center of the arc), and it is lower at the neighbor points i.e. 2, 3, 4 and 5. The minimum temperature is at point 6. To assign the corresponding temperatures from “HEATGEN” table to different points on the weld pool, a user-subroutine is written to select the corresponding elements and assign the respective heating values to them and save it to a table.

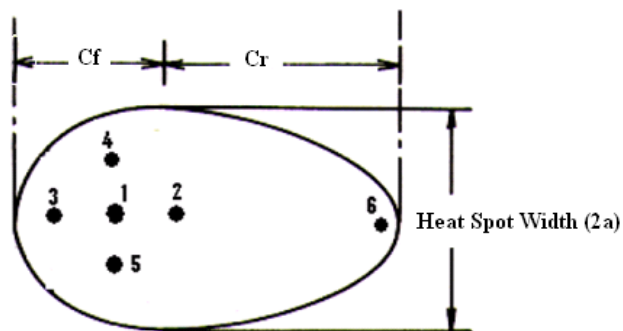


Figure 6.10: Heat distribution (heat spot top view)

10. Allow the cooling time, solve and save the results for use in structure analysis.

6.4 SOLUTION CONTROL

Extremely high heating and cooling rates – which cause extremely high gradients of thermal, micro-structural and mechanical properties - can occur in a welding process. Due to high peak temperatures, large spatial temperature gradients, and rapid temporal temperature fluctuations imposed by the weld heat source, it is necessary to have very small element sizes and consistent time steps. These gradients have to be numerically controlled by the program with reasonable time expenditure. A fine mesh to capture the spatial gradients implies a small time step. That is, it is necessary to choose a time step which is small enough to resolve these large temperature variations for a given mesh.

When transient analysis is dealt with, the determination of time steps is always difficult, and even intrinsically impossible in many cases, as the time steps depend both on the variation in time of the thermal loads applied to the model and the thermo-physical properties of the material. These considerations oblige the user to select a number of options before starting the computation and to restart the computation if convergence is not obtained, or if the resulting precision is considered insufficient. With this in mind different models have been established.

All FEM calculations were carried out to include non-linear thermal and structural properties. The temperature distribution is calculated by assuming a steady-state condition, but the problems are otherwise treated as transient. This is so, because the source itself does not change shape, only location, during welding. The dependency of the materials parameters on the temperature is illustrated in Load step options are options that can be changed from load step to load step, such as number of substeps, time at the end of a load step, and output controls.

In ANSYS, there are two important load-related terms which are load step and substep. A load step is simply a configuration of loads for which a solution is obtained. Load steps are also useful in dividing a transient load history curve into several segments. Substeps are incremental steps taken within a load step. They are mainly used for accuracy and convergence purposes in transient and nonlinear analyses. Substeps are also known as time steps - steps taken over a period of time. The ANSYS program uses the concept of time in transient analyses as well as static (or steady-state) analyses. In a transient analysis, time represents actual time, in seconds, minutes, or hours. In a static or steady-state analysis, time simply acts as a counter to identify load steps and substeps. The ANSYS program uses time as a tracking parameter in all static and transient analyses. Time simply becomes a counter that identifies load steps and substeps. By default, the program automatically assigns time = 1.0 at the end of load step 1, time = 2.0 at the end of load step 2, and so on. Any substeps within a load step will be assigned the appropriate, linearly interpolated time value.

In this thesis work, a moving cylindrical coordinate system is used to move the heat source. Instead of moving the heat source continuously, it is moved in steps, that is, heat is applied at each successive point one after the other chronologically. By making the distance between successive points very small, a close approximation to the continuous movement can be achieved. Figure 6.11 shows the unfold spiral welded pipe showing the weld path. The coordinate system is moved after each load step. At every load step a set of elements in the shape of the Goldak model are selected and a heat flux is applied on the surfaces of the elements. APDL (ANSYS parametric design language) is used to write a subroutine for a looping transient moving heat source model.

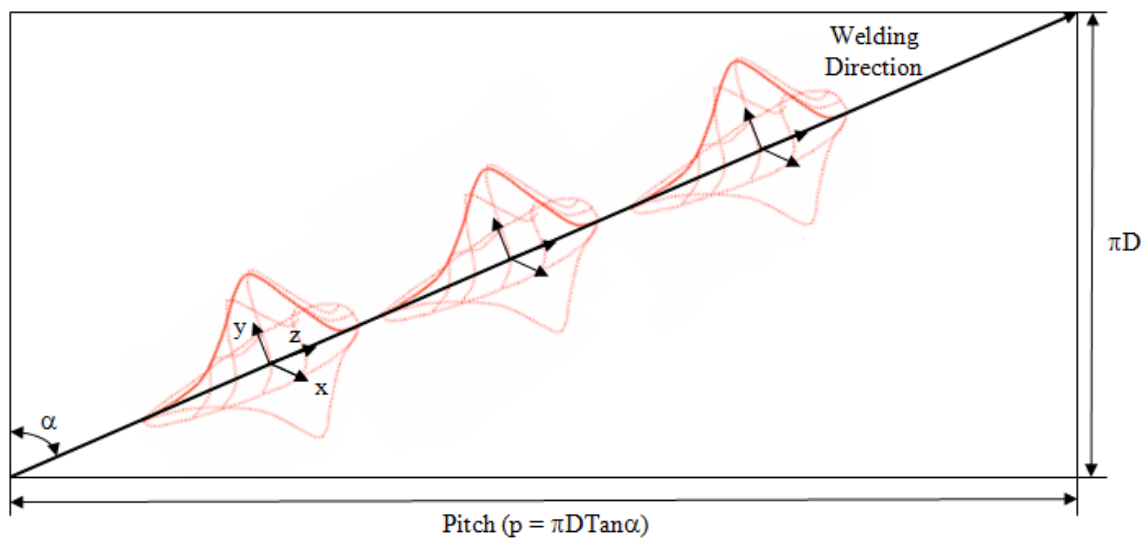


Figure 6.11: Unfolding spiral welded pipe showing the spiral line as straight line

The heat source which was defined in a local coordinate system moves with time. When the heat source moves to the next load step, the former load step is deleted. The

welding time step, which the heat source is applied in each load step, can be defined as follow:

$$\text{Welding Time Step} = \frac{\text{Segment Length}}{\text{Welding Speed}} \quad (6.16)$$

where

$$\text{Segment Length} = \frac{\text{Length of Ring Spiral Path}}{(\text{Predetermined No. of Load Step} - 1)} \quad (6.17)$$

The length of the spiral path to complete the 150-mm ring (from X to Y) as shown in Figure 6.12) was calculated as follow:

$$\text{Length of Ring Spiral Path} = \frac{\sqrt{(\pi D)^2 \times (\text{Pitch})^2} \times 150}{\text{Pitch}} \quad (6.18)$$

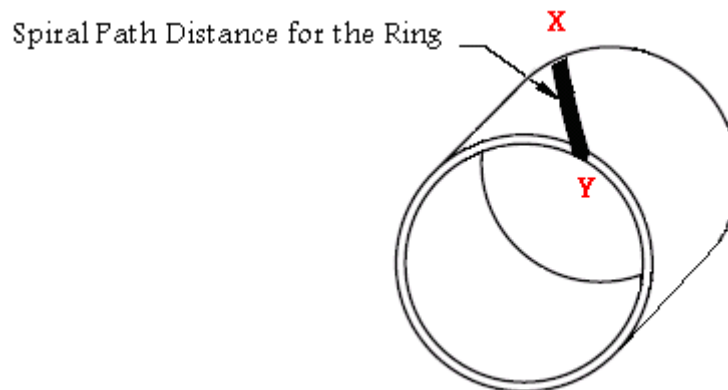


Figure 6.12: 150-mm ring spiral path (XY length)

The intermediate and final cooling time step was set to be 10 times the welding time.

$$\text{Cooling Time Step} = 10 \times \text{Welding Time Step} \quad (6.19)$$

After the first load step, the heat source moves forward to the next position in a distance of the segment length. For better computational results, the heat source is supposed to stay at least once on each element along the weld path, so that the heat input algorithm does not miss elements passed during an increment. The required time for the heat source to complete welding along a spiral path is calculated as follow for both one complete pitch and for the 150-mm ring:

$$Time_{One\ Complete\ Pitch} = \frac{\sqrt{(2\pi r)^2 \times (Pitch)^2}}{Weld\ Speed} \quad (6.20)$$

$$Time_{Ring} = \frac{\sqrt{(2\pi r)^2 \times (Pitch)^2} \times 150}{Pitch \times Weld\ Speed} \quad (6.21)$$

Moreover, the ramped load step (KBC,0) was adopted in this thesis work. In ANSYS, there are two ways for applying the loads (Stepped or Ramped). When more than one substep in a load step is specified, the question of whether the loads should be stepped or ramped arises. If a load is stepped, then its full value is applied at the first substep and stays constant for the rest of the load step, as shown in the Figure 6.13. If a

load is ramped, then its value increases gradually at each substep, with the full value occurring at the end of the load step.

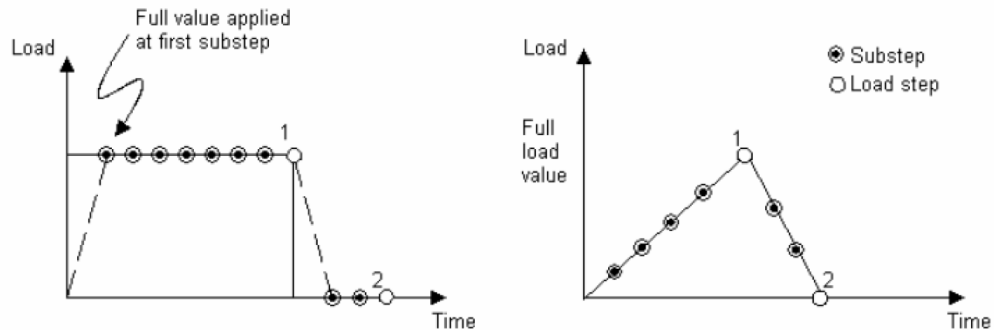


Figure 6.13: Stepped versus ramped loads [ANSYS 2007]

Once the thermal simulation is done, the data regarding the temperature distribution in the buildup structure during the process is stored to a database. That data is used in the next step (structural analysis) as the only load that is applied as the body force. The structural simulation consists of the same steps during the welding and cooling stages as in the case of the thermal simulation. So, the temperature distribution scheme from some specific load step in the thermal analysis is applied to the corresponding load step in the structural analysis.

6.5 THERMAL BOUNDARY CONDITIONS

Heat transfer coefficient for convection is only calculated and applied on all the applicable surfaces. The heat loss from the surfaces is modeled from equation 6.22.

$$q_{\text{loss}} = q_{\text{convection}} \quad (6.22)$$

$$q_{\text{loss}} = h \times A(T - T_{\infty}) \quad (6.23)$$

where A is the surface area, T is current temperature, T_{∞} is the ambient temperature and h is the thermal convection coefficient.

The heat losses by free convection were modeled by Newton's cooling law. Boundary conditions were applied to all free surfaces of the pipe. The surfaces exposed to the environment were subjected to the same convective boundary conditions, using an average heat transfer convection coefficient of $h = 200 \text{ W/m}^2\cdot\text{K}$ to ambient air. The ambient temperature for both parent and weld metal was set at 300 K which is equal to the room temperature. The heat transfer coefficient is the thermal equivalent of an elastic constraint. This is a condition which is normally applied to a surface of the elements. Because of its nature, this condition can be defined either as a constraint or as a load (temperature) in ANSYS. In transient analysis the convective heat transfer is applied as a surface-load. The ANSYS command "SF" is used for applying surface load and "CONV" is used to represent type of surface load.

6.6 VALIDATION OF THE FEM THERMAL MODEL

In order to validate the model before discussing the results of the thermal analysis and then proceeding with the thermo-mechanical analysis of welding, the first step is to

match the FEM predicted temperature with the actual, because it is applied as thermal load in the subsequent structural analysis for stresses calculations. In order to validate the thermal model, several samples from the 56-inch Spiral Welded Pipe underwent destructive metallurgical evaluation in order to document the weld characteristics. The extraction location of the Metallographic Specimen is shown in Figure 6.14.

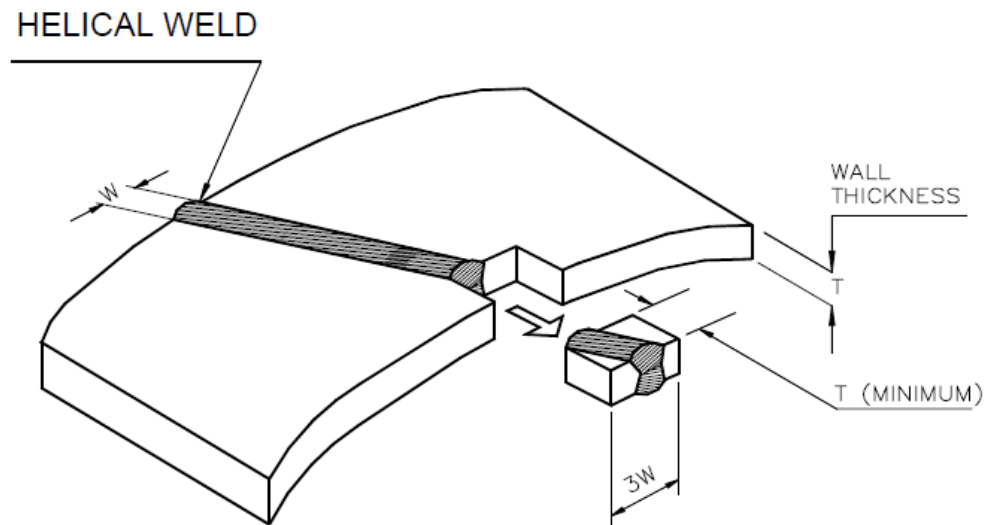


Figure 6.14: Metallographic specimen extraction location

The spiral welded specimen was cut and the weld section was polished and chemically etched as shown in Figure 6.15 to reveal liquidus isotherms (1773 K) and outer HAZ isotherms (1173 K).

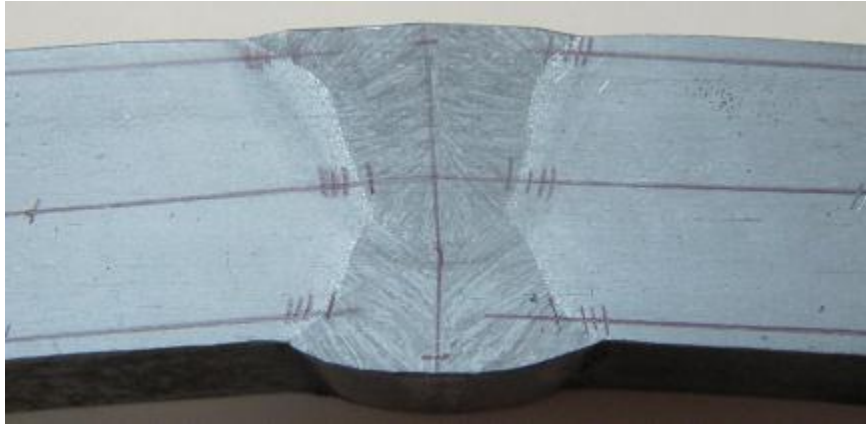


Figure 6.15: Cross Section showing the macrograph of the spiral weld joint

This evaluation included cross-sectioning the weld. The cross-sections were mounted and measured for overall size of weld, fusion zone (FZ) size, and heat affected zone (HAZ) size in x and y directions. In general, welded joint consists out of a molten pool zone, a fusion zone (FZ) and a heat affected zone (HAZ). The heat-affected zone (HAZ) is the portion of the base material that was not melted but whose properties (and, usually, structure) were altered by the heat of welding through some phase transformation or reaction.

In this study a peak temperature 1173 K is defined as the temperature at which the structure and properties of the base mild steel material are altered by some metallurgical transformation, and then the HAZ width is determined by the temperature profile. Figure 6.16 shows a schematic for the inner and outer weld beads with the weld zones

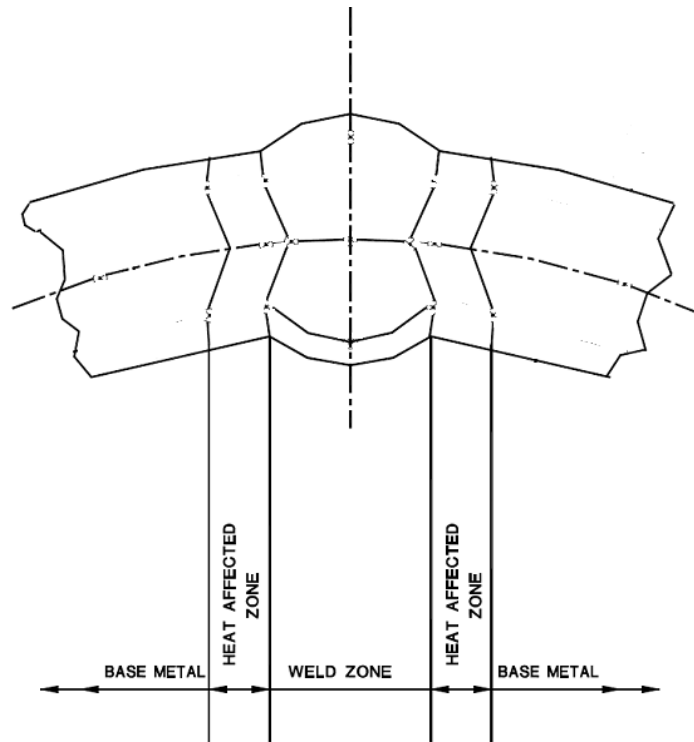


Figure 6.16: Cross section showing the spiral weld configuration

This zone is indicated by region 4 to 1 in Figure 6.17. In region 1 the temperatures were close to melting point. The heat treatment has refined the grain structure and austenitic grain growth takes place. There is an improvement in toughness of the mild steel. If the cooling rate is high, the microstructure can readily change to martensite. The heat from the welding process has raised the temperature in region 2 to just above the lower critical point. At this temperature the ferrite remains unchanged, but the pearlite is dissolved to austenite. Upon cooling, the carbon is precipitated in the form of small globules of cementite in ferrite. This type of structure is acceptable as it produces softness and good ductility. In region 3 the metal was heated to just above 873 K and consists of newly formed fine equiaxed grains of ferrite and pearlite. This temperature

region undergoes relieving of residual stress. Temperatures below 723 K remain unchanged.

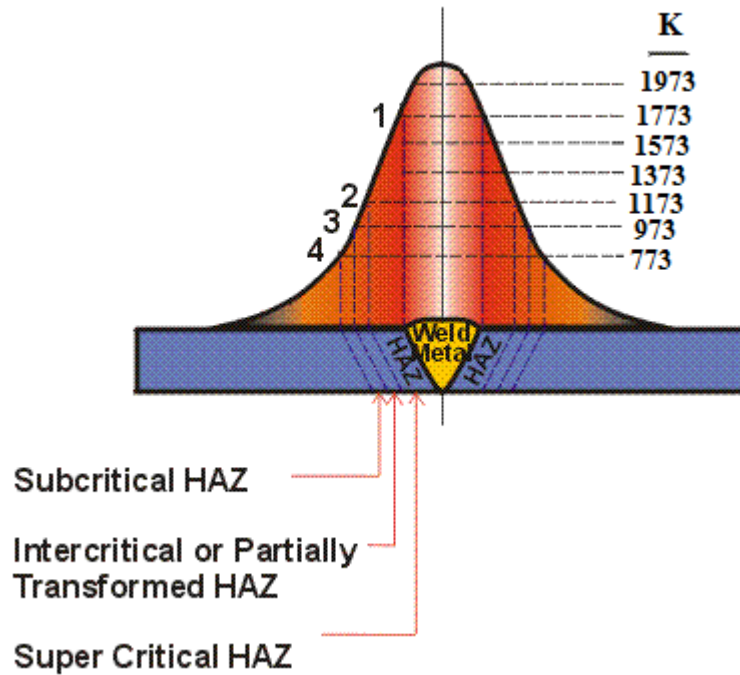


Figure 6.17: Temperature gradients across the weld joint for mild steel

The measurements of FZ and HAZ shown the welding data sheet and in the weld sample microscopic photograph were used to set values of Goldak parameters for the 56-inch pipe (a, b and c for the heat source modeling). Moreover were used to validate the thermal FE model.

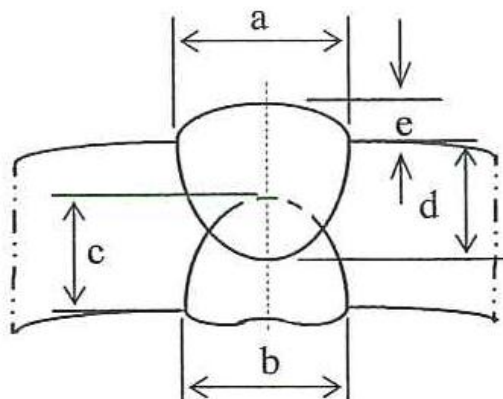


Figure 6.18: Weld bead shape as per the welding data sheet
 ($a=17\pm 3\text{mm}$, $b=16\pm 3\text{mm}$, $c=7.5$ to 8.8mm , $d=8.1$ to 9.5mm , $e=0.5$ to 2.5mm)

The FEM temperature distribution throughout the pipe joint at the end of the bottom and top welding is shown in Figure 6.19.

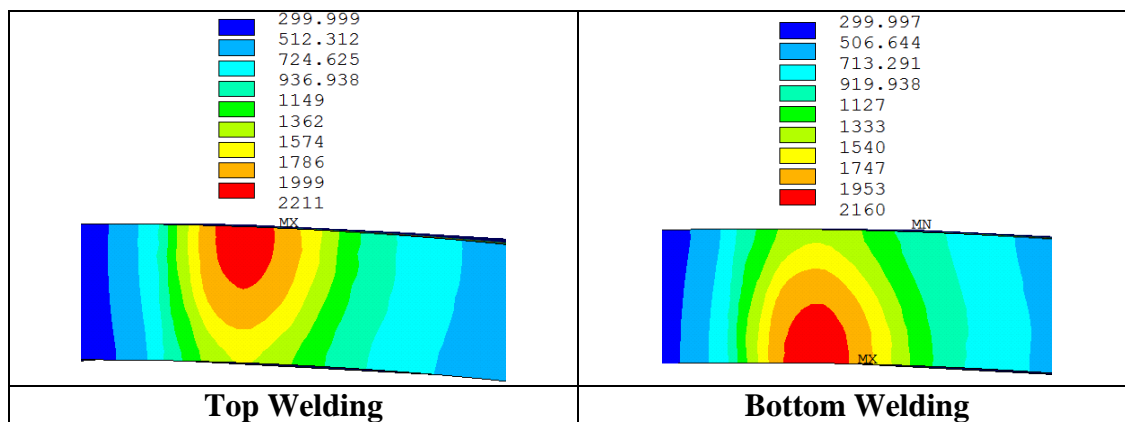


Figure 6.19: Temperature contours throughout the spiral weld joint at the end of bottom and top welding

The temperature profiles at pipe inside and outside surfaces were measured numerically for selected nodes across the weld joint at the moments of bottom welding (Load Step#100) and top welding (Load Step#250). Figure 6.20 shows the representation

of the nodes within the weld area at the ring end side where the temperature profiles numerically predicted.

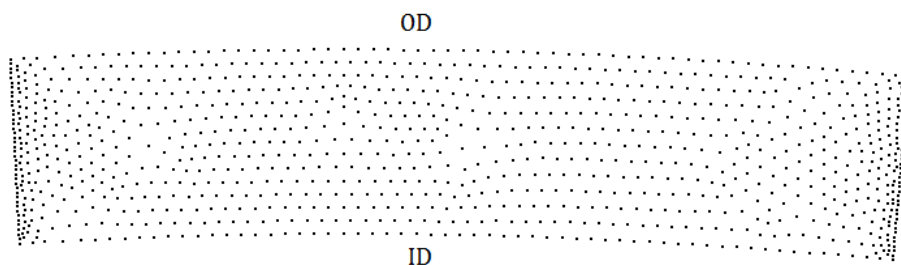


Figure 6.20: Representation of the nodes within the weld area at the ring end side

It can be seen clearly from Figure 6.21 and Figure 6.24 that the width of the fusion zone at both pipe ID and OD are in agreement with the actual measurement from the sample microscopic photograph.

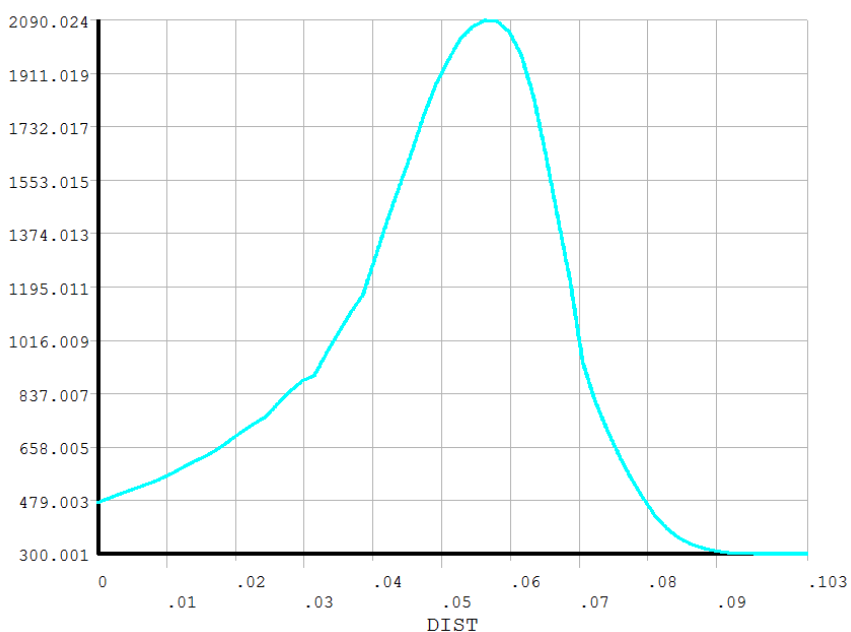


Figure 6.21: Temperature profile at selected nodes along the pipe ID at the end of the bottom welding (Load Step#100)

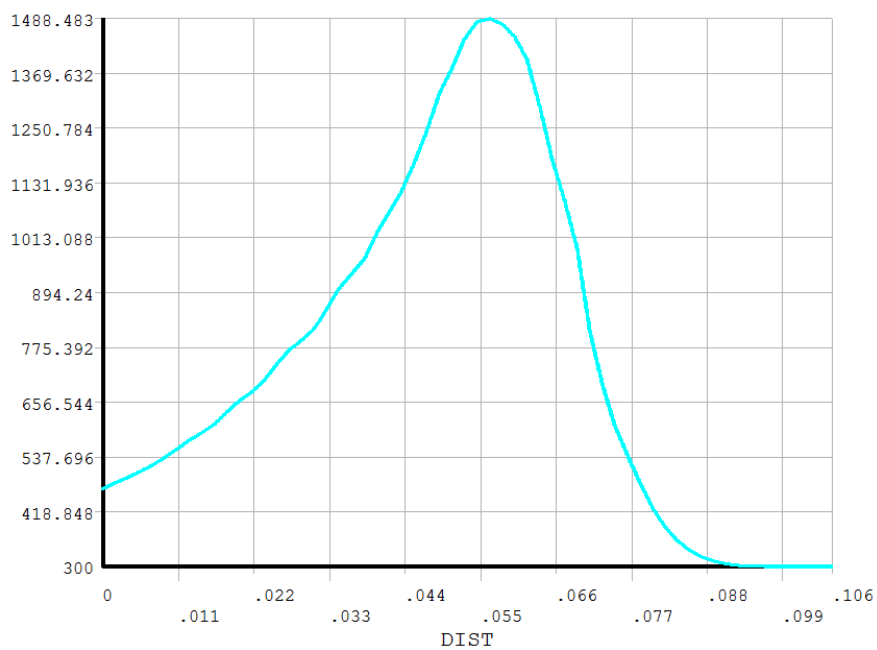


Figure 6.22: Temperature profile at selected nodes along the pipe OD at the end of the bottom welding (Load Step#100)

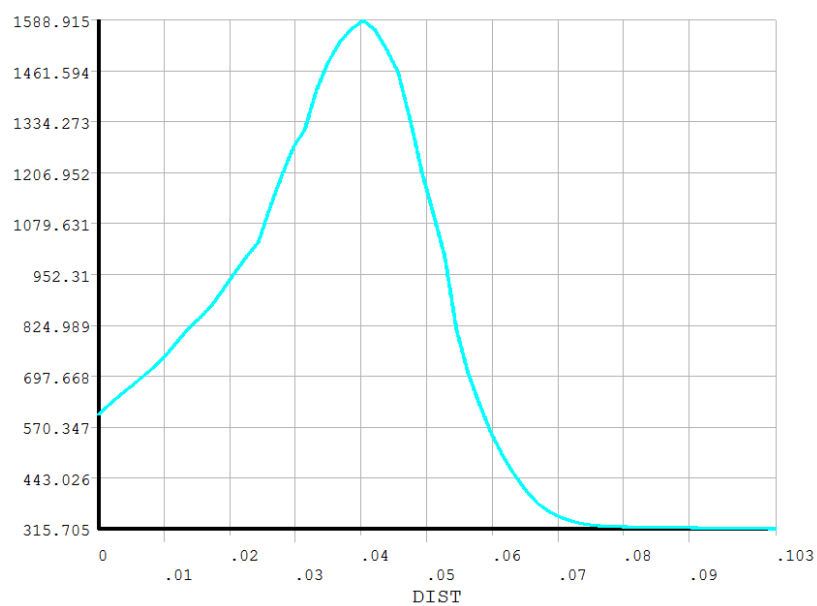


Figure 6.23: Temperature profile at selected nodes along the pipe ID at the end of the top welding (Load Step#250)

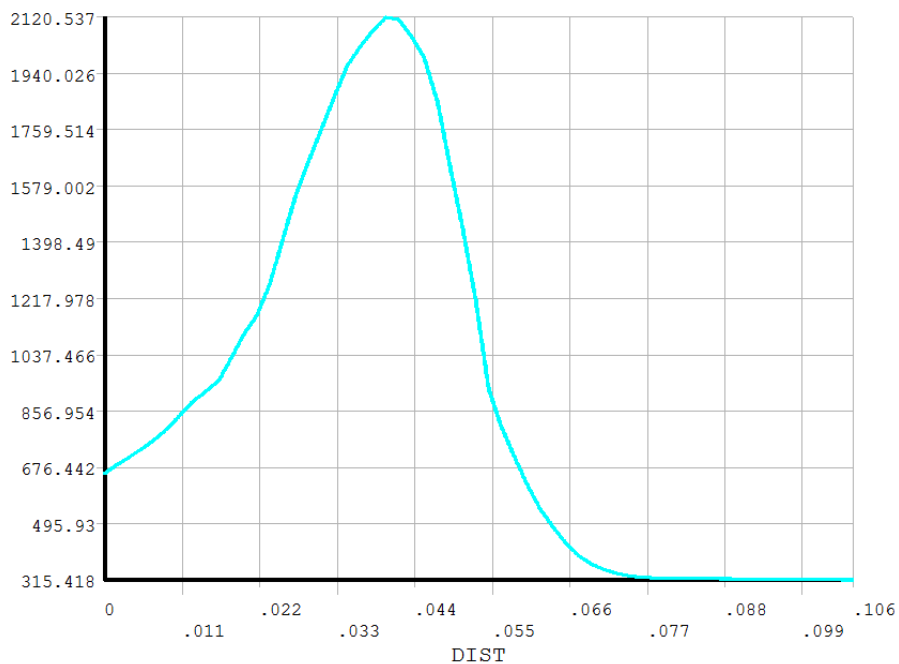


Figure 6.24: Temperature profile at selected nodes along the pipe OD at the end of the top welding (Load Step#250)

Table 6.3 summarizes the Fusion Zone (FZ) measurements.

Table 6.3: Weld measurements for experimental samples

<i>Location</i>	<i>FZ width, mm</i>	
OD	Data Sheet	17±3
	Actual	21
	FEM	18
ID	Data Sheet	16±3
	Actual	18
	FEM	18

From Figure 6.19, Figure 6.21, Figure 6.24 and Table 6.3, it is evident that predicted FEM results agreed well with the experimentally measured FZ and HAZ. Thus, the developed models have been experimentally validated.

6.7 FEM THERMAL RESULTS AND DISCUSSIONS

Using the geometrical model built in the previous chapter with the thermal model demonstrated in this chapter, we present now the results of the simulated weld for the welding speed of 0.019 m/sec. The thermal simulation is divided into 4 different computations:

1. Heat transfer analysis of the bottom welding stage
2. Heat transfer analysis of the intermediate cooling stage
3. Heat transfer analysis of the top welding stage
4. Heat transfer analysis of the final cooling stage

In this thermal analysis for 56 inch spiral welded pipe, heat flux is calculated as a moving heat source. The welding speed was incorporated in terms of load step time. At the end of the heat load an extra load step with time equal to the cooling time is added without any heat input. In the solution phase, this part of the analysis gives the temperature distribution as the output and this result is stored in a separate file.

Table 6.4 shows the solution plan for the thermal analysis with 300 Load Steps. The total spiral welding time of 28.83 seconds was divided into 100 solution steps for each of the top and bottom welding. The program determined the number of sub-steps automatically. Another 50 load steps of different time duration were used for each of the intermediate and final cooling of the pipe. Total run time for this solution plan was about 3 hours for the thermal analysis using an Intel® Core™ i7 CPU workstation with 2.93 GHz CPU and 12.00 GB RAM.

Table 6.4: Solution plan for welding speed=0.0192 m/s with 300 load steps

<i>No.</i>	<i>Solution Phase</i>	<i>Load Step Range</i>	<i>No. of Load Step</i>	<i>Time of Each Load Step (sec.)</i>	<i>Total Time (sec.)</i>
1	Bottom Welding	1-100	100	0.2884	28.8353
2	Intermediate Cooling	101-150	50	4.3253	216.2648
3	Top Welding	151-250	100	0.2884	28.8353
4	Final Cooling	251-300	50	4.3253	216.2648
	TOTAL		300		490.2001

Figure 6.25 shows the temperature distributions on the 150-mm ring at the end of each of the thermal analysis stages mentioned before.

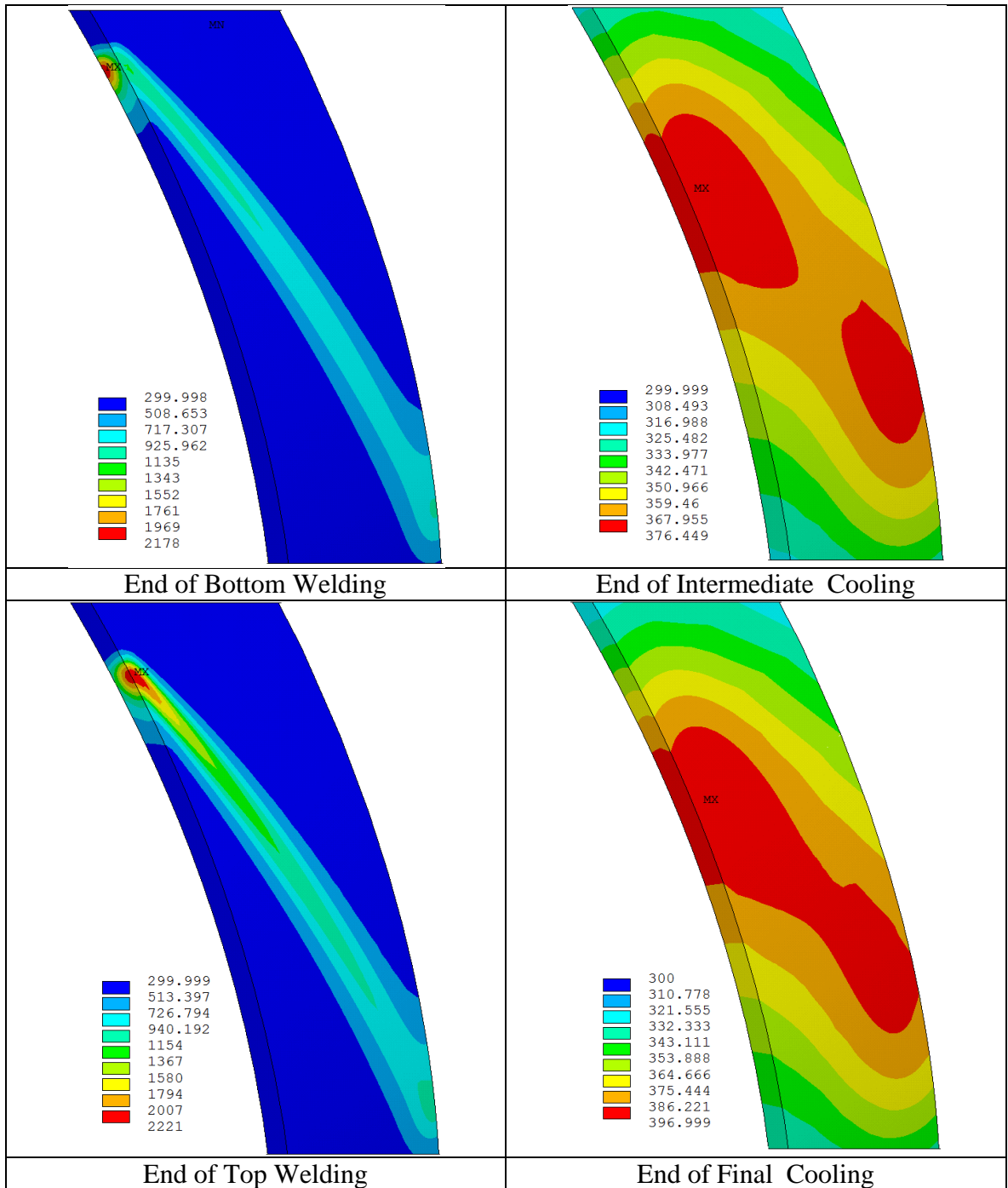


Figure 6.25: Temperature distributions at different stages

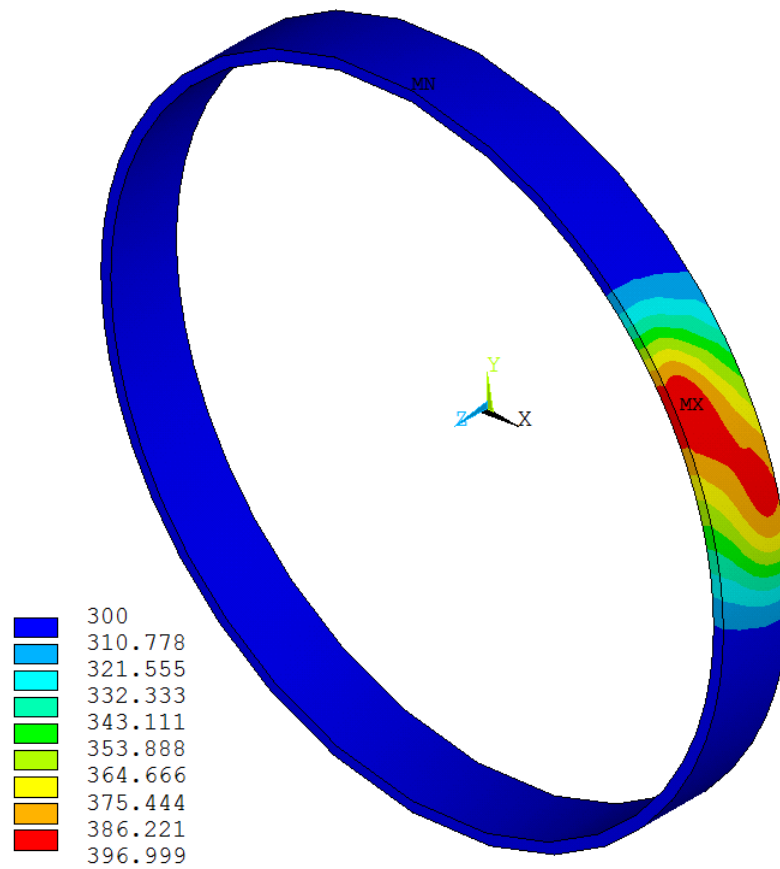


Figure 6.26: Temperature distributions after final cooling stage

Figure 6.27 shows the numerical temperature distributions with time for selected nodes along the spiral welding path at the pipe inside surface (ID). The temperatures at the first 25 seconds increased sharply and then they decrease slowly due to the bottom welding then these points again are affected by the top welding where their temperatures increase again but not to the melting temperature as this effect was not seen on the outside surface of the pipe (OD).

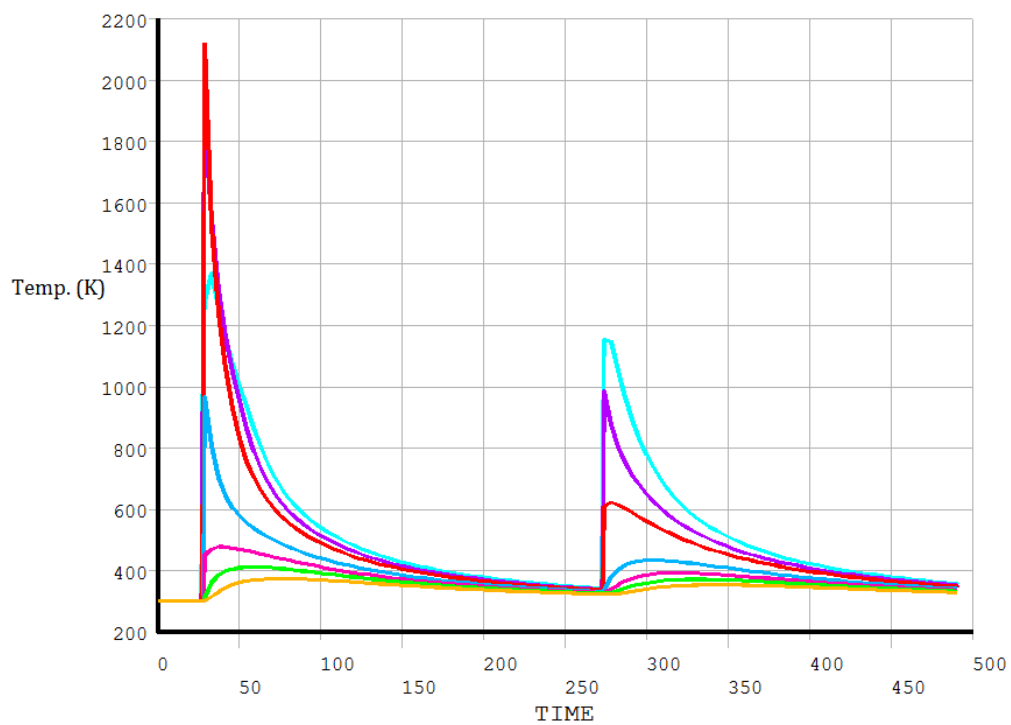


Figure 6.27: Temperature profiles for selected nodes on pipe ID

Figure 6.28 shows the numerical temperature distributions with time for selected nodes along the spiral welding path at the pipe outside surface (OD).

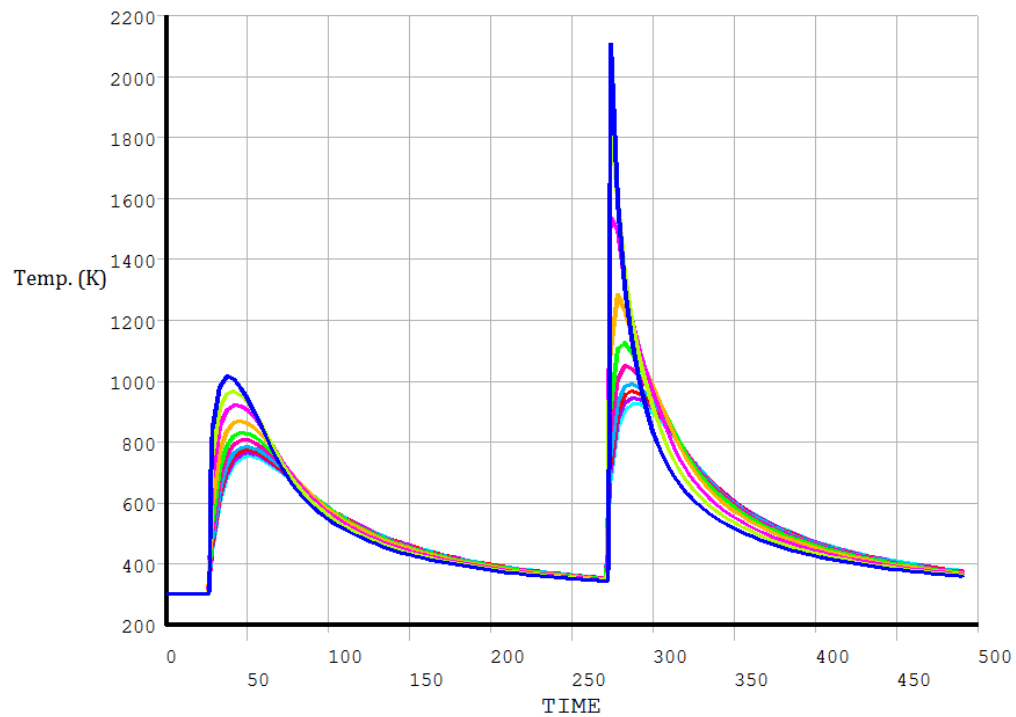


Figure 6.28: Temperature profiles for selected nodes on pipe OD

It can be easily noticed that a big thermal gradients between those points is developed. This is a typical characteristic of a welding process especially with double sided welding (bottom and top welding). The following conclusions are drawn from the above investigations:

- Heat source modeling of the submerged arc welding of the spiral welded pipe in ANSYS has been done.
- The results obtained compared fairly well with those of the experimental results.

6.8 EFFECT OF WELDING SPEED ON THE TEMPERATURE FIELD PREDICTION

Welding speed represents the distance traveled by the welding arc along the weld line per unit of time. The welding speed has an important effect on the heat distribution pattern in the vicinity of the heat source. The effect of welding speed on the shape of the isotherms has been studied for three cases of welding speed by maintaining all other input parameters same in all cases. Table 6.5 shows the cases of welding speed that were studied.

Table 6.5: Cases for welding speed effect study

<i>Case</i>	<i>1</i>	<i>2</i>	<i>3</i>
<i>Welding Speed (m/s)</i>	<i>0.0250</i>	<i>0.0192</i>	<i>0.0125</i>

The predicted surface temperature for all cases can be compared using the top view of the isothermal temperature field over the pipe's surface. The non-linear FEM analysis prediction is shown in Figure 6.29. The maximum temperature and the temperature distribution in all cases are shown after cooling.

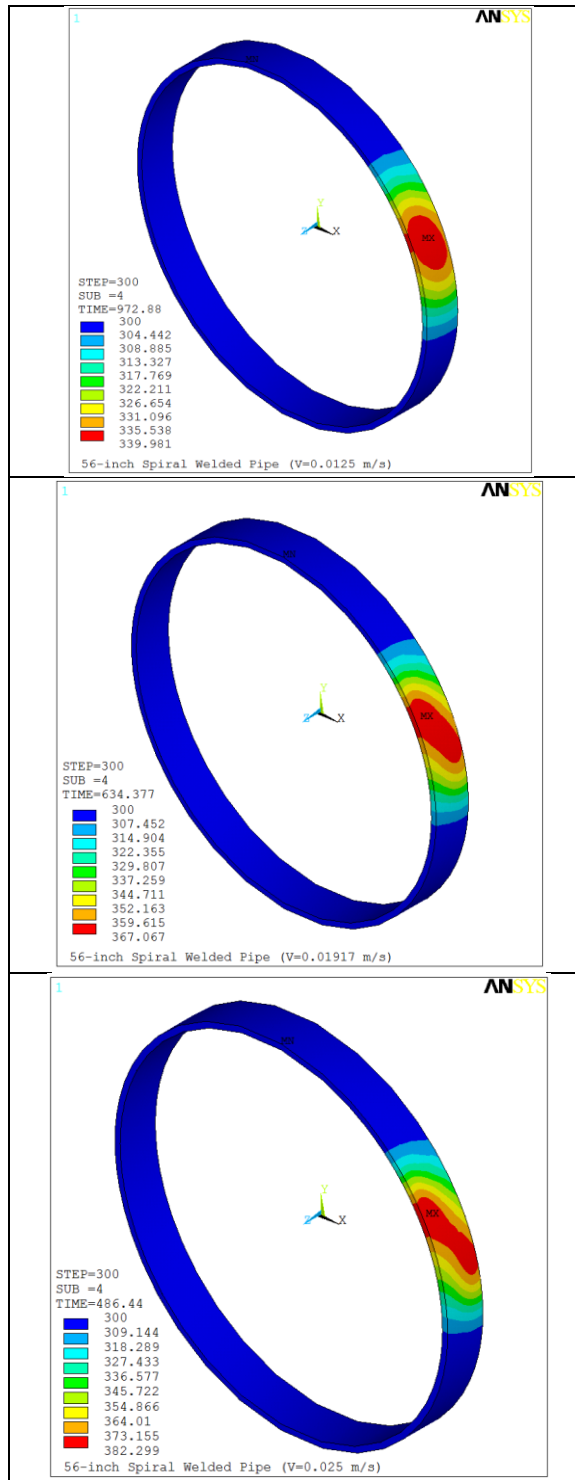


Figure 6.29: Temperature distributions after final cooling stage for different welding speeds

If we compare the temperature variation in time predicted by all cases for a single node (#6409) in the welding path we obtain Figure 6.30.

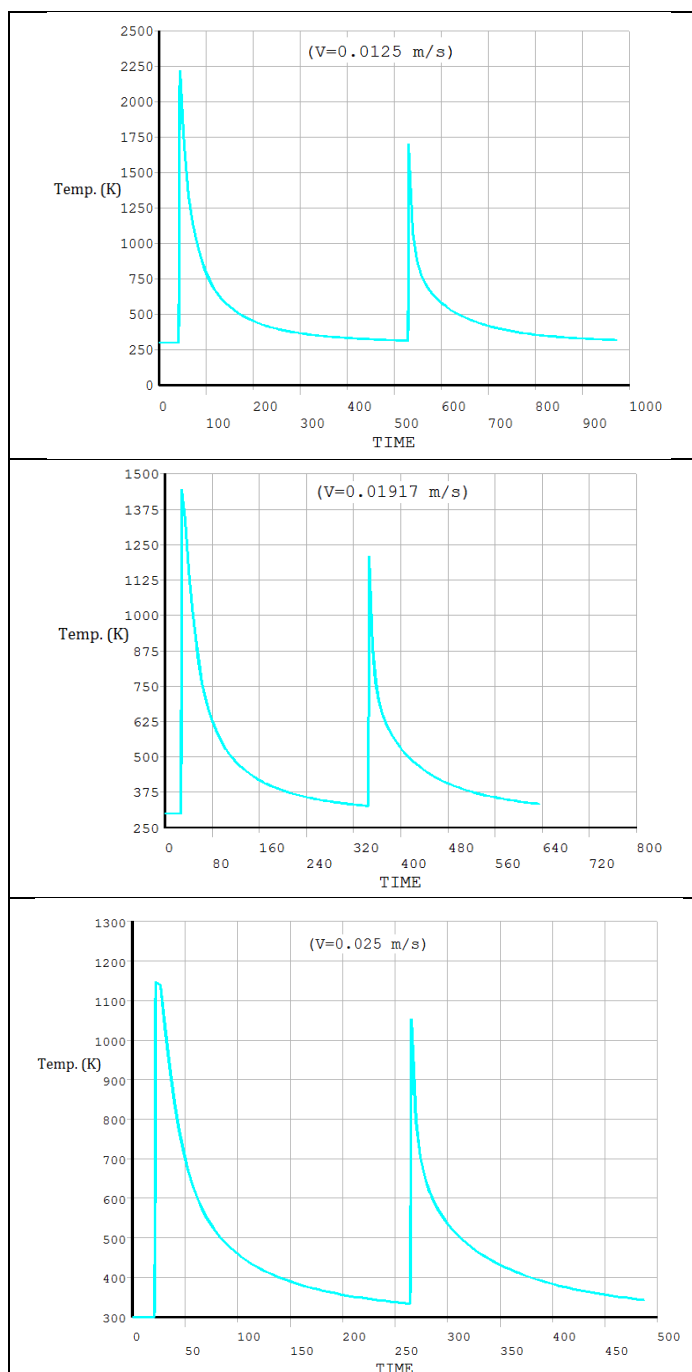


Figure 6.30: Temperature variations at a single node (#6409) located at the OD for different speeds

Figure 6.31 shows the temperature contours through the wall thickness at the end of bottom welding (Load Step#100).

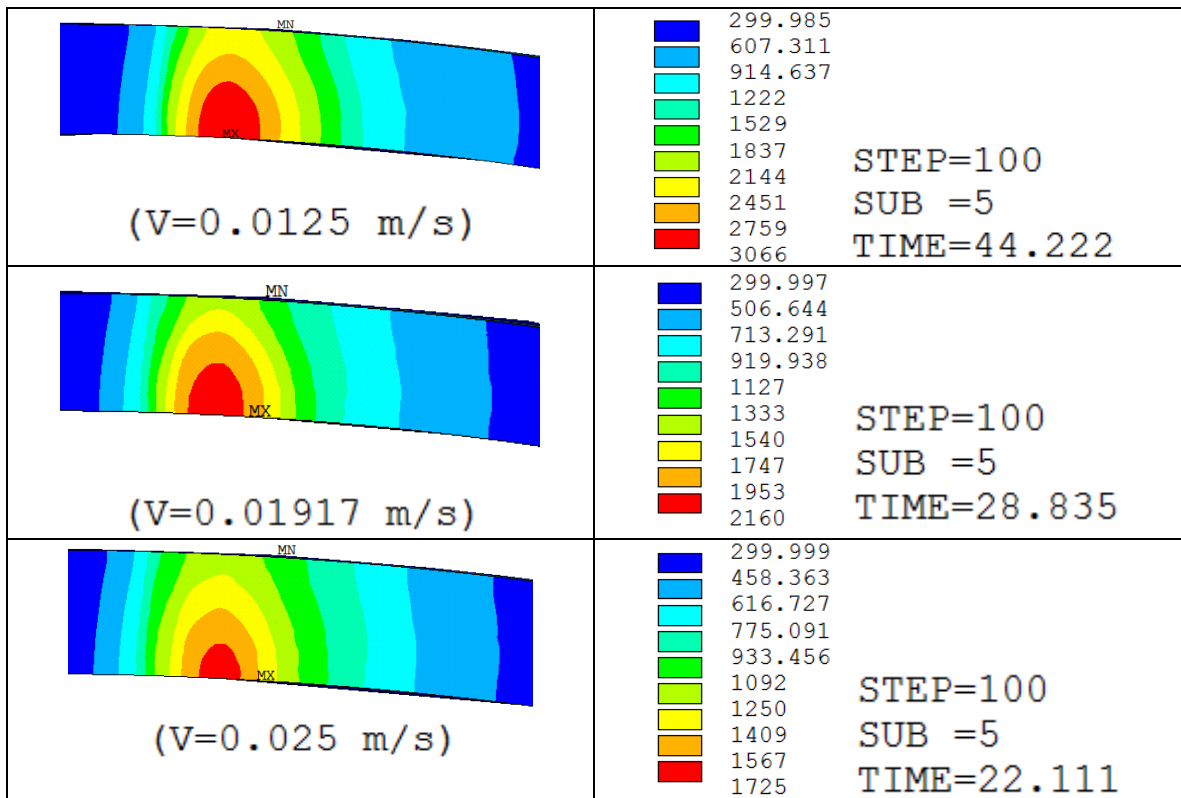


Figure 6.31: Temperature contours through the wall thickness at the end of bottom welding (Load Step#100) for the three welding speed cases

It can be concluded that the speed of welding affects the shape of the isotherms.

The lower the speed, the more elongated the isotherms with value of temperature.

CHAPTER 7

STRUCTURAL ANALYSIS USING FINITE ELEMENT METHOD

7.1 STRUCTURAL ANALYSIS (SEQUENTIALLY COUPLED THERMAL-STRESS ANALYSIS)

Welding processes induce residual stresses and distortions which can play a major role in the mechanical strength of a component. Numerical simulation of processes is of big help to control these effects as it provides the evolution of physical quantities such as temperature stresses and strains at any point in the structure. Prediction of residual stresses is far much difficult as it needs 3D simulations to accurately take account of the constraining conditions induced by the weld bead.

To simplify the welding simulation, it is computationally efficient to perform the thermal and mechanical analyses separately. Physically, it is assumed that changes in the mechanical state do not cause a change in the thermal state. That is, a change in stress and strain does not cause a change in temperature. However, a change in the thermal state causes a change in the mechanical state. Computation of the temperature history during welding and subsequent cooling is completed first, and then this temperature field is applied to the mechanical model to perform the residual stress analysis.

A sequentially coupled thermal-stress analysis is commonly used in simulations of welding processes since the rather slow stress development affects heat transfer very little. Such an analysis is not only fast and computationally economical, but also allows for all useful features of individual thermal and stress analyses available in FEA packages to be applied. Three-dimensional transient thermal analysis is conducted first to obtain the global temperature history generated during the spiral welding process. A transient stress analysis is then developed with temperatures obtained from thermal analysis entered as loading to the stress model. A sequentially coupled thermo-mechanical analysis was conducted to simulate the spiral welding process for the pipe.

Same meshing parameters from thermal analysis to facilitate the nodal data mapping and elements with same topology to enhance the convergence during the structural analysis are used. Creep strains were not included in the stress analysis because the time spent at high temperature was deemed to be very short. Different material laws have been utilized in weld simulations. The available material laws typically include an elastic-perfectly plastic model or a plasticity model which takes into account strain hardening, either kinematic (anisotropic) or isotropic.

Three idealized stress-strain curves for a prismatic, metal bar subjected to uniaxial tension are shown in Figure 7.1. Rigid, perfectly plastic, elastic, perfectly plastic, and elastic, strain-hardening behaviors are shown in parts (a), (b), and (c), respectively, of the figure. The yield strength of the material is denoted by σ_y in the plots. The rigid, perfectly

plastic idealization neglects elastic strains and hardening. The elastic, perfectly plastic curve includes elastic strains but neglects hardening. The elastic, strain hardening curve includes elastic strains and assumes linear hardening. When large deformations are prevented, say, by a surrounding elastic material, then plastic deformation is contained. For contained plastic deformation, neglecting strain hardening, or work-hardening, is a reasonable assumption. Large deformations by cold-working occur in metal-forming processes such as drawing, rolling, and extrusion. Cold-working involves hardening and the plastic deformations in these processes are much larger than elastic deformations, so that neglecting elastic deformation is a reasonable assumption.

The yield strength of a metal is measured in the tension test, which is a uniaxial state of stress. The question of what governs yielding in a multi-axial state of stress is determined from σ_y

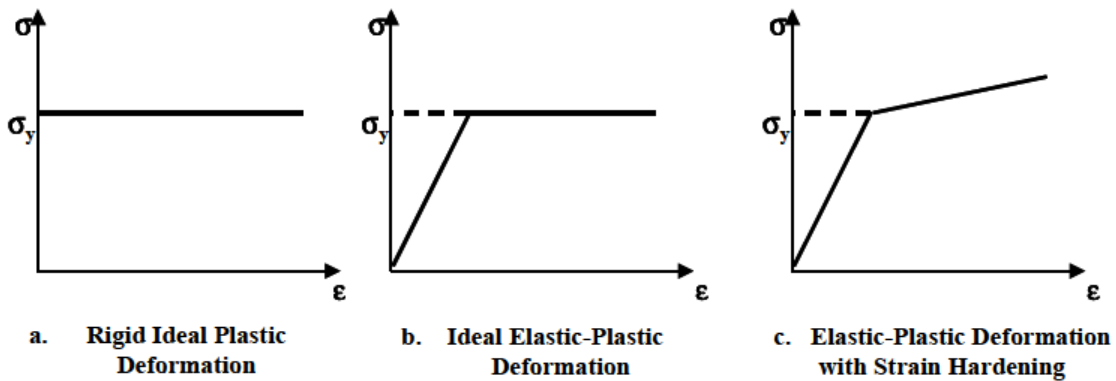


Figure 7.1: Idealized flow curves from uniaxial tension test [Hsu 1986]

Large deformation and thermo-elasto-plastic material formulation were considered. The most important factors when calculating residual stresses introduced by thermal strains in welds are the effects of temperature and the thermal history on the mechanical properties. These temperature histories were obtained from the thermal analysis and were used as thermal loading on to the structural model to calculate thermal strains and stresses for each time increment (load step). The thermal strains and stresses were then accumulated to produce the final state of residual stresses.

Thermo-elastic-plastic material formulation as shown by equation 7.1 with von Mises yield criteria is employed with σ_1 , σ_2 , and σ_3 being the three principal stresses, coupled to a isotropic hardening rule.

$$\sigma_v = \sqrt{\frac{1}{2} [(\sigma_1 - \sigma_2)^2 + (\sigma_2 - \sigma_3)^2 + (\sigma_3 - \sigma_1)^2]} \quad (7.1)$$

For isotropic hardening, it is assumed that the center of the yield surface is fixed in stress space while the size is increased to represent work hardening. This is schematically shown in Figure 7.2.

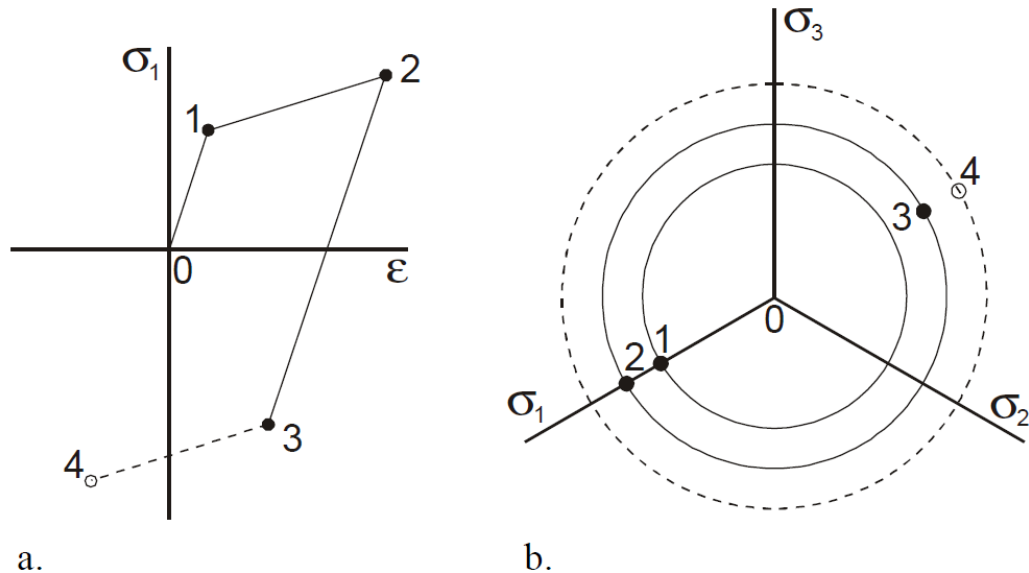


Figure 7.2: A schematic representation of the isotropic hardening model [Horn 2002]

In Figure 7.2(a), a loading history is shown while in Figure 7.2(b); the corresponding points are plotted in stress space. Starting from the origin and loading to point 1, the material behaves elastically; and in stress space, the yield surface is reached at point 1. From point 1 to point 2 the material is plastically loaded and the size of the yield surface is increased. By reversing the loading direction at point 2, elastic unloading and reloading will occur from point 2 to point 3. The equivalent stress, i.e. the distance to the axis of the yield cylinder, at both points is the same. By plastically loading the material from point 3 to point 4, the size of the yield surface is further increased.

For kinematic hardening, it is assumed that the size of the yield surface is constant while the work hardening is represented by translating the center of the yield surface.

This is schematically shown in Figure 7.3.

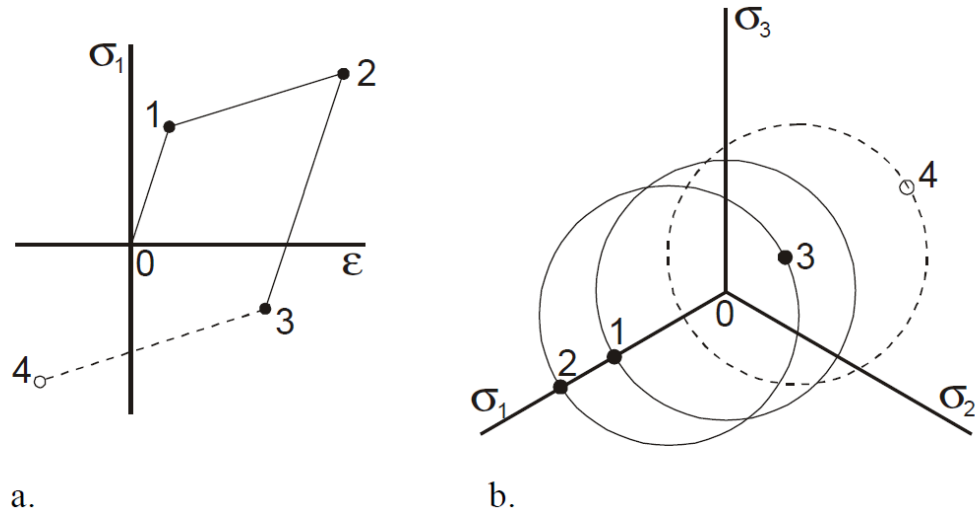


Figure 7.3: A schematic representation of the kinematic hardening model [Horn 2002]

In Figure 7.3(a), a loading history is shown while in Figure 7.3(b), the corresponding points are plotted in stress space. Starting from the origin and loading to point 1, the material behaves elastically; the yield surface is reached at point 1. From point 1 to point 2 the material is plastically loaded and the yield surface now moves from point 1 to point 2 in stress space, but the size remains the same. By reversing the loading direction at point 2, elastic unloading and reloading occurs between point 2 and point 3. The yield stress at point 3 is now lower than if the reversed loading direction was taken from the start. By plastically loading the material from point 3 to point 4, the yield surface now moves in the other direction.

In this thesis work, the material was assumed to be thermo elasto-plastic using rate independent plasticity. The von Mises yield criterion and the associated flow rule

were used. Linear isotropic hardening was assumed. All of these introduced material non-linearity in the thermo-mechanical analysis.

7.2 MECHANICAL BOUNDARY CONDITIONS

The specified mechanical boundary conditions are those just sufficient to prevent rigid body motion of the model. The model is supported so that the two lines (A-A and B-B) in the opposite direction of the spiral weld were restrained in both the radial and tangential directions as shown in Figure 7.4 to Figure 7.6.

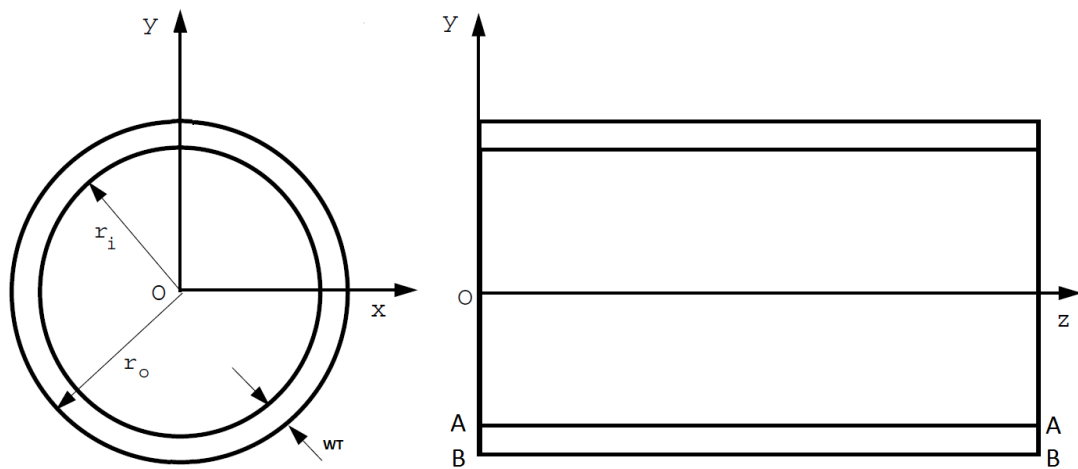


Figure 7.4: Mechanical boundary conditions

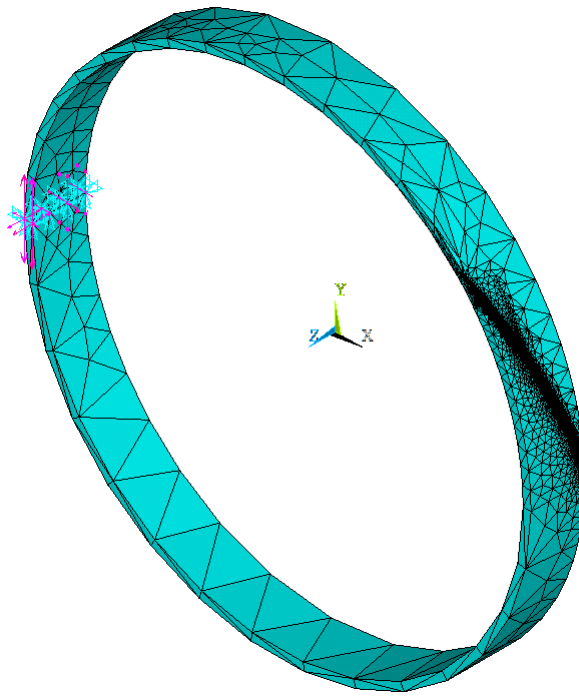


Figure 7.5: Mechanical boundary conditions applied on the ring

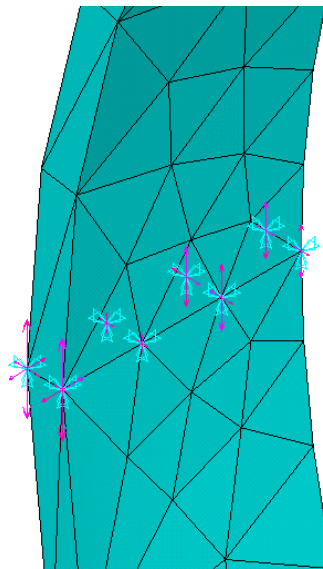


Figure 7.6: Close-up to the lines that were restrained in both the radial and tangential directions

7.3 TRANSIENT NON-LINEAR STRUCTURE ANALYSIS PROCEDURE

The following Procedure was adopted for the transient non-linear structure analysis:

1. Draw same geometry and same number of mesh as in case of thermal analysis.
2. Define element type, which is SOLID 45. This is because it has the capabilities to give good structural results like stresses and deformation.
3. Assign material properties.
4. Free-mesh the model. Mesh should be same as in case of thermal analysis. It must have same number of elements as in case of thermal analysis.
5. Apply the structural boundary conditions. It may contain to restrict the degrees of freedom of the fixed portions of the pipe and the application of force/pressure etc.
6. Solve with transient analysis
7. In the Solution, use thermal result file created in thermal analysis to be read by the software and to apply it on to the target areas as a body load on the pipe.
8. Allow the cooling time, solve and save the results.

This completes the welding simulation using ANSYS.

7.4 VALIDATION OF FE STRUCTURAL MODEL

The maximum von Mises Stress, predicted by the FE analysis, was 0.269×10^9 Pa (269 MPa). The final von Mises residual stress state for the ring after cool-down is shown in Figure 7.7.

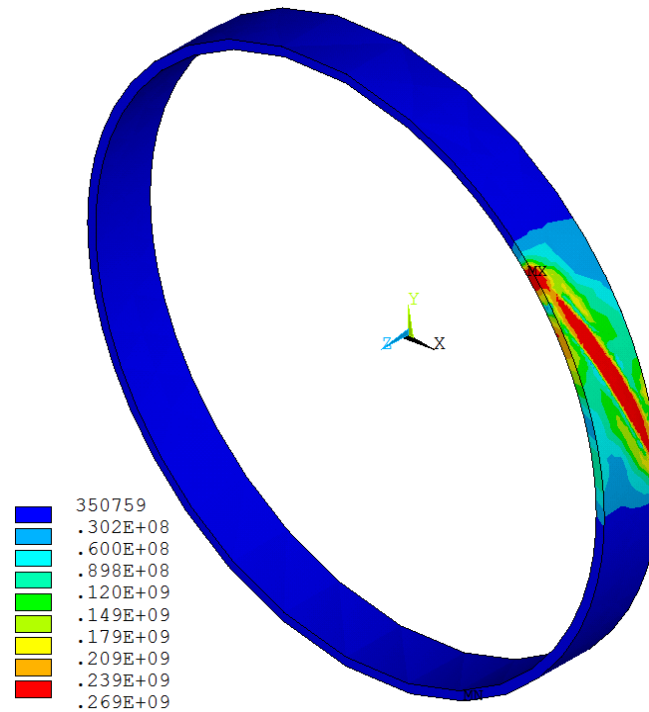


Figure 7.7: Surface contours of the von Mises stress after final cooling

In industry, the computed stresses by ring splitting method in spiral welded pipe are limited to $\pm 10\%$ of the pipe Specified Minimum Yield Stress (SMYS). The modeled pipe is made out X65 material grade so the acceptable residual stress is ± 44.8 MPa (6500 psi).

Table 7.1: SMYS and acceptable residual stress values for X65 pipe

	<i>Specified Minimum Yield Strength</i>		<i>Acceptable Residual Stress</i>	
	<i>(SMYS)</i>		<i>(10% of SMYS)</i>	
	MPa	psi	MPa	psi
X65	448	65,000	± 44.8	± 6500

However, the computed maximum von Mises stress by the model is in good agreement with the one measured by the Drilling Hole Technique and Cutting Method (shown in Figure 7.8 and Figure 7.9). The maximum experimental measured Microscopic Residual Stress (MIRS), both parallel and perpendicular to weld bead In HAZ, was 320 MPa by drilling hole technique while the maximum MIRS measured experimentally by cutting method with strain gauges was around 300 MPa.

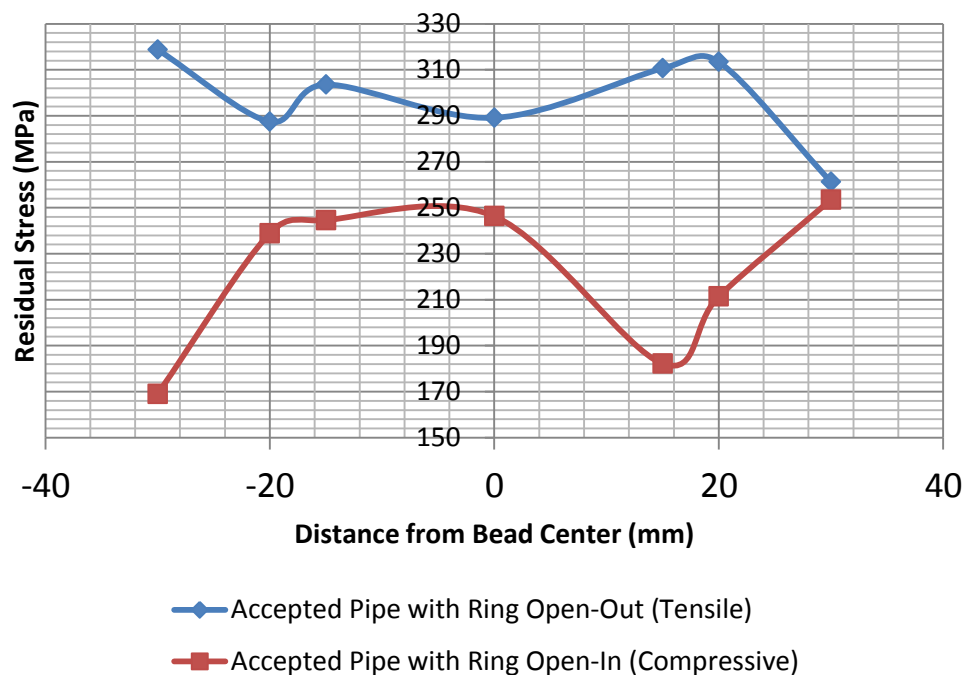


Figure 7.8: Residual stress measured by drilling hole technique for 56-inch spiral welded pipe

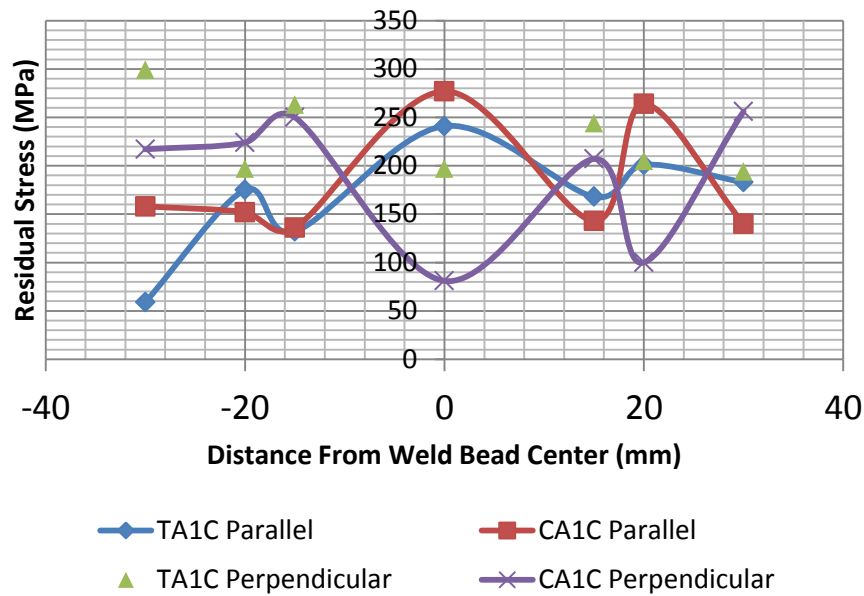


Figure 7.9: Residual stress measured by cutting method for 56-inch spiral welded pipe

For validation, good agreements between 3D predictions and experimental data have been obtained. However, while there exists a great deal of confidence in the modeling technique itself, the final results need always to be treated with caution. Some literatures showed drastically different residual stress distributions reported for the same joint configuration and welding conditions. The inconsistencies can be attributed to the following:

1. Existing residual stress profiles are based on limited experimental data.
2. Depending on size, geometry, and weld parameters, weld axial residual stresses can range from the 'self-equilibrating' to the 'through-thickness bending' type.
3. Earlier measurements of such stresses have focused on the weld area where large scatter in data can be expected due to the high stress gradients there.

4. Residual stress measurement techniques, such as the blind hole technique, are similar to the use of strain gauges. They tend to give averaged data that can hardly be comparable with FE data obtained at integration points or even averaged in a finite element, especially in regions where high stress gradients exist.
5. Data obtained by the FE method can also be strongly dependent on the model, material properties, boundary conditions, and other assumptions.

Finally, despite the comments listed above, the computational model described here has the potential to be applied to spiral pipe welding for residual stress prediction. The results of the FEM done by ANSYS are presented with more details in the next section.

7.5 FEM STRUCTURAL ANALYSIS RESULTS AND DISCUSSIONS

Previously in Chapter 3 and 4, welding residual stresses were only assessed by experimental methods (Ring Splitting and Drilling Hole Techniques). However, experimental residual stress measurements have practical limitations. First, they are expensive and require special equipment. Methods, such as the drilling hole technique, are also destructive. Second, even when non-destructive (e.g. diffraction technique), residual stresses are measured only at discrete locations near the weld surface, and such data not only tend to show significant scatter but also spatial variations. Consequently, it is impossible for any experimental technique to give a complete mapping of three-

dimensional (3D) residual stress distributions. Moreover, the results obtained from one particular weldment may not be directly applicable to other weldments.

With modern computing facilities, the finite element technique has become an effective method for prediction and assessment of welding residual stress. However, the accurate prediction of residual stresses and distortions induced by welding is extremely difficult. This is because the thermal and mechanical behaviors in welding include highly localized temperatures, temperature dependent material properties, large deformation, and a moving heat source. The thermo-structural (stress) analysis is carried out with the temperatures obtained from the thermal analysis as the loading to the stress model. The output obtained out of this analysis is the residual stress distribution throughout the pipe after cooling. Residual stress is obtained at the required nodes by using the time history postprocessor. Usually, residual stresses are found in the weld bead and in the pipe/weld bead interface.

It is necessary to mention that all meshes have a predefined refinement area close to the region where the weld line is located. This is done in order to avoid an excessive coarsening of elements in this region during the cooling time, which would lead to a poor approximation of the mechanical computations. For the mechanical results, we are mainly interested on analyzing the stress development in the material, and the plastic effects resulting from the welding and cooling processes during welding.

The stress simulation for the 56-inch pipe was divided into 4 different computations:

1. Structural analysis of the bottom welding stage
2. Structural analysis of the intermediate cooling stage
3. Structural analysis of the top welding stage
4. Structural analysis of the final cooling stage

The mechanical model starts with zero stresses for all the nodes and reads the temperature file at the corresponding time increments defined for the thermal analysis. The model applies the resulting temperature field at the nodes, varying the temperature dependent mechanical properties of the pipe inducing residual stresses of the pipe itself. The computational results provide the residual stresses on the spiral welded ring (after final cooling) as shown in Figure 7.10 and Figure 7.11 for pipe OD and ID respectively, which also have been be decomposed into the x; y; z stress components as shown also in the same figures. The required results can be tabulated for any node in the pipe or in the weld bead using the time-history postprocessor. X and Y-components residual stresses are dominantly tensile (at yield magnitude) within the weld area. While the Z-component residual stress are relatively compressive within the weld area, with noticeable tensile bands seen slightly away from the weld zone (yellow and red color). The stress reduction trend is observed as we move away from the spiral weld line both for inner and outer surfaces. It was also observed, further remote from the spiral weld line, the stresses are

almost constant. Away from the spiral weld path, the stresses becomes almost uniform tends to approach minimum level.

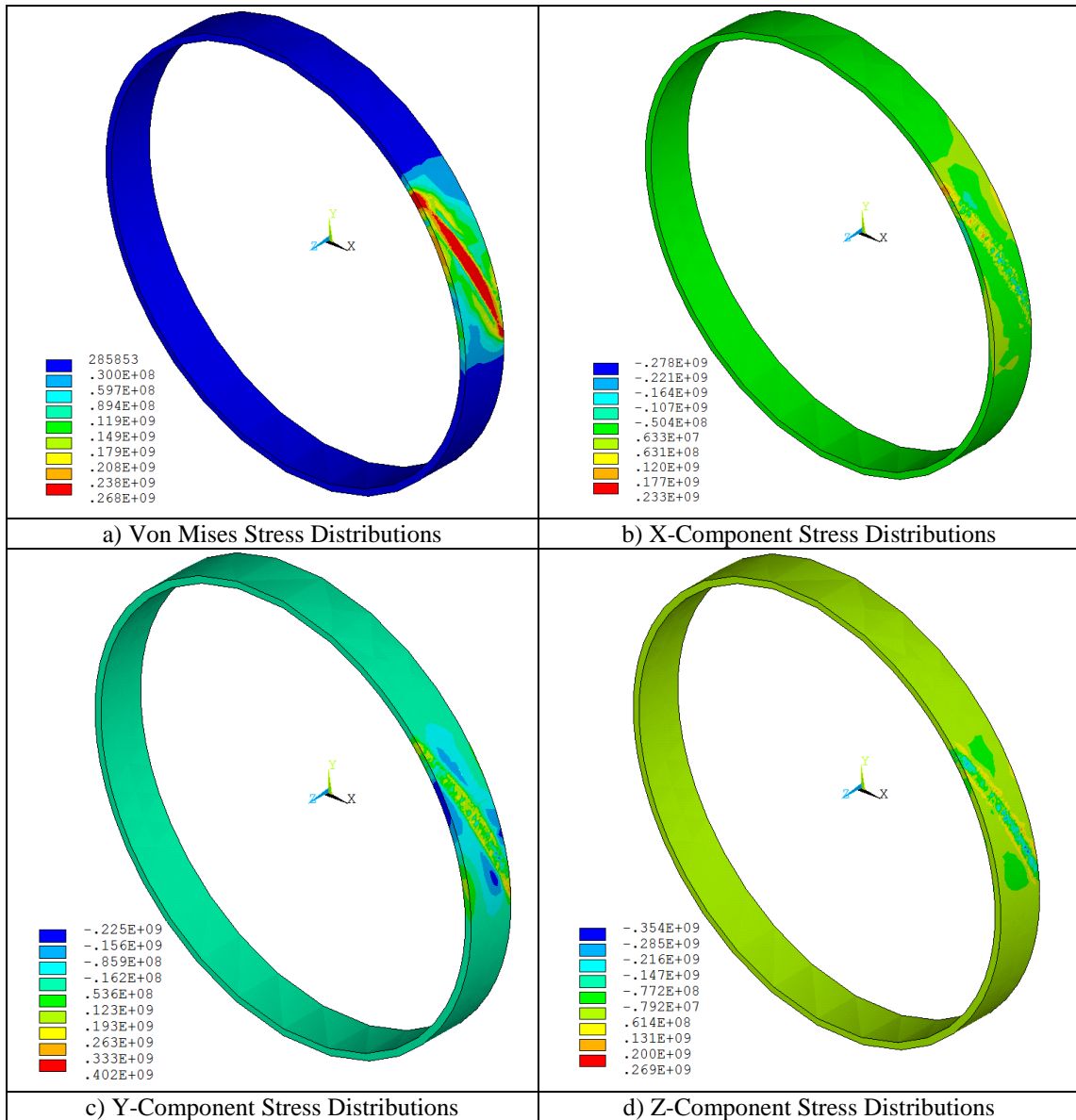


Figure 7.10: Stress distribution throughout the OD of spiral welded ring

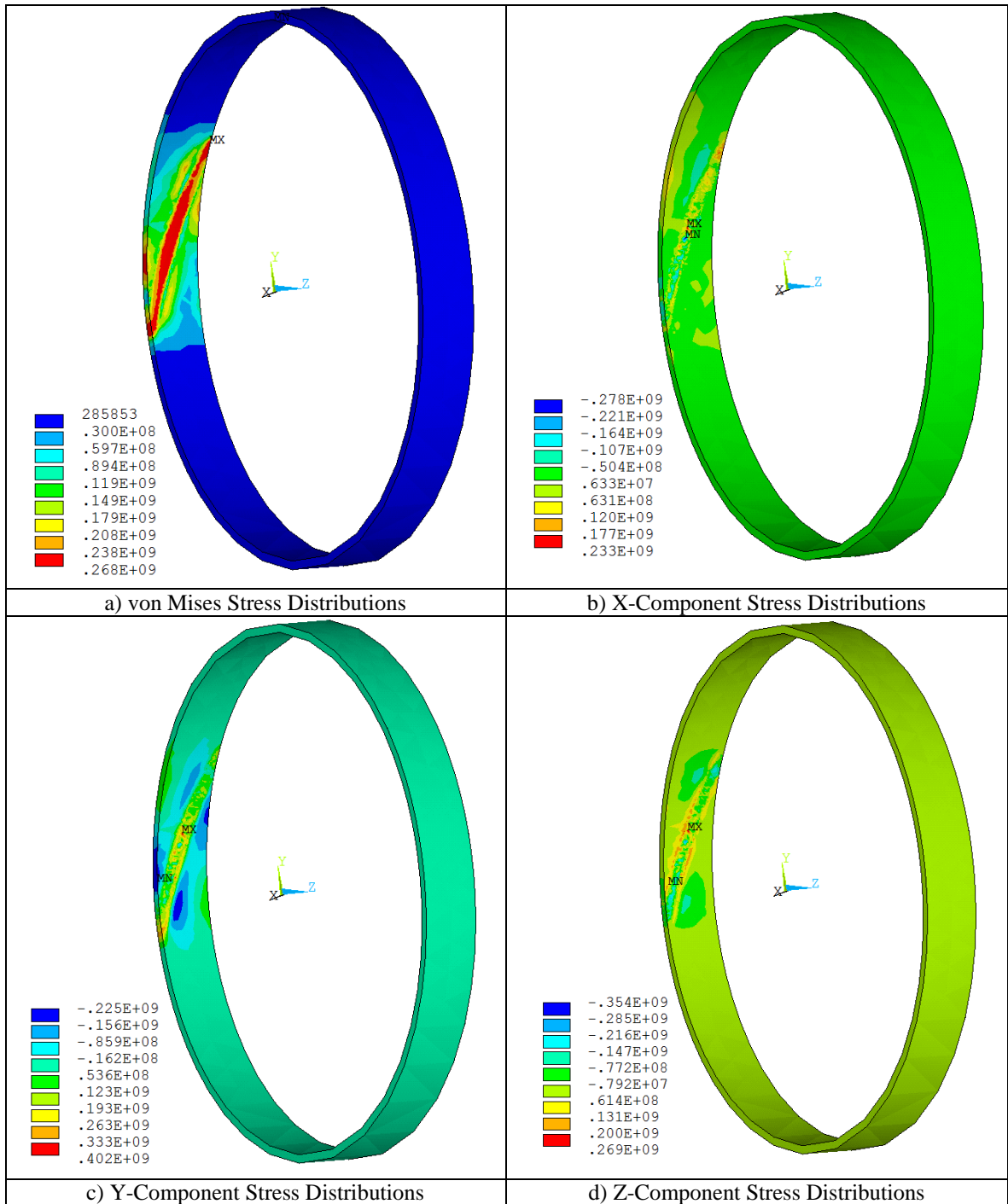


Figure 7.11: Stress distribution throughout the ID of spiral welded ring

It can be seen from Figure 7.10 and Figure 7.11 that the von Mises residual stress at the top and bottom surfaces of the pipe is tensile near the weld metal and less tensile away from it. Residual stresses start to grow at a distance from both ends of the weld. High stresses exist in the central region of the welds. Residual stresses become uniform in the central region for pipe ring. Maximum residual stresses in welds are usually close to the 50% of the yielding limit σ_Y . Gradually decreasing away from the weld axis in the plastic deformation zone, the tensioning stresses then relax down to less tensioning values in the adjacent areas. The cooling rate during welding process and the initial state of the steel can have a serious effect on the stress distribution. von Mises residual stress (Figure 7.10-a and Figure 7.11-a) shows significant tension in the weld and in the HAZ (Heat Affected Zone). During welding, the weld material is liquid and the structure material in the adjacent area is very soft because of high temperature (See Figure 7.12 to Figure 7.14 for the calculated stress during welding). This allows the weld zone to expand without developing stress. In the cooling process, these areas (the weld and the area adjacent to the weld) shrink. These areas develop a tensile state of von Mises stresses, due to the strength of the surrounding structure.

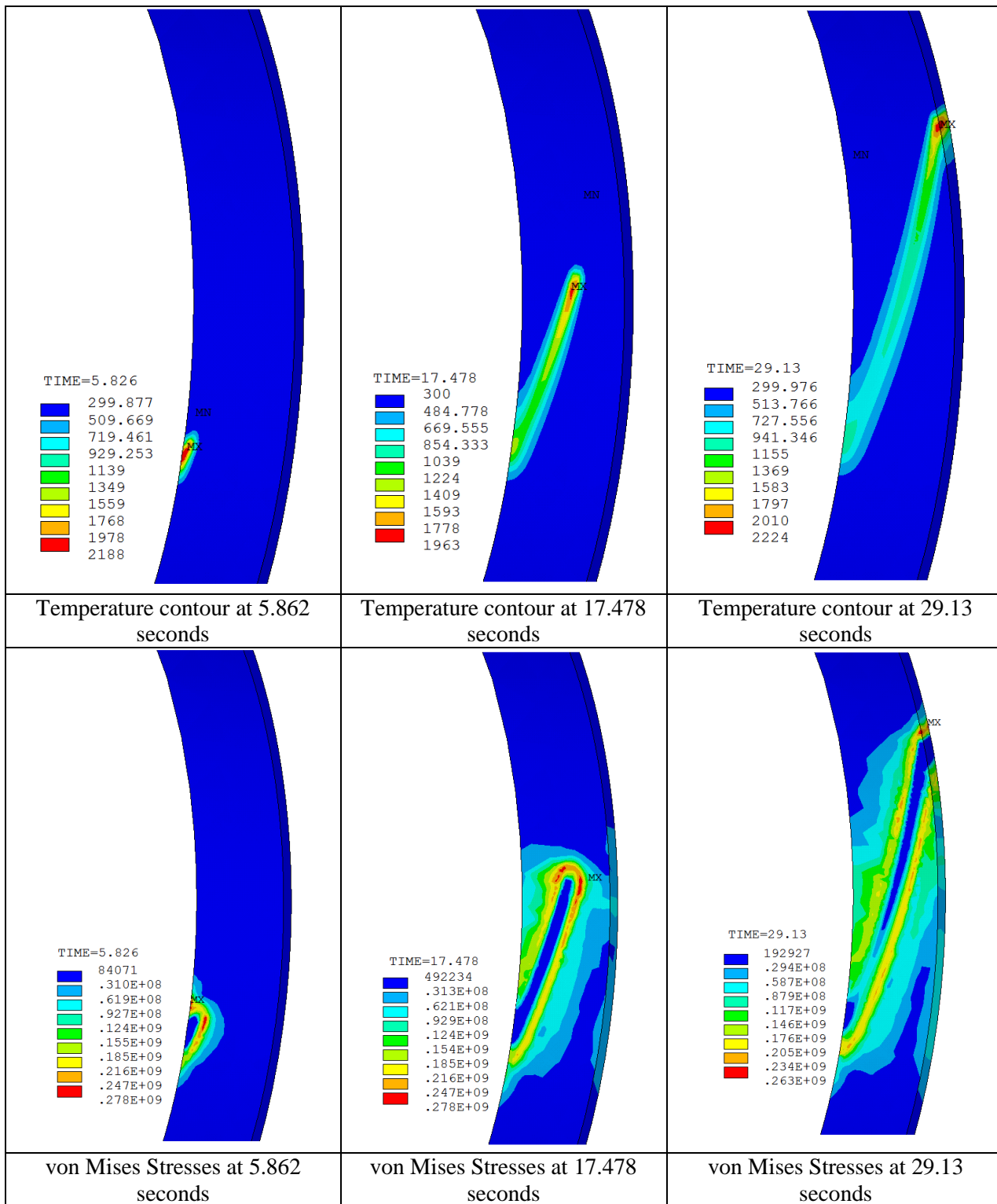


Figure 7.12: Temperature fields and von Mises stress distributions during bottom welding

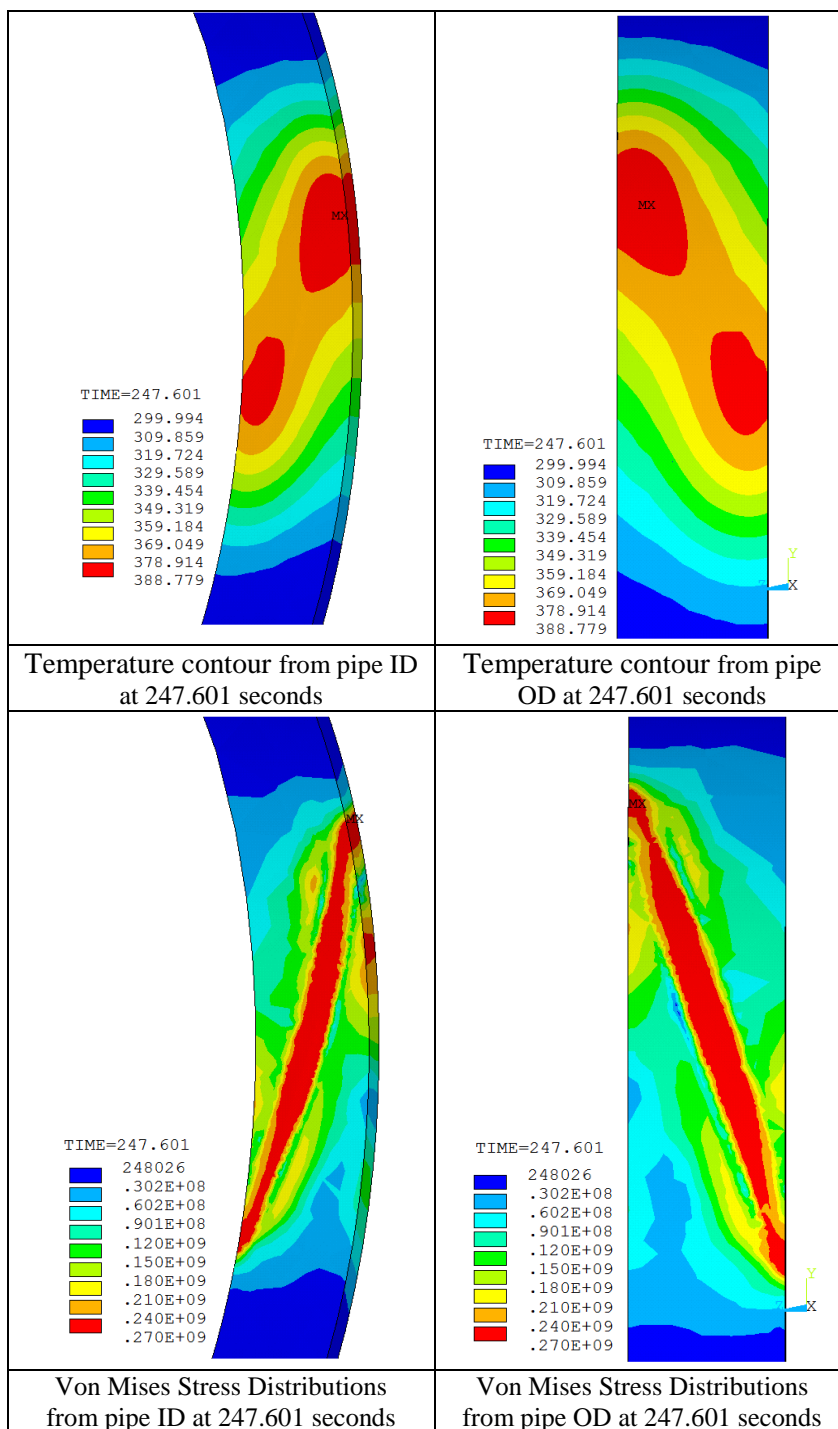


Figure 7.13: Temperature fields and von Mises stress distributions during at the end of the cooling

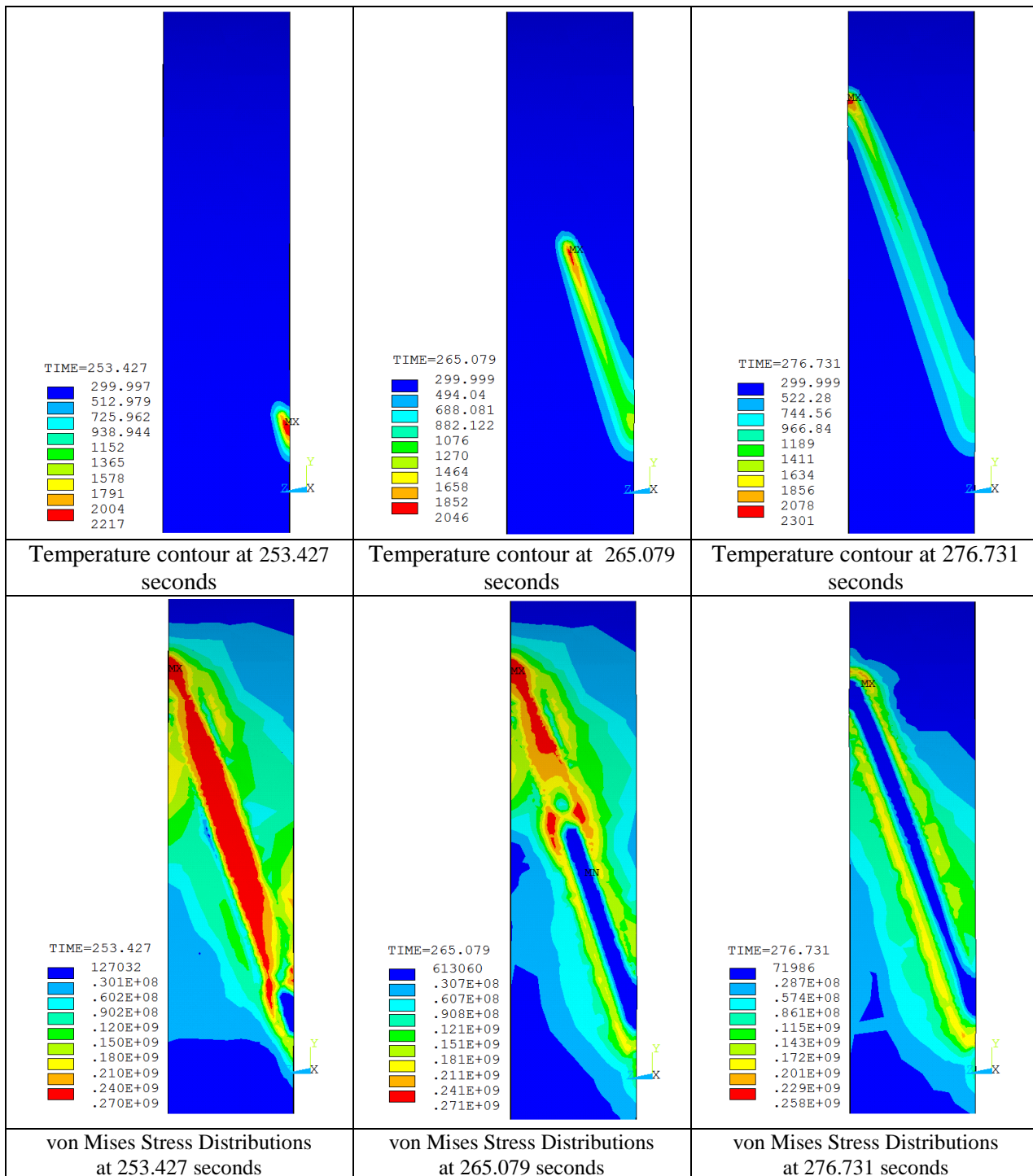


Figure 7.14: Temperature fields and von Mises stress distributions during top welding

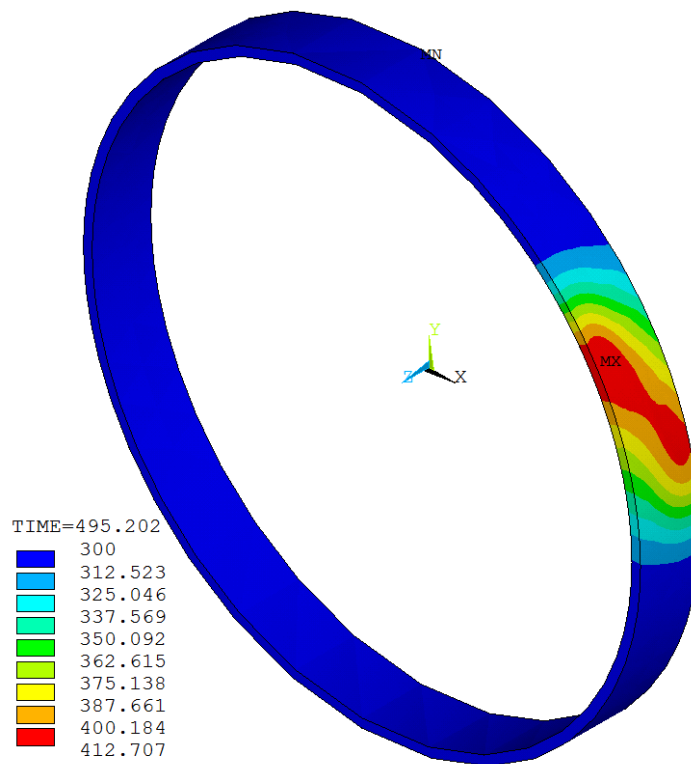


Figure 7.15: Temperature distributions after cooling

The equivalent von Mises plastic strain developed in the welding process is shown in Figure 7.16. As it can be seen, plastic strain is developed in the entire weld area and into the base material. It should be noted that the plastic zone extends in a sufficiently large surrounding area to generate the fusion of the base material with the weld.

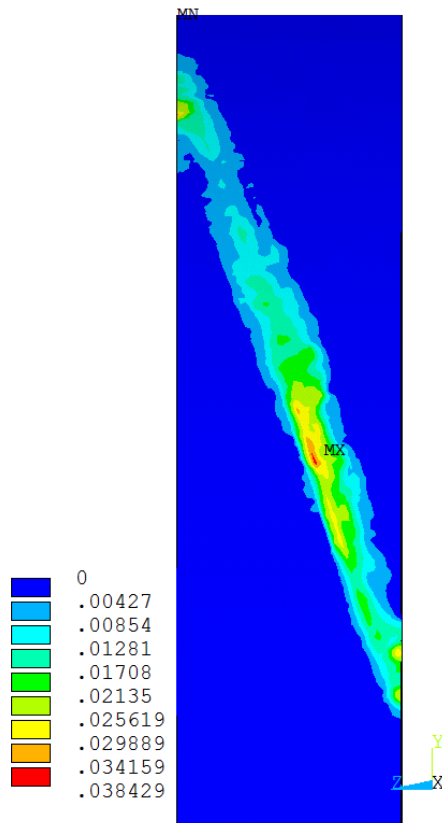


Figure 7.16: Equivalent (von Mises) plastic strain after the welding

Residual stresses in a path weld are produced primarily by shrinkage of the weld metal in the direction parallel to the weld or in the circumferential direction and shrinkage of the weld metal in the direction perpendicular to the weld or in the radial direction. Stresses in short distance from heat source are compressive during welding, because the expansion of these areas is restrained by the surrounding metal where the temperatures are lower. Since the temperatures of these areas are high and the yield strength of the material low, stresses in these areas are as high as the yield strength of the material at corresponding temperatures. The magnitude of compressive stress passes through a maximum increasing distance from the weld or with decreasing temperature.

Stresses in regions away from the weld are tensile and balance with compressive stresses in areas near the weld.

After the welded spiral pipe ring was cooled down, due to the transverse and longitudinal material shortening, residual stresses arise in the pipe. If the pipe were welded in a free condition (without tack welds and additional clamps), then the transverse stresses are not too large. The greatest values are reached near the ends of the weld. Stresses there can be both compressive and tensile. Due to the non-uniform heating process during spiral welding of the pipe, a stress state with a high level of volumetric stress may arise. Figure 7.18 to Figure 7.21 give an overall representation of the complex residual stress distributions on the pipe OD for selected nodes across the weld as shown in Figure 7.17. Typical reparative M-shaped curves of residual stresses are found in the weld area.

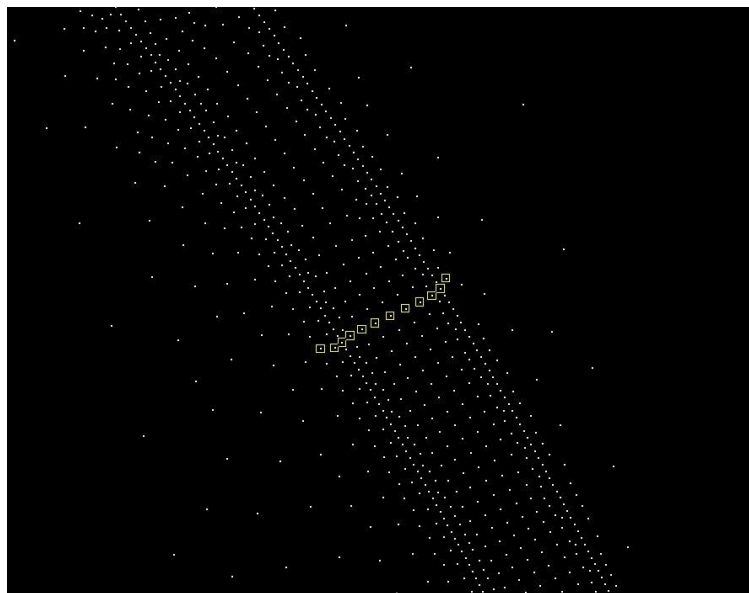


Figure 7.17: Selected nodes across the spiral weld on the OD surface

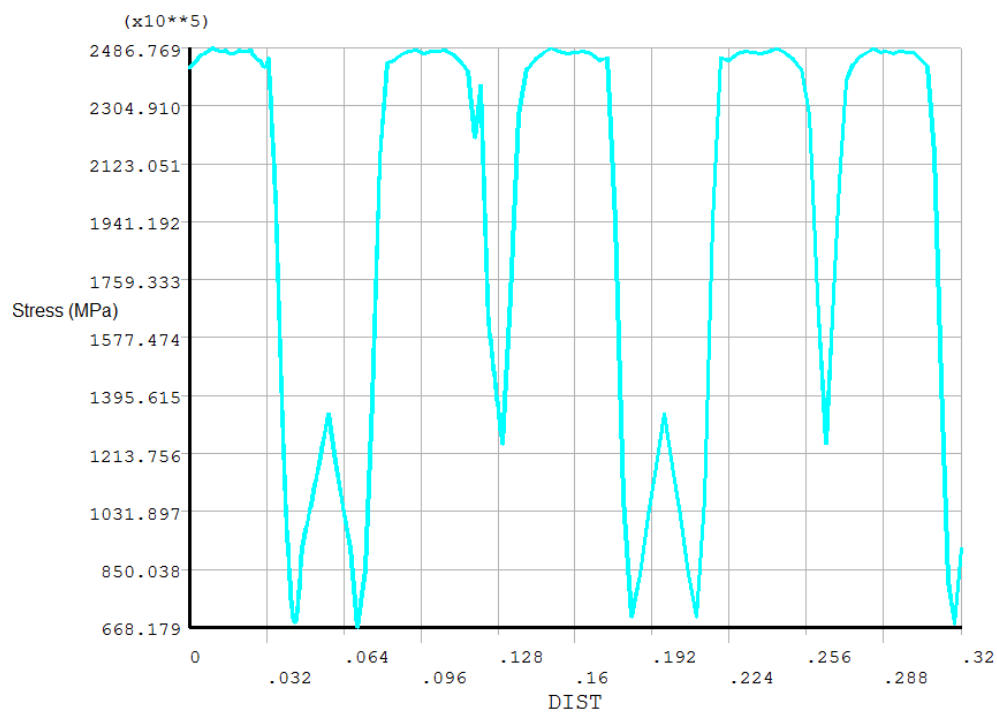


Figure 7.18: von Mises stress distributions across the weld on the OD

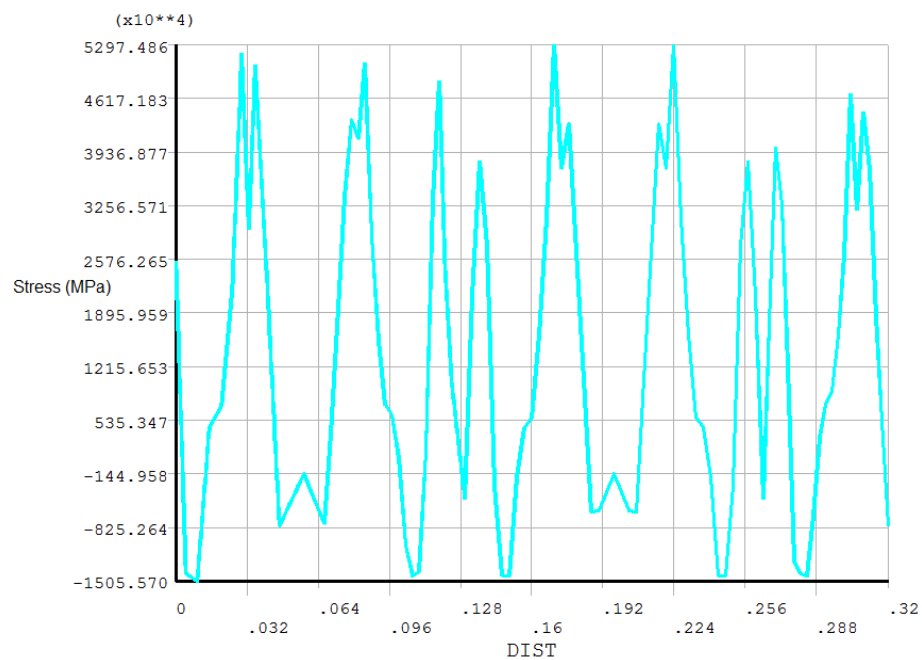


Figure 7.19: X-Component stress distributions across the weld on the OD

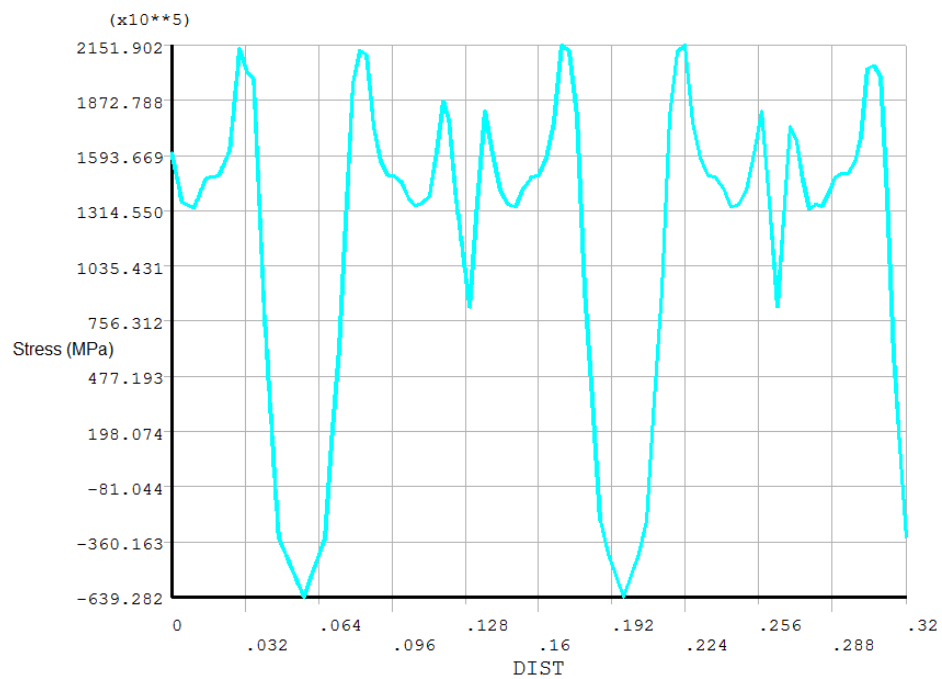


Figure 7.20: Y-Component stress distributions across the weld on the OD

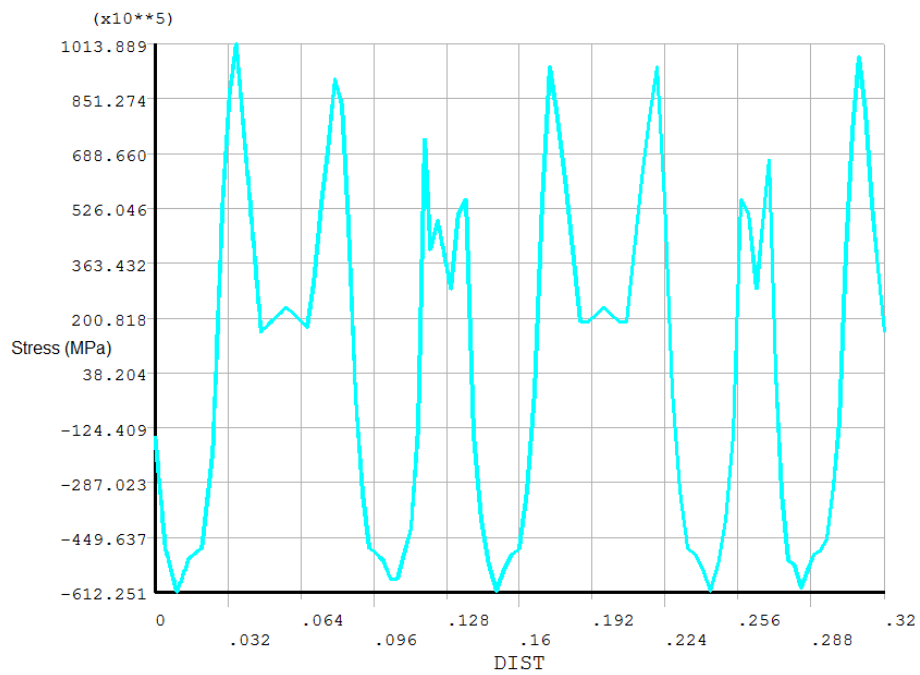


Figure 7.21: Z-Component stress distributions across the weld on the OD

The major finding from this work specific to spiral-seam residual stresses includes the presence of residual stresses with complex 3D distribution. Based on the FEM and experimental results presented on the residual stress profile for the 56-inch spiral welded pipes, it is possible to conclude that the profile of residual stresses in spiral welds can present significant variations causing non-uniformity of profiles. Apparently, the maximum stress can reach values as high as the yield strength, or much lower. Although it is not possible to conclude which variables have the most distinct effect on residual stresses, a part of this effect can be attributed to the adequate choice of weld parameters, which can bring about better stress profile behavior.

7.6 EFFECT OF WELDING SPEED ON THE RESIDUAL STRESS MEASUREMENTS

Welding speed represents the distance traveled by the welding arc along the weld line per unit of time. The welding speed has an important effect on the heat distribution pattern in the vicinity of the heat source. It is important to identify how the welding speed distribution influences the residual stress level and magnitude. The effect of welding speed on the level of residual stress has been studied for three cases of welding speed by maintaining all other input parameters same in all cases. Table 7.2 shows the cases of welding speed that were studied. All other parameters are kept at constant value.

Table 7.2: Cases for welding speed effect study

Case	1	2	3
Welding Speed (m/s)	0.0250	0.0192	0.0125

The predicted von Mises Stresses for all cases can be compared using the top view of the stress field over the pipe's surface. Figure 7.22 shows the von Mises residual stress distributions for different welding speeds used in numerical simulations.

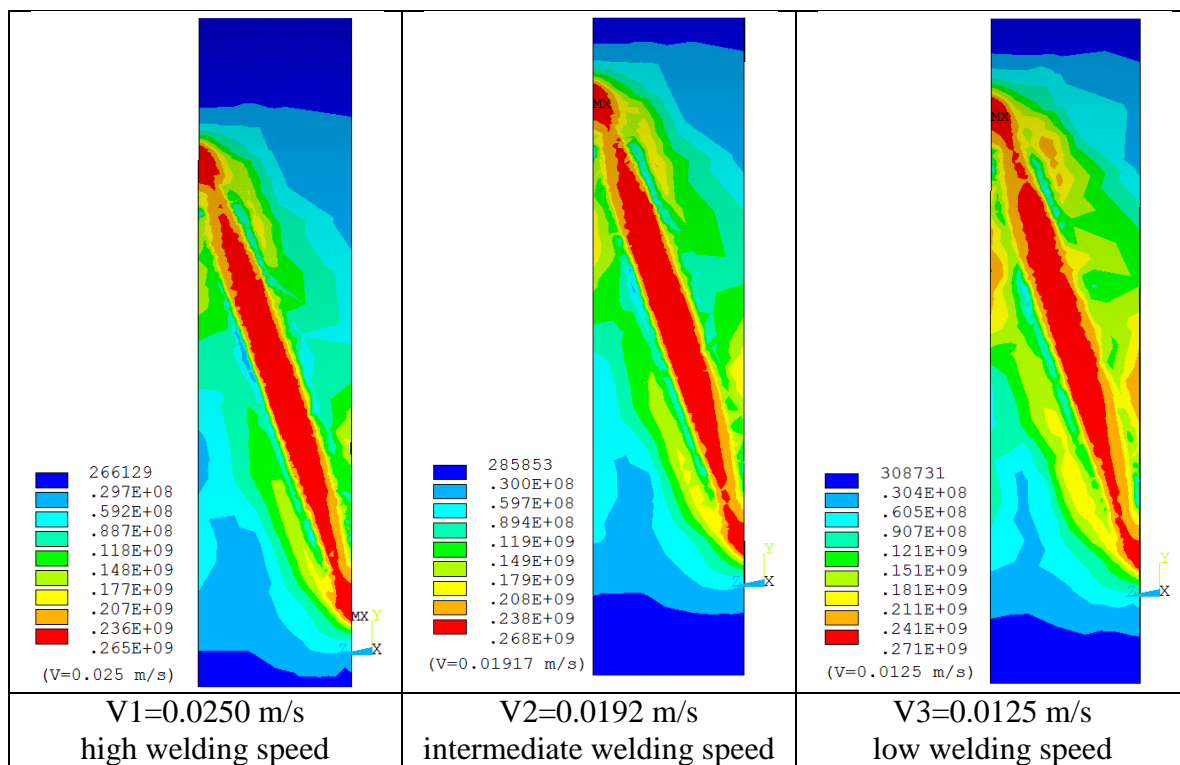


Figure 7.22: von Mises stresses for different welding speeds

Based on the theories the heat input is inversely proportional to the welding speed. Therefore, when the welding speed increases the heat input rate decreases. It was noted by FE analysis that in case of lowest welding speed of 0.0125 m/s (Case#3), wider distributions of residual stresses are observed along the spiral welding path. Technically, it is justified that the lower welding speed results in more heat input per unit volume, consequently wider fusion and HAZ zones are obtained as shown in Figure 7.22.

The width of HAZ is observed to be decreasing with increasing the welding speed. Since the current and voltage are constant for all the three cases, as the welding speed increases, less time is available for heat to flow into the base metal in front of the arc. Hence base metal absorbs complete heat required for melting from the instantaneous heat delivered by the arc. Also the time available for the heat to be transported away in the width direction is less. Thus, both these factors (welding speed, time) will lead to a decrease in the fusion zone width. Since the heat input is the same in all the cases, the decrease in width and consequent additional heat will give rise to a longer fusion zone.

It was found that the magnitude and distributions of residual stress is strongly affected by the temperature gradients and distributions for different welding speeds through the pipe wall thickness. However, it was also concluded from the results that, in general, the welding speed has minor effect on the final magnitude of residual stresses. It can be concluded that, the main welding parameters are the heat input and the welding speed. During welding, the higher value of q , the wider the plastic deformation zone.

Decreasing the welding speed, with constant q and insignificant heat loss from the free surfaces, leads to more elongation of the isotherms. Decreasing the welding speed, with constant q , results in increasing the width of the plastic deformation zone (wider residual stress distribution with insignificant increase on the level of residual stress magnitude).

CHAPTER 8

LASER WELDING

8.1 INTRODUCTION

Spiral welded tube is a circular and straight tubing manufactured by helically forming and automatically welding continuous strip. Spiral welded tubes have found world-wide application. Typical applications include water and pulp in paper mills, product and effluent lines in chemical processing, water lines for brewing, dust fume extraction, furnace and boiler flues, storm water down-pipes in high-rise applications and ventilation ducts and condensation lines for air conditioning. Spiral welded tubes are usually manufactured by the processes of welding using Tungsten Inert Gas (TIG) or Metal Inert Gas (MIG). High-energy welding processes, such as laser or electron beam welding, are being applied in an increasing array of industrial applications because of the narrow heat-affected zone, low residual distortion, high productivity, flexibility and lower operating costs compared to traditional joining processes. Laser welding has the capability of focusing the beam power to a very small spot diameter. In laser welding, a high energy density laser beam is used to melt the material. Laser welding is most efficient for thin plate applications.

In this chapter, laser welding of spiral welded tube is simulated using finite element method to predict the temperature and stress fields. The tube is 1.6 mm thick and 75 mm in diameter. Temperature-dependent thermal and mechanical properties of mild steel are included in the model. The heat input to the model is assumed to be a 3-D volumetric heat source. The finite element code ANSYS is employed to obtain the numerical results. The spiral weld is made using a laser having a maximum power of 1.0 kW.

8.2 MATHEMATICAL MODEL OF LASER WELDING

The modelling of laser welding is a highly non-linear thermo-mechanical phenomenon. The moving heat source results in localized heat generation and large thermal gradients. In addition, the thermo-physical properties of the material depend on the temperature.

8.2.1 THERMAL ANALYSIS

Consequently, for thermal analysis, the transient temperature field T of the plate is a function of time t and the spatial coordinates (x, y, z) , and is determined by the non-linear heat diffusion equation:

$$\rho(T)C_p(T)\frac{\partial T}{\partial t} = \frac{\partial}{\partial x}\left(k(T)\frac{\partial T}{\partial x}\right) + \frac{\partial}{\partial y}\left(k(T)\frac{\partial T}{\partial y}\right) + \frac{\partial}{\partial z}\left(k(T)\frac{\partial T}{\partial z}\right) + q \quad (8.1)$$

where x , y and z are the axes as shown in Figure 8.1, T is the temperature, t is time, and q is the heat generation rate per unit volume. $\rho(T)$, $C_p(T)$ and $k(T)$ are the temperature dependent density, specific heat and conductivity of the plate material, respectively.

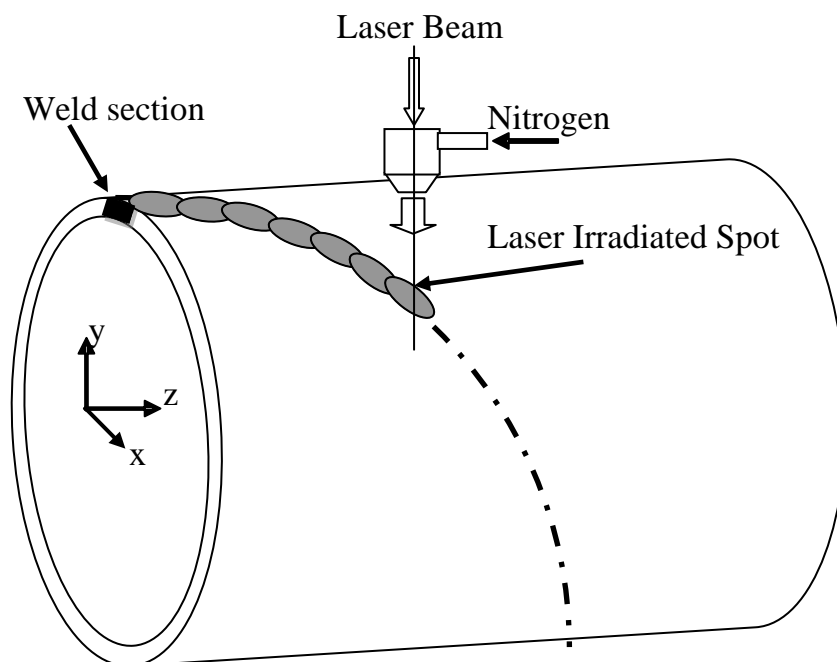


Figure 8.1: View of laser welding process

Heat losses from all surfaces of the tube by convection q_c and radiation q_r are introduced as boundary conditions, using the following equation:

$$q_c = h(T - T_\infty) \quad (8.2)$$

$$q_r = \xi \times \Sigma (T^4 - T_\infty^4) \quad (8.3)$$

where h is the convection coefficient, T_∞ is the room temperature, ξ is the emissivity of the body's surface ($\xi = 0.9$ is considered), and Σ is the Stefan-Boltzman constant ($\sigma = 5.67 \times 10^{-8} \text{ W/m}^2\text{K}$). Initially, the substrate material is assumed to be at a reference temperature equal to the room temperature T_∞ . Therefore, the initial condition becomes: at $t = 0$, $T = T_\infty$.

Equation (8.1) is solved numerically with the appropriate boundary conditions to predict the temperature field in the substrate material. In order to consider the fusion latent heat (phase change), the value of the heat capacity suffers an abrupt increase followed by an abrupt decrease at fusion temperature leading to numerical non-convergence. Therefore, to analyze the phase change problem, a nonlinear transient thermal analysis is performed employing enthalpy method. To account for latent heat evolution during phase change, the enthalpy of the material as a function of temperature is incorporated in the energy equation.

8.2.2 HEAT SOURCE MODEL

Proper modeling of the heat source is crucial as it controls the thermal load, and consequently the weld-bead profile. For a volumetric distribution, a finite three-dimensional Gaussian distribution on an ellipsoid or a double ellipsoid is the most common. The most widely acceptable model for simulation of arc welding processes was presented by Goldak et al. [1984]. Goldak proposed a double-ellipsoidal heat source model, which has the capability of analyzing the thermal fields of deep penetration welds given above. The power densities of the ellipsoidal heat source, $q(x,y,z)$ describing the heat flux distributions inside heat source and it can be expressed as:

$$q(x, y, z) = \frac{6\sqrt{3}fQ}{abc\pi\sqrt{\pi}} e^{(-3\frac{x^2}{a^2})} e^{(-3\frac{y^2}{b^2})} e^{(-3\frac{z^2}{c^2})} \quad (8.4)$$

where

Q is the energy input rate,

f is the fractional factor of the heat deposited in the front and rear quadrant, and

a, b, c are heat source parameters

Goldak's model has been modified in the present work to model laser beam as heat source as shown in the Figure 8.2. The spatial heat distribution in a moving frame of reference can be calculated as follows:

$$q = \frac{6\sqrt{3}}{\pi\sqrt{\pi}} \frac{\alpha Q}{br_0^2} e^{-3\left(\frac{x}{r_0}\right)^2} e^{-3\left(\frac{y}{b}\right)^2} e^{-3\left(\frac{z-Vt}{r_0}\right)^2} \quad (8.5)$$

Where

α = Absorption coefficient

Q = Laser power (W)

r_0 = Laser beam radius at focused surface

V = Laser welding speed

b = Heat source parameter which depends on the focal spot dispersion

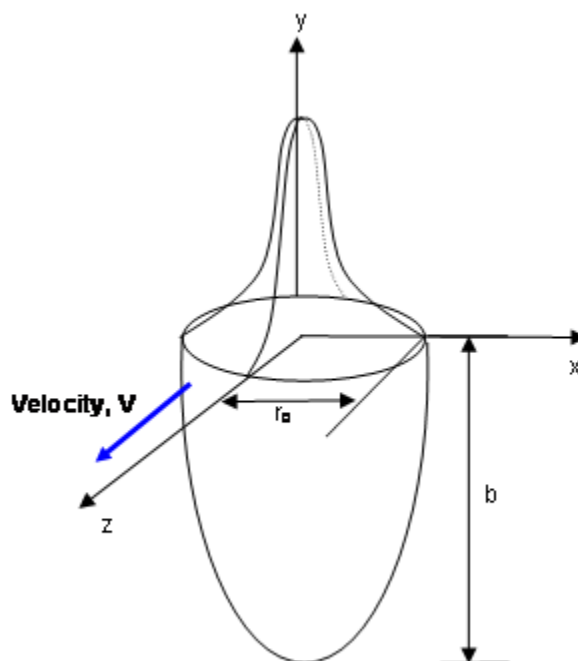


Figure 8.2: The spatial heat distribution in the volumetric heat input model

Figure 8.2 shows 3D heat source model, where the power density deposited region is maximum on the top surface along the weld path, and is minimum at the inner surface. Along the wall thickness, the diameter of the power density distribution region is linearly decreased.

8.2.3 STRESS ANALYSIS

From the principle of virtual work (PVW), a virtual (very small) change in the internal strain energy (δU) must be offset by an identical change in the external work due to the applied loads (δV). Considering the strain energy due to the thermal stresses resulting from the constrained motion of a body during a temperature change, PVW yields:

$$\{\delta u\}^T \int_{vol} [B]^T [D][B] dv \{u\} - \{\delta u\}^T \int_{vol} [B]^T [D] \{\varepsilon^{th}\} dv = \{\delta u\}^T \int_{Area} [N_s]^T \{p\} dS + \{\delta u\}^T \{F_N\} \quad (8.6)$$

Noting that the $\{\delta u\}^T$ vector is a set of arbitrary virtual displacements common in all of the above terms, the condition required to satisfy the above equation reduces to:

$$[K] \{u\} = \{F^{th}\} + \{F^{pr}\} + \{F^n\} \quad (8.7)$$

where

$$\begin{aligned} [K] &= \int_{vol} [B]^T [D][B] dv = \text{Element stiffness matrix} \\ \{F^{th}\} &= \int_{vol} [B]^T [D] \{\varepsilon^{th}\} dv = \text{Element thermal load vector} \\ \{\varepsilon^{th}\} &= \{\alpha\} \Delta T = \text{Thermal strain vector} \\ \{\alpha\} &= \text{vector of coefficients of thermal expansion} \\ \{F^{pr}\} &= \int_{Area} [N_s]^T \{p\} dS = \text{Element pressure vector} \\ \{F^n\} &= \text{Nodal force vector} \end{aligned}$$

In the current work, the effect of mechanical deformation on the heat flow has been ignored and the thermo-mechanical phenomenon of melting is idealized as a sequentially-coupled unidirectional problem. Based on this simplified approach a fully coupled thermo-metallurgical analysis is performed first, which is followed by a structural analysis. During the thermal analysis, micro-structural evolution can be modeled by either more sophisticated direct calculation procedure or by relatively simpler but common method of indirect incorporation of micro-structural aspects into the material model. During the structural analysis, temperature and microstructure dependence of stresses and deformations are accommodated by invoking the results of thermal-metallurgical analysis into the stress analysis.

8.3 FINITE ELEMENT MODEL

Prediction of temperature field and resulting residual stresses foremost relies on accurate prediction of the weld thermal cycle. In this work, a nonlinear, transient, three dimensional finite element analysis of the spiral laser welding process is adopted. The problem analyzed was that of a spiral welded tube with 75 mm outer diameter and 1.6 mm wall thickness. The length of the modeled tube ring was 30 mm. A spiral weld path can be described by the global cylindrical coordinate system (Figure 8.3) whose origin coincides with the curve passing through the tube's cross section center. This spiral line is characterized by the pitch length, pipe diameter (D) and forming angle (α). Figure 8.3

represents, schematically, a weld joint model dragged over a spiral weld line with a pitch (p) and pipe radius R.

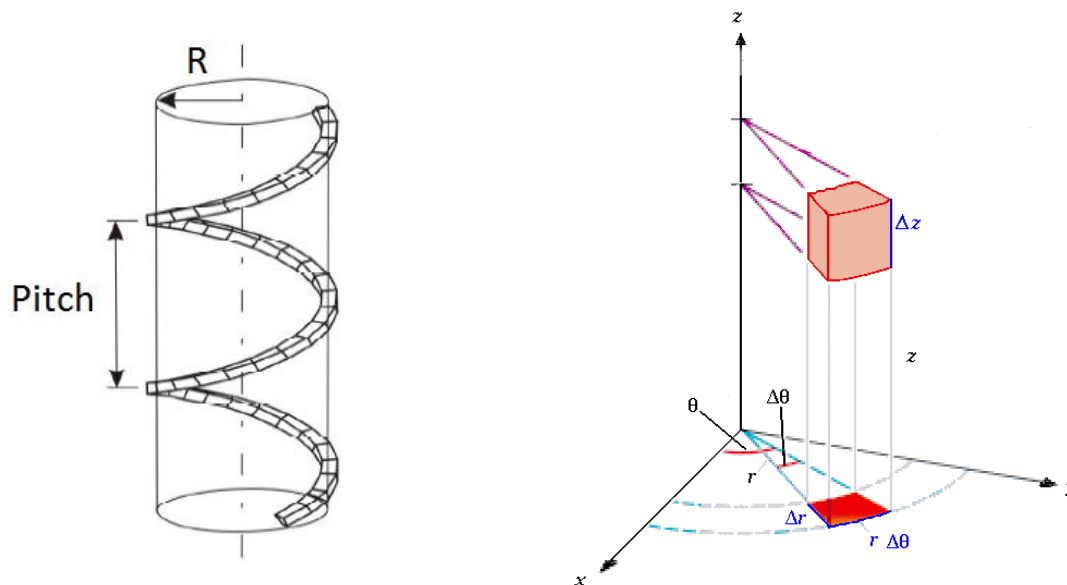


Figure 8.3: Basic concept for weld spiral path in cylindrical coordinate system

The spiral weld path is defined by n discrete points equally positioned along the spiral path. The x , y , z points are created to cover only the 30 mm tube section which represent the ring. To generate the weld path, the weld joint model developed before is revolved (dragged) along a spiral weld path. A user subroutine was developed to create these points for spiral weld path and then creating the line. After creating the weld joint area and the spiral line, dragging has been performed in order to create the weld volume. The final model for the 75 mm Spiral Welded Ring is shown in Figure 8.4 for one

complete spiral pitch. The geometric and welding parameters used in this work are given in Table 8.1.

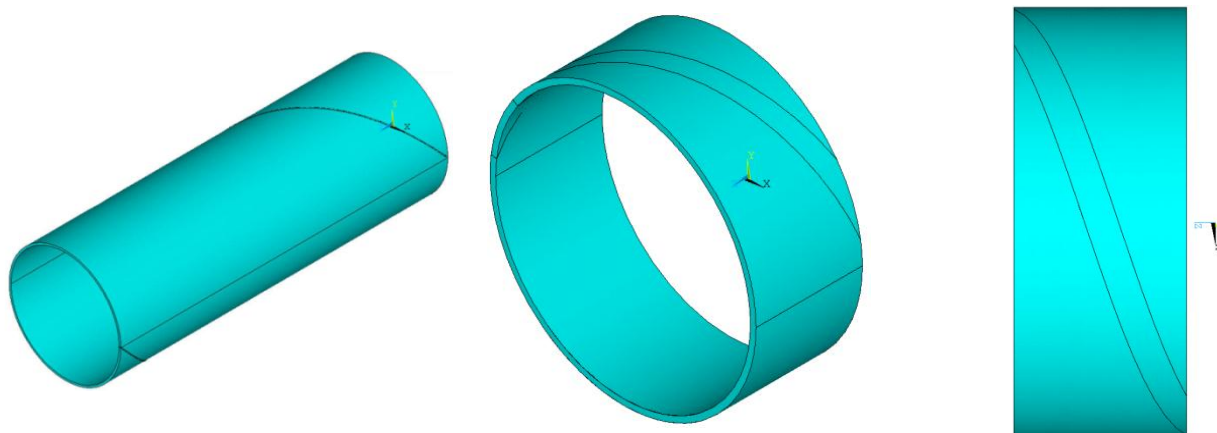


Figure 8.4: (a) 3D model of 75 mm spiral welded tube for one complete pitch, (b) Tube ring of 30 mm length, (c) Weld geometry in the ring

Table 8.1: Pipe and welding parameters

<i>Thickness, t</i> (mm)	<i>Pipe diameter,</i> <i>D</i> (mm)	<i>Alpha</i> (degree)	<i>Pitch, p</i> (mm)	<i>Ring width,</i> <i>w</i> (mm)	<i>Ratio</i> (w/p)	<i>Welding speed</i> (mm/s)	<i>Laser power</i> (W)
1.6	75	19	79	30	0.38	30	1000

The thermal and structural properties used in the current simulations are given in the Table 8.2 to Table 8.4 [Mahapatra et al. 2006]. To avoid the sharp change in the value of specific heat with melting, enthalpy was used as the material property. This was done by defining the enthalpy of a material as a function of temperature as given in Table 8.3.

Table 8.2: Temperature-dependent thermal conductivity of steel [Mahapatra et al. 2006]

<i>Temperature (K)</i>	273	373	573	723	823	873	993	1073	1783	1853
<i>Thermal Conductivities (W/m.K)</i>	51.9	51.1	46.1	41.05	37.5	35.6	30.64	26	29.7	31

Table 8.3: Temperature-dependent enthalpy properties used for steel

<i>Temperature (K)</i>	300	1,640	1,809	3000
<i>Enthalpy (J/m³)</i>	0	5.02E+09	7.12E+09	1.12E+10

Table 8.4: Temperature-dependent mechanical properties of steel [Mahapatra et al. 2006]

Temperature (K)	Yield Stress, σ_y (MPa)	Young's Modulus, E (GPa)	Poisson's Ratios	Thermal Expansion Coefficient, α (1/°C)
273	290.0	200.0	0.2786	1.0E-05
373	260.0	200.0	0.3095	1.1E-05
573	200.0	200.0	0.3310	1.2E-05
723	150.0	150.0	0.3380	1.3E-05
823	120.0	110.0	0.3575	1.4E-05
873	110.0	88.0	0.3738	1.4E-05
993	9.8	20.0	0.3738	1.4E-05
1073	9.8	20.0	0.4238	1.4E-05
1473	2.0	20.0	0.4538	1.5E-05
1783	2.0	2.0	0.4738	1.5E-05
1853	1.0	0.2	0.4990	1.5E-05

In the present work, the effect of mechanical deformation on heat flow has been ignored and the thermo-mechanical phenomenon of melting is idealized as a sequentially-coupled unidirectional problem. For thermal analysis, the given structure is modeled using thermal element (SOLID70). SOLID70 has a 3-D thermal conduction capability [ANSYS 2007]. The element has eight nodes with a single degree of freedom, temperature, at each node. The element is applicable to a 3-D, steady-state or transient thermal analysis. Since the model containing the conducting solid element is also to be analyzed structurally, the element is replaced by an equivalent structural element (such as SOLID45) for the structural analysis. SOLID45 is used for the 3-D modeling of solid

structures. The element is defined by eight nodes having three degrees of freedom at each node: translations in the nodal x, y, and z directions. The element has plasticity, creep, swelling, stress stiffening, large deflection, and large strain capabilities.

For laser, individual element quality directly determines the overall mesh quality and the consequent analysis including thermal and structural. Another important aspect of laser welding modeling is the mesh density, especially along the weld line and the Heat Affected Zone (HAZ). This is mainly due to the very small diameter of the heat source. A sequence of trials has been conducted to select suitable number of elements particularly at the area closer to the weld line and in the thickness direction. More specifically geometries with 4, 6 and 8 elements through the thickness were tested for tube with 1.6 mm thickness. It was decided to use 8 elements for the 1.6 mm thick tube since this mesh required reasonable convergence and solution time with no significant loss of accuracy. A dense mesh was used in the area along the weld line, as shown in Figure 8.5, and a coarser mesh for the rest of the structure. The final mesh was the result of compromise between computing time and accuracy. The mesh has 132,713 eight-node elements and 16,108 nodes. An appropriate time-stepping scheme was used for each analysis to achieve fast convergence of the solution and reasonable accuracy.

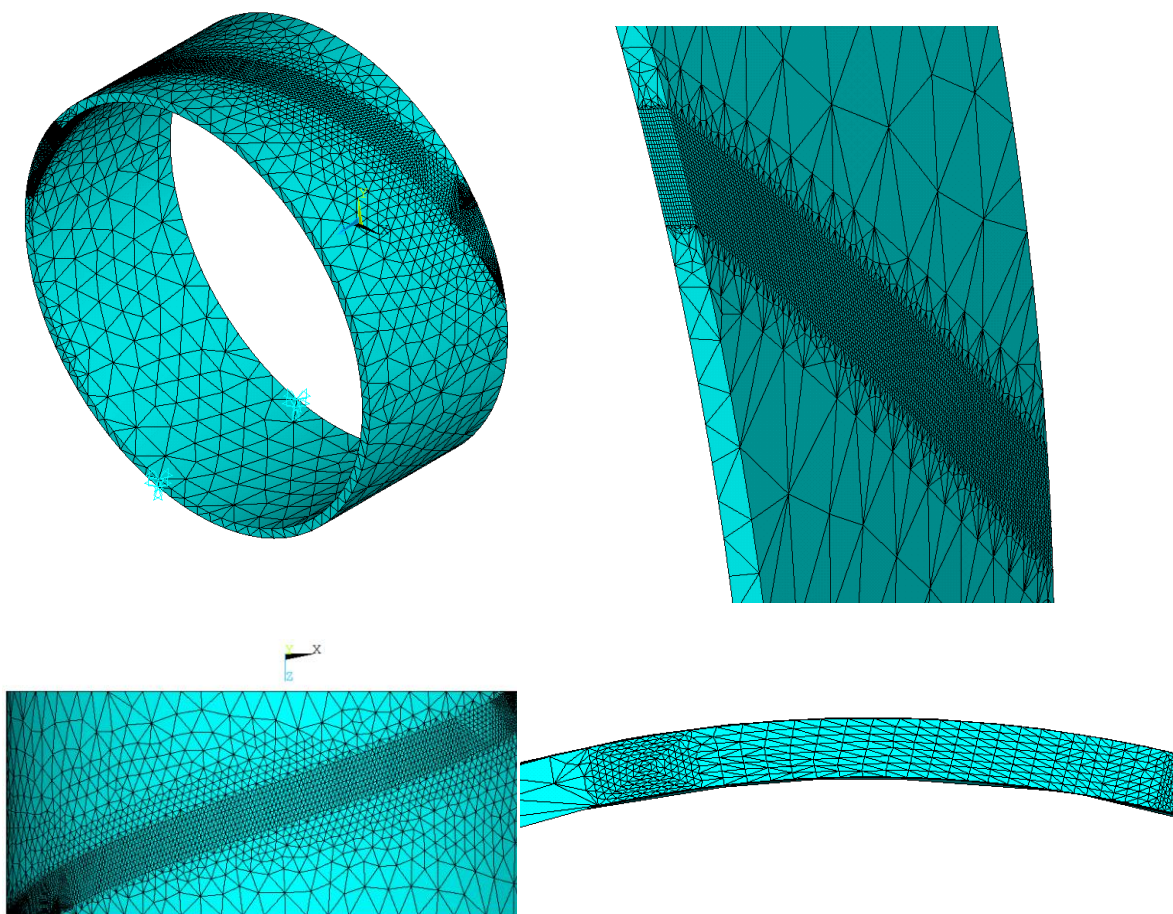


Figure 8.5: Finite element mesh

In this study, a moving cylindrical coordinate system is used to move the heat source as shown in Figure 8.6. Instead of moving the heat source continuously, it is moved in steps, that is, heat is applied at each successive point one after the other chronologically. By making the distance between successive points very small, a close approximation to the continuous movement can be achieved.

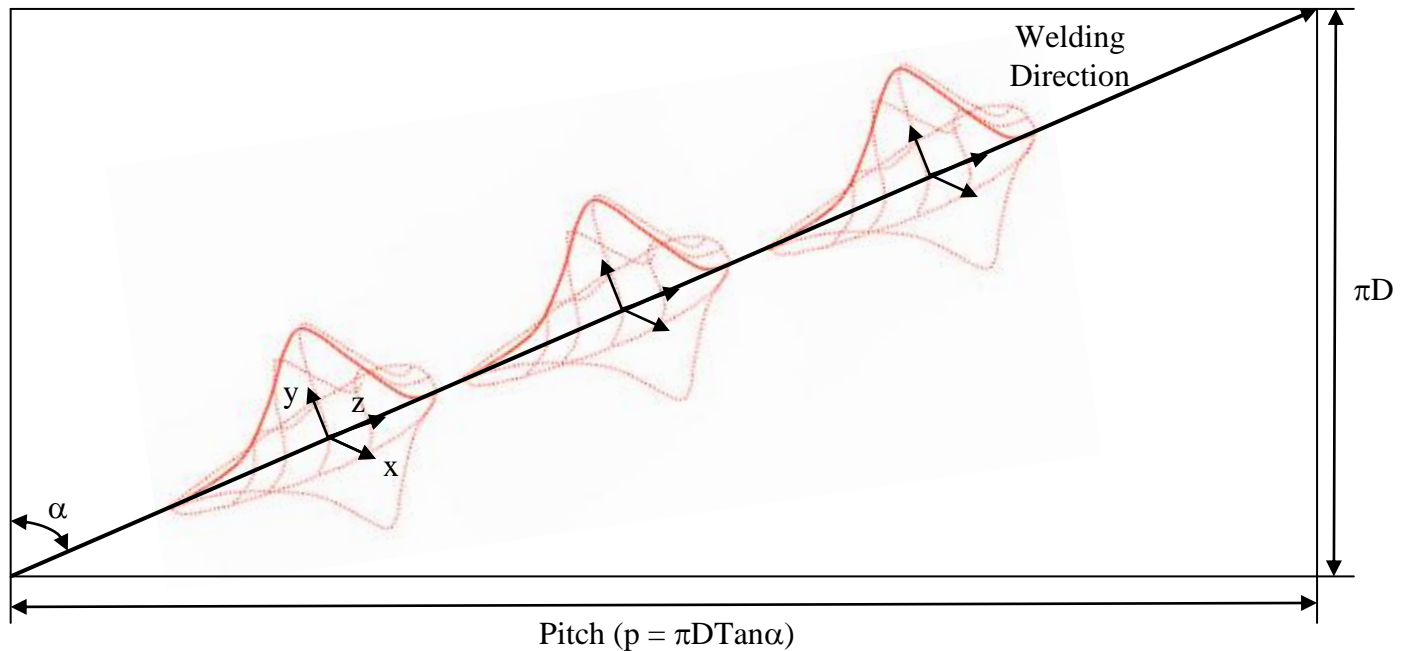


Figure 8.6: Showing the movement of the heat source along the unfolded spiral weld path

Figure 8.7 shows the heat source at different positions at different times along the weld path. The coordinate system is moved after each load step. At every load step a set of elements in the shape of the tool are selected and a volumetric heat generation is applied to the selected elements. The added advantage of volumetric heat generation is that the elements lying on the surface can be used to model the surface heat convection which otherwise require additional two dimensional surface elements for this purpose. APDL (ANSYS parametric design language) is used to write a subroutine for a looping transient moving heat source model. The welding speed, the fraction value f , and the semi-axis of Goldak's heat source parameters used in the calculation are shown in Table 8.5.

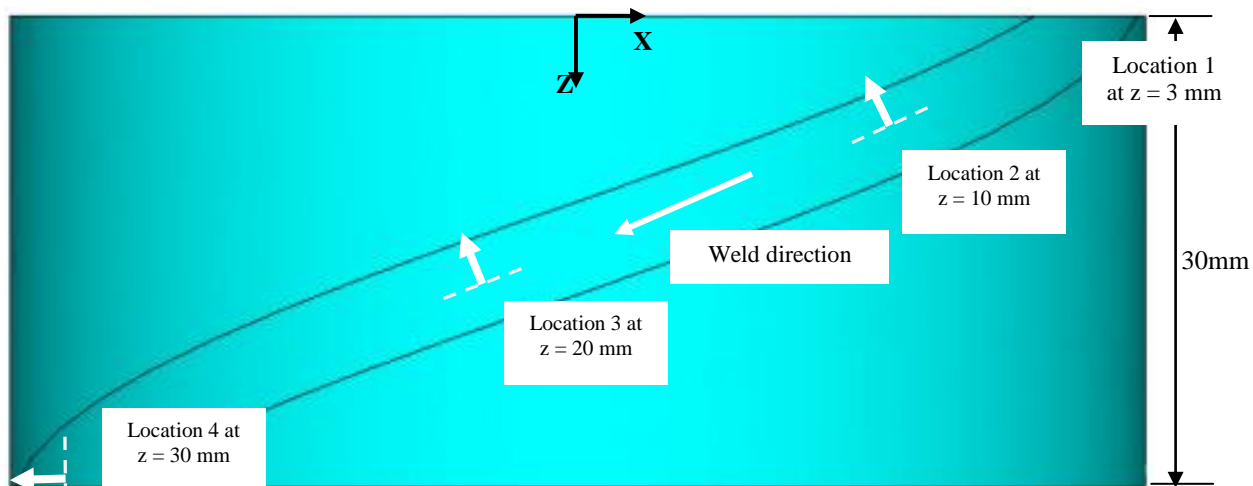


Figure 8.7: Schematic showing welding direction and distance measured across weld at four locations.

Table 8.5: Heat source parameters

<i>Diameter of Laser Beam</i>	<i>d (mm)</i>	<i>1.2</i>
<i>Front heat spot distance= (2/3 d)</i>	<i>c (mm)</i>	<i>0.8</i>
<i>Welding heat spot half width= (2/3 d)</i>	<i>a (mm)</i>	<i>0.8</i>
<i>Welding heat spot depth</i>	<i>b (mm)</i>	<i>5</i>
<i>Goldak Factor</i>	<i>f</i>	<i>1</i>
<i>Welding speed</i>	<i>v (mm/sec)</i>	<i>30</i>
<i>Welding Power</i>	<i>Q (Watt)</i>	<i>1000</i>

8.4 RESULTS AND DISCUSSIONS

Laser welding of mild steel spiral tube is carried out. Temperature and stress fields developed during the welding are computed using the finite element method. Figure 8.7 shows the position of laser heat source at three locations. The corresponding z-

axis location from the welding starting point, time when the laser beam spot center at the location, load step number for finite element simulation and distance along weld path from the starting point are given in Table 8.6.

Table 8.6: Details of locations

<i>Location</i>	<i>z-coordinate</i> <i>(mm)</i>	<i>Time</i> <i>(sec)</i>	<i>Load step</i>	<i>Distance along</i> <i>weld path (mm)</i>
<i>Location 1</i>	3	0.371	10	8.73
<i>Location 2</i>	10	1.112	30	31.0
<i>Location 3</i>	20	2.224	60	64.5
<i>Location 4</i>	30	3.188	86	91.0
<i>After cooling</i>	--	12.456	136	--

Figure 8.8 shows two-dimensional view of temperature distribution on the outer surface of the tube at four different times. The effect of the moving heat source on the distribution of temperature on the outer surface of the tube with time and the rapid heat transfer in the welding zone is evident from this figure. It also appears that the isotherm line presents ellipse. The isotherm line is dense in front of the laser source and the temperature level is high there while in the back of the moving laser source, the complexion is contrary. The heat inputs generated by the moving heat source along the welding line are gradually transferred in all directions of the tube by conduction, convection and radiation. The temperature variation along the weld path is shown in Figure 8.9. It can be seen from the figures that the outer surface temperature along the spiral line is higher than the temperature along the inner surface spiral line. It is also

clearly noticed from the peaks that temperature is substantially higher when the welding laser beam just passes the plane but it decreases rapidly with time. The sharp increase in temperature occurs at a location where the laser beam intensity is the maximum. This is due to the absorption of the laser beam energy by the substrate material, which enhances significantly the internal energy gain in this region. Therefore, temperature increases sharply in the molten material. At location 2 (Figure 8.7), the distance along the spiral weld path is 31 mm from the welding starting point (Figure 8.9) and it should be noted that the time $t = 1.112$ seconds corresponds to the laser beam spot center at that location. The temperature is 2055 K on the outer surface and it decays sharply as the distance in the welding direction increases. Similar trend is observed on the inner surface region except that due to time taken by heat diffusion in tube thickness, the peak temperature of 1915 K occurs at a distance of 29 mm from the starting point. As expected, the temperature in the weld region over the thickness exceeds the melting temperature of the substrate material. In addition, temperature profiles at other locations along the weld path on both outer and inner surfaces become almost self-similar.

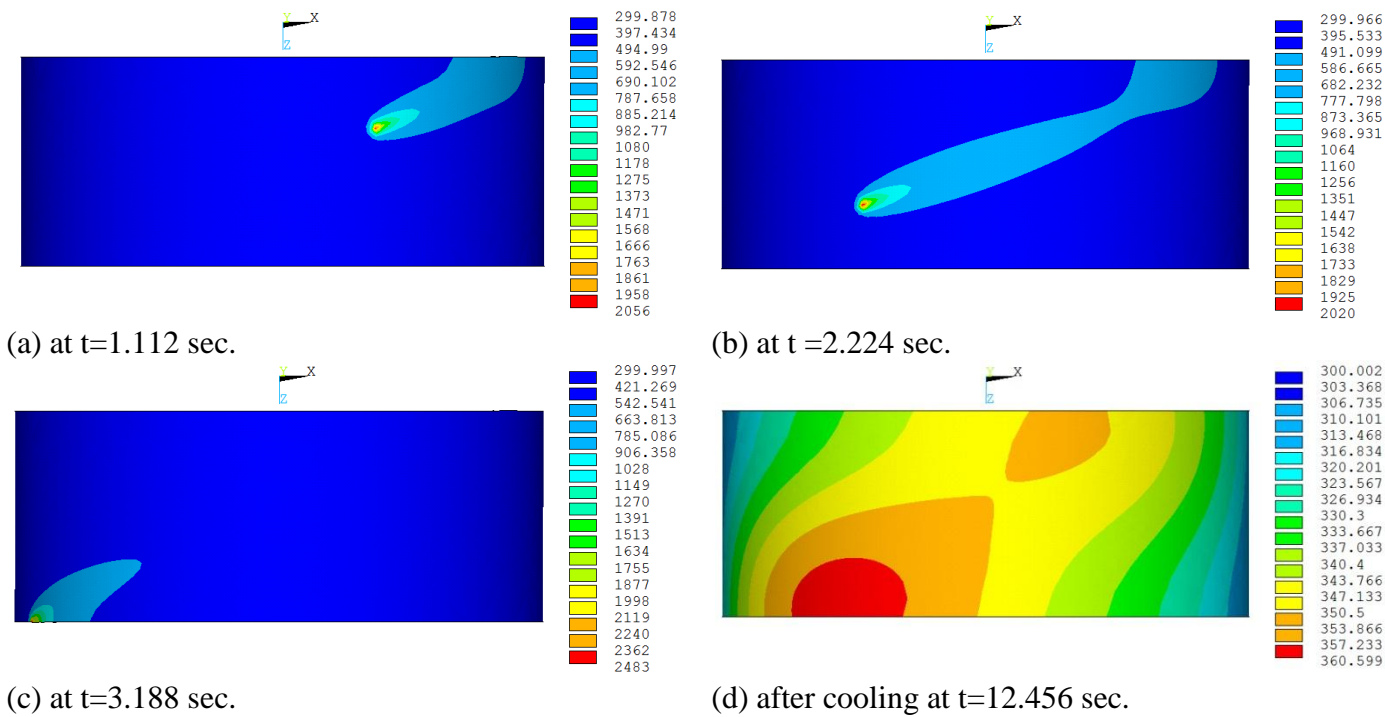


Figure 8.8: Temperature distribution on the outer surface at different times.

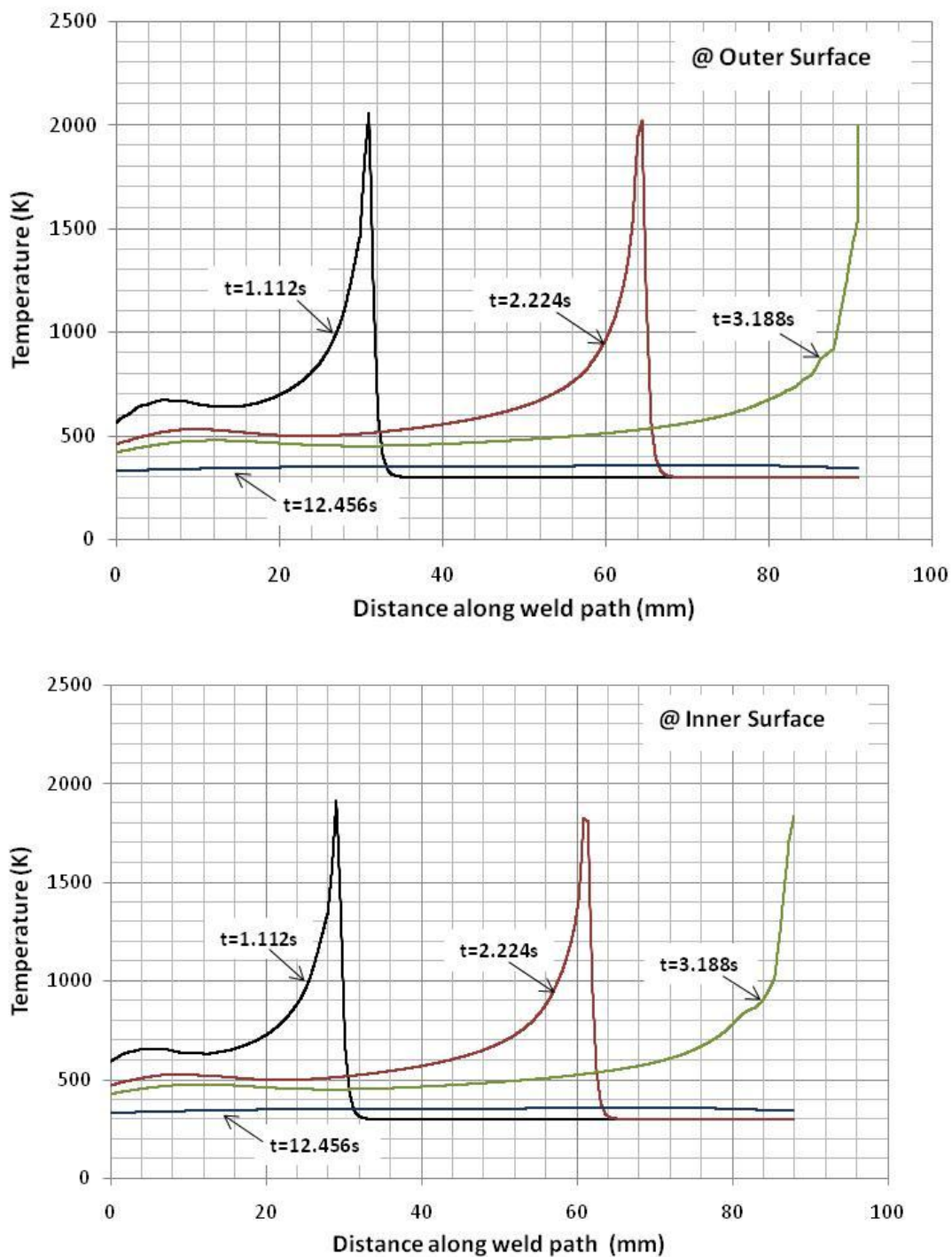


Figure 8.9: Temperature distribution along the spiral weld path on the outer and inner surfaces.

Figure 8.10 shows the temperature distribution across the weld at a distance of 91 mm from the starting point along the weld path (location 4). The temperature distribution on both the outer and inner surface is not symmetric due to spiral weld path. Heat dissipation due to conduction will always be more on the left side of the weld path and, therefore, the temperature is higher on the left side as compared to right side. Thus, an unsymmetrical heat affected zone is expected in spiral welded tubes. Although temperature at the melting solid interface will remain the same - due to the influence of latent heat of fusion on the energy transfer in the vicinity of melting-solid interface - temperature gradient in the molten region becomes different that in the solid phase. Moreover, the decay rate of temperature as well as its magnitude changes at different locations on outer and inner surface in the melting zone.

Figure 8.11 shows temporal variation of temperature at three different locations. Temperature attains high values when the laser beam reaches at locations shown in the figure. However, time taken for laser beam to reach at different locations is not the same. Since the length scale as seen by the laser beam is not same. It should be noted that the laser scanning speed is kept constant during the welding process. Temporal decay of temperature after its maximum is almost the same at different locations (“1”, “2” and “3” in Figure 8.7), provided that the difference in the decay rate is more pronounced after the time of sharp decay of temperature at each locations. This is because of the conduction heating before the laser beam reaching these locations. Consequently, temperature

remains almost 500 K for location “1”, 450 K for location “2”, and 400 K for location “3” after 3 seconds of the welding duration.

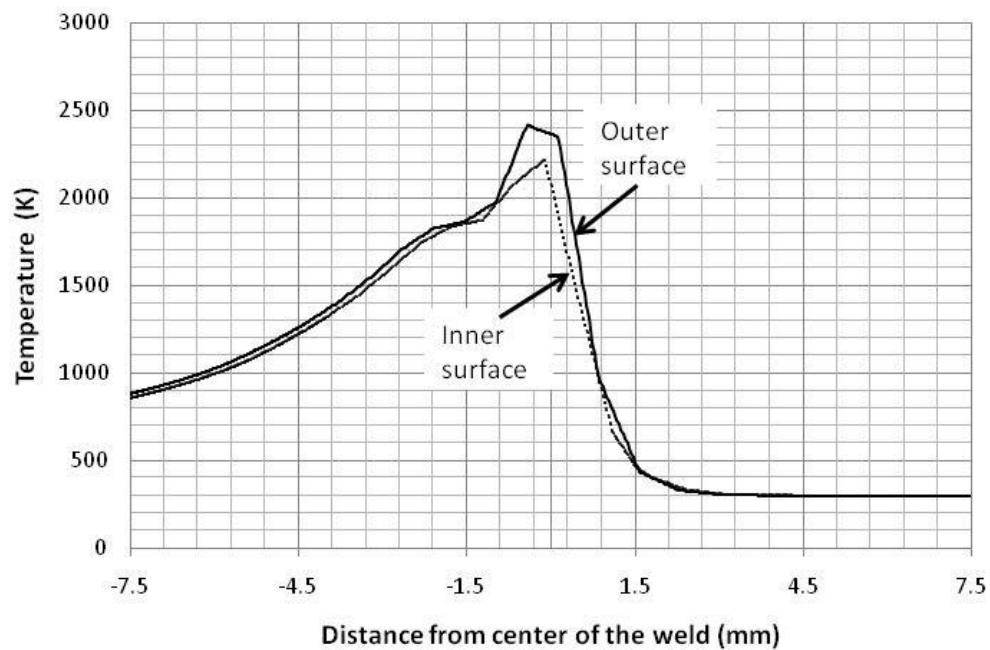


Figure 8.10: Temperature Distribution across the weld at location 4.

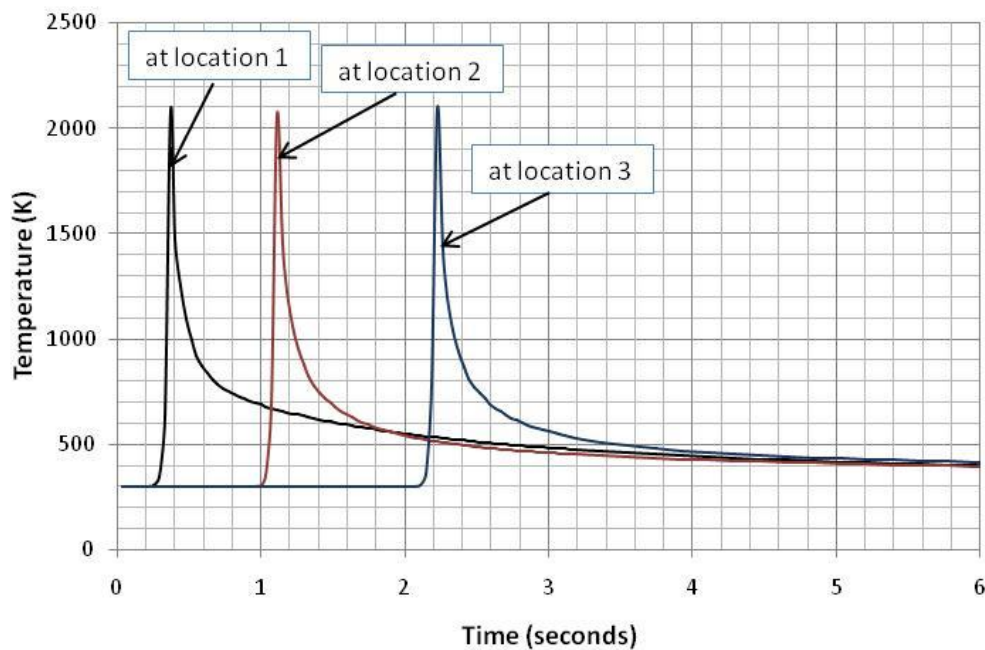


Figure 8.11: Temporal variation of temperature at three different locations.

Figure 8.12 shows von Mises stress along the spiral weld path at four different times while Figure 8.13 shows a plane view of von Mises stress on the outer surface of the tube. As the heat source approaches, there is sudden drop in von Mises stress at all three locations because of the melting; in which case, molten metal is free to expand in this region. The variation of von Mises stress along the spiral weld line is similar at outer and inner surfaces of the tube, since the difference in the stress magnitude is negligibly small. It should be noted that the time 12.456 seconds corresponds to the cooling period. Consequently, the stress value for the time 12.456 seconds corresponds to the residual stress for these locations. von Mises stress remains high along the weld path behind the heat source, despite the fact that temperature decays gradually along. This is because of the attainment of high thermal strain along the weld path. The von Mises residual stress

fields are identical in trend and magnitude on both outer and inner surfaces of the tube. Thermal stress developed during high temperature heating contributes to the stress field developed during the cooling period. Consequently, von Mises stress at any time does not follow exactly the temperature distribution as shown in Figure 8.8.

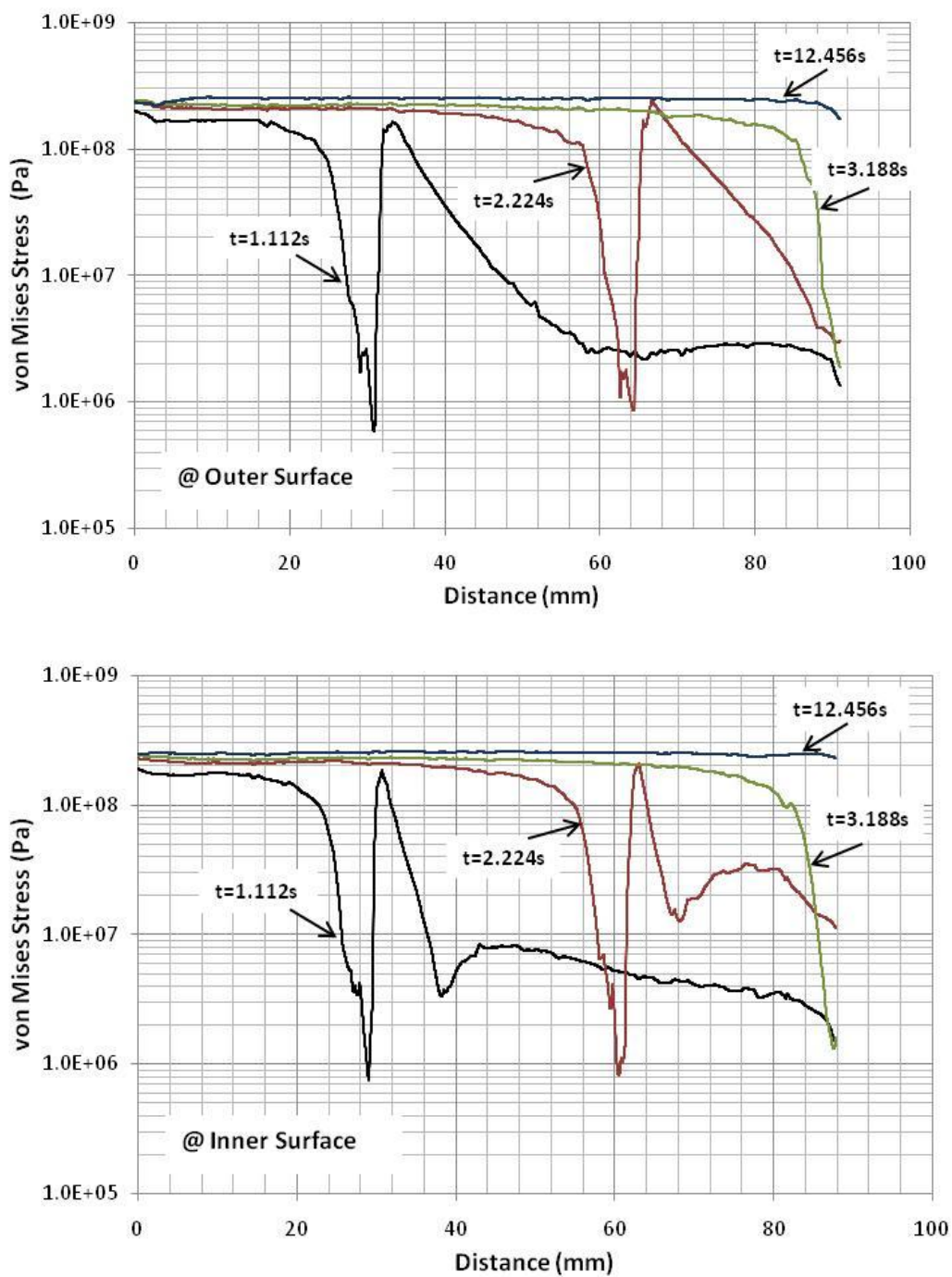


Figure 8.12: von Mises stress distribution along the spiral weld path on the outer and inner surfaces.

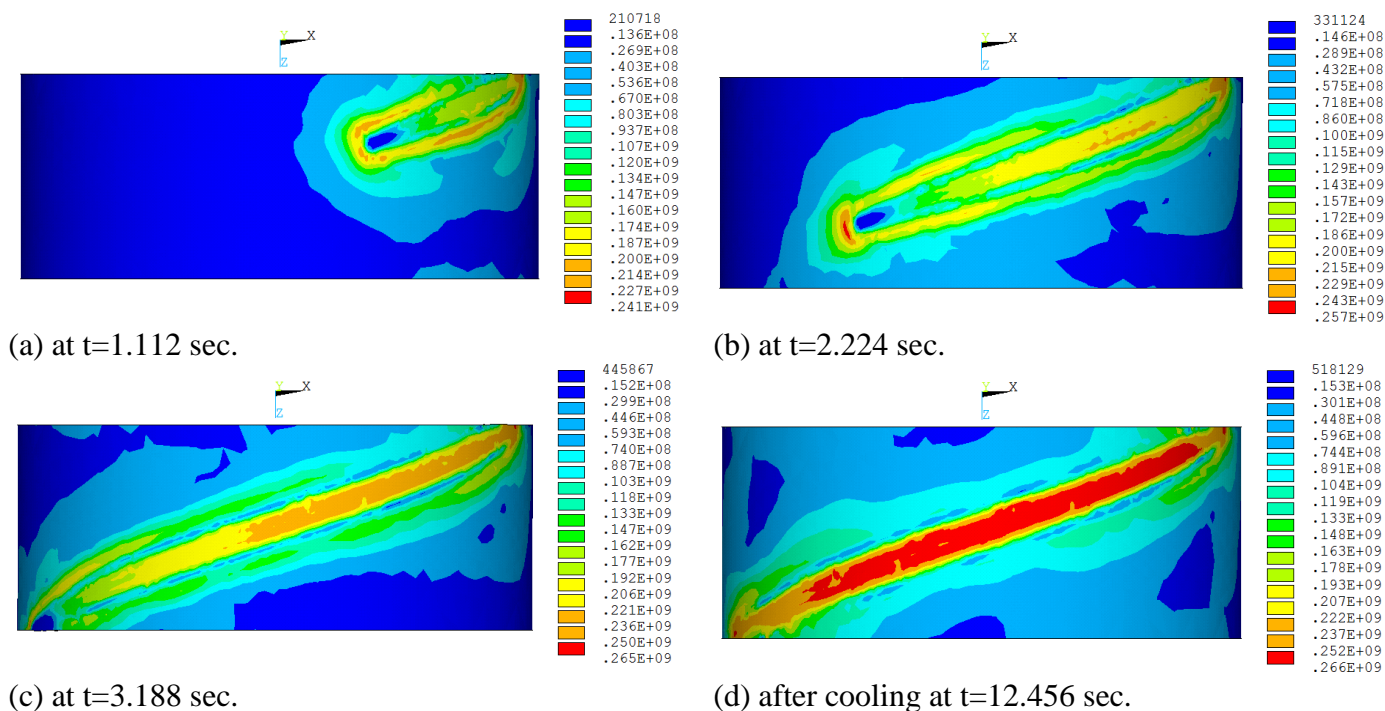


Figure 8.13: von Mises stress distribution on outer surface at different times.

Figure 8.14 shows temporal variation of von Mises stress at the same locations shown in Figure 8.11. von Mises stress increases as the heat source approaches these locations with increasing temperature. During phase change, stress value reduces with minimum at the peak temperature when the substrate material is in molten state. However, von Mises stress attains high values for the time when temperature decay is large. This follows by gradual increase in von Mises stress with the progressing time. Moreover, two local maxima (sharp peaks) are observed in von Mises stress at each location shown in the figure. This can be attributed to the temporal evolution of thermal strain due to the rate of change in the temperature for the time when von Mises stress

reduces to local minimum between the two peaks. Moreover, von Mises stress becomes the residual stress after the time 6.0 seconds.

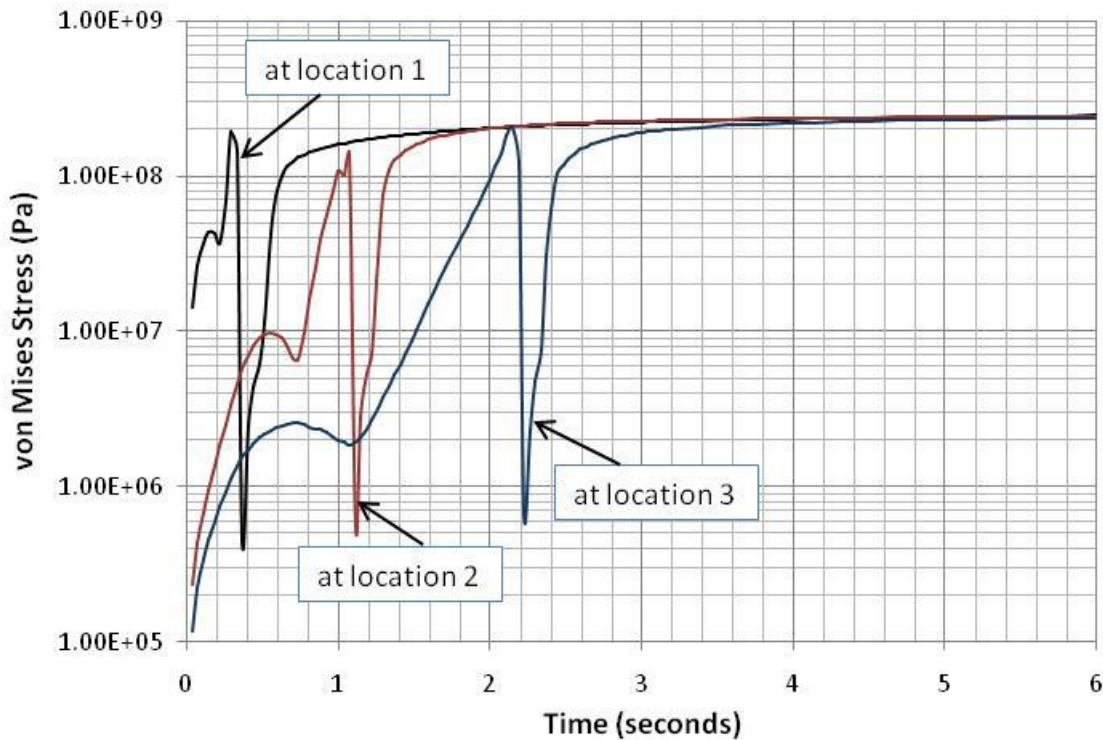


Figure 8.14: Temporal variation of von Mises stress at three different locations.

Figure 8.15 shows von Mises residual stress distribution across the weld path at three locations (Figure 8.7) after cooling at $t = 12.456$ seconds. This figure indicates that although the magnitudes of residual stress developed at each location are close, the width of the region around the center of the weld path is not the same. Location 1, closer to the welding starting point at a distance of 3 mm, has a wider region with high residual stress as compared to other two locations. This is attributed to the thermal strain produced due to high temperature gradient and subsequent cooling rate (temperature decay rate) at each location, which differs after the rapid decay of temperature. The maximum residual

stress is about 250 MPa and, similar to Figure 8.10, the stress field is not symmetric about the center of the weld path. It should be noted that the thermal and mechanical properties of the tube material is considered to be temperature dependent in the simulations. Consequently, the change in the elastic modulus at high temperatures and the temperature gradient variation along the spiral weld path are responsible for the occurrence of the local maximum and minimum in the residual stress.

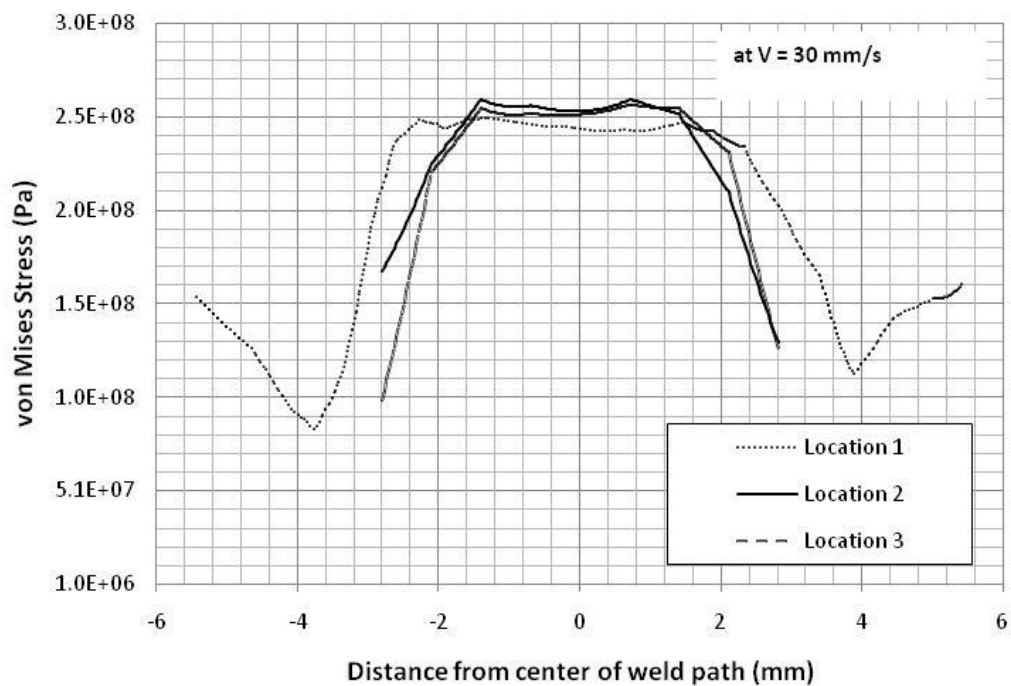


Figure 8.15: Residual stress across the weld path at three different locations.

8.5 EFFECT OF WELDING SPEED

Welding speed represents the distance traveled by the welding arc along the weld line per unit of time. The welding speed has an important effect on the heat distribution

pattern in the vicinity of the heat source. It is in this region that the heated zone is formed, and it is important to identify how the welding speed influences its size and shape. The speed of welding affects the shape of the isotherms. The lower the speed, the more elongated the isotherms and hence the resulting stress field. The effect of welding speed on the stress field has been studied for three cases of welding speeds (25, 30 and 35 mm/s) by maintaining all other input parameters same in all cases as given in Table 8.1.

In Figure 8.16, the temporal variation of von Mises stress for different laser welding speeds at the same location of Figure 8.10 is shown, i.e. location “2”. von Mises stress rises rapidly to reach its maximum for the high welding speed (35 mm/s). This is because of the rapid decay of temperature during the time period immediately after reaching the maximum temperature. Moreover, the rise of stress is relatively slower for the low welding speeds (25 and 30 mm/s) than that corresponding to the high speed. Once the low temperature is attained after cooling, the stress level remains almost steady with progressing time. This situation is true for all the three welding speeds. The magnitude of residual stress remains almost the same for all speeds. The residual stress developed is in the order of 250 MPa, which is less than the elastic limit of the substrate material. Consequently, the crack formation in the corner of the rectangular cut is not probable due to low stress levels developed in this region.

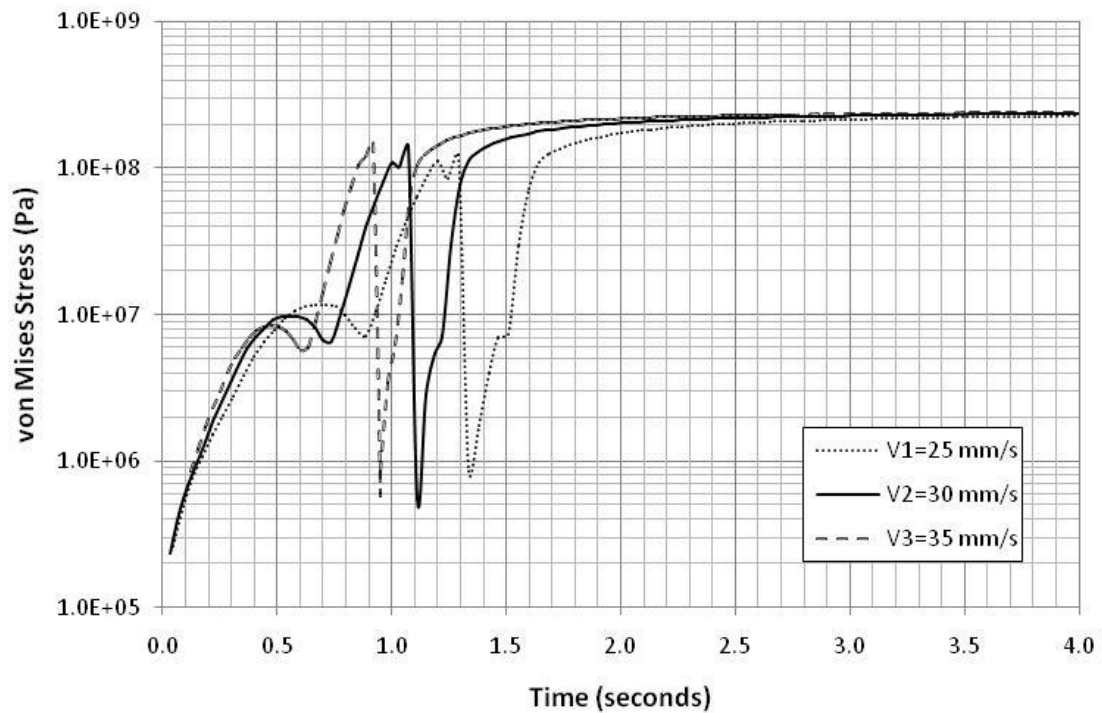


Figure 8.16: Effect of welding speed on the temporal variation of von Mises stress at Location# 2.

It is a well-known theory that the heat input is inversely proportional to the welding speed. Therefore, when the welding speed increases the heat input rate decreases. It is noted by numerical simulation results that in case of lowest welding speed of 25 mm/s, wider distributions of residual stresses are observed across the spiral welding path as shown in Figure 8.17 at all three locations. Technically, it is justified that the lower welding speed results in more heat input per unit volume, consequently wider fusion and HAZ zones are obtained. At all locations, the maximum residual stress is about 250 MPa and, therefore, it is concluded from the results that, in general, the welding speed has minor effect on the final magnitude of the residual stresses. However,

the residual stress distribution is not symmetric about the center of the weld path due to spiral weld line. The high magnitude of residual stress extends almost 2 mm on both sides of the laser beam at location 1, which is close to the welding starting point. At other two locations (“2” and “3”), it extends almost 1.5 mm on both sides of the center of weld path.

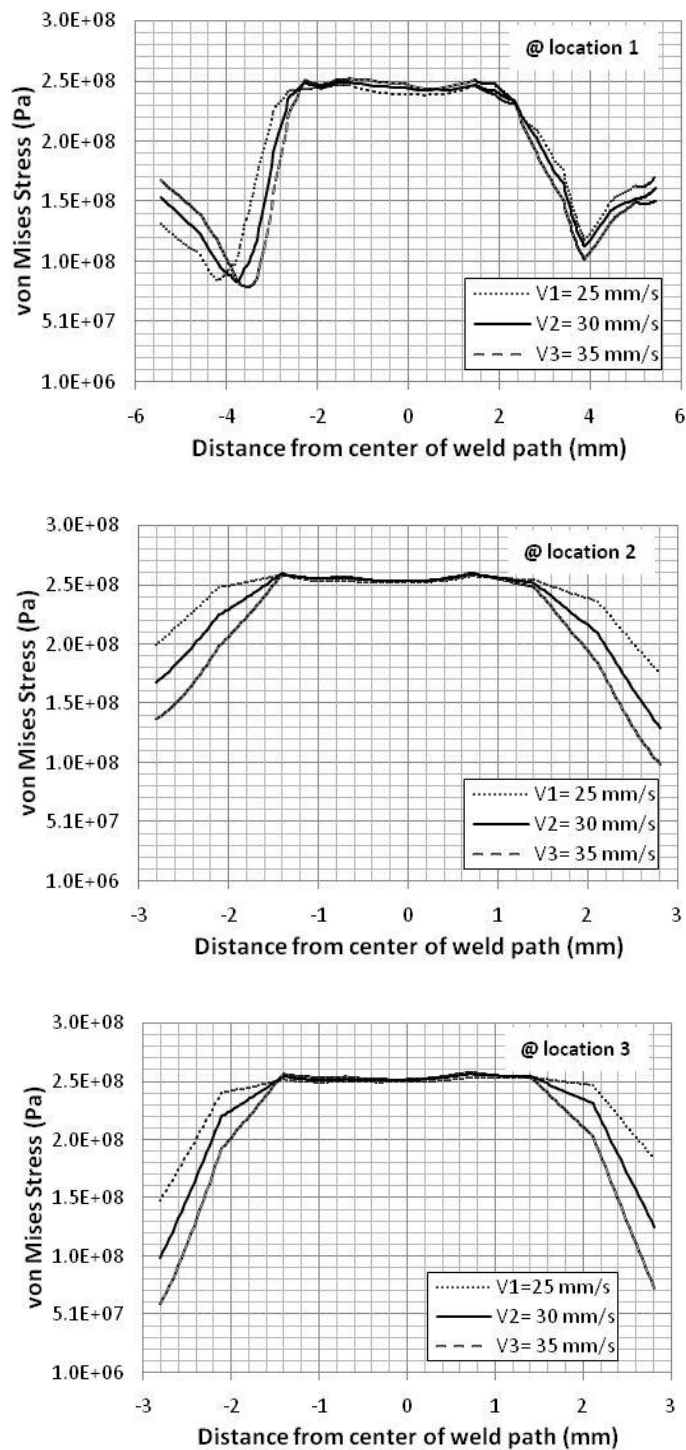


Figure 8.17: Residual stress distribution across the weld at three different locations after cooling at three welding speeds.

CHAPTER 9

CONCLUSIONS

Spiral welded pipe is the process of producing pipe from continuous coil strip formed into a spiral and welded by submerged arc welding process. It is considered suitable for low pressure applications, water supply and structural components. However, Spiral welded pipe gained a poor reputation in some gas, oil industry and petrochemical complex as a result of its high residual stresses. Reducing the residual stresses in spiral welded pipe production will result in a significant acceptance of this product for critical services worldwide.

As stated in this study, residual stresses are major problems associated with welding manufacture of spiral welded pipes. Complex thermal stresses occur during the welding and residual stresses remain, which have various consequences. Most of them are detrimental to the integrity of welded pipes. The objective of this study was to develop a versatile 3D computational model for predicting spiral pipe welding residual stresses on the basis of known material behavior and welding process parameters with little concern as regards geometric simplifications. This included establishing an arbitrary moveable heat source, finite element models, verification measurements of the temperature distribution in a spiral welded pipe and measurements of residual stresses. These objectives were successfully accomplished. The FEM results are here in general

lower than those experimentally measured. Large residual tensile von Mises stresses were observed near the weld fusion line. The magnitude for the residual stresses at the fusion line is 270 MPa. These peak stresses are around 45% of the yield stresses for the base pipe material (480 MPa).

Laser welding of a spiral welded tube with 1.6 mm wall thickness is considered and temperature as well as thermal stress fields is predicted using a three dimensional, nonlinear, transient finite element model. Further, the influence of laser welding speed on temperature and stress fields is examined. It is found that temperature rise is sharp in the region of the laser heat source, which results in high temperature gradients in the vicinity of the spiral weld path. Moreover, once the laser beam scans over this region, temperature decays sharply. This causes sharp increase in von Mises stress due to the attainment of high temperature gradient in this region. However, the maximum stress level is less than the elastic limit of the substrate material. von Mises stress attains a local minimum in the neighborhood of the laser source. This is because of the change in the temperature gradient and temperature-dependent elastic modulus of the substrate material. The effect of welding speed on the level of residual stress has been studied. It can be concluded that, increasing the welding speed with constant laser power and insignificant heat loss from the free surfaces leads to proportional growth of the isotherms. Increasing the welding speed, with constant power, results in reduction of the width of the high stress zone. Results show that the current model can be used as a tool

for parametric study of the welding process, which will lead to optimized values of the welding parameters. The most important of these parameters will be laser power and laser speed.

The effects of some spiral pipe welding and process parameters on the change of the circumferences after ring splitting tests have been studied using experimental data. It was found that pipe diameter; wall thickness, pipe grade, coil width, forming angle, welding speed and spiral pitch distance have significant effects on the change in the circumferences after ring splitting test. It has been realized that with the use of the developed regression model, the prediction of the change in circumferences (ΔC) becomes much simpler to anyone who has no prior knowledge of the pipe spiral welding process. The developed regression equation explains 36.48% of the variability in the ring opening. There was no better model found in open literature until now. With this encouraging result, the prediction model can be further improved upon by including other influencing parameters during forming and welding process. It is believed that there are other factors that have effect on the measured change in circumferences ΔC but the above factors were able to be collected for the analysis. These unconsidered factors include the quality of the weld and the steel materials used for pipe production. Presence of inclusion has a great effect on the level of the microscopic residual stress. For this reason, the model should cover additional welding and forming parameters.

Characterization of residual stresses in spiral welded pipes provides the information the engineer or manufacturer needs to properly manage the welding process, optimize product quality, minimize the effects of fatigue and Stress Corrosion Cracking (SCC) and help minimize production costs while enhancing pipe performance. The amount and distribution of residual stresses on the spiral welded pipes can be minimized by optimizing the welding and forming processes.

To gain empirical knowledge of the residual stresses due to welding and to obtain verification data for the computer simulations, measurements using drill hole techniques done on spiral welded pipe have been carried out. The results of the residual stresses shows that spiral welded pipe have microscopic residual stress above 200 MPa. These values were obtained by the FEM simulation too. Three cases of welding speed were investigated. Lower welding speed results in more heat input per unit volume, consequently wider fusion and HAZ zones are obtained. In general, excessively high temperature concentrations should be avoided, however, not only because of possibly locally increased residual stresses, but because of undesired micro-structural changes connected with the temperature gradient over time. The peak residual stresses from drilling hole technique are higher than those calculated from ring splitting test and FEM measurements; this may have implications for spiral welded piping integrity as stresses will be higher at some locations than those indicated from the simple ring splitting test. The drilling hole residual stress measurements were able to determine the axial residual stresses, which were the greatest in magnitude and could not be measured by the ring-

splitting method. The accuracy and good spatial resolution of the drilling hole measurements makes this a useful research tool. The experimental small scale test by drilling hole technique are sometimes questioned for its effectiveness because of the different residual stress conditions from the actual pipe and also criticized due to the limitation in size or area of evaluation.

The spiral welded pipe industry will face severe problems with residual stresses and the best way of dealing with such problems is to develop technologies for controlling and reducing residual stresses during manufacturing.

CHAPTER 10

FUTURE WORK

This research will add a valuable contribution to the field of spiral pipe welding simulation. As mentioned earlier, there are no proven mathematical formulas to calculate the residual stresses in spiral welded pipes. This research is aimed to be a step towards the more accurate determination of welding residual stresses through simulation by modeling the submerged arc welding for spiral pipes. The outlined way of simulating the welding distortions covers the main issues of the nonlinear thermoelasto-plastic problem. However, improvements of the FEM models could be made and additional effects could be included. Effort could be also made in the area of welding stresses during phase transformation. More attention could be focused on the welding mechanics such as volume changes due to phase transformation, plasticity transformation, chemical composition and alloy-specific materials parameters. In the present work the most influential parameters are taken into account. In the present work calculations by a finite element program have been performed. Subsequently, it should be possible to make corrective pre-adjustments of geometry and change the weld joint parameters or meshing in order to improve the accuracy in the measured residual stresses.

REFERENCES

- Abid M. and Siddique M., 2005, Finite-element simulation of tack welds in girth welding of a pipe-flange joint, *Acta Mechanica*, 178, pp. 53–64.
- Andrzej Sluzalec, 2005, *Theory of Thermomechanical Processes in Welding*, Springer, 1 edition.
- ANSI/API 5L, Specification for Line Pipe, 2007, American Petroleum Institute, Forty-Fourth Edition.
- ANSYS User's Manual, 2007, Version 11.0 ANSYS Inc., USA.
- API 579-1/ASME FFS-1, 2007, Recommended Practice for Fitness-for-Service, American Petroleum Institute. Second Edition.
- Arif A. F. M., 2010. On the modeling of laser a moving distributed volumetric heat source for laser cutting simulation, *Advanced Materials Research*. 83-86, 858-865.
- ASME B31.3, 2008, Process Piping, American Society of Mechanical Engineers.
- ASTM E837, 2008, Standard Test Method for Determining Residual Stresses by the Hole-Drilling Strain-Gage Method, American Society Testing & Materials.
- Avagianos J. and Papamantellos K., 2002, New Technology Spiral SAW Pipes for Onshore & Offshore Oil and Gas Pipelines, Proceedings of 4th International Pipeline Conference, Canada.
- Balasubramanian K. R., Siva Shanmugam N., Buvanashakaran G. and Sankaranarayanan K., 2008. Numerical and Experimental Investigation of Laser Beam Welding of AISI 304 Stainless Steel Sheet, *Advances in Production Engineering & Management*, 2, 93-105.
- Barsoum Z., 2007, Residual Stress Prediction and Relaxation in Welded Tubular Joint, *Welding in the World*, Vol. 51, No. 1/2.
- Benyounis K. Y. and Olabi A. G., 2008, Optimization of different welding processes using statistical and numerical approaches – A reference guide, *Advances in Engineering Software*, Volume 39, Issue 6, June 2008, pp.483-496.

- Brensing K. H., Sommer B., Steel tube and pipe manufacturing processes, http://www.mrw.de/downloads/stahlrohre_engl.pdf.
- Cho J. R., Lee B. Y., Moon Y. H. and Van Tyne C. J., 2004, Investigation of residual stress and post weld heat treatment of multi-pass welds by finite element method and experiments, *Journal of Materials Processing Technology*, 155–156, pp. 1690–1695.
- Collins L. and Hamad F., 2006, Manufacture of High strength Spiral Line pipe for Gas Transmission, *Canadian Welding Association Journal - International Institute of Welding Special Edition*, pp. 17-18.
- Conway H. D. and Nickola W. E., 1965, Anticlastic Action of Flat Sheets in Bending, *Experimental Mechanics*, Volume 5, Number 4, pp. 115-119.
- De A., Maiti S. K., Walsh C.A. and Bhadeshia H. K. D. H., 2003, Finite element simulation of laser spot welding, *Science and Technology of Welding and Joining*, 8 (5), 377-384.
- Dhingra A. K. and Murphy C. L., 2005, Numerical simulation of welding-induced distortion in thin-walled structures, *Science and Technology of Welding and Joining*, Vol. 10 No.
- Dittmer J. P., Jensen C. G., Gottschalk M. and Almy T., 2006, Mesh Optimization Using a Genetic Algorithm to Control Mesh Creation Parameters, *Computer-Aided Design & Applications*, Vol. 3, No. 6, pp. 731-740.
- Dong P., Hong J. K., and Leis B. N., 2006, Computational Simulation of Line-Pipe Fabrication Processes”, *Proceedings 6th International Pipeline Conference*.
- Eagar T. W. and Tsai N. S., 1983, Temperature Fields Produced by Traveling Distributed Heat Sources, *Welding Research Supplement*.
- Erdogan Madenci and Ibrahim Guven, 2006, *The Finite Element Method And Applications In Engineering Using ANSYS*, Springer.
- Fassani R. N. S. and Trevisan O. V., 2003, Analytical Modeling of Multipass Welding Process with Distributed Heat Source, *J. of the Braz. Soc. of Mech. Sci. & Eng*, Vol. XXV, No. 3.

- Franz Martin Knoop and Baldur Sommer, 2004, Manufacturing and use of Spiral Welded Pipes for High Pressure Services- State of the Art, Proceedings of 4th International Pipeline Conference, Canada.
- Franzblau Abraham N., 1958, A Primer of Statistics for Non-Statisticians, New York, Harcourt, Brace & World, New York.
- Frewin M. R. and Scott D.A., 1999. Finite Element Model of Pulsed Laser Welding, Welding Research Supplement, 78, 15s-22s.
- Gery D., Long H. and Maropoulos P., 2005, Effects of welding speed, energy input and heat source distribution on temperature variations in butt joint welding, Journal of Materials Processing Technology, 167, pp. 393–401.
- Goldak J., Chakravarti A., Bibby M., 1984, A new finite element model for welding heat source, Metall. Trans. B, 15B, 299-305.
- Goldak J., Patel B., Bibby M. A. and Moore J., 1986, Computational Weld Mechanics, Advanced Joining Of Aerospace Metallic Materials, Conference Proceeding No. 398.
- Hidveghy J., Michel J. and Bursak M., 2003, Residual Stress in Microalloyed Steel Sheet, Metalurgija 42, pp. 103-106.
- Horn Ten C. H. L. J., 2002, Cyclic Plastic Deformation and Welding Simulation, DUP Science, Netherlands.
- Hsu T. R., 1986, The Finite Element Method in Thermomechanics, Allen & Unwin, Inc., Winchester, MA, pp. 24 - 76.
- Jiang W., Yahiaoui K., Hall F. R., and Laoui T., 2005, Finite element simulation of multi-pass welding: full three-dimensional versus generalized plane strain or axisymmetric models, IMechE 2005, J. Strain Analysis, Vol. 40, No. 6.
- Jones L. A., Mendez P., Weiss D., and Eagar T. W., 1997, Dynamic Behavior of Gas Metal Arc Welding, 9th Annual Conference on Iron and Steel Technology, Pohang, Korea.
- Kim I. S., Son J. S., Kim I. G., Kim J. Y. and Kim O. S., 2003, A study on relationship between process variables and bead penetration for robotic CO₂ arc

- welding, *Journal of Materials Processing Technology*, Volume 136, Issues 1-3, pp. 139-145.
- Kubel Jr. and Edward J., 1986, *Modeling the Weld Process*, Advanced Materials and Processing inc. Metal Progress, pp. 77-80.
 - Lee C., 2006, *A Study of an Automatic Welding System*, http://thesis.lib.ncu.edu.tw/ETD-db/ETD-search/view_etd?URN=87343013#anchor.
 - Lu X. and Hassan T., 2001, *Residual Stresses in Butt and Socket Welded Joints*, *Transactions, SMiRT*, 16.
 - Lundback A., Runnemalm H., 2005. *Validation of three dimensional finite element model for electron beam welding of Inconel 718*. *Science and Technology of Welding and Joining*, 10 (6), 717-724.
 - Mackwood P., Crafer R. C., 2005. *Thermal modeling of laser welding and related processes: a literature review*. *Optics and Laser Technology*. 37, 99-115.
 - Macura P. and Fiala A., 2002, *Experimental Residual Stress Analysis at Welded Pipelines*, 40th International Conference Experimental Stress Analysis, 3. – 6. VI., Czech Republic.
 - Mahapatra M. M., Datta G. L., Pradhan B. and Mandal N. R., 2006, *Three-dimensional finite element analysis to predict the effects of SAW process parameters on temperature distribution and angular distortions in single-pass butt joints with top and bottom reinforcements*, *International Journal of Pressure Vessels and Piping*, 83, 721–729.
 - Malik A. M., Qureshi E. M. and Dar N. U., 2007, *Numerical Simulation of Arc Welding Investigation of various Process and Heat Source Parameters*, MED UET Taxila.
 - Nguyen N. T., Ohta A., Matsuoka K., Suzuki N. and Maeda Y., 1999, *Analytical Solutions for Transient Temperature of Semi-Infinite Body Subjected to 3-D Moving Heat Sources*, *Supplement to the Welding Journal*.
 - Okada A., Kasugai T. and Hiraoka K., 1988, *Heat Source Model in Arc Welding and Evaluation of Weld Heat-affected Zone*, *Transactions ISIJ*, Vol. 28.

- Olabi A. G., Benounis K. Y. and Hashmi M. S. J., 2007. Application of response surface methodology in describing the residual stress distribution in CO₂ laser welding of AISI 304. *Strain*. 43, 37-46.
- Paul S. Prév y, 1996, Current Applications of X-Ray Diffraction Residual Stress Measurement, *Developments in Materials Characterization Technologies*, pp 103-110.
- Permyakov I. L., Pumpyanskyi D.A., Pyshmintsev I. Yu and Stolyarov V. I., 2006, Advanced Technologies for Spiral Welded Oil and Gas Line Pipes, *Proceedings of IPC 2006, 6th International Pipeline Conference*, Calgary, Canada. pp. 239-244.
- Poorhaydari K., Patchett B. M., and Ivey D. G., 2005, Estimation of Cooling Rate in the Welding of Plates with Intermediate Thickness, *Welding Journal*, pp. 149-155.
- Prime M. B., 1999, Residual Stress Measurement by Successive Extension of a Slot: The Crack Compliance Method, *Applied Mechanics Reviews*, 52 (2), pp. 75-96.
- Qingren X., Yaorong F. and Chunyong H., 2002, The Measurement and Control of Residual Stress in Spiral Sub-merged Arc Welded Pipe, *Proceedings of 4th International Pipeline Conference, IPC2002*, Calgary, Alberta, Canada.
- Qureshi E. M., Malik A. M., and Dar N. U., 2009, Residual Stress Fields due to Varying Tack Welds Orientation in Circumferentially Welded Thin-Walled Cylinders, *Advances in Mechanical Engineering*, Volume 2009.
- Safdar S., Li L., Sheikh M.A. and Liu Z., 2007. The Effect of Nonconventional Laser Beam Geometries on Stress Distribution and Distortions in Laser Bending of Tubes, *Journal of Manufacturing Science and Engineering*, 129, 592-600.
- Saudi Aramco Materials System Specification, 01-SAMSS-035, "API Line Pipe", July 19, 2010.
- Shin H., Yoo Y. T., Shin H.J., Kim J. H., 2007. Laser welding characteristics of cold rolled carbon steel utilize continuous wave Nd:YAG laser. *Key Engineering Materials*. 345-346.

- Silva C. C. and Farias J. P., 2008, Non-uniformity of residual stress profiles in butt-welded pipes in manual arc welding, *Journal of Materials Processing Technology*, vol. 199, no. 1–3, pp. 452–455.
- Sorenson M. B., 1999, *Simulation of Welding Distortions in Ship Section*. Ph.D. Thesis, Technical University of Denmark.
- Stamenković D. and Vasović I., 2009, Finite Element Analysis of Residual Stress in Butt Welding Two Similar Plates, *Scientific Technical Review*, Vol. IIX, No.1.
- Starling C. M. D., Marques P. V. and Modenesi P. J., 1995, Statistical modelling of narrow-gap GTA welding with magnetic arc oscillation, *Journal of Materials Processing Technology*, Volume 51, Issues 1-4, pp. 37-49.
- Sunar M., Yilbas B. S. and Boran K., 2006, Thermal and stress analysis of a sheet metal in welding, *Journal of Materials Processing Technology*, 172, pp.123–129.
- Sundar M., Nath A. K., Bandyopadhyay D. K., Chaudhuri S. P., Dey P. K. and Misra D., 2007, Finite Element Analysis of Residual Stress and Distortion in Laser Welded Stainless Plate. *International Journal for Manufacturing Science & Production*, 8 (2-4), 123-136.
- Tanala E., Bourse G., Fremiot M., De Belleval J. F., 1995, Determination of near surface residual stresses on welded joints using ultrasonic methods, *NDT&E International*, Vol. 28, No. 2, pp. 83-88.
- Taylor G. A., Hughes M., Strusevich N. and Pericleous K., 1999, *Finite Volume Methods Applied To The Computational Modeling Of Welding Phenomena*, Second International Conference on CFD in the Minerals and Process Industries, Australia.
- Tsai N. S. and Eagar T. W., 1984, Changes of Weld Pool Shape by Variations in The Distribution of Heat Source in Arc Welding, *Modeling of Casting and Welding Processes II*, AIME, New York, 317.
- Vedani M., 2004. Microstructural evolution of tool steels after Nd-YAG laser repair welding. *Journal of Materials Science*. 39, 241-249.
- Walton H. W., 2002, *ASM Handbook of Residual Stress and Deformation of Steel: Deflection Methods to Estimate Residual Stress*, ASM International, Ohio, pp. 89-98.

- Weisman C., 1976, American Welding Society, *Welding Handbook: Fundamentals of Welding*, Seventh Ed. vol. 1.
- Withers P. J. and Bhadeshia H. K. D. H., 2001, *Residual Stress Part 1 – Measurement techniques*, *Materials Science and Technology*, Vol. 17.
- Wu C. S. and Sun J. S., 2002, Numerical analysis of temperature field during double-sided arc welding of thick materials, *Computational Materials Science*, 25 pp. 457–468.
- Wu C. S., Wang H. G. and Zhang Y. M., 2006, A New Heat Source Model for Keyhole Plasma Arc Welding in FEM Analysis of the Temperature Profile, *Welding Journal*, 85 (12), 284s-291s.
- Yaghi A., Hyde T. H., Becker A. A. Sun W. and Williams J. A., 2006, Residual stress simulation in thin and thick-walled stainless steel pipe welds including pipe diameter effects, *International Journal of Pressure Vessels and Piping*, 83, pp. 864–874.
- Yang L. J., Bibby M. J. and Chandel R. S., 1993, Linear regression equations for modeling the submerged-arc welding process, *Journal of Materials Processing Technology*, Volume 39, Issues 1-2, pp. 33-42.
- Yeung K. S. and Thornton P.H., 1999, Transient Thermal Analysis of Spot Welding Electrodes, *Welding Research Supplement*, 78, pp. 1s–6s.
- Yilbas B. S., Arif A. F. M., Abdul-Aleem B. J., 2010. Laser welding of low carbon steel and thermal stress analysis. *Optics & Laser Technology*. 42, 760-768.
- Zhang W., Kim C.-H., and DebRoy T., 2004, Heat and fluid flow in complex joints during gas metal arc welding—Part II: Application to fillet welding of mild steel, *Journal Of Applied Physics*, Volume 95, Number 9, , pp. 5220-5229.
- Zeng-rong H., Jian-zhong Z., Hua-feng G. and Jian-jun D., 2007. Simulation of temperature field of laser welding by ABAQUS. *Laser Technology*, 31, 3, 326-329.
- http://en.wikipedia.org/wiki/Process_capability_index (visited on 17th September 2010).
- <http://www.hall-longmore.co.za/pipes/saw.html> (visited on June 2009).
- <http://www.ozmakboru.com/eng/> (visited on June 2009).

- X-ray Diffraction Residual Stress Measurement,
<http://www.protoxrd.com/pdf/rsintro.pdf>.

VITA

Name: Ahmed Saleh Awadh Al-Omari

Nationality: Saudi

Place of Birth: Dammam, Saudi Arabia

Address: P.O. Box 12919

Dammam 31483

Saudi Arabia

e-mail: ahmad.omari.1@aramco.com

Education:

- **Bachelor of Science in Mechanical Engineering, June 2001**
King Fahd University of Petroleum & Minerals, Dhahran, Saudi Arabia with a GPA of 3.533 on a 4.0 scale (Second Honors, Dean's List).
- **Master of Science in Mechanical Engineering, May 2010**
King Fahd University of Petroleum & Minerals, Dhahran, Saudi Arabia with a GPA of 3.469 on a 4.0 scale.

Work Experience:

- 2001- Present, Materials & Corrosion Engineer – Saudi Aramco

Certifications:

- NACE Corrosion Technologist (Certificate # 21092)
- Certified NACE Coating Inspector Level 1 (Certificate # 20872)
- Certified NACE Cathodic Protection Tester (Certificate # 21092)
- Certified ASM Failure Analysis Engineer